Role of the cholesterol hydroxylase enzyme CYP46A1 in cholesterol metabolism and neuroprotection in Huntington's disease

Radhia Kacher

Sorbonne Université

Doctoral school: “Cerveau Cognition Comportement”

Thesis submitted for the degree of PhD in Neuroscience

Presented by **Radhia KACHER**

Role of the cholesterol hydroxylase enzyme CYP46A1 in cholesterol metabolism and neuroprotection in Huntington’s disease

PhD defended on the 5th of February 2019

In front of the jury composed of

Pr Alexandra Durr	President
Dr Emmanuel Brouillet	Reviewer
Dr Valerio Leoni	Reviewer
Dr Sandrine Humbert	Examiner
Dr Pierre Trifilieff	Examiner
Pr Sandrine Betuing	PhD supervisor
Dr Jocelyne Caboche	Invited member

A Ilyes et Jamila

Remerciements

Je tiens à remercier Emmanuel Brouillet et Valerio Leoni d'avoir accepté d'être rapporteur de ma thèse, merci également à Sandrine Humbert, Pierre Trifieleff et Alexandra Durr d'avoir accepté de faire partie de mon jury. Je suis très honorée de votre présence et vous remercie pour votre disponibilité et l'intérêt accordé à mon travail.

Je remercie particulièrement et chaleureusement Sandrine Betuing et Jocelyne Caboche pour m'avoir recrutée dès le M2, pour m'avoir fait confiance et pour leurs conseils et leur accompagnement tout au long de ma thèse.

Merci Sandrine pour avoir été un mentor exceptionnel et avoir toujours été présente. Pour tes conseils scientifiques bien sûr mais aussi ton recul et ton esprit critique qui m'ont permis d'apprendre énormément au cours de ma thèse. Merci aussi pour ton énergie et ton dynamisme, source de motivation. Et surtout merci pour ta gentillesse et ta confiance, qui m'ont permis d'évoluer dans un cadre positif et de m'exprimer scientifiquement.

Merci Jocelyne pour le temps consacré à cette thèse et pour tes précieux conseils qui ont permis de faire évoluer ce projet vers de nouveaux horizons, j'ai beaucoup appris grâce à toi. Merci aussi pour toutes les conversations, scientifiques ou non, riches d'enseignements. Merci surtout pour ta disponibilité et ton écoute tout au long de ma thèse.

Je remercie la fondation Groupama « Vaincre les maladies rares » pour avoir cru en moi et pour avoir financé ma thèse, sans eux rien n'aurai été possible. Un grand merci à Sophie Dancygier pour sa disponibilité et son aide.

Merci à toute l'équipe SNRG, passée et présente, pour la bonne humeur et toutes les discussions passionnées et passionnantes.

Merci à Peter pour l'intérêt porté à ce projet et toutes tes questions intéressantes. Merci à tous ceux qui m'ont aidé : Nicolas pour tes épines ; Vincent, Monsieur qPCR ; Enejda, acolyte Huntington et merci à Andry, Estefani et Benoit pour toutes les discussions scientifiques et pour les conseils au quotidien.

Merci à ceux qui étaient là alors que je débutais au labo, à Marine et à Marc, pour toutes les discussions et leurs conseils. Je remercie Lydie qui m'a beaucoup aidé lors de mon M2.

A tous ceux qui sont venus ensuite, merci à Enejda, Andry, Estefani, Pierre et Lieng pour votre amitié, votre présence, votre écoute et toutes les conversations sur tous les sujets possibles et imaginables, des plus sérieux aux plus triviaux.

Je remercie également tous les collaborateurs qui se sont investi dans ce projet, qui ont beaucoup apportés pour l'avancée et la réflexion autour de ce sujet. Merci à Antonin Lamazière et Gaëtan Despres pour leur précieux travail de spectrométrie de masse ; merci à Christian Néri et Satish Sasidharan Nair pour l'analyse transcriptomique qui a beaucoup fait avancer le projet ; merci à Frédéric Saudou et Wilhelm Christaller pour leur très intéressante étude de transport sur micro-fluidique ; merci à Laurent Venance, Yulia Dembitskaya et Elodie Perrin pour leur expertise en électrophysiologie ; merci à Valérie Messent pour son aide en microscopie électronique. Merci également à Carole Escartin et Laurene Abjean pour leur précieux conseils en tri cellulaire et merci Elias El-Habr pour m'avoir accompagné sur l'utilisation du FACS. Je remercie également les membres des plateformes de l'institut : Tahar, Jean-François, France et la plateforme ArtBio pour leur aide et leurs conseils. Je remercie aussi les différents stagiaires qui ont travaillé dans l'équipe, en particulier Jamila et Coline qui ont aidé à faire avancer ce projet.

Merci à toutes les personnes de l'institut avec qui j'ai pu interagir, qui ont contribué à évoluer dans un environnement positif et agréable : Mélody, Coralie, Laila, Anaïs, Josquin, Nida, Juliette, Anne-Claire, Dorian, Jean.

Merci à mes amies, Oriane, Solène et Célia, avec qui nous avons beaucoup partagées et nous sommes soutenues pendant toutes ces années.

Je remercie bien sur mes parents pour avoir toujours mis l'éducation de leurs enfants au premier plan et pour leur soutien permanent. Je remercie particulièrement mon frère et ma sœur, Ilyes et Jamila, pour leur soutien, leur complicité et la capacité à toujours apporter une bonne dose d'humour dans les bons moments comme dans les moments plus difficiles.

Enfin, merci Maxime pour ton soutiens inconditionnel, ton écoute et ta présence à chaque instant.

Merci à tous, grâce à vous j'ai beaucoup appris scientifiquement, j'ai pu grandir humainement, c'est donc avec beaucoup d'émotion que j'écris ces lignes, qui marquent la fin de cette aventure.

Table of Content

Abbreviations

24S-OHC	24S-hydroxycholesterol
25-OHC	25-hydroxycholesterol
27-OHC	27-hydroxycholesterol
5HT	Serotonin
7-DHC	7-dehydrocholesterol
ABCA1	ATP-binding cassette transporter A1
ACAT-1	Acetyl-CoA cholesterol acetyltransferase 1
Ach	Acetylcholine
AD	Alzheimer's disease
AMPA	amino-3-hydroxy-5-methylisoxazole-4-propionic acid
ApoE	Apolipoprotein E
APP	amyloid precursor protein
BBB	Blood Brain Barrier
BDNF	Brain Derived Neurotrophic Factor
CBP	cAMP-response element (CREB)-Binding Protein
CH25H	cholesterol-25-hydroxylase
CNS	Central Nervous System
CREB	cAMP-response element
CSF	cerebrospinal fluid
CYP27A1	Sterol 27-hydroxylase
CYP46A1	Cholesterol 24-hydroxylase
Cyp51	lanosterol C14 demethylase
DA/D1/D2	Dopamine/Dopamine receptor subtype 1/Dopamine receptor subtype 2
DHCR24	24-dehydrocholesterol reductase
DHCR7	7-dehydrocholesterol reductase
ER	Endoplasmic Reticulum
ERK	Extracellular signal-regulated kinases
Fdft1	squalene synthase
GABA	Gamma AminoButyric Acid
GAPDH	glyceraldehyde 3-phosphate dehydrogenase
GGTase-I	geranylgeranyl transferase-I
GLT1	glutamate transporter 1
Glu	Glutamate
GluN1/2/3	Glutamate receptor subunit 1/2/3
GPe	external Globus Pallidus
GPi	internal Globus Pallidus
HAP1	Huntingtin associated protein 1
HAP40	Huntingtin associated protein 40
HD	Huntington's disease
HDAC	histone deacetylase
HIP1/R	huntingtin interacting protein 1/receptor
HMG-CoA	3-hydroxy-3-methylglutaryl-CoA
HMGCR	HMG-CoA reductase
Htt	Huntingtin gene
HTT	Huntingtin protein
Kir4.1	potassium channel

LC3	Microtubule-associated proteins 1A/1B light chain 3B
LDL	low-density lipoproteins
LDL-R	LDL receptors
LRP1	low density lipoprotein receptor-related protein 1
LTP	long term potentiation
LXR	Liver X Receptor
mHTT	mutated Huntingtin protein
MRI	Magnetic Resonance Imaging
mTOR	mammalian target of rapamycin
NE	Noradrenaline
NMDA	*N*-methyl-D-aspartate
NMDA-R	NMDA receptors
NPC1 and 2	Niemann-Pick Type C protein 1 and 2
p53	tumor suppressor protein 53
PET	positron emission tomography
PGC1α	peroxisome proliferator activated receptor gamma coactivator 1α
polyQ	poly glutamine stretch
PSD-95	Post-synaptic density protein 95
REST/NRSF	repressor-element 1 transcription factor/neuron restrictive silencer factor
ROS	reactive oxygen species
RXR	retinoid X receptors
SCAP	SREBP cleavage activating protein
sGTPase	small guanosine triphosphate-binding proteins
SN	Substantia Nigra
SNARE	Soluble NSF Attachment Protein Receptor
SNc	Substansia Nigra pars compacta
SNr	Substansia Nigra pars reticulata
SP1	Specificity Protein 1
SPN	Striatal Projection Neurons
SRE	sterol regulatory elements
SREBP	sterol responsive element binding protein
STN	Subthalamic Nucleus
TAFII30	tyrosine amino transferase II
TBP	TAT binding protein
TFIIF	transcription factor F
TrkB	Tyrosine kinase B

Context

Huntington's disease (HD) is an autosomal dominant genetic disorder, caused by an increase in the number of CAGs in exon 1 of Huntingtin's gene. The neuropathology of HD mainly affects the striatum and the cortex at early stages of the disease and progressively spreads to other brain structures. The main clinical manifestations of this pathology are choreic movements, cognitive deficits and psychiatric disorders. Currently, treatments are only symptomatic, there is no disease modifying treatment on the marker for HD, which is why research on HD remains essential to understand and treat this disease. A major challenge in the management of HD is to delay the age of onset of the disease and slow down its progression. Over the last decade, a growing number of potential therapeutic targets has been tested in HD clinical trials but the rate of success remains low with only 3,5% of trials progressing to the approval phase (Travessa et al., 2017). The goal of our team is to understand the molecular mechanisms involved in neurodegeneration in order to propose new therapeutic targets. In the past 10 years, alterations in cerebral cholesterol homeostasis have been described in HD (Valenza and Cattaneo, 2011). However, the relevance of targeting cholesterol metabolism for therapeutic interventions in HD remains to be established. Cholesterol is an essential membrane component in the central nervous system, alterations of its homeostasis will have serious consequences on neuronal functions. Since cholesterol does not cross the blood-brain barrier, it is synthesized and renewed in the central nervous system. The metabolite derived from the catabolism of cholesterol in the brain, the 24S-hydroxycholesterol (24S-OHC), is decreased in the plasma of patients at early stages and is correlated with the atrophy of the putamen measured by MRI (Leoni et al., 2008). In addition, the expression of CYP46A1, the neuronal protein and the rate-limiting enzyme that catabolizes cholesterol into 24S-OHC, is strongly reduced in the putamen of patients, as well as in the striatum of R6/2 HD mouse models (Boussicault et al., 2016).

The team previously demonstrated, in the R6/2 HD mouse models, that restoration of appropriate CYP46A1 expression in striatal neurons is neuroprotective and directly reinstates cholesterol metabolism, including production of sterols (lanosterol and desmosterol) and 24S-OHC (Boussicault et al., 2016). The zQ175 mice are a recently characterized Knock-In murine model carrying the human first exon with 190 CAGs in the mouse's endogenous *Htt* gene (Menalled et al., 2012). This model has the advantage of respecting the genetic context of the pathology and displays several phenotypes which can be quantified to evaluate therapeutic approaches and to study early events in HD pathogenesis. As cholesterol metabolism appears like an interesting target in HD, my thesis project was focused on the impact of a restoration of CYP46A1 expression in the striatum of the zQ175 mice and the underlying molecular and cellular mechanisms involved in the beneficial effects of CYP46A1.

In this context, a better understanding of the cell-type-specific mechanisms underlying the dysregulation of brain cholesterol signaling are essential to develop an efficient neuroprotective strategy in HD. Therefore, the second part of my project was focused on the specific regulation of transcription and cholesterol metabolism in purified astrocytes and neurons. Indeed, astrocytes are the main site for cholesterol synthesis, whereas neurons mainly degrade cholesterol through CYP46A1 expression and the production of 24S-OHC. Thus, because cholesterol metabolism in the brain is complex and strongly relies on astrocytes, we need to complete our understanding of the neuroprotective mechanisms provided by CYP46A1. We thus started a more precise study on the impact of neuronal CYP46A1 restoration in isolated and purified astrocytes and neurons from striatal extracts. This study on neuronal and astrocytic populations will allow the identification of relevant molecular targets involved in CYP46A1-mediated neuroprotection, which could be of therapeutic interest in HD.

Therefore, my thesis project aimed at further understanding the cellular and molecular mechanisms that drive CYP46A1-mediated neuroprotection and dissecting the cell type-specific mechanisms that ensure an appropriate regulation of cholesterol metabolism.

INTRODUCTION

Chapter 1 - Huntington's disease

Epidemiology

Huntington's disease (HD) is a hereditary neurodegenerative disease, one of the most common neurological disorders with an autosomal dominant inheritance. HD is endemic to all population; however, it is most common in population of European descent. Indeed, in a Canadian study, HD prevalence was estimated at 13.7 per 100 000 in the general population and 17.2 per 100 000 in the population of European descent (Fisher and Hayden, 2014). Japan represents the most non-Caucasian population studied, with a prevalence of 0.72 per 100 000 (Adachi and Nakashima, 1999). In France, the number of people concerned is estimated at 6 000 patients and 12 000 asymptomatic carriers (www.orpha.net). The mean age of onset is typically between 30 and 50 years, with a range of 2 to 80 years (Myers, 2004). The early onsets, before 21 years old, are known as Juvenile Huntington's Disease and concern 3 to 10% of the patients (Gonzalez-Alegre and Afifi, 2006). After the first symptoms appear, the mean progression of the disease is 17 to 20 years (Myers, 2004).

Symptoms

Motor symptoms

Motor symptoms are characteristic of HD, with an evolution of the pattern of symptoms along with the disease progression. Early in the disease, involuntary movements such as chorea are predominant, causing limb incoordination. At later stages, chorea will decrease, replaced by dystonia (sustained or repetitive muscle contraction leading to abnormal posture), rigidity and bradykinesia (slowness of movement) (Novak and Tabrizi, 2010). Other motor symptoms include abnormal eye movement and dysphagia (difficulty in swallowing). In the late stages of the disease, dysphagia is associated with a high morbidity, with complication such as pneumonia, malnutrition and dehydration (de Tommaso et al., 2015).

Cognitive symptoms

Cognitive symptoms tend to begin before motor disorders and can profoundly affect the daily life of patients, especially because patients themselves may not be aware of the beginning of these symptoms. Cognitive decline starts with subtle signs more than 10 years before diagnosis, worsening with the course of the disease (Papoutsi et al., 2014). Patients are frequently impulsive; they will

experience executive dysfunctions at early stages, causing problems of planning, concentration and multi-tasking. They can also have difficulty in learning new skills. Patients can experience perceptual changes, visuospatial deficits, especially perception of their own bodies in their environment (Craufurd and Snowden, 2002).

Psychiatric and behavioral symptoms

Psychiatric symptoms, like cognitive symptoms, often precede motor decline and highly impact patients and their interaction with family members and care takers. Depression is common in HD, as an intrinsic feature, independently of other symptoms. Suicide in pre-symptomatic and symptomatic carriers is higher than in the general population (Paulsen et al., 2005). Other common symptoms include anxiety, irritability and apathy (Paulsen et al., 2001). Apathy can be a challenging symptom to manage because difficult to distinguish from depression. Apathy occurs early and worsens with the progression of the disease (Camacho et al., 2018). Sleep disorders may be misinterpreted as consequences of depression, but are characteristic of HD. Disturbed nocturnal sleep and increased daytime somnolence have been described in patients (Arnulf et al., 2008; Videnovic et al., 2009).

Peripheral symptoms

HD symptoms are not restricted to the central nervous system (CNS) (van der Burg et al., 2009). Weight loss is a prominent hallmark of HD; it is progressive and seems to be associated with an increased metabolic rate. For instance, the pancreas is affected with an impaired glucose tolerance. Skeletal muscle atrophy is another feature of HD and study of patient's myocytes showed several cellular defects. Cardiac failure is observed in 30% of HD patients and is an important cause of death in HD. A recent study showed a cardiac electrical remodeling in HD patients, with changes in advanced ECG variables (Cankar et al., 2018). Other described features include testicular atrophy, osteoporosis and dysfunction of blood derived cells (van der Burg et al., 2009). Risk of cancer is significantly reduced in HD, despite the high incidence of risk factors in patients, except for skin cancer where incidence is higher (Coarelli et al., 2017).

Neuropathology

Neurodegenerescence in HD

HD is associated to a progressive and severe neurodegeneration, with at late stages a decrease in brain weight up to 25% (Vonsattel and DiFiglia, 1998). The main affected structures are the striatum (caudate-putamen), the cortex and the white matter (***Figure 1***). Morphometric analysis of coronal brain slices showed important loss in the putamen (64% reduction), the caudate (57%), the white

matter (29-34%), the cortex (21-29%) and the thalamus (28%), associated to larger ventricles (de la Monte et al., 1988).

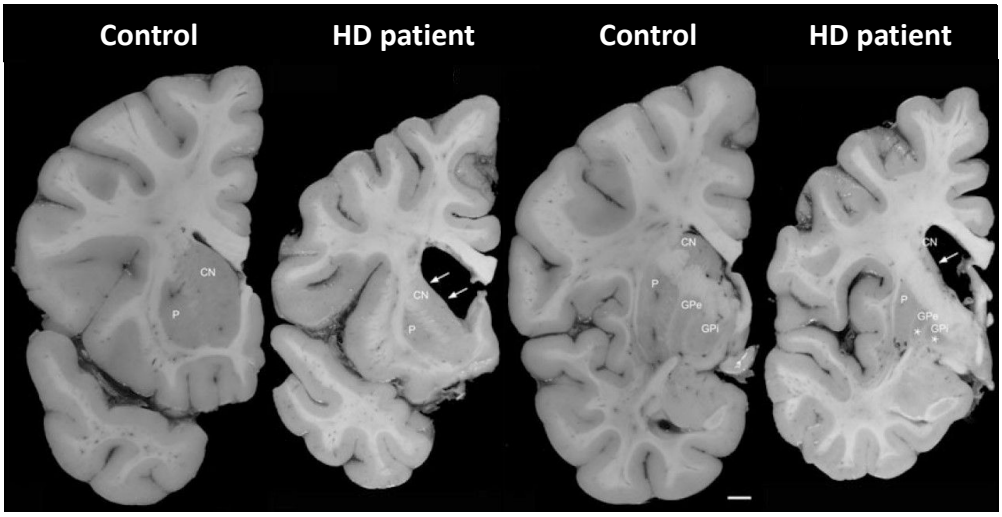

Figure 1. Neuropathology of HD. Brain coronal section at 2 levels of a representative control and a 35-year-old male. We can observe a severe atrophy of the caudate (arrows), the globus pallidus (asterisks) and the cortex. CN: Caudate Nucleus, P: Putamen, GPe: external Globus Pallidus, GPi: internal Globus Pallidus. Scale bar: 1cm (Waldvogel et al., 2015)

Progression of the neurodegenerescence

The neurodegenerescence starts before the first symptoms and worsen with the disease progression. A grading system was established based on the striatal atrophy, from 0 to 4 with increased severity (Vonsattel et al., 1985): grade 0 with no macroscopic changes but 30 to 40% of striatal neurons are already lost, grade 1 with a slight striatal atrophy and 50% neuronal loss. Striatal atrophy becomes severe at grade 3 and 4 with a loss of 95% of striatal neurons. Atrophy in other brain structures is clearly visible at grade 3 and 4. In the cortex, the atrophy is especially visible in in layers III, V and VI (Sotrel et al., 1991). At grade 4, 50% of the globus pallidus volume is decreased, with a more severe atrophy of the external globus pallidus (Lange et al., 1976). The thalamus and the subthalamic nucleus are also affected at grade 3 and 4.

Recent MRI studies showed that brain atrophy starts at pre-symptomatic stages, with reduced volume of the striatum before disease onset. White matter atrophy is also detectable very early (***Figure 2***). Indeed, measure of corpus callosum volume, the largest and one of the most important white matter structure, showed a significant decrease in pre-symptomatic gene-carriers, years before disease onset (Crawford et al., 2013).

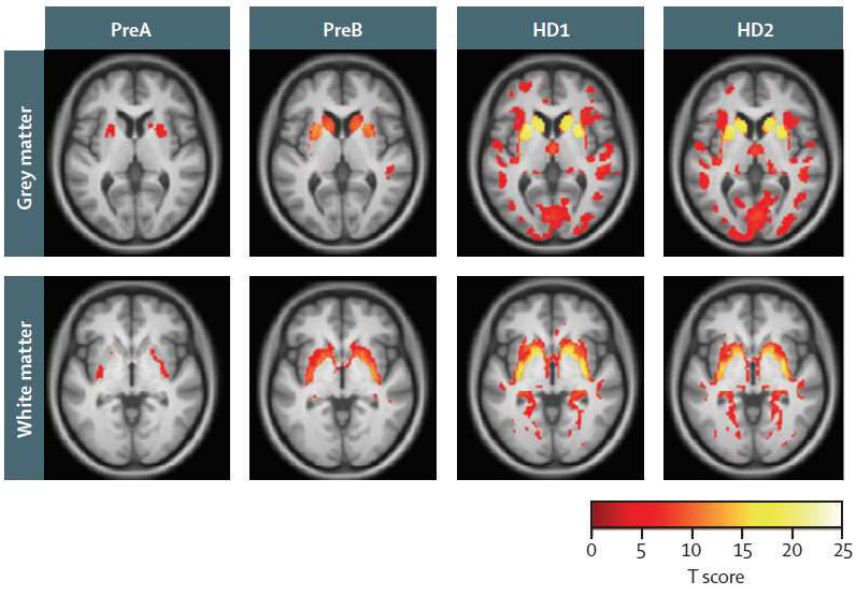

Figure 2. MRI evaluation of brain atrophy in HD. Voxel based morphometry of pre-symptomatic gene-carriers (PreA: more than 10 years from onset, PreB: less than 10 years from onset) and symptomatic HD patients at 2 stages (HD1, HD2). Atrophy is indicated with a color code from red (substantial atrophy) to yellow (severe atrophy). (Ross et al., 2014)

Differential vulnerability of cell population

This specific pattern of neurodegeneration is associated to a differential vulnerability of some neuronal population. As described previously, the striatum is one of the main affected areas, it is mostly composed of projections neurons called striatal projection neurons (SPN), which are medium spiny GABAergic inhibitory neurons, representing up to 95% of the neurons of the striatum. Based on their projection target, SPNs can be classified in two main groups:

- SPN from the direct pathway projecting to the GPi (internal Globus Pallidus) and SNr (Substantia Nigra pars reticulata) expressing dopaminergic receptors of D1 subtype (D1R) and substance P as co-neurotransmitter.
- SPN from the indirect pathway projecting to the GPe (external Globus Pallidus) expressing dopaminergic receptors of D2 subtype (D2R) and encephalin as co-neurotransmitter.

SPN from the indirect pathway are the most vulnerable in HD and are the first affected by the degeneration, followed later on by the SPN from the direct pathway (***Figure 3***) (Augood et al., 1996; Reiner et al., 1988; Richfield et al., 1995). In the cortex, the most vulnerable cells are large pyramidal projection neurons from layer V, VI and to a lesser extent layer III (Cudkowicz and Kowall, 1990; Hedreen et al., 1991). These pyramidal neurons from layer V and VI are the glutamatergic neurons projecting to the striatum. Interneurons of the striatum and the cortex are less impacted in HD (Cicchetti and Parent, 1996) (***Figure 3***).

Anatomical location	Cell type	Relative vulnerability	NT receptor	NT	Peptides
Striatum	SPN (direct pathway)	+++	D1, NMDA, AMPA	GABA	Substance P / Dynorphin
	SPN (indirect pathway)	+++++	D2, NMDA, AMPA	GABA	Enkephalin
	Interneurons	+	D2, NMDA, AMPA	ACh	Neuropetide Y, Parvalbumin
Cerebral cortex	Pyramidal neurons (layer V/VI)	+++	Glu, ACh, DA, NE, 5HT	Glu	-
	Interneurons	+	Glu, GABA	GABA	Somatostatin, Neuropeptide Y

Figure 3. Differential vulnerability of cell population in HD. Neurons in the striatum and the cortex display different degrees of vulnerability in HD, the most vulnerable being the SPN (Striatal Projection Neurons) expressing D2 receptors and enkephalin, and the pyramidal neurons of layer V/VI. Degree of vulnerability: from least (+) to most (+++++) vulnerable. NT: neurotransmitter (Adapted from Han *et al*, 2010)

The basal ganglia are sub-cortical nuclei involved in the control of mood, movement, as well as motor learning, executive functions, behaviors and emotions. It includes the striatum (composed of the caudate and putamen in primates), the globus pallidus (GPe and GPi: external and internal segment), the subthalamic nucleus (STN) and the substantia nigra (SN) (Carpenter et al., 1976). The striatum represents the main input structure of the basal ganglia, as it integrates contextual information from the whole cerebral cortex, thalamus and amygdala (glutamatergic afferents), along with dopaminergic inputs released in response to unexpected rewards and other salient stimuli.

In the indirect pathway, the excitatory pyramidal neurons of the cortex project onto the inhibitory SPN of the striatum. These SPN will send projections to the inhibitory neurons of the GPe, lifting the inhibition of the excitatory neurons of the STN, resulting in the excitation of inhibitory neurons of the GPi which will inhibit the thalamus. In the direct pathway, the cortical excitatory neurons project onto the SPN, which will inhibit the inhibitory neurons of the GPi and thus lifting the disinhibition of the thalamus output onto the cerebral cortex (Smith et al., 1998). In the direct pathway, SPN also project to the GABAergic neurons in the SNr (***Figure 4***).

Thus, the result of cortical activation in the direct pathway is opposite to that of the indirect circuit:

- Indirect pathway: inhibition of cortical activity which inhibits movements.
- Direct pathway: reinforcement of cortical activity which facilitate initiation of movements.

In this system, the dopaminergic neurons from the SNc (pars compacta) send projections to the striatum (***Figure 4***) and the dopamine release modulates SPN activity, allowing an increased activation of SPN expressing D1 receptor from the direct pathway and the inhibition of SPN expressing D2 receptor from the indirect pathway.

At grade 0, the initial symptoms of hyperkinesia and chorea are caused by the damage in the indirect pathway (***Figure 4***), reducing the inhibition of the GPe which increases inhibition on the STN. The STN becomes hypo-functional, reducing disinhibition of the thalamus and leading to the over-activation of the motor cortex which results in chorea (hyperactivity). At grade 1, SPN from the direct pathway projecting to the SNr are degenerating (Glass et al., 2000). At grade 3, in the later stages of the disease, the loss of SPN from the direct pathway projecting to the GPi causes increased inhibition of the thalamus which decreases the activation of the motor cortex leading to rigidity (hypoactivity).

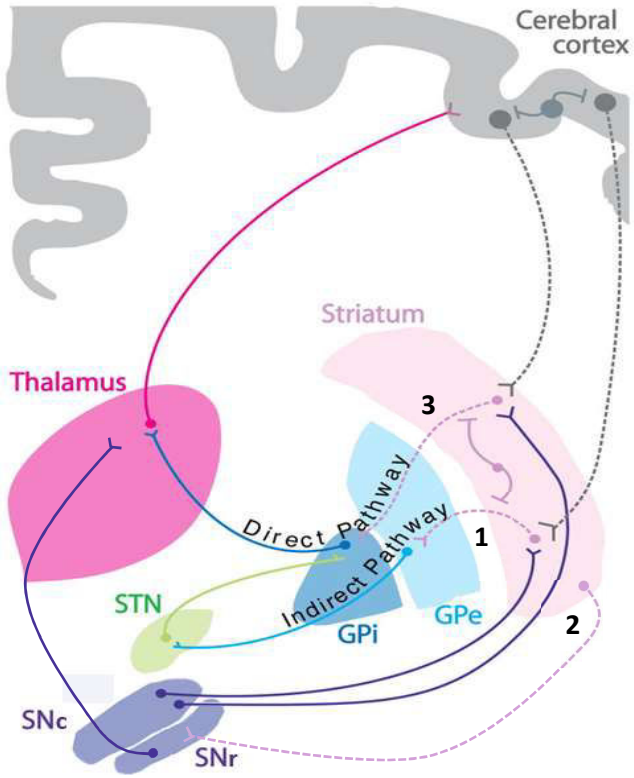

Figure 4. Representation of the cortico-basal ganglia pathways and the affected pathways in HD. Within the striatum, the inhibitory SPN will either connect with the GPi through the direct pathway, or with the GPe through the indirect pathway which will then connect to the STN and finally to the GPi. The dopaminergic neurons from the SNc send projections to the striatum to modulate SPN activation. The most vulnerable neurons in HD, the SPN and the pyramidal neurons are represented by dashed lines. **1**. Degeneration of SPN from the indirect pathway projecting to the GPe at early stages. **2**. Degeneration of SPN projecting onto the SNr. **3**. Degeneration of SPN from the direct pathway projecting to the GPi. STN: Subthalamic nucleus, GPe: external Globus Pallidus, GPi: internal Globus Pallidus, SN: Substantia Nigra. (Modified from Han *et al*, 2010)

Huntingtin's gene

Discovery of the gene

George Huntington was the first physician to give a comprehensive and thorough description of HD in 1872. His father and grandfather were also physician and by gathering observations from these 3 generations he was able to describe a hereditary transmission of the disease. Mendel's work in the 1900s allowed the association of George Huntington's description to a Mendelian dominant pattern of transmission of HD. In the 1980s, the first HD gene-mapping project was launched and HD was the first genetic disease to be mapped to a chromosome in 1983, without prior knowledge of its chromosomal location (Gusella et al., 1983). Once the technology was available, the gene was cloned by the Huntington's Disease collaborative research group in 1993 and the mutation responsible for the disease was identified (MacDonald et al., 1993).

Description of Huntingtin's gene

Huntingtin's gene (*Htt*) is located on the short arm of chromosome 4 at position 16.3 (4p16.3) (Gusella et al., 1983) (***Figure 5***). Using cloned trapped exons, the Huntington's disease collaborative research group was able to isolate the IT15 (Interesting Transcript 15) reading frame encoding for HD gene. The human *Htt* gene is a large locus of 180 kB containing 67 exons. The first exon contains a $(CAG)_n$ repeat and the abnormal expansion of this repeat is responsible for the disease. This repeat is located 17 codons after the ATG initiation site (***Figure 5***). In the normal population, the CAG repeat is on average 17 and in the HD population the CAG repeat is superior to 40 copies (MacDonald et al., 1993). A subset of single nucleotide polymorphism (SNP) was identified in *Htt* gene with three common HD haplotypes (A1, A2, A3) highly associated to the disease (Lee et al., 2012a; Warby et al., 2011). Characterization of *Htt* gene promotor allowed the identification of GC rich regions and binding sites for regulatory element such as SP1, AP2, p53, but this promotor lacks TATA and CAAT boxes (Feng et al., 2006; Holzmann et al., 2001).

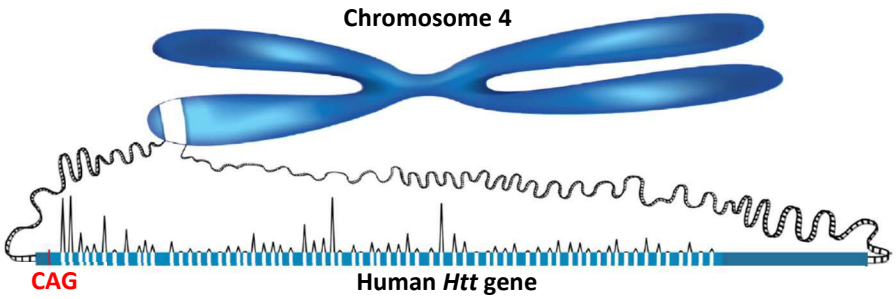

Figure 5. Localization of Huntingtin gene. *Htt* gene is located on the small arm of chromosome 4. (Modified from Déglon, 2017)

Expression of Huntingtin's gene

There is a differential polyadenylation of *Htt* gene, giving two forms, a larger 13.7 kb transcript which is the predominant form in the human brain and a 10.3 kb transcript widely expressed (Lin et al., 1993). Huntingtin mRNA is ubiquitously expressed with variability depending on the structures. *Htt* mRNA is expressed in all brain regions, with high levels in the cerebellum, the hippocampus, the cerebral cortex, the substantia nigra pars compacta and pontine nuclei, in the striatum the levels are intermediate and they are low in the globus pallidus. mRNA expression is higher in neurons but still significant in glial cells (Landwehrmeyer et al., 1995). A recent study showed that, in neuronal cells, 50% of wild type *Htt* mRNA is located in the nucleus, where it is more stable than in the cytoplasm (Didiot et al., 2018). No difference was observed between wild type and mutant *Htt* (*mHtt*) mRNA localization in post mortem tissue (Gourfinkel-An et al., 1997). However, *mHtt* mRNA levels are higher in the cortex and striatum of patients at early stages (Liu et al., 2013).

CAG instability and disease onset

In the normal population, the polymorphic range of CAG repeat is between 6 and 35 repeats. Between 36 and 39 repeats, the penetrance is incomplete, meaning that the risk of developing HD is increased but some individuals will never develop HD symptoms. With more than 40 CAG repeats HD penetrance is total (Rubinsztein et al., 1996). The number of CAG repeat is unstable and can change size during transmission from one generation to the next, especially for intermediate CAG repeat (27-35), with more instability with increased CAG length. Typically, the increase or decrease involve one or a few CAG, larger modification are rare but often associated to paternal transmission, suggesting a higher instability during spermatogenesis (Duyao et al., 1993). Although rare, de novo mutation were described in HD and epidemiologic analysis of the disease showed ≥10% new mutation rate in each generation (Falush et al., 2001). There is an inverse relationship between the size of the CAG repeat and disease onset (***Figure 6***). The allele with the longer CAG repeat will determine disease onset, in a dominant manner, regardless of the length of the second allele (normal or not) (Lee et al., 2012b). Juvenile HD is associated to alleles with more than 70 CAG repeats, however alleles with more than 80 repeats are extremely rare (Telenius et al., 1993). Interestingly, the size of the CAG repeat is not the only factor associated with age of onset, it is estimated to contribute to 50-77% of the variance in HD (Andrew et al., 1993). Indeed, several genetic modifiers have been identified in HD that could influence disease onset (***Figure 6***). Genome wide association analysis showed a locus at chromosome 15 that could accelerate or delay onset by 6.1 years and 1.4 years respectively and a locus at chromosome 8 that could increase onset by 1.6 years. These loci are strongly associated to pathways involved in DNA repair and also to mitochondria, oxidative stress and proteostasis (Genetic Modifiers of Huntington's Disease (GeM-HD) Consortium, 2015). Another association was detected in chromosome 3, near the *MLH1* gene, involved in DNA mismatch repair (Lee et al., 2017).

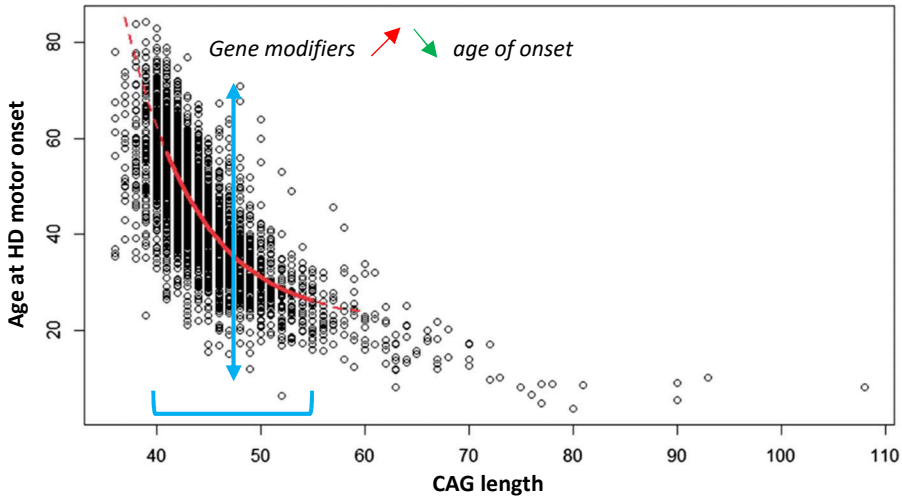

Figure 6. Huntingtin CAG length against age of motor onset in HD. Increased CAG length is associated to early age of onset. In blue: influence of gene modifiers on age of onset (Modified from Holmans *et al*, 2017)

Modeling Huntington's disease

Before the discovery of HD gene, the first models relied on striatal lesions using toxins, based on the knowledge that it is the most affected structure (Beal et al., 1986; Brouillet et al., 1993). The identification of the mutation responsible for HD allowed the establishment of many models to decipher HD molecular and cellular mechanisms and to evaluate the potential of therapeutic strategies. Since then, many strategies and species have been used to model HD and address different questions (***Figure 7***). The size of the genomic sequence and the variable phenotype depending on the CAG repeat gave rise to several questions to establish the appropriate genetic strategy: use of the full-length or the mutated fragment of *Htt*, the size of the CAG repeat, use of the endogenous mouse promoter or the human *Htt* promoter…

The most commonly used animals to model HD are rodent models. The N-terminal transgenic model usually exhibits rapid phenotype onset (Mangiarini et al., 1996; Schilling et al., 1999), whereas full length knock-in models are closer to the human genetic context and have a more progressive phenotype (Lin et al., 2001; Menalled et al., 2003; Wheeler et al., 2002) (***Figure 7***). Other full length model were created using YAC (Yeast Artificial Chromosome) and BAC (Bacterial Artificial Chromosome) technology, also giving a progressive phenotype (Hodgson et al., 1999; Yu-Taeger et al., 2012) (***Figure 7***). Another technic to generate HD models is based on the transfer of viral vectors expressing the mutated *Htt* (Déglon and Hantraye, 2005). Lentiviruses coding for the 171 first amino acids of Htt with 82 CAGs (N171-82Q) were largely used, this model develops a neuropathological phenotype but no behavioral changes (Damiano et al., 2013; Galvan et al., 2012). Adeno-associated viruses (AAV) coding for the mutated *Htt* were also developed, with AAVs coding for *Htt* fragments with 97 or 100 CAGs (DiFiglia et al., 2007; Senut et al., 2000) and more recently the N171-82Q *Htt* fragment, which is associated to motor dysfunctions (Jang et al., 2018).

A few large animal models were created to be closer to the human physiology and anatomy. A rhesus macaque model was established using fragments of human *Htt*, they reproduced HD phenotype, however this model was very severe and the animals died quickly (Yang et al., 2008). A sheep model was established using the full length *Htt*, neuropathological hallmarks and metabolic disruptions were reported, however, no motor symptoms were observed up to 3 years (Jacobsen et al., 2010; Skene et al., 2017). A new knock-In mini-pig model was established using CRISPR/Cas9 and characterization of this model showed promising recapitulation of HD symptoms (Yan et al., 2018).

Non-mammalian models such as C. Elegans and Drosophila melanogaster have also been established and can be useful for high throughput genetic and pharmacological screening (Parker et al., 2001; Romero et al., 2008) (***Figure 7***).

Cellular models are also useful tools to dissect cellular mechanisms (***Figure 7***). For instance, a striatal cell line was established from HdhQ111 knock-in embryos, with a strong dominant phenotype caused by the mutant HTT protein (mHTT) and a high sensitivity to stress (Trettel et al., 2000). The recent use of induced pluripotent stem cells (iPSC) opened the new possibility to model HD using cells derived directly from patients, giving new resources to gain further mechanistic insight and explore novel drug targets for HD (HD iPSC Consortium, 2012).

Model	Transgene	Promoter	(CAG)n	Motor phenotype
Non-mammalian models				
C. Elegans	N-terminal human *Htt* cDNA	Osm-10 (sensory neurons)	95,150	5 days
Drosophila melanogaster	N-terminal human *Htt* cDNA Full-length human *Htt* cDNA	Gmr (Glass multimer reporter)	128	10 days 20 days
N-terminal transgenic and fragment models				
R6/1 mice	67 amino acids of N-terminal fragment (human *Htt*)	Human *Htt* promoter	116	4.5 months
R6/2 mice	67 amino acids of N-terminal fragment (human *Htt*)	Human *Htt* promoter	144	6 weeks
N171-82Q mice	171 amino acids of N-terminal fragment (human *Htt* cDNA)	Murine prion promoter	82	3 months
Rhesus Monkey	Human *Htt* exon 1	Human polyubiquitin-C	84	1 week
Transgenic full-length models				
YAC128 mice	Full-length human *Htt*	Human *Htt* promoter and regulatory elements	128	6 months
BACHD rats	Full-length human *Htt*	Human *Htt* promoter and regulatory elements	97	2 months
Sheep OVT73	Full-length human *Htt*	Human *Htt* promoter	73	-
Knock-In models				
CAG140 mice	Full-length chimeric human *Htt* exon 1:mouse *Htt*	Endogenous mouse *Htt* promoter	140	4 months
zQ175 mice	Full-length chimeric human *Htt* exon 1:mouse *Htt*	Endogenous mouse *Htt* promoter	188	2 months
HdhQ111 mice	Full-length chimeric human *Htt* exon 1:mouse *Htt*	Endogenous mouse *Htt* promoter	111	24 months
HdhQ150 mice	Full-length chimeric human *Htt* exon 1:mouse *Htt*	Endogenous mouse *Htt* promoter	150	10 months
Mini-pig	Full-length chimeric human *Htt* exon 1:pig *Htt*	Endogenous pig *Htt* promoter	150	5 months
Cellular models				
STHdhQ111/Q111	Full-length chimeric human *Htt* exon 1:mouse *Htt*	Endogenous mouse *Htt* promoter	111	-
iPSC	Full-length human *Htt*	Endogenous human *Htt* promoter	60, 109, 180	-

Figure 7. Overview of HD models. (Crook and Housman, 2011; Pouladi et al., 2013)

The zQ175 knock-in mouse model

Knock-In models are the most appropriate models to mimic the genetic context of HD. Among these models, the zQ175 mice derived from a spontaneous expansion of the CAG repeat in the CAG140 knock-in mice (Menalled et al., 2012). They develop impairment of motor behavior (Menalled et al., 2012; Smith et al., 2014), cognitive deficit (Heikkinen et al., 2012), apathy (Oakeshott et al., 2012) and sleep disorder (Loh et al., 2013). They display striatal and cortical atrophy (Heikkinen et al., 2012; Peng et al., 2016), along with neuropathological landmarks of HD such as the formation of aggregate (Carty et al., 2015) and decreased myelination (Ma et al., 2015). In other knock-in models, working on homozygous mice has been necessary to observe clear phenotypic changes, whereas with the zQ175 mice, heterozygous mice display characteristic HD phenotype. Since in humans most of patients are heterozygous for HD, heterozygous zQ175 mice are mouse models with robust behavioral, electrophysiological and histopathological features that may be valuable in furthering our understanding of HD pathophysiology. Therefore, it is an interesting model to evaluate potential therapeutic strategies. Recently, the zQ175 mice were crossed with the FVB/N strain, which is highly susceptible to neurodegeneration, giving the Q175F line. The zQ175 Knock-In allele retains a floxed neomycin resistance cassette upstream of *Htt* gene, decreasing the expression of mutant *Htt*. This neo cassette was removed from the Q175F mice, generating the Q175FDN line, with an increased expression of m*Htt* and an enhanced phenotype severity (Southwell et al., 2016).

Structure and function of huntingtin

Structure of Huntingtin protein

Huntingtin (HTT) is a highly conserved protein of 348 kD containing 3144 amino acids. The CAG repeat of *Htt* gene translates into a poly glutamine stretch (polyQ) at the N-terminus of the protein, which is preceded by 17 amino acids and followed by a proline rich domain (PRD). This PRD domain can interact with proteins containing tryptophans and Src homology 3 domains (Harjes and Wanker, 2003). The polyQ tract, which forms a polar zipper, can also interact with other proteins (Perutz et al., 1994). HTT has several HEAT domains (acronym for the four proteins where these structures are found: **H**untingtin, Elongation factor 3: **E**F3, protein phosphatase 2A: PP2**A**, lipid kinase **T**OR) which are tandem repeats composed of two alpha helices linked by a short loop. HEAT domains are involved in the formation of inter and intra-molecular interactions (Palidwor et al., 2009) (***Figure 8***). With partner proteins HEAT can act as scaffold structures and within HTT it allows the formation of different three-dimensional conformation for HTT (Seong et al., 2010). HTT is subjected to several post-translation modifications: phosphorylation, acetylation, palmitoylation, ubiquitylation and sumoylation (***Figure 8***), which regulate its functions, localization and stabilization. HTT has PEST proteolytic sites (for cleavage

at proline, glutamic acid, serine, threonine amino acids), targeted by proteins such as caspases, calpain, cathepsins and the metalloproteinase MMP10 (Gafni and Ellerby, 2002; Kim et al., 2001) (***Figure 8***). Both wild-type and mHTT have functional cleaving sites, but proteolysis activity is increased in mHTT, with generation of various mHTT fragments (Weiss et al., 2012), accumulation of N-terminal fragment containing the polyQ stretch (Lunkes et al., 2002) and production of non-polyQ fragments (El-Daher et al., 2015), both involved in cell toxicity.

Integrated studies crossing experimental methodologies, such as affinity purification, combined to network based investigation of potential interactors, allowed the identification of 395 partners for HTT (Schaefer et al., 2012) (HIPPIE data base). The mutation of HTT can change its interactions, indeed, in striatal cells 349 interactors have been identified, 200 being more abundant in complexes containing mHTT and 149 more abundant in complexes containing wild type HTT (Ratovitski et al., 2012). Through these numerous interactions, HTT has important functions in several cellular pathways. The structure of HTT was recently determined using cryo-electron microscopy, by isolating the HTT-HAP40 complex to access a stable form of HTT; allowing a high resolution description of HTT and its HEAT domains (Guo et al., 2018). This more precise structure of HTT will be of great interest to further examine HTT interactors and to improve our knowledge on its functions and regulations.

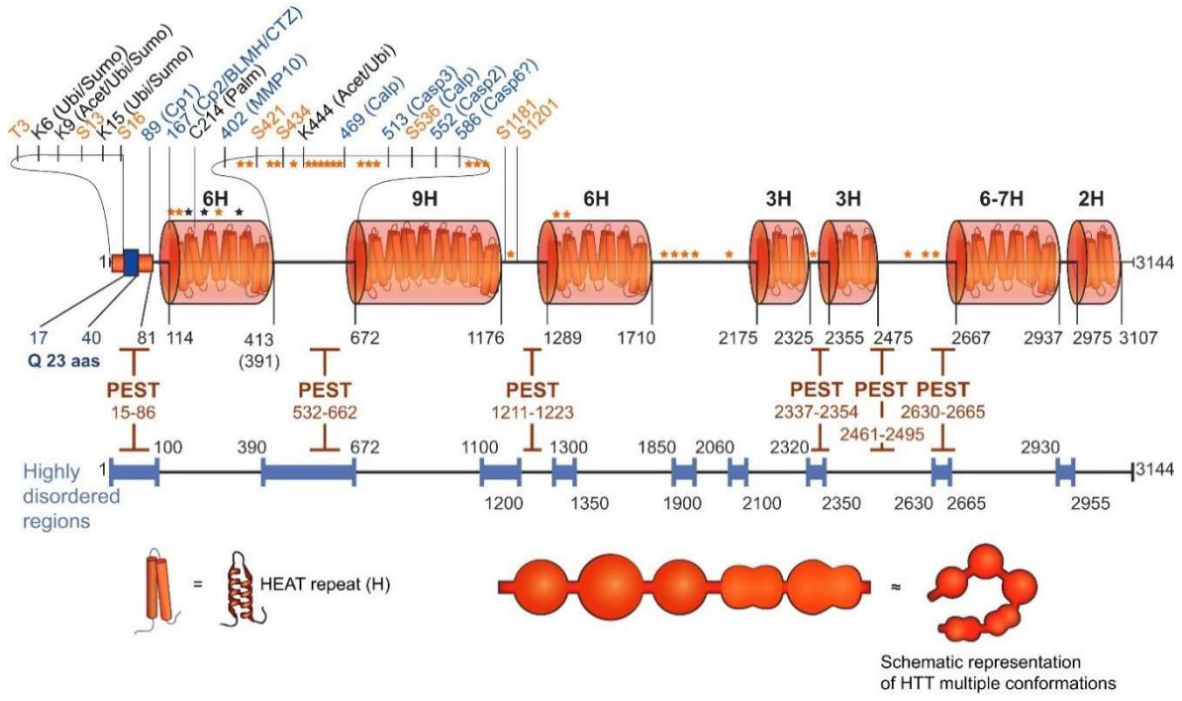

Figure 8. Scheme of the human huntingtin protein sequence. Orange amino acid (aa): phosphorylation sites. Black aa: sites of indicated modifications. Blue aa: cleavage sites. Orange and black stars: potential phosphorylation and acetylation sites. Numbers bellow the 2D structure: limits of the indicated domains (HEAT, PEST, Highly disordered regions). H: number of predicted HEAT repeats organized in larger domains. PEST: proteolysis-sensitive domains. Bottom: Schematic HTT with spheres corresponding to stretches of HEAT repeats. Ubi: ubiquitin; Sumo: sumoylation; Acet: acetylation; Palm: palmitoylation; MMP10: metalloproteinase 10; Calp: calpain; Casp: caspase. (Saudou and Humbert, 2016)

Huntingtin expression and localization

HTT is a stable protein with a half-life of about 24h (Persichetti et al., 1996). It is an ubiquitous protein found in all cell types, with high levels in neurons (Sharp et al., 1995). HTT is mainly cytoplasmic but can also go to the nucleus. Indeed, the first 17 amino acids sequence has a nuclear export signal (NES) and is subjected to post-transcriptional modifications that can affect HTT clearance and localization (Atwal et al., 2007; Thompson et al., 2009). HTT co-localize with several cellular compartments such as the endoplasmic reticulum, the mitochondria, the Golgi apparatus, the cytoskeleton and vesicles (DiFiglia et al., 1995; Gutekunst et al., 1995; Sharp et al., 1995). HTT is enriched in cortical neurons from layers V, which project to the striatum. Interestingly, HTT is less abundant in the striatum, and in this region, the cells expressing the highest levels are the cholinergic interneurons (less affected in HD), SPN expressing intermediated levels (Fusco et al., 1999).

Huntingtin and development

After the gene discovery, invalidation of *Htt* gene was undertaken to understand HTT function. However, homozygous invalidation was lethal in mice, with abnormal gastrulation at E7.5 (Duyao et al., 1995) and heterozygous mice had increased motor activity and cognitive deficits (Nasir et al., 1995). These studies highlighted the role of HTT during development, especially in the nervous system. Indeed, decreased expression of HTT severely affects brain formation, with the most evident malformation in the fore and mid-brain and abnormal organization of the striatal subventricular zone (White et al., 1997). More specifically, silencing of HTT in cortical progenitors favors neuronal differentiation instead of maintaining their proliferative status by disturbing mitotic spindle orientation (Godin et al., 2010). Knock down of *Htt* in neuroepithelial cells of the neocortex was associated to a defect in migration, reduced proliferation and increased cell death (Tong et al., 2011). A recent study showed that HTT is essential for the establishment of the proper morphology and positioning of cortical neurons during the development of the neocortex. This regulation of newborn neurons polarization by HTT is mediated by RAB11 recycling of N-cadherin (Barnat et al., 2017).

Huntingtin and mitosis

HTT is involved in the coordination of cell division, by being targeted to spindle poles through its interaction with dynein. HTT mediates the localization and accumulation to the cell cortex of NUMA and LGN, proteins that are necessary to generate the pulling forces on astral microtubules in order to properly position the spindle (Elias et al., 2014). Moreover, the specific loss of HTT function has been shown to lead to spindle mis-orientation, highlighting HTT role in mitosis (Godin et al., 2010).

Huntingtin and transcription

HTT interacts with major transcription factors such as CBP, Sp1, p53 and might act as a scaffold for the transcriptional machinery. Importantly, HTT sequestrates the REST/NRSF complex in the cytoplasm, allowing *bdnf* transcription (***Figure 9***). HTT binds to nuclear receptors LXR (Liver X Receptor), acting as a co-activator, and others such as PPARγ (Proliferator Activated Receptor γ) and VDR (vitamin D receptor) (***Figure 9***). HTT can interact with proteins involved in epigenetic modification like PRC2. Through these interactions, HTT can facilitate transcription activation or the repression, having large potential consequences on cellular functions. HTT itself can also bind DNA acting as a co-factor, indeed exon 1 can directly bind DNA and alter its conformation, however, polyQ expansion increases this interaction, altering the binding of transcription factors (Benn et al., 2008).

Name	*Action of HTT*	*Target - Role*	*Reference*
Transcription factors			
cAMP-response element (CREB)-Binding Protein (CBP)	Interaction	Transcription activator	(Steffan et al., 2000a)
NeuroD	Facilitates activation	Neuronal development and survival	(Marcora et al., 2003)
SP1 (Specificity Protein 1)	Scaffold	Cell differentiation, apoptosis, chromatin remodeling	(Dunah et al., 2002)
NF-κB (Nuclear Factor κB)	Scaffold	Stress response	(Takano and Gusella, 2002)
p53 (tumor suppressor protein 53)	Scaffold	Cell cycle, apoptosis, DNA repair	(Steffan et al., 2000a)
Transcriptional activators or repressors			
Co-activator TAFII130	Scaffold	Transcription co-activator	(Dunah et al., 2002)
REST/NRSF (repressor-element 1 transcription factor/neuron restrictive silencer factor)	Sequestration of REST/NRSF Promotes *bdnf* transcription	REST: NRST silencer NRSF: Neuronal development and maintenance	(Zuccato et al., 2003)
CtBP (Corepressor C-terminal-Binding Protein)	Scaffold	Transcription co-repressor	(Kegel et al., 2002)
Nuclear receptors			
LXRα (Liver X receptor α)	Co-activator	Lipid homeostasis Inflammation	(Futter et al., 2009)
Chromatin remodeling			
PRC2 (Polycomb Repressive Complex 2)	Facilitates histone catalytic activity	Tri-methylation at H3K27	(Seong et al., 2010)

Figure 9. HTT interacts with proteins involved in the transcription.

Huntingtin and vesicular transport

HTT interacts with molecular transporter, directly with dynein or through the Huntingtin associated protein 1 (HAP1) (***Figure 10***) (Colin et al., 2008; Engelender et al., 1997; McGuire et al., 2006). It is involved in the anterograde and retrograde transport of organelles like autophagosomes (Wong and Holzbaur, 2014), endosomes and lysosomes (Caviston et al., 2010). In neurons, HTT is important for

the transport of vesicles in axons and dendrites, for instance for the transport of vesicles containing synaptic precursor, vesicles containing GABA receptor (Twelvetrees et al., 2010), the transport of BDNF vesicles (Brain Derived Neurotrophic Factor) from cortical neurons to striatal neurons (Gauthier et al., 2004) and the transport of BDNF receptor, TrkB, in dendrites of striatal neurons (Liot et al., 2013). HTT involvement in vesicular transport has been supported by experiments showing that HTT silencing decreases vesicles transport whereas its overexpression favors transport (Zala et al., 2013a). Some evidence suggests that HTT participate to the transport of mitochondria, but the role of wild type HTT is less clear since it has been mostly studied in the context of mHTT. Vesicles velocity might also be increased by HTT thanks to its ability to bind GAPDH (glyceraldehyde 3-phosphate dehydrogenase), providing a local source of energy for vesicles (Zala et al., 2013b).

Huntingtin and endocytosis

Among its partners, HTT interacts with complexes associated to endocytosis. Through its interaction with HIP1 (huntingtin interacting protein 1) and HIP1R (HIP1 receptor), HTT is involved in the assembly of clathrin at the membrane for membrane invagination (Waelter et al., 2001). Dynamin 1, which is involved in clathrin-mediated endocytosis, is inactivated after artificial proteolysis of HTT, suggesting a role of HTT in dynamin 1 activation (El-Daher et al., 2015). HTT also participates to the recycling of vesicles by interacting and activating GTPase Rab11 (Li et al., 2008). To regulate endocytosis and vesicle recycling, HTT may also be involved in a larger complex containing endophilin A3, endophilin B1, amphiphysin and dynamin (Modregger et al., 2003). HTT interacts with HAP40, which can bind Rab5 to regulate endosomal trafficking. Doing so, HTT allows the switch of cargo from microtubules to actin filaments by interacting with actin and decreasing endosome motility (Pal et al., 2006). This transition could also be mediated by HTT interaction with complexes such as Rab8-optineurin-myosin VI and HAP1-dynactin (Hattula and Peränen, 2000; Sahlender et al., 2005).

Huntingtin and autophagy

HTT has an important role in the regulation of autophagy, which is an essential pathway for the elimination of unfolded or aggregated proteins and defective organelles. HTT can act as a scaffold protein for the specific macroautophagy by interacting with p62 (autophagy cargo receptor) which facilitate its association with LC3 (involved in autophagosome membrane formation and fusion) and ubiquitinated cargo (Ub-K63). By doing so, HTT facilitates cargo loading into autophagosomes. Moreover, HTT promotes autophagy induction by binding to ULK1 (a kinase initiating autophagy), releasing it from the negative regulation by mTOR (Rui et al., 2015). The structural similarities between HTT and yeast autophagy proteins give further support that HTT is a key component as a scaffold protein for autophagy (Ochaba et al., 2014). In neurons, autophagosomes formed at the periphery

need to be transported to the soma, to do so, HTT and its partner HAP1 promotes the retrograde axonal transport of these autophagosomes by regulating dynein and kinesin motor complex (Wong and Holzbaur, 2014). Interestingly, deletion of the polyQ stretch in mice increased autophagy and was associated to an extended lifespan (Zheng et al., 2010). Therefore, HTT role in autophagy may rely on the polyQ stretch, thus modification of its length could impact this function.

Huntingtin and cell survival

Because of the neuronal loss observed in HD, it seems that the mutation of HTT is associated to pro-apoptotic pathways and potentially that wild type HTT might be involved in cell survival. Indeed, wild type HTT was shown in several studies to be associated to pro-survival pathways, for instance overexpression of HTT protects against excitotoxic cell death (Leavitt et al., 2006). HTT can also directly act on the pro-apoptotic pathway by preventing caspase 3 activity and inhibiting pro-caspase 9 processing (Rigamonti et al., 2001; Zhang et al., 2006). The striatum does not produce BDNF (brain derived neurotrophic factor) and relies mostly on cortical delivery of this trophic factor for neuronal survival (Baquet et al., 2004). As seen previously, HTT promotes BDNF transcription (Zuccato et al., 2003). HTT is also involved in the axonal transport of BDNF vesicles along cortical axons (Gauthier et al., 2004) and upon release, BDNF will activate TrkB receptors, which are then endocytosed and transported to striatal cell soma where they can activate pro-survival pathways. This transport of TrkB is mediated by HTT interaction with dynein IC-1B (Liot et al., 2013). By acting at different levels of BDNF transport, HTT participates to the survival of striatal neurons (***Figure 10***).

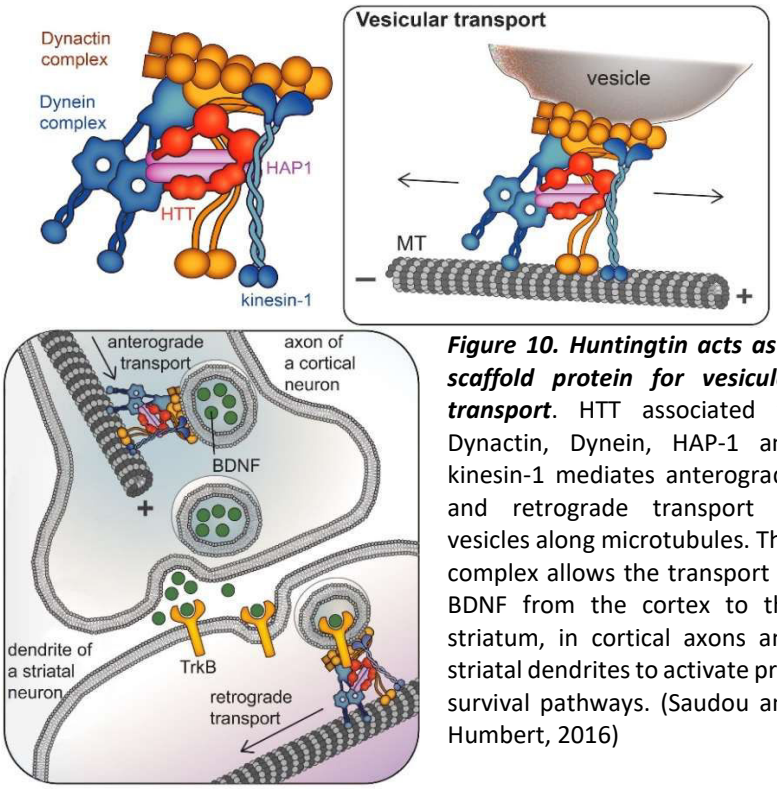

Figure 10. Huntingtin acts as a scaffold protein for vesicular transport. HTT associated to Dynactin, Dynein, HAP-1 and kinesin-1 mediates anterograde and retrograde transport of vesicles along microtubules. This complex allows the transport of BDNF from the cortex to the striatum, in cortical axons and striatal dendrites to activate pro-survival pathways. (Saudou and Humbert, 2016)

Physiopathology of Huntington's disease

Because of the mutation, the normal function of HTT is altered (loss of its normal functions) and the cleavage of mHTT, leading to the accumulation of the N-terminal fragments, disrupts several cellular pathways (gain of toxic functions).

Accumulation of mHTT fragments

The presence of intracellular aggregates of mHTT is one of the prominent neuropathological hallmarks of HD, as an early event in the disease course (Davies et al., 1997; Weiss et al., 2008). Aggregates were observed in different neuronal compartment: cytoplasmic aggregates, intranuclear inclusion and aggregates in neuronal processes which are more abundant than in the nucleus and present before disease onset in human brains (DiFiglia et al., 1997; Gutekunst et al., 1999).

Formation of toxic species

The mHTT is cleaved at the accessible proteolytic sites by caspases, calpain and endoproteases (***Figure 8***), giving rise to a variety of N-terminal fragments. Particularly, cleavage by caspase 6 was linked to neuronal dysfunctions. Indeed, in mice expressing mHTT, resistance to cleavage by caspase 6 was protective from induced neurotoxicity, whereas resistance from caspase 3 cleavage did not protect from excitotoxicity (Graham et al., 2006).

Aberrant *Htt* splicing can generate short polyadenylated exon 1 mRNA, translating into the N-terminal fragments. Levels of this exon 1 mRNA are proportional to the CAG repeat length and was found in mouse models and in patients tissues (Neueder et al., 2017). This study showed that the production of N-terminal fragments can also be independent from proteolytic cleavage (***Figure 11***).

Recently, repeat-associated non ATG (RAN) translation was described in HD from both sense and antisense *Htt* strands. RAN translations generate abnormal protein products with either poly-alanine, poly-serine, poly-leucine or poly-cysteine (***Figure 11***). These proteins can accumulate and form aggregates in the brain of patients, displaying toxic properties in neurons (Bañez-Coronel et al., 2015).

Different form of toxic species

The N-terminal fragment is disordered as a monomeric fragment; it will favor a condensed state. PolyQ fragments display polymerization kinetics of nucleated growth, in which polyQ monomers rapidly join the growing aggregate. These aggregates are formed of aligned β-sheet fibrils, forming amyloid-like fibers that associate to form aggregate inclusions (Bates, 2003; Jayaraman et al., 2012).

Other intermediate structures have been described from N-terminal fragment association. For instance, smaller oligomeric structures could be formed by direct interaction via the polyQ tract (Legleiter et al., 2010).

Consequences on cellular dysfunctions

PolyQ aggregates can participate to cellular dysfunctions by sequestrating essential proteins: transcription factors like p53 and CBP (Nucifora et al., 2001; Steffan et al., 2000a), ubiquitin-proteasome system components, cytoskeleton proteins, proteins from the nuclear pore complex (Suhr et al., 2001), transport protein (Trushina et al., 2004) and normal HTT (Martindale et al., 1998).

However, the toxic properties of aggregates have been largely debated. Some studies in mouse models support that aggregates are not correlated to the neurodegeneration, showing that neuropathological changes can occur without the presence of aggregates (Slow et al., 2003) and that aggregates can be present without neuronal loss or dysfunction (Slow et al., 2005). Suppressing the formation of mHTT inclusions *in vitro* actually resulted in an increased cell death (Saudou et al., 1998). Cell death might rather be correlated to the amount of diffuse mHTT, aggregates formation would thus function as a coping response to the more toxic soluble mHTT (Arrasate et al., 2004).

Therefore, the most toxic species would be intermediate conformers rather than aggregates. *In vitro* studies suggest that the toxic conformers are composed of short β strands interspersed with β turns (Poirier et al., 2005). Further observations of the different forms adopted by the N-terminal fragment showed that the soluble oligomers of mHTT fragments are associated with direct toxicity, causing for instance endoplasmic reticulum stress (Leitman et al., 2013).

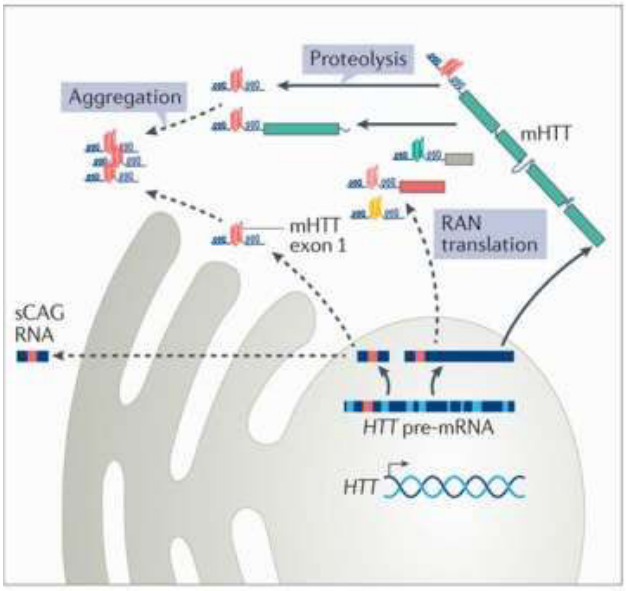

Figure 11. Toxic species of mHTT. Expression of mHTT can produce multiple toxic variants that may contribute to different extents to HD pathogenesis. These include, abnormal RAN translation protein products, the N-terminal HTT fragment generated from exon 1 which is formed by aberrant splicing and full-length mutant HTT (mHTT), that can be further processed to generate smaller fragments. These species can form oligomers or aggregate into large inclusion bodies. HTT mRNA can also give RNA hairpins formed by small CAG-repeated RNAs (sCAG RNAs). (Caron et al., 2018)

Transcriptional dysregulations and alteration of gene expression

Early transcription dysregulations were described in patients' striatum with altered gene expression for D1 and D2 receptors (Augood et al., 1997), reduced levels of enkephalin and substance P mRNA (Augood et al., 1996). Interestingly, gene deregulation was measurable in patients' blood, indicating a wide alteration of transcription in HD (Anderson et al., 2008). Study of mice models showed a nice recapitulation of the dysregulations seen in patients, without significant modification depending on mHTT length (Kuhn et al., 2007). However, co-expression network analysis from brain and peripheral tissue samples, from HD knock-in mice with increasing CAG repeat length, revealed 13 striatal and 5 cortical networks that highly correlated with CAG length and age (Langfelder et al., 2016). Overall, dysregulation of genes encoding for neurotransmitter receptors, cytoskeletal and structural proteins and cell signaling were described (Cha, 2007).

mHTT directly interfere with transcription factors and regulators

As described previously, HTT can interact with transcription factors and regulators (***Figure 9***). The mHTT will also interact with transcription factors, interfering with their normal functions. As aggregate or soluble form, mHTT will interact with proteins necessary for the basal machinery of transcription like TBP (TAT binding protein), TFIIF (transcription factor F), TAFII30 (tyrosine amino transferase II) (Shimohata et al., 2000; Suhr et al., 2001). PolyQ aggregates bind an sequester transcriptions factors and regulators such as CBP (Nucifora et al., 2001), p53 (Steffan et al., 2000b), SP1 (Li et al., 2002), NCoR (Boutell et al., 1999), which alter their normal function and is associated to cellular toxicity. mHTT interfere with the transcriptional regulation of BDNF by preventing the normal sequestration of REST into the cytoplasm and its release into the nucleus where it can repress BDNF transcription and expression (Strand et al., 2007; Zuccato et al., 2001). The sterol responsive element binding protein (SREBP), a transcription factor involved in cholesterol and lipid metabolism, has a decreased nuclear translocation in the presence of mHTT (Valenza et al., 2005).

Chromatin remodeling in HD

Chromatin remodeling allows the compaction or decompaction of DNA through epigenetic modifications, favoring or not the access of certain genes for transcription. It is critically controlled by post-translational modifications of histones, a group of highly basic proteins tightly linked to DNA. Acetylation of histone favors decompaction whereas histone methylation favors compaction. Administration of HDAC (histone deacetylase) inhibitors improved behavior and neuronal survival in several HD models (Ferrante et al., 2003; Steffan et al., 2001). Expression of the methyltransferase ESET is increased in patients and R6/2 mice. Pharmacological inhibition of ESET improved R6/2 phenotype and survival (Ryu et al., 2006). These studies showed a potential role of favoring DNA

decompaction, either by promoting acetylation or inhibiting methylation, thus highlighting the role of global transcription regulation in HD. Another post-translational modification involved in chromatin compaction is histone phosphorylation. The mitogen- and stress-activated kinase-1 (MSK-1), a kinase involved in H3 phosphorylation is deficient in the brain of patients and HD models (Roze et al., 2008). Restoration of MSK-1 *in vivo* in HD models prevented dysfunction and death of striatal neuron and up-regulated the expression of PGC1α, indicating a role of MSK-1 deficiency in transcriptional dysregulation in HD (Martin et al., 2011a)

Modification of gene expression in HD: non-coding RNAs

microRNAs are small non-coding RNAs that act as post-transcriptional regulators of gene expression by targeting 3' untranslated regions of mRNAs and repressing their translation or degrading them. Interestingly, evaluation of microRNA levels in the cerebrospinal fluid (CSF) of pre-symptomatic gene carriers revealed a specific increase of 6 microRNAs compared to control (Reed et al., 2018), revealing them as biomarkers of prodromal and diagnosed patients. In HD models, altered microRNA expression was described with differential levels throughout development, along with changed expression of proteins involved in microRNA function (Lee et al., 2011). The transcriptional repressor REST is involved in the regulation of a family of microRNA including the brain specific miR124a, allowing the persistence of non-neuronal transcripts (Conaco et al., 2006). Changes in the expression of these specific microRNAs could also result from mHTT-induced release of REST in the nucleus. There was evidence suggesting that mutant *Htt* RNA give rise to small CAG repeated RNAs (sCAG RNA) that contribute to neuronal toxicity (***Figure 11***). These sCAG RNA can then silence gene expression through the microRNAs machinery (Bañez-Coronel et al., 2012). Overalls these alterations impact mRNA related regulations. Therefore, these mechanisms give another level of complexity to the alteration of gene expression in HD.

Lack of trophic support

The normal HTT has an essential role in the transport of vesicles. However, abnormal polyQ alters its interaction with components of the molecular motor complex. Altered axonal transport of BDNF form cortical neurons to striatal neurons was shown in HD (Gauthier et al., 2004). Transport defect also applies to trafficking of endosomes containing TrkB receptors, which are internalized after BDNF binding and need to be transported to the soma to activate intracellular signaling. mHTT impairs the binding of endosomes to the microtubules, reducing TrkB endosomal transport from dendritic terminals to the soma (Liot et al., 2013). Combined to the decreased expression of BDNF, the global impairment of BDNF and TrkB transport are thought to participate to the striatal vulnerability in HD, by weakening the related pro-survival signaling, including ERK phosphorylation pathway.

Impairment of autophagy

Autophagy is an important process for the clearance of aggregated proteins and defective organelles. As described previously HTT plays a role in autophagy, facilitating its activation and autophagosomes transport. In HD, an increased number of autophagosomes is observed, however they are empty of content indicating a deficit in cargo loading (***Figure 12***) (Martinez-Vicente et al., 2010). mHTT can activate autophagy by segregating mTOR (mammalian target of rapamycin) in aggregates (Ravikumar et al., 2004), but because of a deficit of cargo loading, autophagosomes have a slower turnover and accumulate, triggering a negative feedback loop where mHTT increases autophagy initiation but impairs the next steps. Furthermore, autophagosomes motility through HTT and HAP1 is prevented by mHTT, disrupting fusion of autophagosomes with lysosomes (***Figure 12***) (Wong and Holzbaur, 2014). In addition, mHTT has a reduced interaction with optineurin/rab8 complex, impairing lysosomes trafficking (del Toro et al., 2009). Ubiquitinated cargos are usually recognized by autophagy receptor p62, which can then bind to LC3 at the autophagosomes membrane. p62 was shown to bind mHTT aggregates (Bjørkøy et al., 2005), however, the subcellular localization of p62 bodies is modified, suggesting a less efficient targeting of aggregates to the autophagy machinery (Huang et al., 2018). A recent study showed that polyQ domains interact with the deubiquitinating enzyme ataxin-3, enabling its interaction with beclin-1, a key initiator of autophagy. Ataxin-3 can then deubiquitinate beclin-1, protecting it from degradation by the proteasome complex, thereby enables autophagy. In polyQ disorders, there is a competition for ataxin-3, with longer polyQ tract increasing interactions. Thus, in cells expressing mHTT, there is an impairment of autophagy, which is also observed in HD mouse model brains and patients cells (Ashkenazi et al., 2017).

Impairment of the ubiquitin-proteasome system in Huntington's disease

The ubiquitin-proteasome system (UPS) is involved in the recycling and degradation of misfolded proteins. Ubiquitin was shown to co-localize with HTT aggregates, suggesting that mHTT might initially be targeted for degradation, yet still accumulates (Davies et al., 1997; DiFiglia et al., 1997). Impairment of the UPS activity was reported in HD cell models and in the brain of patients (Hunter et al., 2007; Seo et al., 2004), which could potentially participate to the accumulation of mHTT. Accumulation of poly-ubiquitin chains was demonstrated as an early event in R6/2 mice (Bennett et al., 2007). Interestingly, UPS activity is decreased in the synapses of HD mice, decreasing protein turnover, which could alter synaptic plasticity (Wang et al., 2008a). However, the proteasome is still dynamically recruited to HTT aggregates (Schipper-Krom et al., 2014). Therefore, the mechanisms underlying UPS impairment are still debated, even though there are several evidences implicating UPS in HD pathogenesis.

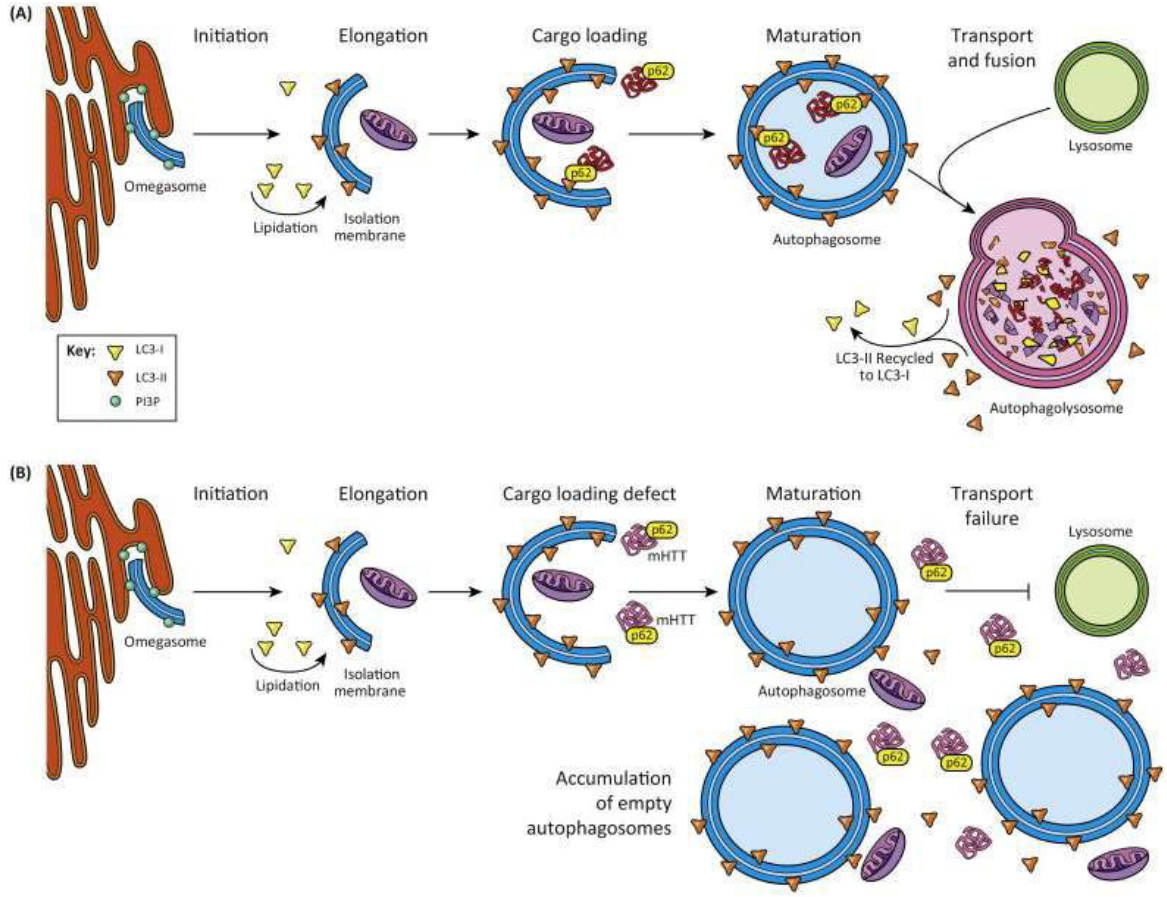

Figure 12. Autophagy is impaired in Huntington disease. (**A**) Vesicles are formed and elongated and can incorporate damaged organelles and/or aggregated proteins, and fuse with the lysosome for degradation. (**B**) Autophagy is altered in HD at several levels including a defect in cargo loading, trafficking of autophagosomes, and decreased fusion of autophagosomes with lysosomes leading to a build-up of defective materials in the cytoplasm and empty autophagosomes. (Martin et al., 2015)

Astrocytes dysfunction in Huntington's disease

Astrocytes are critical component of the CNS, involved in neurotransmission, calcium signaling and brain metabolism. In response to a homeostatic dysregulation, astrocytes become reactive, adapting their morphology and transcriptional regulation to respond to the changing environment. Astrocyte reactivity is observed in post mortem tissue of patients, with increased reactivity from grade 1 to 4 (Vonsattel et al., 1985). However, it is worth noting that evidence of astrocyte reactivity in HD models is not clear, instead astrocytes show functional alteration rather than morphological changes (Tong et al., 2014). Aggregates are present in astrocytes, but are smaller and less present than neuronal inclusions (Jansen et al., 2017). Interestingly, specific expression of mHTT in astrocytes is sufficient to induce neurological symptoms in mice (Bradford et al., 2009) and contributes to neuronal excitotoxicity *in vitro* (Shin et al., 2005). Thus, astrocyte dysfunction needs to be considered as a contributor in HD pathogenesis.

Astrocytes and neurotransmission

Astrocytes participate to the glutamatergic neurotransmission by reuptake of glutamate at the synapse. One of the major transporters is the glutamate transporter 1 (GLT1), which is highly expressed in astrocytes (Rothstein et al., 1996). Expression of GLT-1 is decreased in patients, visible from grade 0 and with increased loss with HD severity, and in various mouse models (Faideau *et al*, 2010; Behrens *et al*, 2002; Arzberger *et al*, 1997), causing a decreased re-uptake of glutamate. This is due to a specific decrease of GLT1 in astrocytes, indeed when mHTT is expressed only in astrocyte GLT1 expression is affected, whereas specific neuronal expression of mHTT did not affect GLT1 expression (Bradford et al., 2009; Faideau et al., 2010). mHTT can alter GLT1 expression by affecting SP1 binding to GLT1 promoter in astrocytes. In non-pathological conditions, astrocytes regulate extracellular potassium (K^+) levels, mainly through Kir4.1 potassium channel, which is essential to support SPN excitability (Nwaobi et al., 2016). In HD mouse models, Kir4.1 expression was decreased and associated to an increase of extracellular K^+ in the striatum, which increased SPN excitability. A viral delivery of Kir4.1 channels into astrocytes rescued SPN excitability and ameliorated motor phenotypes in these mice (Tong et al., 2014). This study highlights the fact that astrocytic homeostasis is pivotal for the development of HD phenotype. Astrocytes from HD mouse models had reduced spontaneous Ca^{2+} signals but had robust evoked Ca^{2+} signals after cortical stimulation. These signals were dependent on GLT1 and to a lesser extent on Kir4.1 channel. These Ca^{2+} dependent action potentials were mediated by astrocytes mGluR2/3 receptors, likely due to glutamate spillover (Jiang et al., 2016).

Astrocytes and metabolism

The CNS preferred energy substrate is glucose; in HD patient, positron emission tomography studies showed an impairment of glucose metabolism (Grafton et al., 1992). According to the lactate shuttle hypothesis, neurons rely on astrocytes for its energy supply. When neuronal activity is increased, astrocytes take up glucose from the blood, oxidize it through glycolysis and redistribute it to neurons in the form of lactate (Pellerin and Magistretti, 1994). Study in mouse models showed a decreased glucose uptake in the striatum and *in vitro* expression of mHTT in astrocytes indirectly impairs glucose uptake in neurons (Boussicault et al., 2014). Another important metabolic pathway regulated by astrocytes is cholesterol metabolism, which will be addressed in detail in a specific chapter.

Glutamatergic excitotoxicity

Excessive stimulation of NMDA receptors (NMDA-R) can lead to an aberrant Ca^{2+} signaling and the induction of cell death, this mechanism is called excitotoxicity. The first evidence linking excitotoxicity to HD was the observation that injection of NMDA-R agonists in the striatum recapitulates the degeneration and was used to generate the first HD models (Beal et al., 1986; Coyle and Schwarcz, 1976). At pre-symptomatic stages, glutamate release is increased, SPN are abnormally depolarized and dendritic spines loss starts. After onset of motor symptoms, the excitatory transmission is decreased whereas inhibitory transmission is increased (André et al., 2010). Expression of GLT-1 is decreased in patients and HD models (Arzberger et al., 1997; Behrens et al., 2002; Faideau et al., 2010), causing a decreased re-uptake of glutamate. This excess of glutamate will affect Ca^{2+} homeostasis through NMDA-R, because of their high permeability to calcium. NMDA-R are hetero-tetramers containing two GluN1 subunits associated to GluN2 (GluN2A-D) and/or GluN3 (GluN3A-B) with different properties depending on this subunit composition (Paoletti et al., 2013). GluN2A containing receptors are preferentially located at the synapse and are associated to pro-survival pathways, whereas GluN2B containing receptors are more extra-synaptic and associated to apoptosis (Hardingham and Bading, 2010). In YAC128 mice, extra-synaptic GluN2B-NMDA-R are increased and associated to enhanced apoptosis (Milnerwood et al., 2010, 2012). The inhibition of extra-synaptic NMDA-R with memantine antagonist improved YAC128 phenotype, validating the role of this pathway in HD deleterious mechanisms (Milnerwood et al., 2010). Interestingly, the striatum expresses high levels of GluN2B, thus, GluN2B-mediated excitotoxicity could participate to the striatal vulnerability in HD (Küppenbender et al., 2000). Several cellular events have been described for the localization of GluN2B-NMDA-R. Phosphorylation of GluN2B at Tyrosine 1472 (Tyr^{1472}) by the tyrosine kinase Fyn favors its localization at the synapse. Early in HD, STEP (Striatal Enriched protein tyrosine Phosphatase), which inhibits Fyn, has an increased activity, reducing GluN2B phosphorylation and synaptic localization (Gladding et al., 2012). Another mechanism relies on the cleavage of GluN2B C-terminus by the protease calpain, which activity is enhanced at early stages in HD models, weakening GluN2B anchor at the synapse (Gladding et al., 2012). These modifications lead to an increased extra-synaptic localization of GluN2B-NMDA-R (***Figure 13***). Early at post-natal stages, GluN3A expression peaks and participate to the elimination of immature synapses, then levels of GluN3A progressively decrease (Paoletti et al., 2013). In YAC128 mice, mHTT alters the endocytosis of GluN3A by interacting with its adaptor PACSIN-1, thus GluN3A membrane expression remains persistent (***Figure 13***) (Modregger et al., 2002). NMDA-R containing GluN1-GluN2B-GluN3A are then more likely addressed to the extra-synaptic domains (Martínez-Turrillas et al., 2012). These changes in receptor localization lead to several deleterious cellular events along with activation of pro-apoptotic signaling pathways. Rhes

activity (Ras-homolog enriched in the striatum) is increases by extra-synaptic NMDA-R activity. Rhes will disaggregate mHTT by increased sumoylation, leading to smaller and more toxic mHTT fragments (Subramaniam et al., 2009). These fragments can sequester CBP, preventing the transcription of CREB. In the nucleus, mHTT blocks PGC-1α expression by interfering with CREB and TAF4-mediated transcription. Reduced PGC-1α, in turn, increases extra-synaptic NMDA-R currents, giving a toxic positive feedback loop. Extra-synaptic NMDA-R activation may also contribute directly to PGC-1α transcriptional shut-off by CREB inhibition (Okamoto et al., 2009). Overall, enhanced extra-synaptic activity is associated with decreased pro-survival pathways (***Figure 13***).

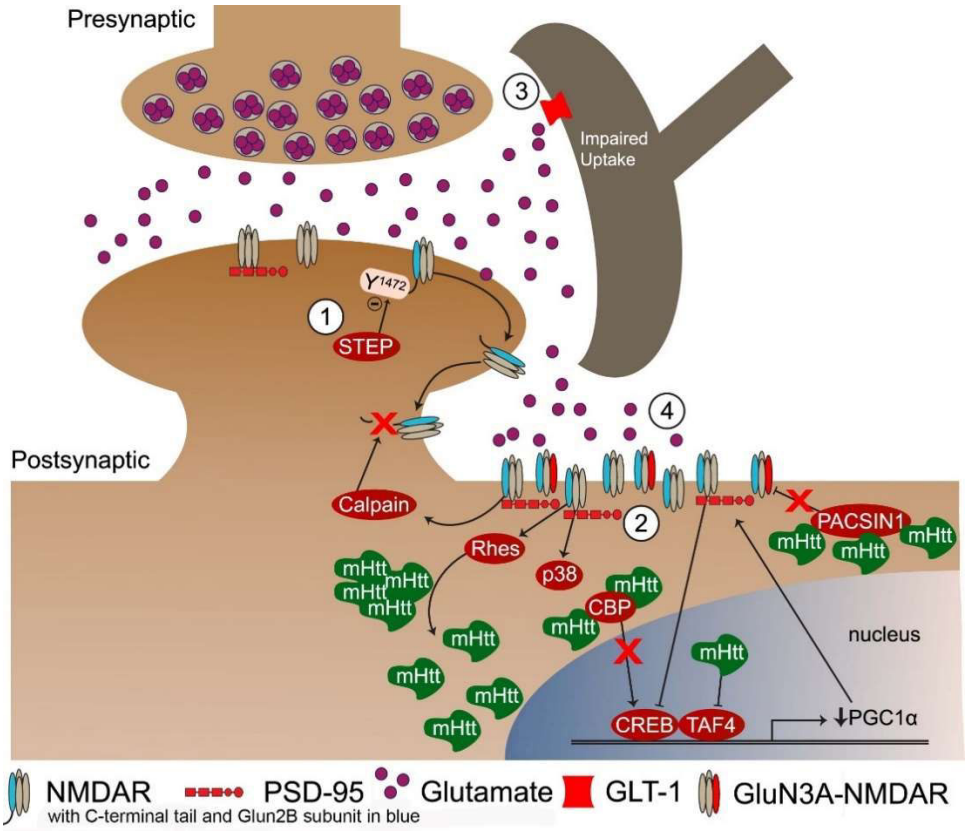

Figure 13. Mechanisms underlying glutamatergic excitotoxicity **1**. Post-translational modifications of GluN2B alter its localization towards the extra-synaptic compartment **2.** Increased Rhes activity favors mHtt disaggregation, leading to the sequestration of CBP. In the nucleus PGC-1α expression is suppressed by mHtt, increasing extra-synaptic NMDAR currents. **3**. Decreased uptake of glutamate by GLT-1 **4**. Expression of GluN3A-containing NMDA-R is increased due to decreased endocytosis by PACSIN1. (Parsons and Raymond, 2014)

Mitochondrial dysfunctions and energy metabolism

Mitochondria regulate key homeostatic events in the cell, from energy metabolism, Ca^{2+} levels to apoptosis. In HD, numerous studies have shown a dysregulation of this homeostasis leading to cellular stress and dysfunction. Targeting the mitochondria, using toxins such as 3-nitropropionic acid (3-NP), was actually among the first *in vivo* model used to cause specific striatal degeneration and HD phenotype in mice (Brouillet et al., 1993, 1995).

Respiratory chain and ATP production

The enzymatic activity of the respiratory chain complexes is strongly and specifically reduced in post-mortem caudate and putamen (Browne et al., 1997) (***Figure 14***), with a preferential and major decreased expression of the complex II (Benchoua et al., 2006). Loss of pyruvate dehydrogenase complex was also described in patients' brains (Sorbi et al., 1983). Reliable measures of ATP levels can be challenging, so to measure high-energy phosphates in the brain a study used microwave fixation *in vivo* to inactivate enzymes that could modify ATP levels. Using this method, a decrease of ATP levels in the striatum, hippocampus and cerebral cortex was shown in R6/2 mice, associated to an early increase of phosphocreatine (Mochel et al., 2012).

Mitochondrial membrane properties and Ca^{2+} homeostasis

Mitochondrial membrane potential is decreased in patients' lymphocytes (Panov et al., 2002) and in clonal cells STHdhQ111/Q111 (Milakovic et al., 2006). These cells also display high sensitivity to Ca^{2+} induced mitochondrial permeability, and when treated with 3-NP they have higher vulnerability to permeability and death (Ventura et al., 2013). N-terminal fragment of mHTT can directly interact with the outer mitochondrial membrane to trigger permeability changes and loss of membrane potential (Choo et al., 2004).

Significant changes of intracellular Ca^{2+} concentration are toxic for neurons, however Ca^{2+} buffering is altered in patients' lymphocytes and in cells expressing mHTT (Panov et al., 2002). STHdhQ111/Q111 mitochondria for instance have reduced capacity to take-up Ca^{2+} (Milakovic et al., 2006). In *vivo* some models showed decreased Ca^{2+} buffering (R6/2 and YAC128) but not all (HdhQ150) (Brustovetsky et al., 2005; Wang et al., 2013). (***Figure 14***)

Transcription dysregulation and mitochondria

As described previously, transcriptional disruptions are found in HD. PGC1α is a nuclear co-activator involved in mitochondria biogenesis and levels of this protein are decreased in HD patients and models (McGill and Beal, 2006) (***Figure 14***). mHTT repress PGC1α gene transcription by association with its promotor and interfering with CREB/TAF4 (Cui et al., 2006). Downstream targets of PGC1α are also dysregulated and participate to HD pathogenesis, like the nuclear respiratory factor NRF1 and 2 and the peroxisomes proliferator activated receptor (PPARs) (Dickey et al., 2016; Scarpulla, 2008).

Mitochondria dynamic and recycling in the cell

In vitro, cells expressing mHTT showed increased fission and decreased fusion (Shirendeb et al., 2011, 2012). Dynamin related protein (DRP1) is a GTPase involved in mitochondria's fission. mHTT can interact with DRP1, which results in enhanced and increased mitochondria fission. The pro-fusion GTPase OPA1 (optic atrophy 1) is also affected with an abnormal oligomerization in R6/2 mice (Hering et al., 2017) (***Figure 14***). Inhibition of DRP1 GTPase activity rescued mitochondria fragmentation and transport (Song et al., 2011). Indeed, DRP1 also mediates mitochondrial transport, a mechanism that is overall altered in HD. Moreover, studies have shown that aggregates impair mitochondria trafficking along neuronal processes, causing mitochondria accumulation and immobilization (***Figure 14***) (Chang et al., 2006). The N-terminal fragment can interact with mitochondria, preventing its interaction with microtubules (Orr et al., 2008).

Mitophagy, the cellular self-degrading process for defective mitochondria, is altered in HD. Indeed, this mechanism is dependent on macroautophagy (Martinez-Vicente et al., 2010; Wong and Holzbaur, 2014) which is impaired in HD, as described previously. Another mechanism called micro-mitophagy also allows mitochondria elimination, where GAPDH activation under oxidative stress condition leads to the detection and degradation of damaged mitochondria by fusion with lysosomes. But since GAPDH is inactivated by mHTT, this mechanism is blocked, causing an accumulation of damaged mitochondria which is deleterious for the cell (Hwang et al., 2015).

Mitochondria and cell survival

General dysfunction of the mitochondria can alter neuronal survival in HD. In addition of protein fusion, OPA1 is crucial for the mitochondrial cristae stability, where many cytochromes involved in apoptosis are concentrated. In HD, the integrity of the mitochondrial cristae is compromised, most likely due to the impairment of OPA1 oligomerization (***Figure 14***). This structural defect could thus impact the regulation of apoptosis (Hering et al., 2017). Global alteration of mitochondria can induce an increased production of ROS (reactive oxygen species), which is associated to cell death (Liot et al., 2009).

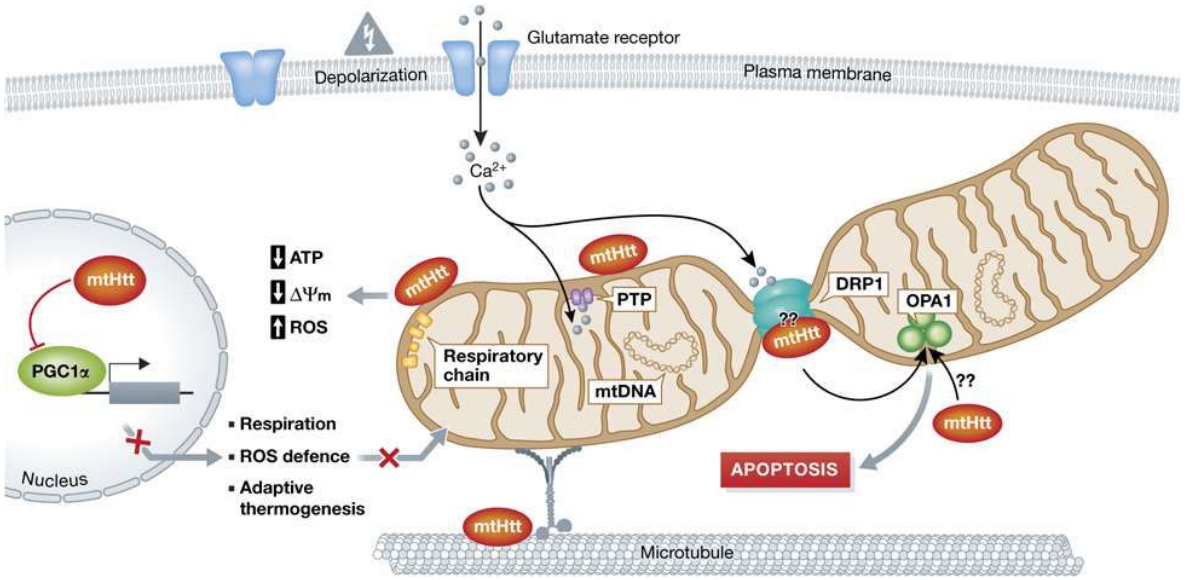

Figure 14. Alteration of mitochondria homeostasis in HD. The respiratory chain complex function is impaired in HD, along with decreased ATP levels. mHTT leads to a decrease of membrane potential. HD mitochondria are less able to buffer Ca^{2+} in the cell. PGC1α transcription is inhibited by mHTT, leading to a decrease of ROS defense. Mitochondria fission/fusion equilibrium is destabilized and mitochondria recycling through autophagy are decreased. PTP: permeability transition pore (Costa and Scorrano, 2012)

Myelination defect in Huntington's disease

White matter degeneration was well described in HD, appearing at early stages before disease onset, and correlates with clinical progression (Bohanna et al., 2011; Zhang et al., 2018). For instance, myelin damage and breakdown was found in pre-symptomatic gene-carriers (Bartzokis et al., 2007). Deficient myelination was also observed in HD models, prior to neuronal loss (Teo et al., 2016). This last decade, studies have been done to explore whether white matter defects are due to direct effects of mHTT on oligodendrocytes, the myelinating cells in the CNS, or to secondary effects from neuronal damage. Selective expression of mHTT in primary oligodendrocytes was associated to a decreased expression of myelin associated genes such as PGC1α (peroxisome proliferator activated receptor gamma coactivator 1α), and MBP (myelin basic protein) (Xiang et al., 2011). Generation of transgenic mice specifically expressing mHTT in oligodendrocytes showed age dependent demyelination, reduced expression of myelin genes, associated to a strong motor decline, weight loss and early death. This study showed that mHTT directly binds MYRF (myelin regulatory factor), which is a specific regulator that activates and maintains the expression of myelin genes in mature oligodendrocytes, affecting its transcriptional activity (Huang et al., 2015). Therefore, there are building evidences implicating oligodendrocytes dysfunctions in HD pathogenesis.

Microglial activation and inflammation in Huntington's disease

Microglia are the resident immune cells of the CNS; they monitor the environment and when activated can release pro-inflammatory and/or anti-inflammatory molecules, along with growth factors to respond to changes in their environment. Microglial activation can either be neurotoxic or protective depending on the factors released, the duration of activation and the stage of activation: pro-inflammatory M1 microglia or pro-repair M2 microglia (Yang et al., 2017). In HD, microglial activation was detected in patient post mortem's brain (Singhrao et al., 1999) and by positron emission tomography (PET), where it was significantly increased in affected areas (Pavese et al., 2006). Interestingly, microglial activation was also detected in pre-symptomatic gene carriers by PET (Tai et al., 2007), indicating that it is an early event in HD. Over-activated microglia can be neurotoxic, whereas initial normal activation can be protective by increasing survival of mHTT expressing neurons (Kraft et al., 2012). Patients' monocytes are hyperactive in response to stimulation, suggesting a cell-autonomous effect of the mHTT on immune cells (Björkqvist et al., 2008). This is supported by a study showing that specific expression of mHTT in microglia induces pro-inflammatory transcriptional activation, by enhancing the expression of myeloid lineage determining factors PU.1 and C/EBPs, and is associated to an increased ability to induce neuronal death without external inflammatory signals (Crotti et al., 2014). It must be noted that reactive astrocytes can also produce pro-inflammatory and/or anti-inflammatory molecules. A recent study showed that activated microglia can induce the activation of pro-inflammatory astrocytes, favoring cell death (Liddelow et al., 2017). The neuroinflammation observed in HD most probably arise from a combination of cell-autonomous and non-cell autonomous activation of microglia, with a communication between damaged neurons, reactive astrocytes and microglia.

General mechanism for Huntington's disease dysfunctions

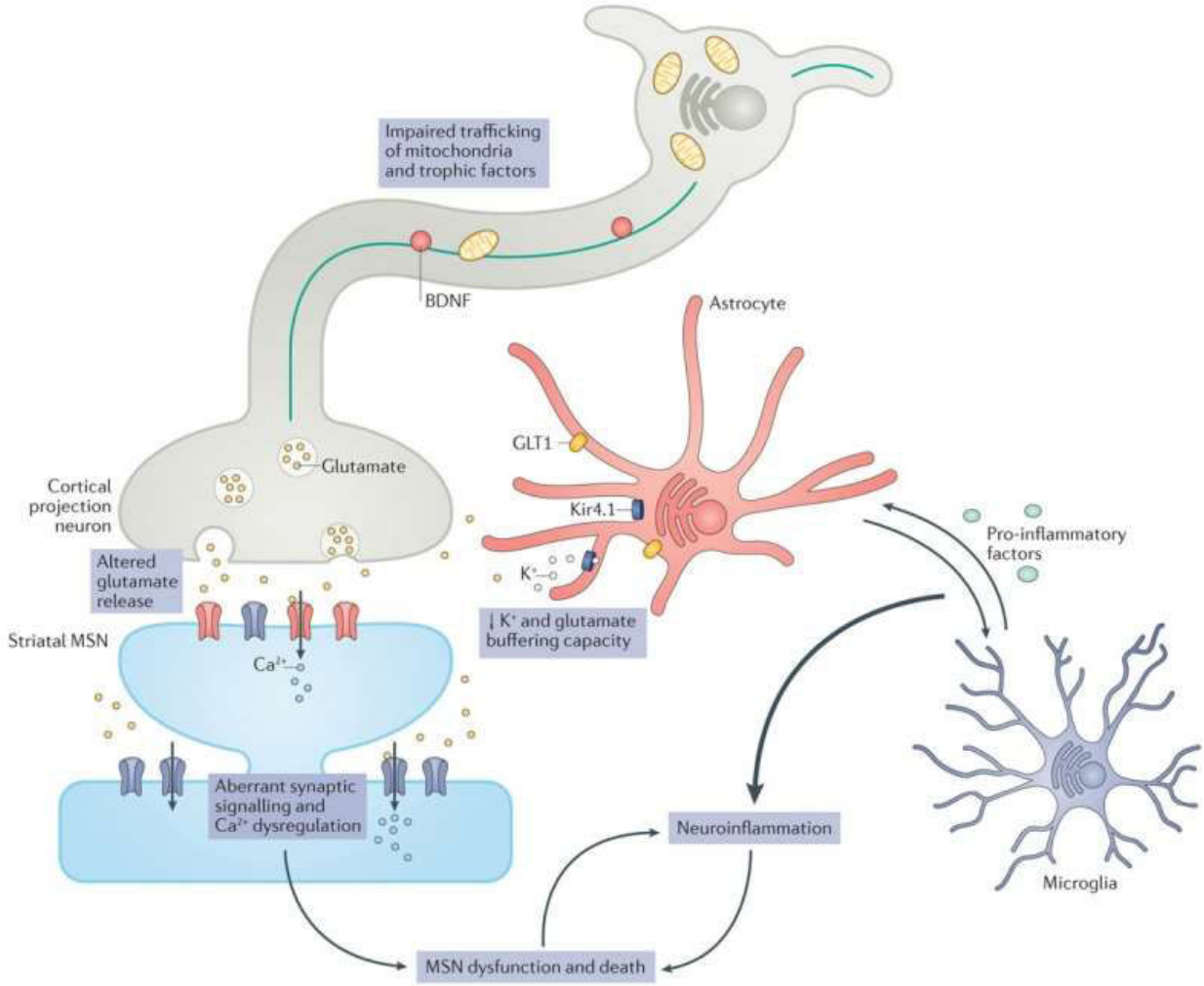

Intracellular mechanism

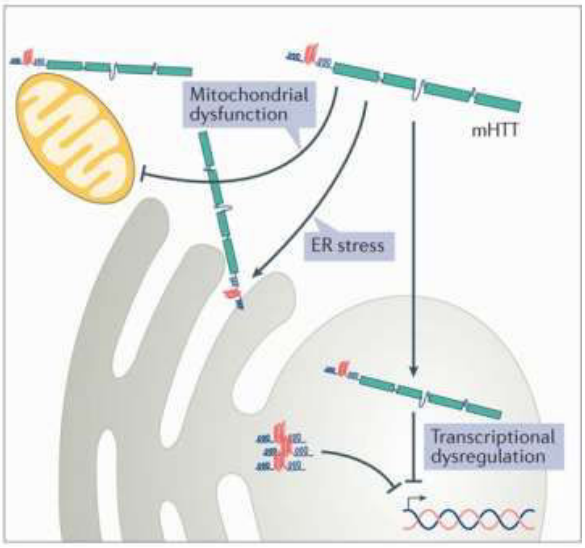

Figure 15. General mechanisms for HD dysfunctions. mHTT can act through several pathogenic mechanisms, including transcriptional dysregulation, impaired mitochondrial function, synaptic dysfunction, endoplasmic reticulum (ER) stress and loss of trophic support to striatal neurons. mHTT impairs extracellular ion homeostasis and glutamate uptake by astrocytes at the synapse by altering the expression of potassium channel Kir4.1 and glutamate transporter GLT1, which can lead to increased SPN excitability and activation. Moreover, mHTT can cause aberrant immune activation, resulting in neuroinflammation. (Caron et al., 2018)

The multiple dysfunctions of vital processes seen in ***Figure 15*** and others like autophagy, lead to toxicity over time, promoting neurodegeneration in both a cell autonomous and non-cell autonomous manner. Of special interest, cholesterol metabolism will be further discussed in the next chapter.

Chapter 2 - Cholesterol in the central nervous system

Cholesterol exerts key functions as a structural component of membranes, myelin sheaths but also through its complex metabolism composed of numerous metabolites, which are involved in cell signaling. It is also the precursor of bile acids, steroid hormones and oxysterols. Cholesterol is a major component of the CNS, with a highly regulated metabolism.

Cholesterol content in the brain

In the human brain, the mean concentration of cholesterol is 20 mg per gram of tissue, accounting for 23% of the total body cholesterol, when the brain volume account for about 2.1% of the body mass (Dietschy, 2009). Brain cholesterol is mainly unesterified; the larger pool of cholesterol is found in myelin sheaths of oligodendrocytes (70% of the brain cholesterol), with a very slow turnover giving the half-life of approximately 5 years. The 30% remaining is found in the membranes of neurons and astrocytes, with a faster turnover and a half-life of 5 to 10 months (Andersson et al., 1990; Davison, 1965).

Cholesterol synthesis

Cholesterol cannot cross the blood brain barrier (BBB), due to its association with lipoproteins, so it is synthesized *de novo* in the CNS (Jeske and Dietschy, 1980). The main origin for newly synthesized cholesterol switches from neurons during embryogenesis to oligodendrocytes during postnatal myelination, to mainly astrocytes in the adult brain (Saher and Stumpf, 2015).

Cholesterol synthesis in mammals CNS involve a complex series of reactions that are catalyzed by over 30 enzymes, which require energy and oxygen (***Figure 16***) (Gaylor, 2002). The first step is the conversion of acetyl-CoA into HMG-CoA (3-hydroxyl-3-methylglutaryl-coenzyme A) via the reaction catalyzed by HMG-CoA synthetase and then by HMG-CoA reductase (HMGCR) into melanovate. This reaction catalyzed by HMGCR is an irreversible and rate limiting step in cholesterol synthesis (Rodwell et al., 1976). It is followed by a sequence of enzymatic reactions converting mevalonate into 3-isopenenyl pyrophosphate, farnesyl pyrophosphate, squalene and lanosterol, followed by 19 steps involving two related pathways. These two pathways for cholesterol production in the brain seemingly have preferential cell localization: neurons preferentially go throw the Kandutsch-Russel pathway via synthesis of 7-dehydrocholesterol (7-DHC) and astrocytes preferentially go throw the Bloch pathway via synthesis of desmosterol. In the adult brain, the Bloch pathway seems to be preferred, via production of desmosterol (Pfrieger and Ungerer, 2011). Desmosterol is converted into cholesterol by 24-dehydrocholesterol reductase (DHCR24), while 7-DHC is converted into cholesterol by 7-dehydrocholesterol reductase (DHCR7) (***Figure 16***).

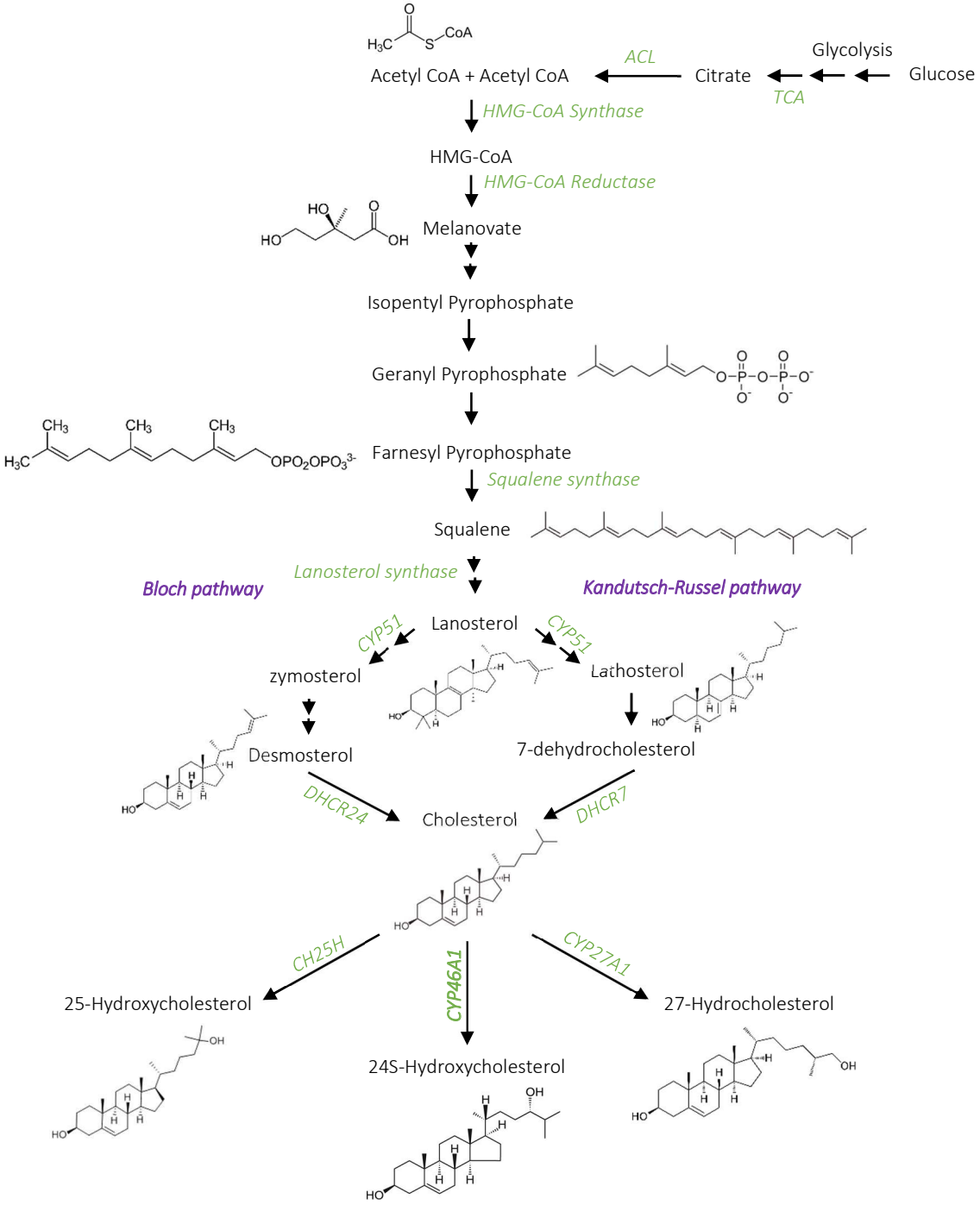

***Figure 16. Cholesterol metabolism*.** Cholesterol synthesis involves a complex chain of enzymatic reaction, from acetyl-CoA to the melanovate pathway that then divides into two possible pathways: the Bloch and Kandutch-Russel. The main product of cholesterol hydroxylation in the brain is the 24S-hydroxycholesterol, it can also be hydroxylated into 27-hydroxycholesterol and 25-hydroxycholesterol to a lesser extent. ACL: ATP citrate lyase, TCA: tricarboxylic acid cycle, CH25H: Cholesterol 25 hydroxylase, CYP51: lanosterol 14 alpha-demethylase, DHCR7: 7-dehydrocholesterol reductase, DHCR24: 24-dehydrocholesterol reductase, CY46A1: cholesterol 24-hydroxylase.

The machinery for cholesterol synthesis resides in the endoplasmic reticulum (ER). One of the main regulators of cholesterol synthesis in the brain is SREBP-2 (sterol regulatory element binding protein 2), which is a transcription factor functioning as a sensor of cholesterol in the cell (***Figure 17***). When inactive, it is anchored to the ER membrane and binds to SREBP cleavage activating protein (SCAP). When cholesterol concentration is high in the cell, SCAP, which has a cholesterol sensing domain, binds to insulin induced protein (INSIG), maintaining the SREBP-2/SCAP complex in the ER membrane. When cholesterol levels decrease, SREBP-2/SCAP complex is dissociated from INSIG, allowing SCAP to escort SREBP-2 to the Golgi, where SREBP-2 is cleaved by SCAP releasing an active N-terminus domain. This N-terminus domain translocate into the nucleus and binds to the sterol regulatory elements (SRE) in the promoter region of target genes involved in the synthesis and uptake of cholesterol, fatty acids, triglycerides and phospholipids (Horton et al., 2002). Cholesterol biosynthesis has an important feedback control on HMGCR activity and degradation (Goldstein and Brown, 1990). Accumulation of sterols in the ER membranes triggers the proteasome-mediated degradation of HMGCR through an INSIG/GRP78 dependent ubiquitination (***Figure 17***) (Tsai et al., 2012). Cholesterol synthesis is regulated by a negative feedback loop dependent of sterol levels.

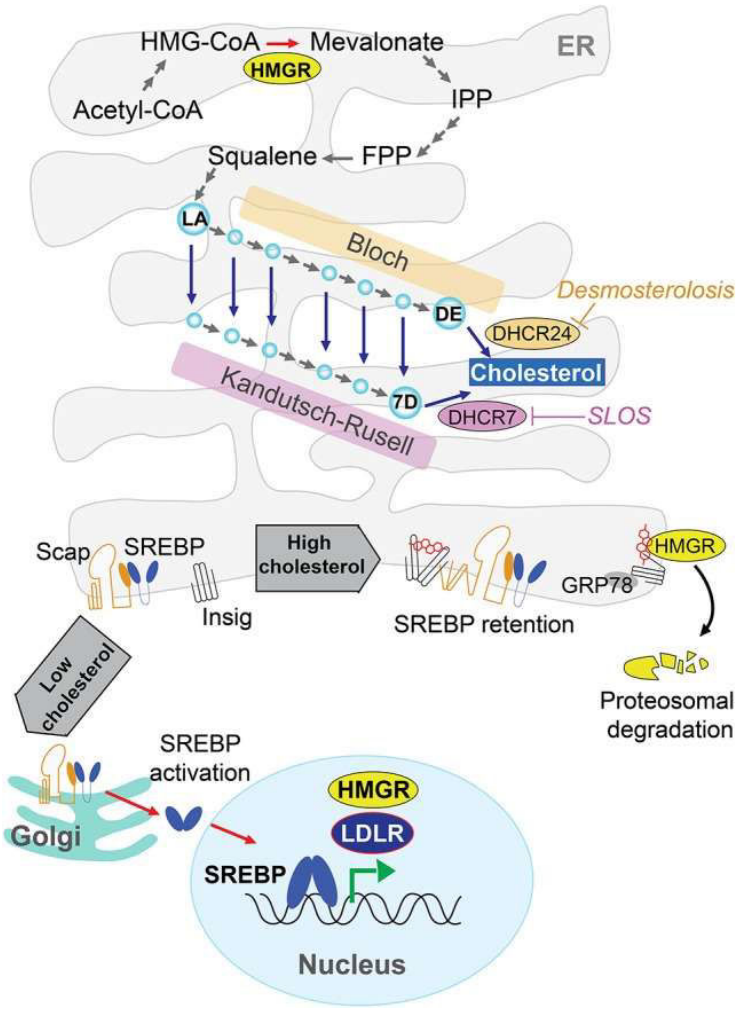

Figure 17. Cholesterol synthesis pathway. Cholesterol is synthesized in the endoplasmic reticulum (ER) from acetyl-CoA through several enzymatic steps. The rate-limiting enzyme HMGCR irreversibly converts HMG-CoA to mevalonate, then isopentenyl-pyrophosphate (IPP), farnesyl-pyrophosphate (FPP), followed by multiple enzymatic reactions until lanosterol (LA), which is succeeded by 19-steps involving the Bloch and Kandutsch-Russel pathways. These pathways use desmosterol (DE) or 7-dehydroxycholesterol (7D) as precursors of cholesterol through DHCR24 and DHCR7 enzymes, respectively. Sterol accumulation triggers proteasome-mediated degradation of HMGCR through an Insig/GRP78-dependent mechanism and the ER-retention of SREBP-2, which is controlled by SCAP. Decreased cholesterol allow SREBP-2 activation in the Golgi and its translocation to the nucleus (Arenas et al., 2017)

Cholesterol storage

The excess of cholesterol can be stored in cells as lipid droplets after esterification (***Figure 18***), which constitutes about 1% of cholesterol in the adult brain. These lipid droplets are a direct pool of cholesterol and fatty acids that can be used for myelination and synaptogenesis. The enzyme responsible for cholesterol esterification is ACAT-1 (Acetyl-CoA cholesterol acetyltransferase 1) and its expression can increase when cholesterol levels are high in the ER, but oxidative stress can also enhance ACAT-1 expression. In the CNS, cholesterol ester levels are stable and can be unesterified back by hydrolases. (Chang et al., 2009)

Cholesterol trafficking

In the mature brain, neurons rely on astrocyte for their cholesterol supply. To be transported to neurons, cholesterol needs to be associated to lipoproteins because it is lipophilic. In the CNS, the main lipoprotein for cholesterol transport is the Apolipoprotein E (ApoE), which is associated to phospholipids to form lipoprotein complexes. In accord with the role of astrocyte in cholesterol synthesis, ApoE is mainly synthesized by astrocytes (Pitas et al., 1987). The core of ApoE lipoproteins is formed in the ER and is then lipidated and secreted by ATP binding cassette transporters (ABC), (***Figure 18***) mainly ABCA1 (Wahrle et al., 2004), also ABCG1 and ABCG4. These lipoproteins are then mainly targeted to neurons where they can be internalized by receptors from the family of low-density lipoproteins (LDL) (***Figure 18***): LDL receptors (LDL-R) and LDL-R like proteins (LRP). LRP1 is expressed on neurons and has a high transport capacity for ApoE lipoproteins due to its elevated rate of endocytic recycling, whereas LDL-R is primarily expressed on glial cells (Vance and Hayashi, 2010). After endocytosis, lipoproteins fuse with late endosomes/lysosomes where acid lipase hydrolyzes cholesterol ester, unesterified cholesterol can then exit endosomes through Niemann-Pick Type C (NPC) proteins, NPC2 (luminal protein) and NPC1 (transmembrane protein) to then reach the plasma membrane or ER membrane (***Figure 18***) (Ramirez et al., 2011). ApoE lipoproteins interaction with their receptors not only allows cholesterol transport but also triggers signaling pathways essential for nerve regeneration (Ignatius et al., 1986), neuronal survival (Aono et al., 2002; Hayashi et al., 2009) and synaptic plasticity (Herz and Chen, 2006).

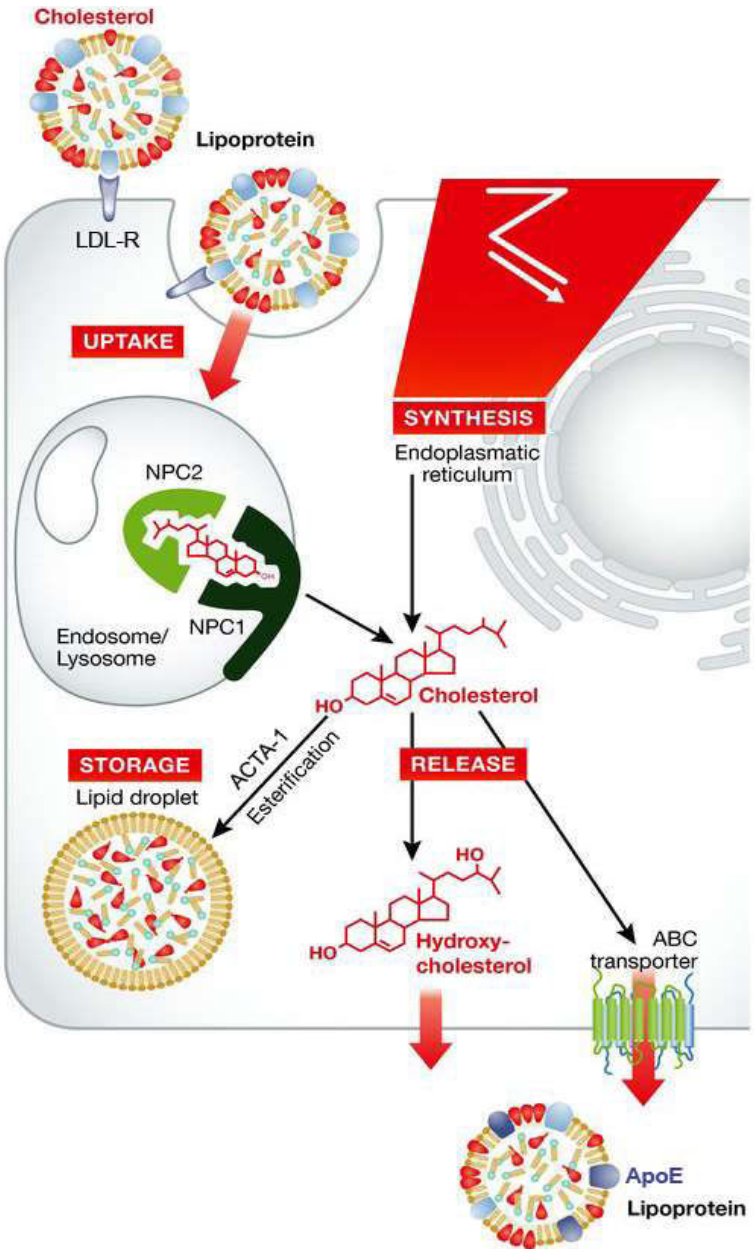

Figure 18. Global model for cholesterol trafficking. The relative contribution of each pathway to cholesterol homeostasis is cell type-specific. Cells can take up cholesterol by receptor-mediated endocytosis of lipoproteins bearing apolipoproteins, through LDL receptors (LDL-R). Lipoproteins are then directed to the endosome/lysosome pathway where Niemann-Pick Type C Protein 1 and 2 (NPC1 and NPC2) cooperatively mediate the exit of cholesterol allowing its incorporation into the intracellular pool. Overload of cholesterol is prevented by its intracellular esterification by ACAT-1 and subsequent storage in lipid droplets. Cholesterol is released either in ApoE lipoproteins via members of the ATP-binding cassette (ABC) transporters or after conversion into hydroxycholesterol. (Martín et al., 2014)

Cholesterol turnover in the brain

To cross the BBB, cholesterol needs to be converted to a more hydrophilic form, to do so it has to be hydroxylated into oxysterols (***Figure 16***). The main enzyme for cholesterol conversion in the brain is cholesterol-24-hydroxylase (CYP46A1), converting cholesterol into 24(S)-hydroxycholesterol (24S-OHC) (Lund et al., 1999; Smith et al., 1972), the role of this enzyme will be detailed in the next chapter. 24S-OHC is transported out of the brain at a rate of 6 to 8 mg per day (Lütjohann et al., 1996), by crossing the BBB through diffusion or anion transporter. Once in the blood stream, 24S-OHC binds to LDL, which are taken up by hepatocytes and excreted mainly as bile acids. Studies from *cyp46a1* knock-out showed that a third of cholesterol is excreted through another pathway, probably using lipoproteins, which could account for cholesterol turnover in glial cells (Xie et al., 2003). Other

oxysterols are found in the brain, the 27-OHC, which is one of the major oxysterols in the general circulation, can be produced by neurons, astrocytes and oligodendrocytes but at a very low rate. It is synthesized in the mitochondria thanks to CYP27A1 enzyme. 27-OHC can also access the brain from the blood stream, but the normal ratio of 27-OHC/24S-OHC is 1 to 8 in the frontal cortex, 1 to 5 in the occipital cortex and 1 to 10 in the basal ganglia (Heverin et al., 2004). 27-OHC can be then converted by CYP7B1 into 7α-hydroxy-3-oxo-4-cholestenoic acid. 25-hydroxycholesterol (25-OHC) formation is dependent on cholesterol-25-hydroxylase (CH25H), which expression is increased after innate immune activation (Diczfalusy et al., 2009). Oxysterols levels can be implicated in neurodegenerative diseases. Indeed, under oxidative stress, cholesterol can be converted into 27-OHC, which can increase the risk of neurodegenerative diseases (Marwarha and Ghribi, 2015). Brain levels of 25-OHC can be elevated in neurodegenerative diseases (Jang et al., 2016) and levels of 24S-OHC are decreased in neurodegenerative diseases (Leoni et al., 2008; Testa et al., 2016).

Oxysterols and sterol activation of LXR in cholesterol metabolism

Liver X receptor (LXR) transcription factors are activated by oxysterols such as 24S-OHC (Lehmann et al., 1997; Yang et al., 2006) and some of cholesterol precursors such as desmosterol (Spann et al., 2012). LXR form heterodimers with retinoid X receptors (RXR) which recognize the LXR response elements (LXRE) in the promoter regions of their target genes (***Figure 20***). In the absence of ligand, the complex is associated to co-repressors, which are replaced by co-activators upon binding of LXR with oxysterols and RXR with 9-cis retinoic acid, allowing gene expression (***Figure 20***). LXR regulate the expression of cholesterol synthesis enzymes *Fdft1* (squalene synthase) and *Cyp51* (lanosterol C14 demethylase) (Wang et al., 2008b) and of protein involved in cholesterol transport like ApoE and ABCA1 (Abildayeva et al., 2006). LXR activation is also important for oligodendrocyte differentiation and myelination (Meffre et al., 2015; Xu et al., 2014), and is implicated in the modulation of inflammation (Morales Jesús R. et al., 2008; Zelcer et al., 2007).

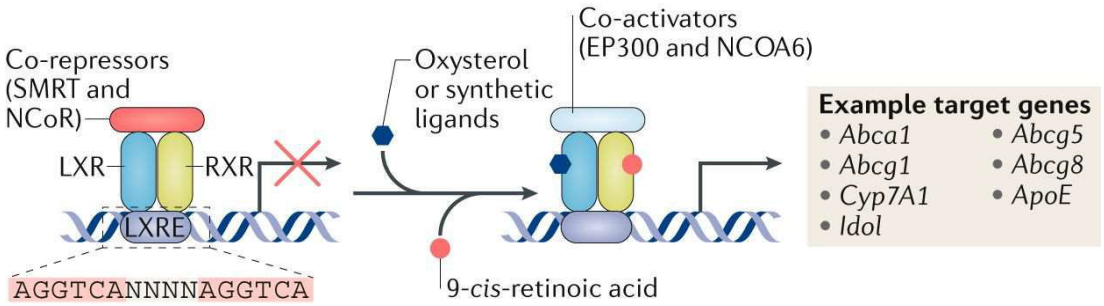

Figure 20. Activation of transcription factors LXR. LXRs and RXRs form heterodimers and bind to LXRE. Without ligands, LXR/RXR binds co-repressors. After activation of LXRs by oxysterols or synthetic ligands and RXR by 9-*cis*-retinoic acid, co-repressors are replaced by co-activators, activating the expression of target genes. NCOA: activating signal co-integrator 2; EP300: histone acetyltransferase p300; NCoR: nuclear receptor co- repressor; SMRT: silencing mediator of retinoic acid and thyroid hormone receptor. (Wang and Tontonoz, 2018)

Differential cholesterol metabolism in brain cell types

Throughout development, brain cells have differential role in cholesterol synthesis and homeostasis. Cholesterol synthesis is the highest at postnatal stages during active myelination, then it gradually decreases (Saher et al., 2005). Cholesterol synthesis switches from neurons during embryogenesis to oligodendrocytes during postnatal myelination and mainly to astrocytes in the adult brain (Saher and Stumpf, 2015). Oligodendrocytes have a higher capacity to synthesize cholesterol than astrocytes, which themselves have 2 to 3 fold higher capacity than neurons (Björkhem and Meaney, 2004; van der Wulp et al., 2013).

Myelin is composed of a multi-layered stack of extended oligodendrocyte membranes. Cholesterol in myelin serves essential brain functions including proper insulation of axons allowing fast transduction of neuronal signals. Cholesterol for myelin formation is synthesized locally (Jurevics and Morell, 1995), mostly by oligodendrocytes. Indeed, when cholesterol synthesis is abolished in oligodendrocytes, CNS myelination is severely disturbed and mutant mice have ataxia and tremor. Interestingly, in these mutant mice, myelination is not completely abolished and transport proteins (ApoE and LRP) are strongly increased, along with astrocyte activation, suggesting a partial compensation mechanism where astrocytes provide cholesterol for oligodendrocytes (***Figure 21***) (Saher et al., 2005). Moreover, oligodendrocytes specifically express LDL receptors at post-natal stages, which then progressively decrease, indicating that a complementary source of cholesterol could come from uptake from other brain cells during active myelination (Zhao et al., 2007). Before myelination the levels of desmosterol are high in the brain, making it the most represented sterol in the brain (Fumagalli and Paoletti, 1963; Jurevics and Morell, 1995). However, the decrease of desmosterol precedes the increase of cholesterol for myelination. Desmosterol most likely reflects sterol synthesis by astrocytes (Nieweg et al., 2009). This high production of desmosterol could be used by astrocytes as a substrate for progesterone, which in turn participate to the differentiation of oligodendrocytes towards myelination (Goodman et al., 1962; Schumacher et al., 2004). All major myelin proteins are associated to cholesterol rich domains such as the proteolipid protein (PLP) which is of particular interest because of its direct association to cholesterol (Simons et al., 2000). PLP is involved in cholesterol enrichment in myelin membranes (***Figure 21***), and in PLP knock-out mice, cholesterol content in myelin is strongly reduced (Werner et al., 2013).

In the adult brain, cholesterol synthesis and transport strongly depends on astrocytes (***Figure 21***) (Nieweg et al., 2009). Importantly, specific inhibition of cholesterol synthesis by SREBP-2 knock-out in astrocytes, strongly impact brain development and mice behavior, and causes a switch of metabolism toward glucose oxidation as a compensation mechanism (Ferris et al., 2017). Furthermore, astrocytes

express ApoE lipoproteins and ABCA1 receptor essential for lipidation and export of these lipoproteins (Pitas et al., 1987; Wahrle et al., 2004). This allows astrocytes to regulate cholesterol efflux towards neurons, with an important role of LXR dependent transcription of ApoE and ABCA1 (Chen et al., 2013).

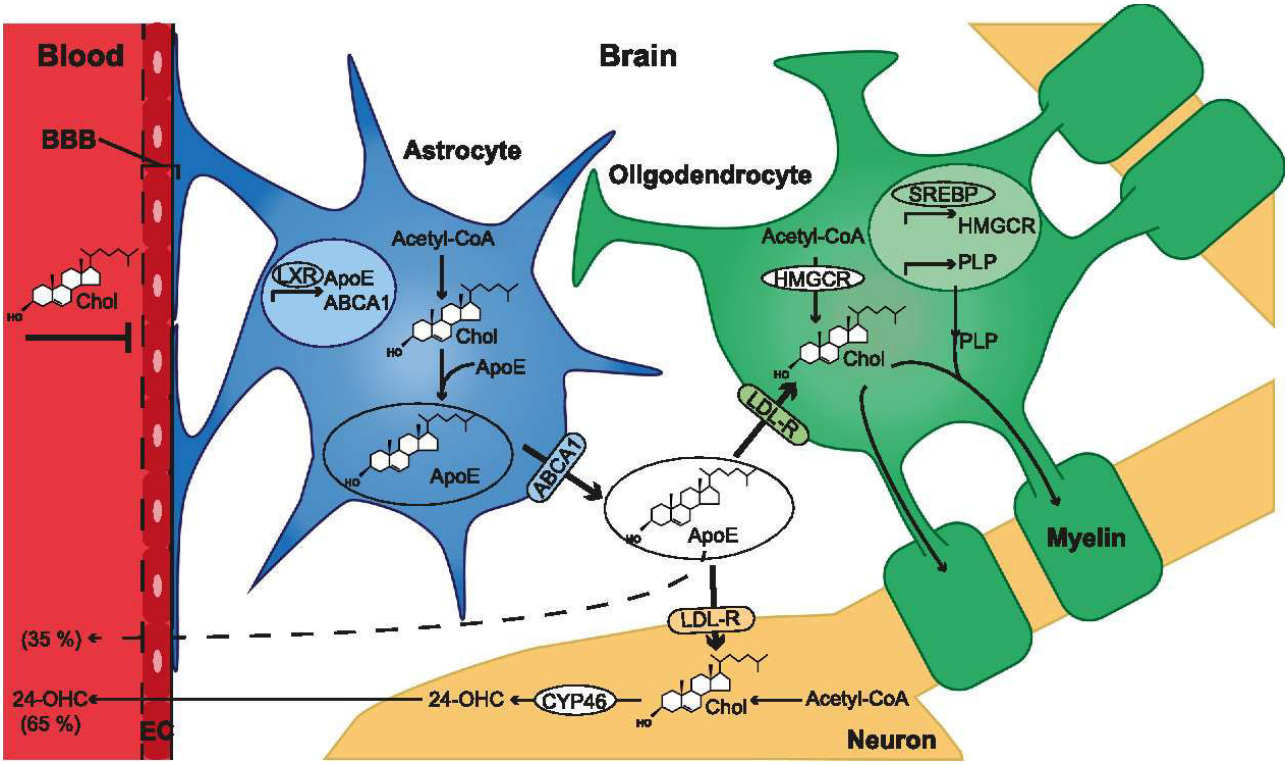

Figure 21. Model for cholesterol homeostasis in the CNS. Peripheral cholesterol (Chol) does not cross the blood–brain barrier (BBB) which is mainly constituted of endothelial cells (EC). ApoE facilitates the transport of cholesterol between cells. ApoE containing lipoproteins are lipidated, then secreted by ABC transporter (ABCA1), predominantly by astrocytes. Lipoproteins are endocytosed by LDL-R, providing neurons and oligodendrocytes with cholesterol. During myelination, cholesterol associates with the proteolipid protein (PLP) and is integrated into the myelin sheath. One excretion pathway for cholesterol is achieved by conversion into 24-OHC, catalyzed by cholesterol 24-hydroxylase (CYP46). 24-OHC can cross the BBB into the blood stream where it gets transported to the liver for excretion. About one third of cholesterol is excreted by another route potentially involving lipoproteins. (Saher and Stumpf, 2015)

Roles of cholesterol

Cholesterol at the membrane

Cholesterol has a rigid apolar ring structure, associated to a small polar hydroxyl group, giving it very specific biophysical properties (***Figure 22***). Cholesterol hydrocarbon ring is deeply immersed in the lipid bilayer, reducing membrane dynamic and fluidity (Sankaram and Thompson, 1990). Cholesterol promotes the formation of highly ordered domains called liquid ordered domains (van Meer et al., 2008). The increase of cholesterol in membranes slows down the lateral diffusion of lipids and proteins (Rubenstein et al., 1979). Cholesterol can also impact the bending and compressibility properties of the membrane (Chen and Rand, 1997). Due to its polar head, cholesterol can generate intrinsic negative curvature in lipid bilayers (Wang et al., 2007). An increased order of membrane by enhanced

cholesterol can influence the conformation of membrane proteins, changing for instance their binding properties with ligands and their stability (Gimpl et al., 1997; Saxena and Chattopadhyay, 2012). Protein membranes can directly interact with cholesterol through specific binding sites (Fantini and Barrantes, 2013).

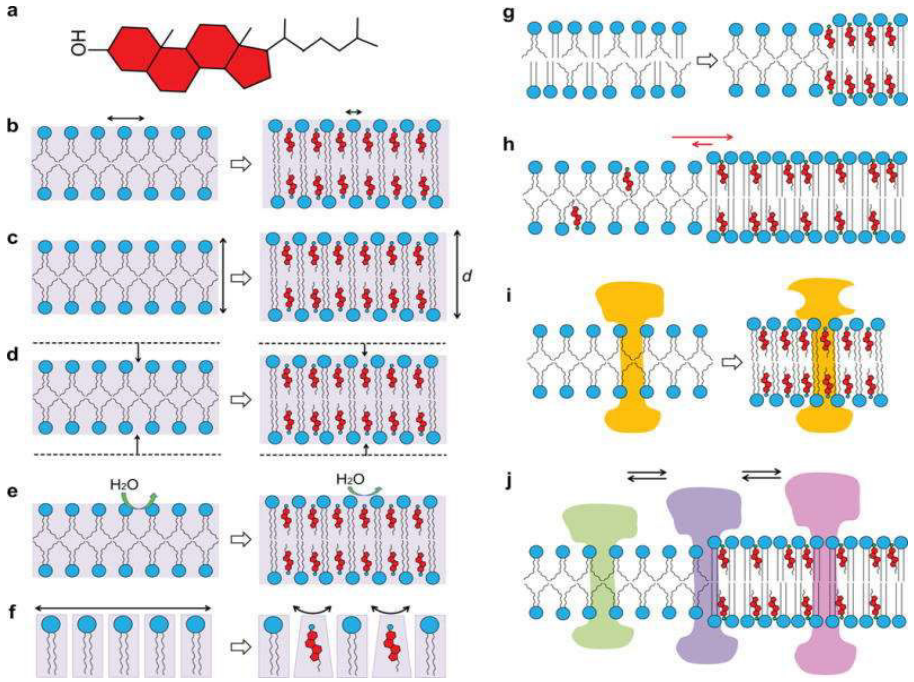

Figure 22. Multiple effects of cholesterol on lipid bilayers. (a) Cholesterol changes the fluidity (b), thickness (c), compressibility (d), water penetration (e), and intrinsic curvature (f) of lipid bilayers. Cholesterol also induces phase separations in multicomponent lipid mixtures (g), partitions selectively between different coexisting lipid phases (h), and causes membrane proteins to respond by changing conformation (i) or redistribution (j) in the membrane. (Yang et al., 2016)

Lipid raft

Within the plasma membrane micro-domains called lipid rafts, enriched in cholesterol and sphingolipids, act as a dynamic platform for protein clustering (***Figure 23***). Lipid raft participate to the compartmentation of proteins contributing to spatial and temporal organization of cell signaling. The lipid composition of these micro-domains can vary with the cell type, brain region and developmental stage. Their identification was for long challenging, because of their size and fluctuating nature, but the new technological advances in microscopy and spectroscopy produced compelling data for the existence of these nano-domains (Lingwood and Simons, 2010). Lipid rafts participate to the organization of the post-synaptic density, thus having a critical role in the signal integration at the synapse (Suzuki et al., 2011). Lipid rafts are also found in synaptic vesicle membranes, which have been shown to be enriched in cholesterol (Petrov et al., 2011). Lipid rafts are associated with several proteins, for instance with the scaffold protein caveolin, which has binding domains for metabotropic

receptors, MAP and Src-kinase, protein kinase A and C, adenylate cyclase (Stary et al., 2012). In neurons, caveolin 1 co-localizes with NMDA receptors and PSD-95 in lipid rafts, and caveolin-1 knock-out induces a loss of synapses (Head et al., 2010). Therefore, lipid rafts constitute platforms allowing the organization and compartmentalization of cell signaling.

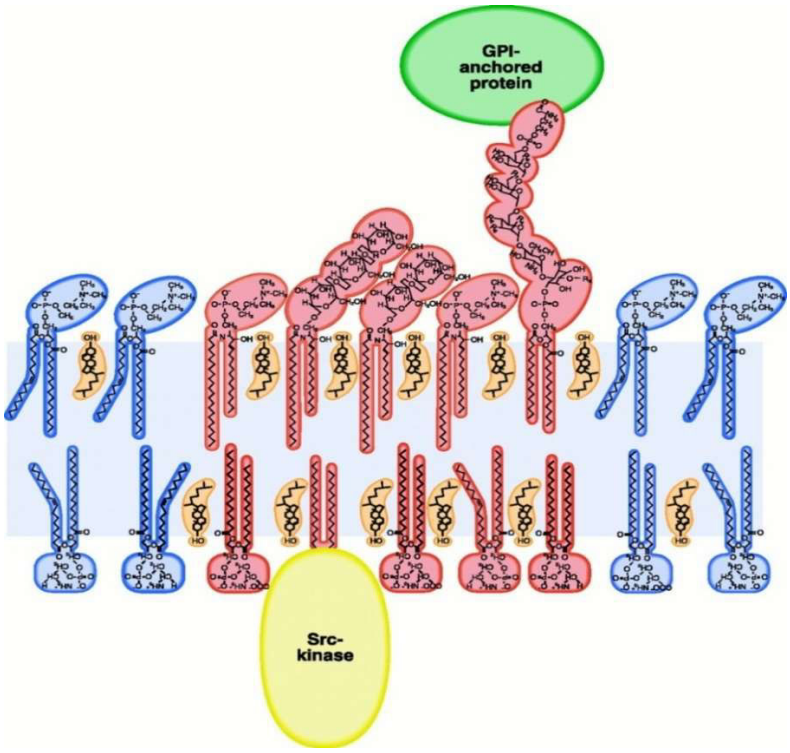

Figure 23. Model of a lipid raft associated to two proteins. A glycosylphosphatidyl inositol (GPI) anchored protein is attached to the extracellular leaflet, and a Src-kinase to the cytoplasmic leaflet. Lipids from the liquid-ordered phase (lipid raft) are shown in red and from the liquid-disordered phase in blue. Cholesterol (in orange) preferentially locates into the liquid-ordered phase. The outer leaflet of the raft is enriched in glycosphingolipids and sphingomyelin and the corresponding inner leaflet in glycerolipids with mainly saturated fatty acyls. (Simons and Ikonen, 2000)

Cholesterol and synaptic vesicle dynamic

In the CNS, cholesterol has an essential role in vesicle dynamics and constitutes 40% of total lipids in synaptic vesicle membranes (Takamori et al., 2006). To illustrate this role, cholesterol depletion by β-cyclodextrin increased the spontaneous neurotransmission in hippocampal cultures, due to an enhanced spontaneous vesicle recycling (Wasser et al., 2007).

Cholesterol and synaptic vesicle exocytosis

Inhibition of cholesterol synthesis has been shown to impair synaptic vesicle exocytosis, the fundamental process for neurotransmitters release (Linetti et al., 2010). This exocytosis process is defined by fast Ca^{2+} triggered fusion, which kinetics is dependent on cholesterol levels within membranes (Churchward et al., 2005). Importantly, cholesterol content influences fusion pore formation and stability during exocytosis (Koseoglu et al., 2011), by directly reducing the fusion pore-bending energy (Stratton et al., 2016). It has been postulated that SNARE proteins (Soluble NSF Attachment Protein Receptor), implicated in the machinery for membrane fusion, are clustered in

cholesterol rich domains of the vesicle membrane (***Figure 24***) (Gil et al., 2005). However, it is debated whether these domains are lipid rafts *per se* or other type of cholesterol ordered domains (Destainville et al., 2016; Lang, 2007). Syntaxin-1 for instance, which is part of the SNARE complex involved in synaptic vesicles exocytosis, was found to form clusters in cholesterol domains (Murray and Tamm, 2009).

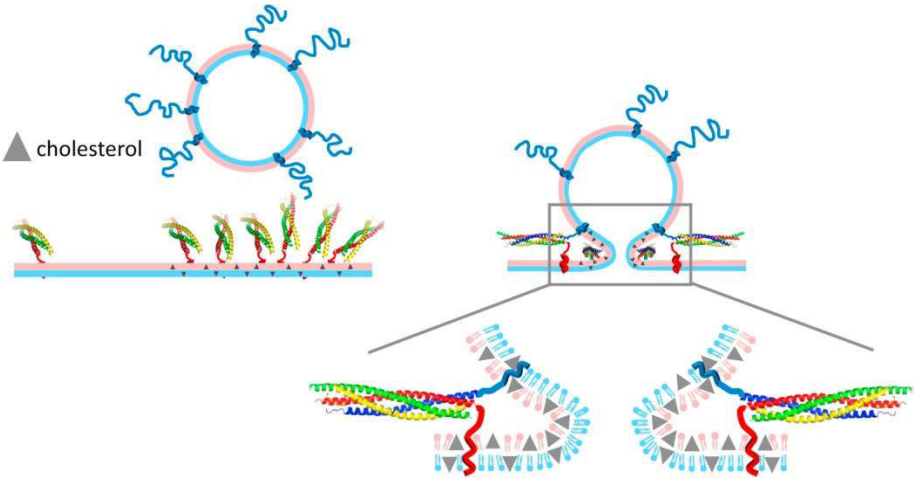

Figure 24. Model for cholesterol implication in SNARE-mediated fusion. Cholesterol content directly influences the formation of fusion-pore and indirectly favors exocytosis by clustering t-SNAREs (in red, green and yellow) into concentrated docking domains. (Stratton et al., 2016)

Cholesterol and synaptic vesicle recycling

Endocytosis of new vesicles is necessary to replenish the pool of synaptic vesicles. As a general mechanism, cholesterol-rich domains are important for the clustering of adaptor proteins. Indeed, cholesterol depletion blocks endocytosis via caveolae and clathrin-coated pits (Subtil et al., 1999). Cholesterol has a critical role in the formation of synaptic vesicles; when associated to synaptophysin, it can promote membrane curvature and the formation of synaptic like vesicles (Thiele et al., 2000). Within vesicles, synaptophysin/synaptobrevin complex promotes the functional build-up of v-SNARE complex (vesicle SNARE); and this interaction critically depends on cholesterol content at the membrane of synaptic vesicles (Mitter et al., 2003).

Cholesterol and synaptic transmission

The content and activity of post-synaptic receptors is critical for synaptic function and plasticity. Due to its role on membrane organization, cholesterol can differentially impact neurotransmitter receptor functions. These functions have mainly been studied in the context of cholesterol depletion. Cholesterol depletion can reduce agonist effectiveness on $GABA_A$ receptors and increase receptor potentiation by benzodiazepines (Nothdurfter et al., 2013; Sooksawate and Simmonds, 2001). AMPA receptors are associated to lipid rafts, acute cholesterol depletion leads to instability of AMPA

receptors and gradual loss of synapses and dendritic spines (Hering et al., 2003). Moreover, alteration of lipid rafts suppresses AMPA receptor exocytosis, reducing its cell surface expression (Hou et al., 2008). After acute cholesterol depletion, NMDA-R responses are decreased due to a reduction of channel opening probability and increased desensitization, impairing long term potentiation (LTP) (Korinek et al., 2015). As seen previously, NMDA-R are associated to lipid rafts with caveolin-1 (Head et al., 2010), which activation pathway is associated to ERK and Src-kinase, promoting cell survival (Head et al., 2008). Astrocytic glutamate transporter EAAT are also associated to lipid raft and upon cholesterol loss, glutamate uptake by astrocytes is reduced (Butchbach et al., 2004). Interestingly, after activation of NMDA-R, a rapid and transient decrease of cholesterol intracellular pool is observed, activating cdc42 dependent trafficking of AMPA receptors from Rab11 endosomes to the post-synaptic membrane, thereby favoring LTP. Overall, cholesterol loss at the synapse is induced by excitatory neurotransmission, which is recovered after stimuli (Sodero et al., 2012). Thus, cholesterol could act as a sensor of NMDA-R activation, triggering downstream signals for LTP (Brachet et al., 2015). Receptor localization and trafficking at the synapse is dependent on the lipid composition of the membrane. At the synapse, NMDA-R and its cytoplasmic scaffold protein PSD-95 move between the post-synaptic density and rafts following learning or ischemia. In this context, PSD-95 has a key role in the localization of GluN2A-containing NMDA-R to lipid rafts (Delint-Ramirez et al., 2010). Moreover, cholesterol depletion can redistribute GluN2B-containing NMDA-R outside lipid rafts (Frank et al., 2004). Dopamine transporters (DAT) cluster into cholesterol-rich nanodomains in the plasma membrane of pre-synaptic varicosities and neuronal projections of dopaminergic neurons; their location in these domains is reversibly regulated by NMDA-R activation. These nano-domains are highly sensitive to cholesterol depletion (Rahbek-Clemmensen et al., 2017).

Cholesterol and transport

The presence of cholesterol domains on vesicles can regulate the recruitment of motor proteins. Lysosomal transport for instance is co-regulated by a multi-protein complex: Rab7-RILP-ORP1L. The Rab7 interacting lysosomal protein (RILP) directly and concomitantly associates to the homotypic fusion and vacuole protein sorting (HOPS) complex and the dynein motor. The oxysterol binding protein related protein 1L (ORP1L) then acts as a cholesterol-sensing switch controlling RILP-HOPS-dynein interactions (Kant et al., 2013). The Rab7-RILP-ORP1L complex couples and regulates transport on microtubule by efficiently recruiting dynein-dynactin motors (Johansson et al., 2007; Jordens et al., 2001). Cholesterol depletion can promote endosome motility towards the plus end of microtubules by suppressing the association of endosomes containing lipid rafts with Rab7 GTPase and promotes their association with Rab4 GTPase (Chen et al., 2008).

Cholesterol and autophagy

Modulation of cholesterol dynamics can affect autophagy. This is clearly described in lysosomal storage disorders like Niemann-Pick type C disease (NPC), where defective cholesterol trafficking leads to altered endocytic trafficking and accumulation of autophagic vesicles (Liao et al., 2007; Sarkar et al., 2013). Interestingly, driving accumulated cholesterol out of the endosome/lysosome compartment prevents neurodegeneration in NPC (Aqul et al., 2011). Accumulation of cholesterol in late endosomes leads to an enlargement of these endosomes and affects their trafficking (Sobo et al., 2007). Cholesterol accumulation in membranes reduces the lysosomes ability to fuse with endocytic and autophagic vesicles, due to an abnormal sequestration of SNARE proteins in cholesterol enriched regions of endolysosomal membranes (Fraldi et al., 2010). High cholesterol content impairs lysosomal fusion by altering Rab7A and SNARE content and distribution (Barbero-Camps et al., 2018). Moreover, acute removal of cholesterol in membranes also strongly reduces autophagosomes/lysosomes fusion (Koga et al., 2010). At physiological levels, cholesterol is critical for autophagosomes fusion and transport. Dynein motors cluster into lipid raft at the membrane of phagosomes as they mature. This organization facilitates the generation of forces, allowing several dynein motors to cooperate to rapidly transport phagosomes to lysosomes (Rai et al., 2016).

Cholesterol and cell survival

Because of its critical role in membrane dynamics and cell signaling, alterations of cholesterol content and homeostasis can have deleterious impacts on cell survival. The binding of BDNF to TrkB receptor triggers ERK and Akt signaling, two major survival pathways. Interestingly, in aging neurons, loss of cholesterol is associated with increased TrkB activity (Martin et al., 2008). Stimulation of cultured neurons and hippocampal slices by BDNF induces an increase of TrkB receptor location in lipid rafts, showing a potential need of selective receptor location for efficient signaling (Suzuki et al., 2004). Because of their high need in energy production, neurons progressively accumulate ROS (reactive species of oxygen). Interestingly, in conditions of oxidative stress related to production of ROS, loss of membrane cholesterol is associated to the activation of the pro-survival receptor TrkA, whereas addition of cholesterol in non-stressed condition inhibit receptor activation and favors stress (Iannilli et al., 2011). Cholesterol overload can decrease cell survival and TrkB signaling (Huang et al., 2016). Thus, changes in cholesterol content might be a way to regulate receptor activity towards cell surviving pathways, acting as a sensor of the cell state. Altogether, cholesterol level seems to be precisely regulated to favor cell survival, within a physiological range of concentration.

General functions of cholesterol in neurons

Overall, cholesterol has many essential functions in the cell, in the CNS, it has particularly major functions in neurons. Cholesterol is an essential structural component for integration of intracellular signaling through the organization of the plasma membrane in microdomains like lipid rafts. It is a major component of the myelin, important for a proper conductance of action potentials. It also regulates the dynamic of synaptic vesicle biogenesis and vesicle fusion. Moreover, cholesterol domains on vesicles participate to the proper transport of vesicles along microtubules (***Figure 25***).

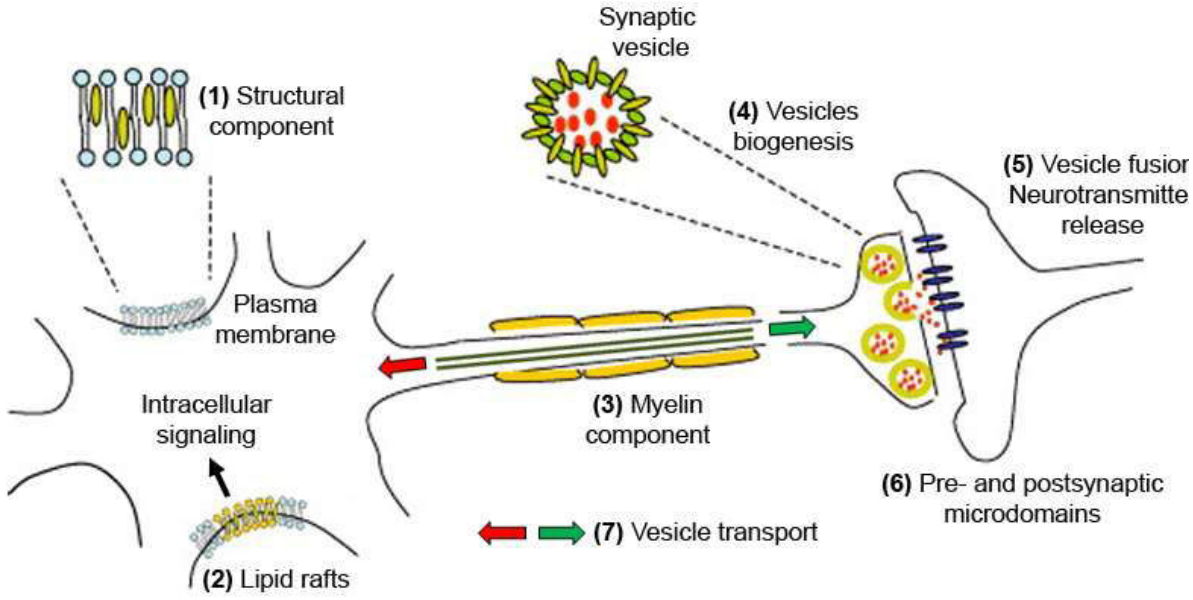

Figure 25. Cholesterol functions in neurons. Cholesterol (yellow ovals) is a major structural component of membranes **(1)**, essential for their structure and organization. It can be concentrated in microdomains in the plasma membranes, also referred to as lipid rafts **(2)**, which participate to the organization of intracellular signaling triggered by different neurotrophic factors and their receptors. Up to 70% of the brain cholesterol is found in the myelin **(3)** surrounding axons. Cholesterol plays a crucial role for vesicles biogenesis **(4)** and for vesicles fusion **(5)**, essential for an optimal neurotransmitter release neurotransmitter release. It is also important to maintain pre- and postsynaptic microdomains **(6)**, in order to organize the signal transduction after binding of neurotransmitters to their receptors. Cholesterol domains on vesicles also participates to the transport of vesicles along microtubules **(7)**. (Valenza and Cattaneo, 2006)

Chapter 3 - Impairment of cholesterol metabolism in neurodegenerative diseases

As seen previously, cholesterol metabolism is tightly regulated and is involved in many essential cellular processes. Therefore, dysregulations of this metabolism will have serious consequences in the brain. During the last decade, a growing number of evidences have implicated impairment of cholesterol metabolism in neurodegenerative diseases.

Cholesterol and ageing

To understand pathological modification of cholesterol metabolism, we should look at its content evolution during normal aging. An age dependent loss of cholesterol was described in the human brain. However, alterations in the amount of cholesterol are highly variable during aging, ranging from no change to a 40% decrease (Söderberg et al., 1990). On average, cholesterol decreases by 47% in women and 53% in men, with a significant loss of myelin lipids (Svennerholm et al., 1997). Cholesterol loss is more pronounced in the white matter than in the cerebral cortex (Svennerholm et al., 1991). Cholesterol synthesis rate declines with aging in the human hippocampus, with lower concentration of lanosterol and desmosterol precursors in elderly subjects (Thelen et al., 2006). In the aging rat brain, there is also a decreased synthesis with altered expression of gene related to cholesterol synthesis (Blalock et al., 2003). In the aging rat hippocampus, lanosterol, desmosterol and lathosterol are decreased, whereas in the cortex only desmosterol is decreased over time (Smiljanic et al., 2013). Age dependent loss of cholesterol was also described in the mouse hippocampus (Martin et al., 2008; Sodero et al., 2011a) and is associated to a cognitive decline (Martin et al., 2014). Regarding 24S-OHC, the major catabolism product of cholesterol, its plasma levels are very high in children, then decreases to become constant in the adult life and tend to increase in more advanced ages (Bretillon et al., 2000a). The exact causes of this loss are not yet clear but some mechanisms have been proposed. An increase of transcriptional activation (Ohyama et al., 2006) and membrane mobilization (Sodero et al., 2012) of CYP46A1 could participate to cholesterol loss during aging. Indeed, CYP46A1 increases in high stress situations, accumulation of cellular stress over time could thus favor cholesterol loss in aging. The age-dependent lowering of cholesterol may also be due to reduced synthesis or impaired delivery from glial cells.

Cholesterol metabolism in neurodegenerative diseases

Some neurodegenerative diseases related to cholesterol metabolism alterations are caused by direct mutations on genes implicated in cholesterol homeostasis and are associated to severe brain development defects. The Smith-Lemli-Optiz syndrome (SLOS) is due to a mutation on *dhcr7* gene, causing a defect of cholesterol synthesis (Nowaczyk and Irons, 2012). Desmosterolosis is also due to a

defect of cholesterol synthesis, with a mutation on *dhcr24* gene (Zolotushko et al., 2011). The Niemann-Pick type C (NPC) disorder is caused by a defect of cholesterol intracellular trafficking, due to a mutation on either NPC1 (95% of cases) or NPC2 (5% of cases) (Zech et al., 2013).

Sporadic neurodegenerative diseases also show impairment of cholesterol metabolism. In Parkinson's disease, there are evidence linking α-synuclein aggregation to cholesterol levels, and in patients, 24S-OHC levels in cerebrospinal fluid (CSF) correlate to the disease duration (Doria et al., 2016). Cholesterol dependence of Muller glial cells in the retina has been implicated in glaucoma and macular degeneration (Lakk et al., 2018). Moreover, oxysterol signature can impact age related macular degeneration (Lin et al., 2018a).

Extensive studies have focused on the role of cholesterol in Alzheimer's disease. Cholesterol turnover is involved in APP (amyloid precursor protein) processing at the membrane and modification of cholesterol levels can influence Aβ formation (Allinquant et al., 2014). Interestingly, oxysterols levels are altered in Alzheimer's disease, with decrease of 24S-OHC and increase of 25-OHC and 27-OHC in patients' brain, which could be linked to neuroinflammation (Testa et al., 2016). Moreover, the ε4 allele of *apoe* gene is more frequent in Alzheimer's patients and is associated to an increased mean age of onset (Farrer et al., 1997). Recent studies showed that expression of ApoE4 causes molecular and cellular alterations associated to Alzheimer's disease (Lin et al., 2018b) and is more potent in stimulating Aβ production than other isoforms (Huang et al., 2017).

Deregulation of cholesterol metabolism in Huntington's disease

An increasing number of studies have implicated dysregulations of cholesterol metabolism in HD (see ***Figure 26*** for references). Studies on rodent models, cell lines and data from patients' samples have shown a global down regulation of cholesterol metabolism. Levels of the precursors lathosterol and lanosterol are decreased in multiple models and in patients' plasma. This global alteration of cholesterol biosynthesis pathway could be caused by a decreased translocation of the transcription factor SREBP to the nucleus and a decreased expression and activity of synthesis enzymes. Especially, expression of enzymes such as HMGCR, CYP51, DHCR7 and DHCR24 are reduced in whole tissue extract and also specifically in astrocytes primary cultures, cells that are essential for cholesterol synthesis in the adult brain HD (***Figure 26***).

Studies of cholesterol content gave rise to more differential results, with decreased, increased or no changes in cholesterol levels in the brain of animal models; whereas studies in human post mortem caudate and putamen showed increased cholesterol levels (***Figure 26***). Interestingly, specific studies on cell cultures showed an accumulation of cholesterol in membranes due to an altered trafficking of

cholesterol by caveolin-1. The methodology used to measure cholesterol levels is critical to have reproducible data. A comparative study demonstrated that biochemical and mass spectrometry methods showed reduced cholesterol levels whereas colorimetric and enzymatic methods showed increased cholesterol levels. Colorimetric and enzymatic methods appear to have lower sensitivity, giving more variable results than analytical methods like gas chromatography-mass spectrometry. The method for sample preparation is also critical to have sensitive and reliable measures (Marullo et al., 2012).

The product of cholesterol degradation in the brain, 24S-OHC is decreased in the brain of several HD models and in patients' tissues. Interestingly, 24S-OHC levels are decreased in patients' plasma at early stages and correlates with caudate atrophy measured by MRI and to motor impairment (***Figure 26***). 24S-OHC seems to be an interesting biomarker for HD, however, it should be noted that peripheral factors can significantly modify its plasma levels like plasma lipoproteins turnover and the rate of excretion of oxysterols by the liver.

Cholesterol transport by astrocytes is less efficient in HD, with decreased expression of *apoe* and *abca1*. Astrocytes expressing mHTT produce and release less ApoE, impacting cholesterol transport to neurons (***Figure 26***). Reduced transport might be associated to a decreased activity of LXR. Indeed, in normal conditions, HTT acts as a co-activator for LXR transcription factors, therefore HTT mutation can potentially lead to a loss of function and thus a decreased LXR activity (Futter et al., 2009).

Of interest in HD, knock-out of PGC1α, which expression is altered by mHTT, causes a reduction of cholesterol synthesis and degradation and is associated to a defect of myelination. Especially, a knock-out of PGC1α in oligodendrocytes impact cholesterol biosynthetic pathway, by decreasing expression of HMGCS1 and HMGCR (***Figure 26***).

Alteration of cholesterol homeostasis	Event associated	Experimental model	Reference
Decreased cholesterol synthesis			
Altered transcription of cholesterol **biosynthesis enzymes**	Early transcriptional events	Striatal derived cells (67Q, 105Q, 118Q)	(Sipione et al., 2002)
Decreased **SREBP** nuclear translocation	Reduced SRE activity	• mHTT cell line ST14A • R6/2 mice	(Valenza et al., 2005)
Reduced mRNA levels of ***hmgcr, cyp51, dhcr7***	Decrease after glial differentiation	Astrocytes: R6/2, YAC128, HdhQ140/7 mice	(Valenza et al., 2010)(Valenza et al., 2015a)
Reduced expression of **DHCR24**	Decreased rate of cholesterol synthesis	• mHTT cell line ST14A • R6/2 mice	(Samara et al., 2014)
Reduced levels of **HMGCR, CYP51, DHCR7**	Decreased rate of cholesterol synthesis	R6/2 mice	(Valenza et al., 2005)
Reduced striatal levels of **lathosterol, lanosterol** (striatum, cortex, hippocampus)	Reduced expression and activity of HMGCR	R6/2 mice	(Valenza et al., 2007a)(Boussicault et al., 2016)
Reduced sterol content in myelin and synaptosomes	Early in synaptosomes, later in myelin	R6/2 mice	(Valenza et al., 2010)
• Early reduction of **lathosterol and lanosterol** in the cortex and the striatum • Increased **desmosterol** at late stages	Plausible reduced activity of DHCR7 and DHCR24 enzymes	R6/1 mice	(Kreilaus et al., 2015)
Reduced brain levels of **lanosterol, lathosterol** (early) and **desmosterol** (later)	• Reduced plasma levels: lathosterol, desmosterol • Reduced hmgcr activity	YAC128 mice	(Valenza et al., 2007b)
Reduced brain levels of **lathosterol**	CAG-dependent reduction in YAC mice	• YAC46, YAC72, YAC128 mice • HdhQ111/Q111 mice • HD transgenic rat	(Valenza et al., 2010)
Reduced brain levels of **lathosterol, zymosterol, stigmasterol**		HdhQ150	(Trushina et al., 2014)
• Reduction of **lathosterol** in the striatum (early) and cortex (late)	Reduced striatal mRNA levels for *hmgcr* and *fdft1*	Heterozygous zQ175 mice	(Shankaran et al., 2017)
Reduction of **lathosterol** content in the striatum and the cortex	CAG-dependent reduction in the striatum	Heterozygous Q80, Q111, Q175 mice	(Shankaran et al., 2017)
Reduced levels of **HMGCR, CYP51, DHCR7**	Decreased regulation of melanovate pathway	Human striatum, cortex post mortem tissues and fibroblasts	(Valenza et al., 2005)
Reduced capacity to activate **cholesterol biosynthesis**	Reduced levels of cholesterol	Human fibroblasts	(Valenza et al., 2005)
Decreased plasma **lathosterol** and **lanosterol**	Lathosterol at pre-symptomatic stages	Human plasma	(Leoni et al., 2011)
Increased **desmosterol, lathosterol, zymosterol, dihydrolanosterol**	Decreased DHCR24 protein levels	Human post mortem putamen	(Kreilaus et al., 2016)
Impairment of cholesterol levels			
Reduced total **cholesterol** content		• mHTT cell line ST14A • HdhQ140 primary neurons	(Valenza et al., 2005)(Ritch et al., 2012)
Reduced brain levels of **cholesterol**		• YAC72, YAC128 mice • HdhQ111 and HdhQ150 mice • HD transgenic rat	(Valenza et al., 2007b)(Valenza et al., 2010)(Trushina et al., 2014)
Reduction striatal levels of **cholesterol**	Decreased cholesterol synthesis rate per day	Heterozygous zQ175 mice	(Shankaran et al., 2017)
Reduced **cholesterol** levels	Striatum and cortex	Heterozygous Q80, Q175 mice	(Shankaran et al., 2017)
Reduced levels of **cholesterol** in the striatum	At 5 weeks and 10 weeks	R6/2 mice	(Valenza et al., 2005)
No changes of **cholesterol** levels in the brain		R6/2 mice	(Valenza et al., 2007a)
Increased **cholesterol** levels in the striatum		R6/2 mice	(Boussicault et al., 2016)
Accumulation of **cholesterol**	mHTT impairs caveolin-1 dependent endocytosis	YAC72 (brain and primary striatal neurons)	(Trushina et al., 2006)
	Increase caveolin-1 levels and excitotoxicity	Primary striatal neurons and cell lines from HdhQ111 mice	(del Toro et al., 2010)

Accumulation of **cholesterol**	mHTT binds caveolin-1 and impair cholesterol exit from the Golgi	Primary striatal neurons from HdhQ150 mice	(Trushina et al., 2014)
Increased levels of **cholesterol** and cholesterol esters	SIRT2 regulates sterols biosynthesis	Striatal neurons infected with lentiviral Htt171-82Q	(Luthi-Carter et al., 2010)
No changes of plasmatic **cholesterol**		Human plasma	(Leoni et al., 2008)
Decreased plasma **cholesterol**	At very late stages	Human plasma	(Leoni et al., 2011)
Increased total **cholesterol** in the caudate	Important neuronal loss	Human post mortem tissues	(del Toro et al., 2010)
Increased total **cholesterol** in the putamen		Human post mortem tissues	(Kreilaus et al., 2016)
Decreased cholesterol degradation			
Decreased **CYP46A1** expression	Decreased cholesterol turnover	• R6/2 mice • STHdhQ111/Q111 cells • Human putamen	(Boussicault et al., 2016)
Decreased **CYP46A1** expression	Decreased protein levels but not mRNA	Human post mortem tissues	(Kreilaus et al., 2016)
Impairment of oxysterols levels			
Reduction of striatal **24S-OHC and 27-OHC**	At late stages	R6/1 mice	(Kreilaus et al., 2015)
No changes of **24S-OHC** levels in the brain		R6/2 mice	(Valenza et al., 2007a)
Reduced brain levels of **24S-OHC**		• YAC46, YAC72, YAC128 mice • HdhQ111/Q111 mice • HD transgenic rat	(Valenza et al., 2007b)(Valenza et al., 2010)
Decreased levels of **24S-OHC** in the striatum (early) and in the cortex (late)	Decreased 24S-OHC synthesis rate per day	Heterozygous zQ175 mice	(Shankaran et al., 2017)
• Reduction of plasma **24S-OHC** • Reduction of **24S-OHC** (striatum and cortex)	Reduction not CAG-dependent	Heterozygous Q80, Q111, Q175 mice	(Shankaran et al., 2017)
Reduced levels of **24S-OHC**	Specifically, in the caudate and the putamen	Human post-mortem tissues	(Kreilaus et al., 2016)
Increased levels of **27-OHC, 7β-OH, 7-keto cholesterol**	Specifically, in the caudate		
Decreased levels of **24S-OHC**	Correlates with caudate atrophy	Human plasma	(Leoni et al., 2008, 2013)
Decreased levels of **24S-OHC** and **27-OHC**	27-OHC: pre-symptomatic	Human plasma	(Leoni et al., 2011)
Impairment of cholesterol transport			
• Reduced genes expression ***abca1*** and ***apoe*** • Reduced **ApoE secretion** by HD astrocytes • Smaller ApoE-containing-lipoproteins in CSF	• Reduced cholesterol transport • Reduced ApoE lipidation	• Primary astrocytes (YAC128 mice) • YAC128 mice	(Valenza et al., 2010)
Reduced **ApoE production** and release by astrocytes	Reduced cholesterol in the medium	HdhQ140/7, HdhQ50/7, HdhQ111/7, R6/2	(Valenza et al., 2015a)
Cholesterol in mitochondrial membranes is altered			
Decreased cholesterol levels in mitochondrial membranes	Increased mitochondrial membrane fluidity	BACHD rats	(Eckmann et al., 2014)
• Increased mitochondrial conjugated cholesterol in the striatum • Decreased cholesterol/phospholipid ratio	Decreased membrane fluidity	Rats 3-NP treated	(Mehrotra et al., 2015)
PGC1α regulates cholesterol metabolism			
PGC1α KO: Reduced brain levels of **cholesterol, lathosterol, lanosterol, desmosterol and 7-DHC, 24S-OHC and 27-OHC**	Reduced expression of **MBP, HMGCS1, HMGCR**	PGC1α KO mice	(Xiang et al., 2011)
	Reduced expression of MBP, HMGCS1, HMGCR	Primary rat oligodendrocytes knocked-down for PGC1α	
	Decrease of PGC1α and its targets: MBP, HMGCS1, HMGCR	mHTT in primary oligodendrocytes	

Figure 26. Impairment of cholesterol metabolism in HD models and patients. Rodent models in purple, cell cultures in orange and human samples in blue. Decreased levels are in red, increased levels in green.

Cellular consequences of altered cholesterol metabolism in Huntington's disease

Altered cholesterol metabolism can have deleterious impacts at several levels. Modification of cholesterol content and dynamics can impact membranes fluidity and the distribution of microdomains. The study of peripheral cells from HD patients showed an alteration of membrane properties and fluidity related to differences in cholesterol and phospholipid content (Muratore, 2013). Higher number of ordered domains was observed in mHTT expressing neurons, suggesting that cholesterol accumulation is associated to increased amount of lipid rafts. This is accompanied by an increased localization of NMDA-R in the cholesterol enriched domains, thus altering NMDA-R distribution; potentially contributing to NMDA mediated excitotoxicity. Moreover, administration of cholesterol lowering drugs such as simvastatin and β-cyclodextrin protected against NMDA mediated excitotoxicity (del Toro et al., 2010). Cholesterol can also influence HTT binding and aggregation to membranes, with decreased HTT insertion as cholesterol content increases (Gao et al., 2016).

Aberrant interaction between mHTT and caveolin-1 impairs the intracellular trafficking of cholesterol, leading to cholesterol accumulation in the Golgi and in lysosomes. This accumulation could impact the normal function of the Golgi apparatus and lysosomes, contributing to cellular toxicity. Interestingly, loss of caveolin-1 in HdhQ150 mouse model was able to rescue cholesterol trafficking and motor decline in these mice (Trushina et al., 2006, 2014).

A proper supply of cholesterol is critical for neurite outgrowth, synapses and dendrites formation and axonal guidance (Fester et al., 2009; Goritz et al., 2005). Cholesterol depletion leads to a decreased synaptic plasticity and neurite degeneration caused by a neurodegenerative break of neurofilaments integrity (Koudinov and Koudinova, 2005). Moreover, targeting cholesterol synthesis by inhibition of HMGCR causes neurite loss by interfering with the melanovate pathway (Schulz et al., 2004). At late stages in R6/2 mice, cholesterol content is decreased in myelin, highlighting a potential link between cholesterol impairment and myelin defects in HD (Valenza et al., 2010). Since cholesterol in myelin is critical for an efficient transmission of action potential, this defect could impair the neuronal transmission. Thus, a global alteration of cholesterol metabolism can affect the neurotransmission.

Studies showed that mHTT decreased mitochondrial membranes fluidity in *STHdh* cells, in isolated mitochondria from HD knock-in mice and BACHD rat, while mitochondrial cholesterol levels were decreased only in BACHD rats (Eckmann et al., 2014). The authors concluded that cholesterol levels might not be the major determinant of membrane fluidity changes found in mitochondria isolated from different HD models.

Overall, altered cholesterol metabolism is associated to a decreased cell survival and re-establishment of normal cholesterol levels is often neuroprotective. Several strategies have been addressed to modulate cholesterol metabolism and content in order to improve cell survival in HD. For example, addition of cholesterol rescues the cell death induced by mHTT in transfected cells (Valenza et al., 2005) and partially alleviates HD phenotype in a mouse model (Valenza et al., 2015b). In another cellular model where cholesterol level was increased by mHTT, inhibition of sirtuin 2 decreased nuclear trafficking of SREBP-2, cholesterol synthesis and protected from mHTT toxicity (Luthi-Carter et al., 2010). Even addition of cholesterol precursors lanosterol and desmosterol are neuroprotective *in vitro* on neuronal models of HD (Boussicault et al., 2016), showing a global need to compensate for impaired cholesterol metabolism even through cholesterol precursors.

Chapter 4 - CYP46A1, the rate limiting enzyme for cholesterol degradation in the central nervous system

Dysregulation of cholesterol metabolism is well described in HD. Most of the studies have focused on sterols, oxysterols and cholesterogenic enzymes. Despite its important role in cholesterol turnover in the brain, CYP46A1 was not studied in HD. In this chapter, we will focus on CYP46A1 function, regulation and its key position in cholesterol homeostasis. Since targeting cholesterol metabolism in HD can be an interesting therapeutic strategy for a global compensation of HD cellular dysfunctions, it is important to have a better understanding of CYP46A1 functions.

CYP46A1 function

Cholesterol 24-hydroxylase or CYP46A1 is an enzyme that converts cholesterol into 24S-OHC in a reaction requiring NADPH, allowing the addition of an hydroxyl group to the lateral hydrocarbon chain of cholesterol (***Figure 27***) (Dhar et al., 1973; Dzeletovic et al., 1995). This conversion allows the crossing of the BBB, thus the elimination of cholesterol. *In vivo* formation of 24S-OHC was detected in human (Lütjohann et al., 1996), rats (Breuer and Björkhem, 1995) and mice (Meaney et al., 2000). CYP46A1 is responsible for 99% of 24S-OHC in the brain, which account for 60 to 80% of 24S-OHC in the serum (Lund et al., 2003). According to the continuous flux of 24S-OHC in the serum (Lütjohann et al., 1996), cholesterol turnover in the brain by CYP46A1 appear like a daily mechanism, that could account for a daily turnover of 20% in certain neurons (Dietschy and Turley, 2004). To a lesser extent, CYP46A1 can also catalyze the formation of 25-hydroxycholesterol, 24,25-dihydroxycholesterol and 24,27-dihydroxycholesterol (Lund et al., 1999; Mast et al., 2003).

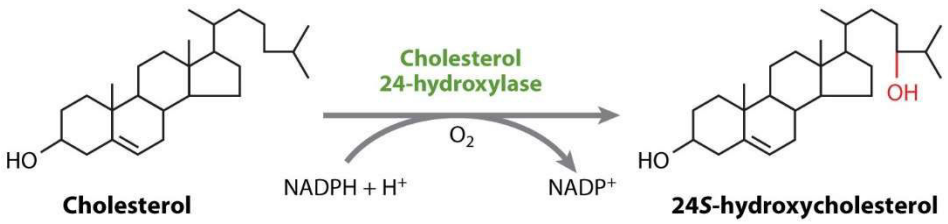

Figure 27. Reaction catalyzed by Cholesterol 24-hydroxylase (CYP46A1). (Russell et al., 2009)

Transcriptional regulation of CYP46A1

Cyp46a1 gene is located on human chromosome 14q32.1 and contains 15 exons (Lund et al., 1999). It has no canonical TATA or CAAT boxes and has a high number or GC, a usual feature of housekeeping genes (Ohyama et al., 2006). The Sp family of transcription factors is involved in the transcriptional control of human *cyp46a1* (***Figure 28***). Binding of Sp3 and Sp4 to GC-boxes is essential for a high activity of the promoter (Milagre et al., 2008). During neuronal differentiation, a shift of Sp factors recruitment at *cyp46a1* promoter occurs with an increase of (Sp3+Sp4)/Sp1 ratio, which might account for CYP46A1 neuronal expression (Milagre et al., 2012a). Interestingly, during neuronal differentiation CYP46A1 levels increases whereas CYP27A1 decreases, suggesting a shift towards a CYP46A1-mediated catabolic pathway in mature neurons (Milagre et al., 2012b). Epigenetic regulations are involved in the control of *cyp46a1* expression. The demethylating agent DAC (5'-Aza-2'-deoxycytidine) and the histone deacetylase inhibitor TSA (trichostatin A) can induce *cyp46a1* expression (***Figure 28***). DAC represses Sp1 and Sp3 expression, decreases Sp3 binding and favors the dissociation of histone deacetylase (HDAC) 1 and 2. However, the effect of DAC does not depend on *cyp46a1* promoter methylation status (Milagre et al., 2010). TSA causes a transient histone hyperacetylation, affecting Sp binding to the promoter, favoring HDAC dissociation (Nunes et al., 2010). Overall, decreased Sp3 binding is associated to an increased transcription of *cyp46a1*. Sp3 is associated to ERK1/2, and upon TSA treatment ERK1/2 phosphorylation decreases, diminishing Sp3 binding. Inhibition of MEK1 (mitogen activated protein kinase 1), the kinase upstream ERK1/2, potentiate TSA effect, consistent with the hypothesis of increased *cyp46a1* transcription after ERK1/2 dephosphorylation (Nunes et al., 2012). Mice acutely treated with TSA had significant increase of *cyp46a1* mRNA in the brain whereas chronic treatment did not affect mRNA levels. Injection of valproic acid (an histone deacetylase inhibitor) also increased *cyp46a1* mRNA (Shafaati et al., 2009).

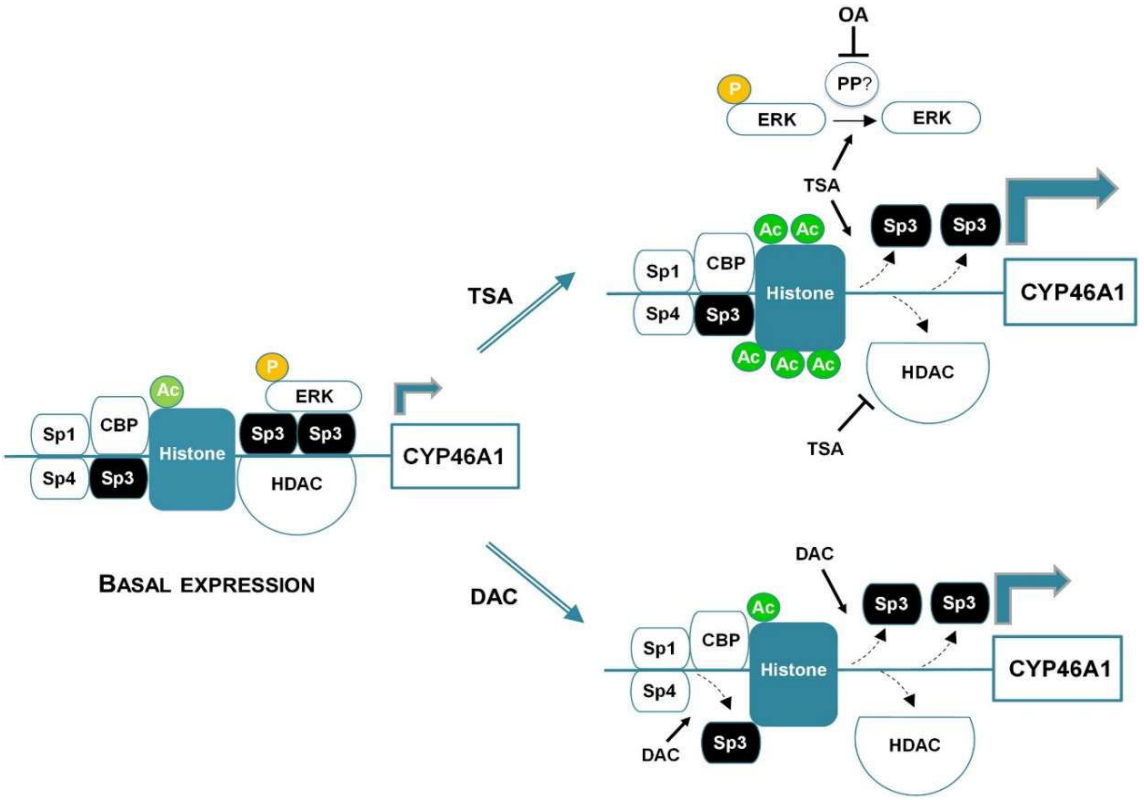

Figure 28. CYP46A1 transcriptional activation. CYP46A1 transcription is significantly increased after DAC and TSA treatment. TSA increases histone acetylation and release HDAC, in a process that is favored by decreased binding of Sp3 to the promoter. TSA effect depends on decreased activation of ERK1/2 signals and Sp3 phosphorylation. Impairment of Sp3 dephosphorylation with okadaic acid (OA), presumably by inhibiting a protein phosphatase (PP) impairs TSA effect. DAC treatment also leads to the reduced binding of Sp3 to the promoter and the detachment of HDAC. (Moutinho et al., 2016a)

CYP46A1 expression and localization

CYP46A1 is mostly expressed in neurons of the brain and the retina (Bretillon et al., 2007; Lund et al., 1999). Small amounts of mRNAs were detected in the mouse testis and liver, without apparent translation in the testis and very low expression in the liver (Lund et al., 1999). Extensive study of CYP46A1 mRNA expression in human tissues confirmed the preferential expression in the brain (Nishimura et al., 2003). Expression is lower during the development and gradually increases from 9 days in the mouse and 1.5 years in humans (Lund et al., 1999), which can correlate with the accumulation of cholesterol during the brain development. CYP46A1 is distributed throughout the cell body and dendrites of multiples type of neurons where it is embedded in the membrane of the smooth endoplasmic reticulum (***Figure 29***). It is highly expressed in pyramidal neurons of the hippocampus and cortex, in Purkinje cells of the cerebellum, in hippocampal and cerebellar interneurons (Ramirez et al., 2008). CYP46A1 sub-cellular localization seems to be dynamic, indeed, upon neuronal excitation it is mobilized from the endoplasmic reticulum to the membrane to locally decrease cholesterol and release 24S-OHC (Sodero et al., 2012).

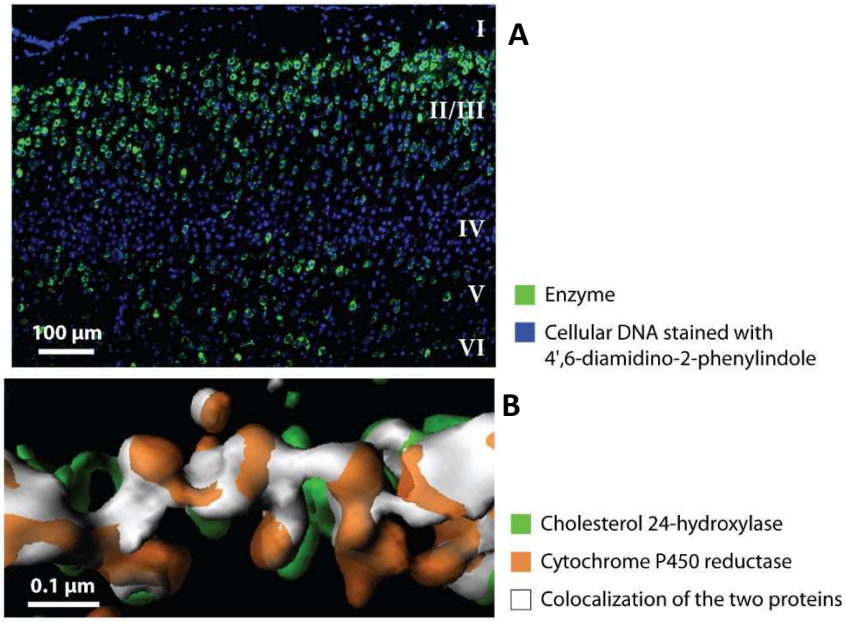

Figure 29. CYP46A1 localization **(A)** Wild-type mouse cortical section showing expression of CYP46A1 (in green) in pyramidal neurons of layers II/III, V, and VI. **(B)** 3D reconstruction of a dendrite from primary cortical neuron showing CYP46A1 staining and cytochrome P450 reductase (marker of the endoplasmic reticulum) colocalization in the endoplasmic reticulum. (Russell et al., 2009)

CYP46A1 structure and activity modulation

CYP46A1 is a 53 kDa protein with 500 amino acids and belongs to the cytochrome P450 family. The protein sequence is highly conserved among vertebrate, with 95% identity between the mouse and human orthologues (Lund et al., 1999). The N and C terminus of the protein are highly conserved; and out of the twenty-two amino acids that are different from the mouse enzyme, twenty are concentrated on one side of the protein (***Figure 30***). A specific poly-proline sequence is found at the C-terminus of the protein in mammals, this type of motif are often binding sites for protein interaction that could play an important role in CYP46A1 function (Zarrinpar et al., 2003). The first three dimensional description of the protein was reported in 2008 (Mast et al., 2008; White et al., 2008), showing a primary sequence formed of 12 α-helices and 4 β-pleated sheets with an heme prosthetic group between two α-helices (***Figure 30***). Identification of the crystal structure of the protein showed a structural flexibility of the protein, allowing the binding of different compounds. *In vitro* studies identified phenacetin, 4'-(2-hydroxyethoxy)-acetanilide and acetaminophen as activators; clobenpropit, thioperamide, and tranylcypromine as inhibitors (Mast et al., 2008). An antifungal drug, voriconazole, was identified as an efficient *in vitro* and *in vivo* inhibitor of CYP46A1, with decreased cholesterol, 24S-OHC and HMGCR mRNA levels (Shafaati et al., 2010). Amongst marketed drug, fluvoxamine was identified as an inhibitor of CYP46A1 *in vitro* (Mast et al., 2012). The anti-HIV marketed drug efavirenz, can activate CYP46A1 activity through a specific allosteric site. However, at high concentration, efavirenz inhibits CYP46A1 activation. *In vitro* and *in vivo* studies showed that at low concentration, efavirenz lead to increased cholesterol turnover, without modifying cholesterol levels (Anderson et al., 2016; Mast et al., 2014).

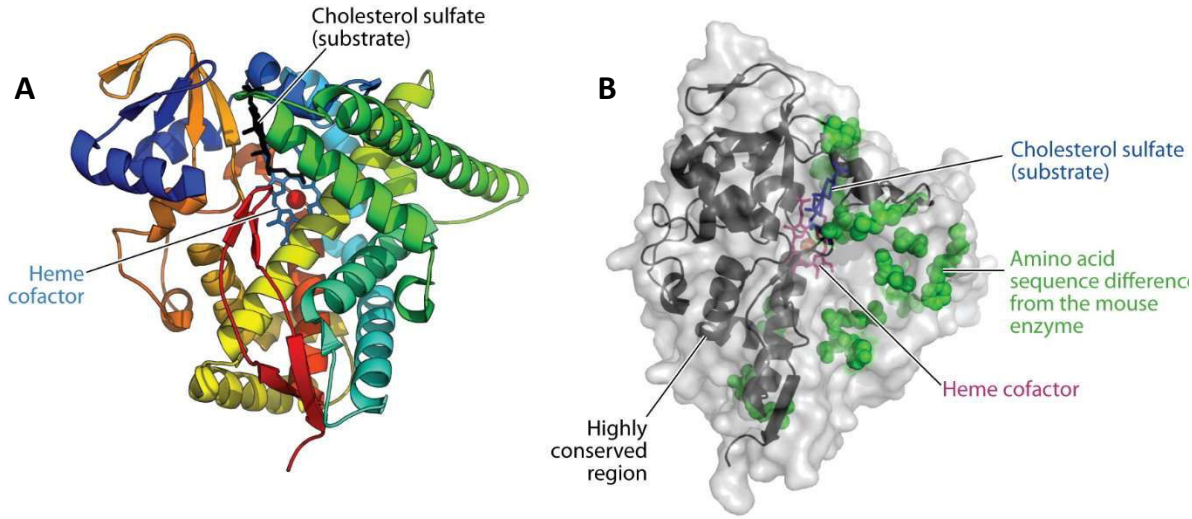

Figure 30. CYP46A1 structure. **(A)** Structure of the human enzyme, determined by X-ray crystallography. Twelve α-helices and four β-pleated sheets are shown together with the heme cofactor and a cholesterol sulfate substrate. **(B)** Surface representation of the human enzyme. In green: amino acids different from the mouse enzyme. Gray ribbons: highly conserved N and C terminus. (Russell et al., 2009)

CYP46A1 role in brain homeostasis and function

To have a better understanding of CYP46A1 function, a knock-out mouse model was generated (*cyp46a1* -/-). In this model, brain cholesterol levels are unchanged but cholesterol synthesis is reduced by 40%, potentially to compensate for the lack of degradation, showing the importance of CYP46A1 in cholesterol turnover (Lund et al., 2003). *Cyp46a1* -/- mice present severe cognitive deficiency, with impairment of spatial, associative and motor learning, associated to deficiency to establishing long term potentiation (LTP) in the hippocampus. The effects on LTP were reversed by treatment with geranylgeraniol, a precursor of cholesterol from the melanovate pathway, but not by adding cholesterol (Kotti et al., 2006). Geranylgeraniol acts rapidly during LTP, just before electrical stimulation and 15 min after. These experiments showed the importance of cholesterol turnover, with a specific and quick action of the melanovate pathway for LTP in the hippocampus (Kotti et al., 2008). 24S-OHC is almost absent from the brain of *cyp46a1* -/- mice and is not replaced by other oxysterols, even if small amounts of 22R-, 24R, 25- and (25R),26-hydroxycholesterol were detected (Meljon et al., 2014). In the brain of *cyp46a1* -/- mice, a compensatory upregulation mechanism takes place on pathways related to cholesterol storage and cholesterol removal, independent from CYP46A1, along with upregulations of some LXR targets such as *abca1*. The phosphorylation level of many proteins is altered in the brain of these mice, including GTPase proteins (RAB8, CDC42, RAC), microtubules associated and neurofilaments proteins (MAP and NEF) and proteins involved in synaptic vesicles and neurotransmission (SLCs, SHANKs). Moreover, protein ubiquitination is increased in proteins important for cognition, cytoskeleton function and energy production (Mast et al., 2017a).

Because of the role of CYP46A1 in the brain, a transgenic mouse model overexpressing human CYP46A1 (C46-HA) was also established to explore the regulatory mechanisms dependent on CYP46A1 function. Production of 24S-OHC was strongly increased (four to seven fold), however, despite the known function of 24S-OHC as an activator of LXR, expression of LXR target genes was not changed (Shafaati et al., 2011). Cholesterol synthesis was enhanced in the brain of these mice, with higher levels of lanosterol, consistent with increased cholesterol turnover by CYP46A1. Interestingly, the C46-HA transgenic mice showed improvement of spatial memory with increased levels of proteins involved in neurotransmission: PSD-95, synapsin-1, synaptophysin, GluN1 and phosphorylated GluN2A subunit of NMDA-R (Maioli et al., 2013). Decreased membrane cholesterol by CYP46A1 in neurons also increases isoprenoid synthesis and small guanosine triphosphate-binding proteins (sGTPase) prenylation *in vitro*. CYP46A1 overexpression *in vitro* increased HMGCR activity and membrane levels of sGTPase Rac1, Cdc42, Rab8 and RhoA, along with a specific increase of RhoA activity. This increase in membrane sGTPases is also observed *in vivo*, in transgenic C46-HA mice (Moutinho et al., 2015). CYP46A1 overexpression increases neuronal dendritic outgrowth and protrusion density *in vitro*, associated to an enhancement of synaptic proteins in synaptosomal fractions. Interestingly, these effects are dependent on geranylgeranyl transferase-I (GGTase-I) activity. Reduction of cholesterol content by CYP46A1 is the trigger for increased phosphorylation of Trk receptor, Trk receptor interaction with GGTase-I, which allows GGTase-I activity. Indeed, GGTase-I is activated through direct interaction with TrkB after BDNF activation. These results were replicated *in vivo*, with an increase of p-Trk and synaptic proteins in synaptosomal fractions prepared from CYP46A1 transgenic mouse cortex (Moutinho et al., 2016b). Overall, CYP46A1 has an essential role in synaptic functions by stimulating cholesterol turnover, particularly through the melanovate pathway.

CYP46A1 and neurodegenerative diseases

Because of its pivotal role in cholesterol metabolism, it can be expected that CYP46A1 dysregulations are associated to brain disorders. Indeed, in the last years, evidences have linked CYP46A1 to neurological disorders.

Levels of 24S-OHC, which are directly correlated to CYP46A1 activity, are changed in several neurodegenerative diseases: Parkinson's disease (Björkhem et al., 2013), Alzheimer's disease (Bretillon et al., 2000b; Lütjohann et al., 2000; Schönknecht et al., 2002), multiple sclerosis (Teunissen et al., 2003), Huntington's disease (Leoni et al., 2013) and dementia (Kölsch et al., 2004). These studies highlight the involvement of cholesterol homeostasis imbalance in neurodegenerative diseases. Moreover, the integrity of the BBB should also be considered when 24S-OHC measures are performed

in the context of brain diseases, the ratio between 24S-OHC and 27-OHC in the CSF can be an interesting way to access the barrier integrity (Leoni et al., 2003).

Some studies have linked CYP46A1 polymorphism to cognitive decline (Fu et al., 2009; Lai et al., 2014), and others have been interested in CYP46A1 polymorphism in Alzheimer's disease (AD). However, association between genetic variant of CYP46A1 and AD are not all consistent. Several studies showed an association between an intronic polymorphism on *cyp46a1* gene with increased risk of AD (He et al., 2012; Johansson et al., 2004; Kölsch et al., 2002; Papassotiropoulos et al., 2003). Other studies have failed to establish a link between AD and CYP46A1 polymorphism (Chalmers et al., 2004; Desai et al., 2002; Tedde et al., 2006). Interestingly, a meta-analysis showed that the particular polymorphism (rs4900442) was associated with a higher risk of developing AD in the Chinese population but not in the Caucasian population (Jia et al., 2016), thus difference between populations could explain the discrepancy between the different studies. In brain tissue from AD patients CYP46A1 pattern of expression is changed with a selective expression around amyloid plaques and in astrocytes, whereas neuronal expression is decreased (Bogdanovic et al., 2001).

Because of these links between CYP46A1 and neurodegenerative diseases, therapeutic strategies have been explored. In AD models, a gene delivery approach in the hippocampus showed reduced amyloid pathology in APP23 mice (Hudry et al., 2010); reduced cognitive deficits, improved LTP and spine density in THY-Tau22 mice (Burlot et al., 2015). In opposition, silencing of *cyp46a1* in the hippocampus of wild-type mice led to cholesterol accumulation, neuronal loss and cognitive deficits; and in APP23 mice amyloid-β production was increased along with a higher neuronal death upon *cyp46a1* silencing (Djelti et al., 2015). Moreover, silencing of *cyp46a1* in mice hippocampus induced epileptic seizures paralleled by neuronal death (Chali et al., 2015). However, crossing *cyp46a1* knock out mice with APP/PS1 AD mice model did not affect amyloid formation but increased mice lifespan (Halford and Russell, 2009). Difference in cholesterol levels may account for these different phenotypes, since silencing of *cyp46a1* increased cholesterol in the hippocampus, whereas *cyp46a1* knock out did not exhibit changes in cholesterol levels. Other works support the idea that increasing cholesterol levels by inhibiting CYP46A1 might be a strategy against AD. It was suggested that cholesterol loss enhance the formation of amyloid peptides (Abad-Rodriguez et al., 2004) and that pharmacological inhibition of CYP46A1 could improve cognition in APP transgenic mice (Uto, 2015). Contrarily to this idea, pharmacological activation of CYP46A1 by efavirenz in AD mice models reduced amyloid formation, microglial activation, improved memory and decreased mortality rate (Mast et al., 2017b). Some controversy appears in CYP46A1 potential role in AD, however, it is clear that targeting cholesterol turnover through CYP46A1 can dramatically impact AD.

In pathological contexts, CYP46A1 pattern of expression is altered, especially with decreased neuronal expression and increase astrocytic expression. Traumatic brain injuries induce CYP46A1 expression in glial cells, associated to an increased LXR activity, potentially acting as a mechanism to remove damaged cell membranes (Cartagena et al., 2008; Smiljanic et al., 2010). When CYP46A1 is specifically expressed in cultured astrocytes, the glutamate transporter EAAT2 is dissociated from lipid rafts, disrupting its function on glutamate uptake, a common feature of neurodegenerative diseases (Tian et al., 2010). Moreover, hippocampal injury triggered by kainic acid induces an increased expression of CYP46A1 in astrocytes (He et al., 2006).

CYP46A1 is also involved to retinal disorders. Indeed, CYP46A1 polymorphism have been associated to an increased risk of primary open angle glaucoma (Fourgeux et al., 2009). After a retinal stress caused by intraocular pressure, CYP46A1 expression is temporarily increased, as an early response to retinal stress (Fourgeux et al., 2012). Interestingly, pharmacological inhibition of CYP46A1 by voriconazol strongly impaired retinal functions and activated retinal glial cells (Fourgeux et al., 2014).

In HD, CYP46A1 expression is decreased in the post mortem putamen of patients and the striatum of R6/2 mouse model (Boussicault et al., 2016; Kreilaus et al., 2016). A recent strategy of gene therapy delivery of CYP46A1 in the striatum of R6/2 mice allowed an improvement of neuronal atrophy, decrease of aggregates and improved locomotor behavior (Boussicault et al., 2016). This study showed a potential role for CYP46A1-mediated neuroprotection in HD.

CYP46A1 and signaling pathways

Modulation of CYP46A1 expression or activity can impact signaling pathways at different levels. As seen previously, the knock-out and transgenic models for CYP46A1 showed its critical role in cholesterol turnover and neuronal function, through a regulation of cholesterol precursors (***Figure 31***). Indeed, isoprenoids are essential for the activity of small GTPases, which play a crucial role in neuronal development (Govek et al., 2005), neuronal migration (Govek et al., 2011), dendritic spine formation and maintenance, neurite outgrowth and axon guidance (Hall and Lalli, 2010).

The primary effect of CYP46A1 is cholesterol clearance, which in specific contexts participates to cell signaling and homeostatic responses to excitotoxicity (***Figure 31***). Aging hippocampal neurons undergo a progressive cholesterol loss in membranes, mediated by CYP46A1 increased expression and translocation, which is associated to an increased phosphorylation and activation of TrkB receptors, triggering a pro-survival signaling pathway (Martin et al., 2011b). CYP46A1-mediated cholesterol loss is up-regulated upon stress, including glutamatergic excitatory neurotransmission (Sodero et al., 2011b). Moreover, upon glutamatergic stimulation, CYP46A1 is mobilized from the

endoplasmic reticulum to the plasma membrane, leading to fast and transient cholesterol loss. This process requires high levels of calcium and functioning stromal interaction molecule 2 (STIM2) an endoplasmic reticulum calcium sensing protein (Sodero et al., 2012). Reduction of cholesterol levels was also shown to protect from NMDA-induced neuronal death, probably by reducing the association of NMDA receptors to lipid rafts (Ponce et al., 2008).

We also need to consider the direct effects of the product of cholesterol degradation by CYP46A1 (***Figure 31***). Indeed, 24S-OHC is an allosteric modulator of NMDA receptors and participates to synaptic plasticity by enhancing NMDA-R mediated LTP (Paul et al., 2013) and by enhancing synaptic vesicle cycling (Kasimov et al., 2017). Moreover, 24S-OHC is an endogenous ligand of LXRs (Lehmann et al., 1997), and could thus activate the transcription of genes involved in lipid metabolism (Ulven et al., 2005) and modulation of inflammation (Ito et al., 2015). Interestingly, *in vitro* treatment with 24S-OHC is able to decrease amyloid-β production by inhibiting intracellular trafficking of APP, showing a potential protective role of 24S-OHC in Alzheimer's disease (Brown et al., 2004; Urano et al., 2013). The direct effect of 24S-OHC on cell survival has been studied. At high concentration, 24S-OHC can induce cell death *in vitro* on neuroblastoma cells and cortical neurons (Yamanaka et al., 2011). However, 24S-OHC toxic effect might be an indirect result of its esterification by ACAT1 (Shibuya et al., 2016; Yamanaka et al., 2014), forming atypical lipid droplets (Takabe et al., 2016). 24S-OHC seems to protect against toxicity mediated by another cholesterol oxidation product, 7-ketocholesterol, by a mechanism dependent on LXR activation (Okabe et al., 2013). If more 24S-OHC is generated, it is likely that it will be converted to some extent by CYP39A1 (expressed mostly in the liver but also in the brain) into 7α,24S-dihydroxycholesterol (Li-Hawkins et al., 2000). Although not tested, it is potentially a ligand of EBI2, which is important for adaptive immune response (Hannedouche et al., 2011).

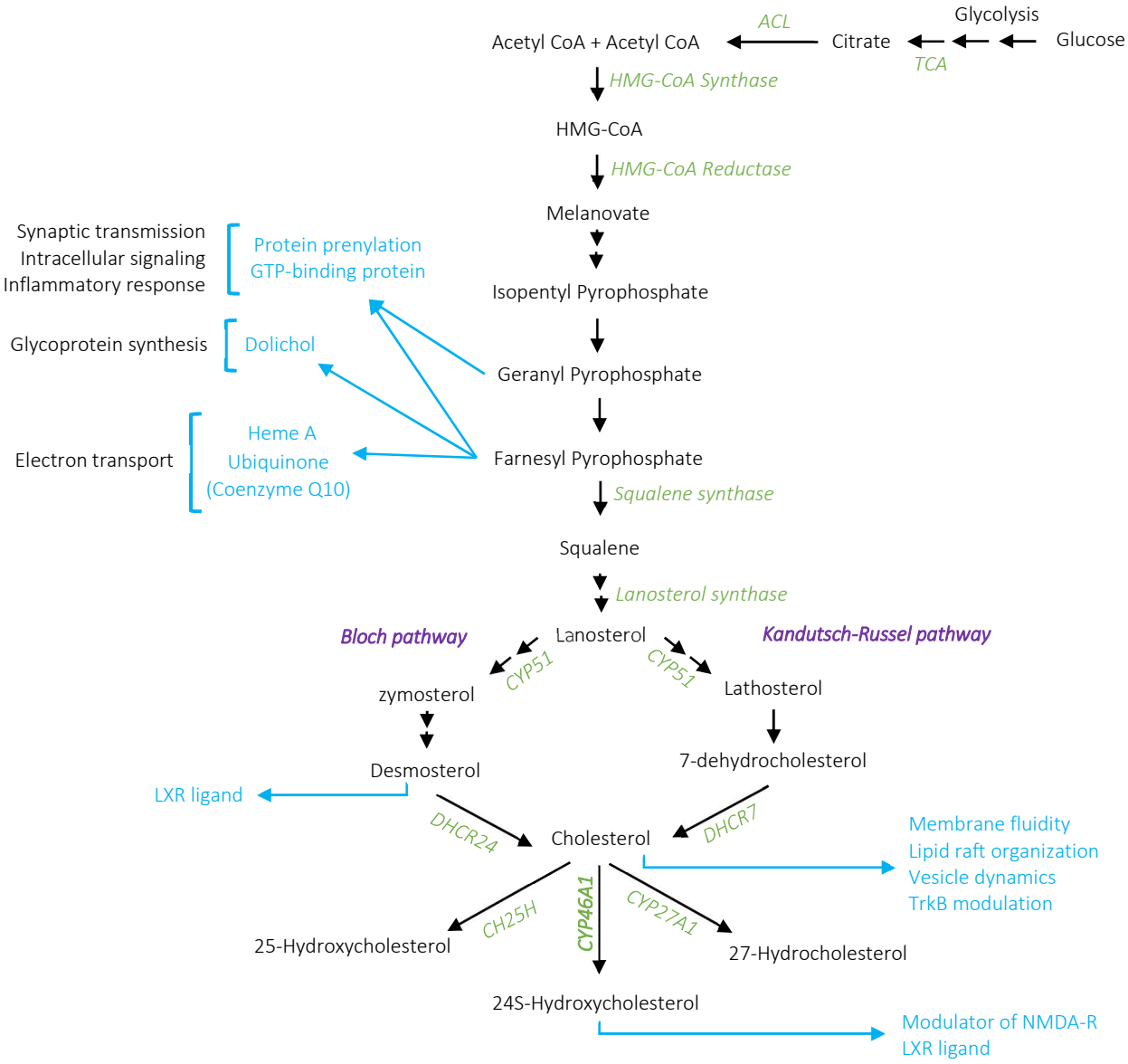

Figure 31. Cholesterol metabolism and regulation of cellular processes. A modulation of cholesterol metabolism can impact cellular processes at different levels. Precursors from the melanovate pathway are involved in protein prenylation, production of dolichol, heme A and Ubiquinone. Cholesterol itself participate to membranes fluidity, organization of lipid rafts, vesicles dynamics and decreased cholesterol by CYP46A1 is involved in TrkB activation. The 24S-hydroxycholesterol is an allosteric modulator of NMDA receptors and a ligand for LXR. ACL: ATP citrate lyase, TCA: tricarboxylic acid cycle, CH25H: Cholesterol 25 hydroxylase, CYP51: lanosterol 14 alpha-demethylase, DHCR7: 7-dehydrocholesterol reductase, DHCR24: 24-dehydrocholesterol reductase, CY46A1: cholesterol 24-hydroxylase.

HYPOTHESIS AND OBJECTIVES

Huntington's disease has a complex physiopathology including transcriptional dysregulations, lack of trophic support, impairment of autophagy, altered neurotransmission, mitochondrial dysfunctions, myelination defects… And in the last years, decreased cholesterol metabolism was described in Huntington's disease. Cholesterol, as a structural component but also through its complex metabolism, is implicated in several critical cellular processes. Interestingly, the enzyme for cholesterol conversion into 24S-OHC, CYP46A1, appears like a key protein in cholesterol metabolism and was recently shown to be decreased in Huntington's disease. Therefore, restoring cholesterol homeostasis could be an interesting strategy to compensate for the dysregulations observed in Huntington's disease. To do so, the team focused on the enzyme CYP46A1 and established a gene therapy strategy to restore CYP46A1 on models of Huntington's disease. The strategy is based on the expression of CYP46A1 using an adenovirus associated AAVrh10, with a neuronal tropism to conserve the neuronal expression of CYP46A1. This strategy was used on the R6/2 mouse model with a single injection in the striatum prior to the motor phenotype. A neuroprotective effect of CYP46A1 in R6/2 mice was described with an improvement of motor behavior, decreased aggregates and increased cholesterol metabolism (Boussicault et al., 2016). However, the mechanism involved in CYP46A1 remained to be explored. The purpose of my thesis was to study these neuroprotective mechanisms in a knock-in mouse model of Huntington's disease, the zQ175. This model has the advantage of being closer to the genetic context of the pathology, with a more progressive development of the phenotype. First, we needed to verify if the neuroprotective effects were conserved in this model by testing the motor behavior and the evolution of the neuropathological landmarks such as neuronal atrophy and aggregates. This analysis is particularly relevant in the context of a gene therapy with a unique injection of the virus, to check if the positive effects of the transgene are prolonged over time. To explore the molecular and cellular mechanisms involved in CYP46A1-mediated neuroprotective effect, we realized a large-scale analysis of the zQ175 transcriptome by RNAseq, to highlight relevant pathways involved in CYP46A1-mediated neuroprotection. This study led us to study the synaptic connectivity, vesicular transport and autophagy mechanisms in this model after CYP46A1 gene therapy.

Moreover, to go deeper into the understanding of CYP46A1 restoration on the global effect on Huntington's disease, we needed to consider the compartmentalization of cholesterol metabolism in the brain. Indeed, CYP46A1 is expressed in neurons, whereas in the adult brain the synthesis in mainly realized in astrocytes, with a tight communication between these two-cell population to adjust cholesterol metabolism to supply or decrease cholesterol. So, the second part of my thesis was focused on establishing a protocol to separate neurons and astrocyte to study the specific regulations

in these cell types. To do so, a protocol of cell sorting was set up to isolate these cells based on specific fluorescence. Thus, the mice were injected with a specific astrocytic virus expressing the dtTomato fluorophore along with the CYP46A1 neuronal virus associated to a GFP fluorescent neuronal virus. The protocol was approved for cell viability and RNA integrity after cell sorting. The objective is to study the transcriptomic regulations using RNAseq and the lipidomic regulation by GC-MS. Expectedly, we should observe a specific pattern of regulation in these two cell types, first related to cholesterol metabolism but also on other pathways related for instance to autophagy and proteasome which are known to be more efficient in astrocytes, also potentially related to LXR anti-inflammatory responses in astrocytes, and in neurons pathways involved in the synaptic connectivity.

Altogether, this study will give us more insights into the role of cholesterol metabolism in a neurodegenerative disease like Huntington's disease and into the potential role of CYP46A1 as a therapeutic strategy for Huntington's disease.

RESULTS

Paper 1 – CYP46A1 gene therapy deciphers the role of brain cholesterol metabolism in Huntington's disease

CYP46A1 gene therapy deciphers the role of brain cholesterol metabolism in Huntington's disease

Radhia Kacher[1], Antonin Lamazière[2], Nicolas Heck[1], Vincent Kappes[1], Coline Mounier[1], Gaëtan Despres[2], Yulia Dembitskaya[3], Elodie Perrin[3], Wilhelm Christaller[4], Satish Sasidharan Nair[5], Valérie Messent[6], Nathalie Cartier[7], Peter Vanhoutte[1], Laurent Venance[3], Frédéric Saudou[4], Christian Néri[5], Jocelyne Caboche[1,8], Sandrine Betuing[1,8]

Affiliations

1. Neuroscience Paris Seine, Institut de Biologie Paris-Seine, CNRS UMR 8246/INSERM U1130., Sorbonne Université, Paris, France.
2. LBM, CNRS UMR7203/INSERM U1157, Sorbonne Université, Faculté de Médecine, AP-HP, Hôpital Saint Antoine, Département PM2, Paris, France.
3. Center for Interdisciplinary Research in Biology, College de France, CNRS UMR7241/INSERM U1050, MemoLife Labex Paris, France
4. Université Grenoble Alpes, Grenoble Institut des Neurosciences, INSERM U1216, CHU Grenoble Alpes, 38000 Grenoble, France.
5. Sorbonne Université, Centre National de la Recherche Scientifique, Research Unit Biology of Adaptation and Aging (B2A), Team Compensation in Neurodegenerative and Aging (Brain-C), F-75252, Paris, France.
6. Neuroplasticity of Reproductive Behaviors, Sorbonne Université, CNRS, INSERM, Neurosciences Paris Seine, Institut de Biologie Paris Seine, Faculté des Sciences et Ingénierie, INSERM/UMR-S 1130, CNRS/UMR 8246, 75005 Paris, France.
7. Biotherapies for neurodegenerative diseases, Institut du Cerveau et de la Moelle (ICM) INSERM Sorbonne Université, Paris, France.
8. Senior authors, equal contribution.

Corresponding Author and lead contact: Dr Jocelyne Caboche, jocelyne.caboche@upmc.fr

Abstract

Huntington's disease (HD) is a fatal autosomal dominant neurodegenerative disease caused by an abnormal CAG expansion in huntingtin's gene. Among the multiple cellular and molecular dysfunctions caused by this mutation, altered brain cholesterol homeostasis has been described in patients and animal models as a critical event in HD. However, how changes in cholesterol metabolism can influence HD pathogenesis is yet to be understood. Here we demonstrate that a gene therapy approach based on the delivery of CYP46A1, the rate-limiting enzyme for cholesterol degradation in the brain, has a long-lasting neuroprotective effect in HD and counteracts multiple detrimental effects of the mutated huntingtin. In zQ175 HD knock-in mice, CYP46A1 prevented neuronal dysfunctions and restored cholesterol homeostasis. These events were associated to a specific striatal transcriptomic signature that compensates for multiple mHTT-induced dysfunctions. We thus explored the mechanisms underlying these compensations and showed an improvement of synaptic activity and connectivity along with the stimulation of the proteasome and autophagy machineries, which participate to the clearance of mHTT aggregates. Furthermore, BDNF vesicle axonal transport and TrkB receptor endosome trafficking were restored in a cellular model of HD. These results highlight the large-scale beneficial effect of restoring cholesterol homeostasis in neurodegenerative diseases and give new opportunities for developing innovative disease-modifying strategies in HD.

Introduction

Huntington's disease is a devastating neurodegenerative disorder, with autosomal dominant heritance, onset in young adults, and a combination of neuropsychiatric, motor and cognitive symptoms (Aylward *et al.*, 2000). The disease is caused by a mono-allelic mutation, an abnormal expansion of CAG trinucleotide repeats, in *HTT*, the gene that encodes the huntingtin protein (HTT) (MacDonald *et al.*, 1993). It results in a progressive and predominant atrophy in the striatum and the cerebral cortex. Mutant HTT protein (mHTT) as well as the loss of HTT activity, results in multiple cellular and molecular dysfunctions, including gene dysregulation (Moumné *et al.*, 2013), alteration of energy metabolism (Cui *et al.*, 2006; Tsunemi *et al.*, 2012), cholesterol homeostasis (Karasinska and Hayden, 2011; Valenza and Cattaneo, 2011), synaptogenesis (Milnerwood and Raymond, 2010), axonal growth (Li *et al.*, 2001), BDNF synthesis (Zuccato *et al.*, 2003) and transport (Gauthier *et al.*, 2004), TkrB receptor trafficking (Liot *et al.*, 2013) and clearance of unfolded proteins (Martinez-Vicente *et al.*, 2010; Wong and Holzbaur, 2014).

Despite these intense discoveries about the pathogenesis of Huntington's disease, there is yet an important challenge to identify Huntington's disease modifying strategies that could be used to delay the onset and progression of Huntington's disease. Recently, disturbances of cholesterol homeostasis have been discovered in patients and Huntington's disease mouse models (Karasinska and Hayden, 2011; Valenza and Cattaneo, 2011), raising the interesting possibility that targeting cholesterol metabolism could be a promising therapeutic strategy in Huntington's disease. However, how changes in cholesterol metabolism influence the pathogenesis of Huntington's disease remains to be fully understood.

A proper balance of cholesterol metabolism is a key feature for the central nervous system (CNS) physiology since it plays an essential role in many neurobiological processes including synaptogenesis, axonal growth and dendrite maintenance (Heacock *et al.*, 1984; Mauch *et al.*, 2001; Fan *et al.*, 2002; Pfrieger, 2003; Goritz *et al.*, 2005). The importance of brain cholesterol homeostasis is highlighted by the negative impact of genetic mutations affecting enzymes of this metabolic pathway, as observed in several neurodevelopmental and neurodegenerative diseases including Smith-Lemli-Opitz syndrome and Niemann-Pick Type C (Korade and Kenworthy, 2008). Brain cholesterol is synthesized *in situ*, primarily by astrocytes in the adult CNS since plasma cholesterol cannot cross the blood-brain-barrier (BBB) under physiological conditions. The major pathway for cholesterol catabolism is achieved by the neuronal cholesterol 24-hydroxylase enzyme (CYP46A1), leading to the conversion of cholesterol into 24 (*S*)-hydroxycholesterol (24S-OHC), a metabolite that can cross the brain-blood barrier, but also acts

locally in neural populations (including astrocytes and neurons) as a ligand of Liver X receptors (LXRs)-target genes (Lund *et al.*, 1999).

Cholesterol metabolism is significantly altered in Huntington's disease patients, animal models and cell lines, with decreased levels of enzymes involved in cholesterol biosynthesis, such as HMG-CoAR (3-hydroxy-3-methyl-glutaryl-coenzyme A reductase), CYP51 (lanosterol 14-a demethylase) and DHCR-7 (7-dehydrocholesterol reductase) along with decreased levels of cholesterol precursors lanosterol and lathosterol (Sipione *et al.*, 2002; Karasinska and Hayden, 2011; Valenza and Cattaneo, 2011; Leoni and Caccia, 2015; Boussicault *et al.*, 2016; Kreilaus *et al.*, 2016; Shankaran *et al.*, 2017). Early in the disease, levels of 24S-OHC are decreased in the plasma of Huntington's disease patients (Leoni *et al.*, 2008), paralleling the caudate atrophy (Leoni *et al.*, 2013). These alterations are associated with a striking reduction of CYP46A1 expression in the putamen of Huntington's disease patients and the striatum of the transgenic R6/2 mouse model (Boussicault *et al.*, 2016; Kreilaus *et al.*, 2016).

Here, we took advantage of the Huntington's disease knock-in mouse model zQ175, which recapitulates the human disease at the genetic level (Menalled *et al.*, 2012; Indersmitten *et al.*, 2015), to study in depth the mechanisms of CYP46A1-mediated neuronal protection. In these mice, a single administration of an AAV for CYP46A1 delivering in the striatum produced a global regulation of cholesterol metabolism and provided a long-lasting improvement of behavioral and neuronal dysfunctions. This regulation of cholesterol metabolism was associated to a specific transcriptomic signature, linked to a compensation of several deleterious effect of mHTT. Based on the data of this large-scale transcriptomic analysis, we unraveled the role of CYP46A1 and regulation of cholesterol metabolism in the improvement of synaptic connectivity and glutamatergic transmission, along with increased axonal and dendritic trafficking. We also report that sterols produced by CYP46A1 increase the clearance of mHTT aggregates through the proteasome and autophagy machineries. Collectively, our results provide new mechanisms by which brain cholesterol metabolism is regulated by CYP46A1 and opposes Huntington's disease detrimental defects, thus opening a novel therapeutic avenue. Given the pivotal role of cholesterol metabolism in the brain homeostasis and function, we speculate that this strategy could be successful in more prevalent neurodegenerative disorders, such as Alzheimer and Parkinson disease, in which cholesterol metabolism has been similarly implicated.

Materials and Methods

Experimental models

In all experiments, both males and females were used and the number of males of females was balanced in each group. Mice were housed in groups of 2 to 5 with access to food and water *ad libitum* and kept at a constant temperature (19-22 °C) and humidity (40-50%) on a 12:12 h light/dark cycle. All experimental procedures were performed in authorized establishments in strict accordance with the recommendations of the European Community (86/609/EEC) and the French National Committee (2010/63) for care and use of laboratory animals under the supervision of authorized investigators (permission (#01435.02 to J. Caboche and S. Betuing for zQ175 mouse studies and #91448 to S.Humbert for *Hdh*CAG$^{140/+}$ mouse studies). The local ethics committee approved the experiments.

zQ175 mice: zQ175 mice (B6J.129S1-*Htt*^{tm1Mfc}/190ChdiJ) were obtained from Jackson Laboratories. zQ175 mice express the human *Huntingtin* exon 1 sequence with a 190 CAG repeat tract, replacing the mouse *Huntingtin* exon 1. All mice used in the study were from the second offspring using Heterozygous mice for breading. Heterozygous, homozygous and wild type littermates were obtained and the genotype was verified by polymerase chain reaction (PCR) using genomic DNA extracted from tail and specific primers according to Jackson Laboratories recommendations (https://www.jax.org/strain/370476).

Hdh$^{CAG140/+}$ mice: *Hdh*$^{CAG140/+}$ knock-in mice are generated on a C57/BL6J background and express human *HTT* exon 1 sequence with 140 repeats of CAG. Regarding controlled crosses, wild type C57/BL6J or *Hdh*$^{CAG140/CAG140}$ male mice were mated for one night with wild type C57/BL6J female.

Production and stereotaxic injection of AAVrh10-GFP and AAVrh10-CYP46A1

All AAV vectors were produced and purified by Atlantic Gene therapies (Inserm U1089, Nantes, France). Viral constructs for AAVrh10-GFP and AAVrh10-CYP46A1-HA contain the expression cassette consisting of either the GFP or the human CYP46A1 sequence, driven by a CMV/β-actin hybrid promoter surrounded by inverted terminal repeats of AAV2. The mice were injected at 4 months at the following stereotaxic coordinates: 1 mm rostral to the bregma, 2 mm lateral to midline and 3.25mm ventral to the skull surface. For the behavioral studies a second group was injected at the following coordinates: 1.5 mm or 0.86 mm rostral to the bregma, 1.5 mm or 2 mm lateral to midline (respectively) and 3.25 mm ventral to the skull surface. The rate of injection was 0.2 µl/min with a total volume of 2 µl per striatum (equivalent to 3.10^9 genomic particles).

Animal behavior

All behavioral tests were performed blind of mouse genotypes and treatments. Mice were tested at 7, 8, 9 and 11 months, once a month for each test.

Rotarod performance: mice were tested over three consecutive days and each daily session included a 5-min training trial at 4 rpm on the rotarod apparatus. After 30 min of resting, mice were tested for three consecutive accelerating trials of 5 min each with a linear increasing speed from 4 to 45 rpm over a time period of 300s. The latency to fall from the rod was recorded for each trial. Mice remaining on the rod for more than 300 s were removed and their time scored as 300s. Data from the training trial were not included.

The locomotor activity was measured as the number of interruptions by the mouse of two adjacent beams in a circular corridor (Imetronic, Pessac, France), containing four infrared beams placed at every 90°. Spontaneous activity was recorded for 2 h.

The rearing frequency was measured as the number of interruptions by the mouse of upper beams in actimeter boxes (Imetronic, Pessac, France). Spontaneous rearing activity was recorded for 1h.

Immunohistochemistry

Mice were deeply anaesthetized by intraperitoneal injection of sodium pentobarbital 250 mg/kg (Sanofi). Intracardiac perfusion of 4% paraformaldehyde in 0.1 M Na2HPO4/NaH2PO4 buffer, pH 7.5 was performed and brains were post-fixed overnight in the same solution at 4°C. Coronal brain sections (30 µm) were done using a vibratome in 0.1 M Na2HPO4/NaH2PO4 buffer. Free-floating sections were permeabilized and blocked with 5% NGS (normal goat serum) 0,2% triton in TBS (Tris-Buffered Saline) for 2h at RT. For bassoon/GluR1 staining, sections were permeabilized for 15min with 0,5% triton in TBS, then incubated in the saturation solution (5% NGS in TBS). Sections were then incubated with primary antibodies in 5% NGS in TBS overnight. For immunofluorescence, sections were incubated in secondary antibodies in 1% NGS in TBS for 2h at RT. Sections were then incubated with Hoescht solution to stain nuclei and mounted under cover slips in ProLong Gold antifade reagent (ThermoFischer). A systematic evaluation of the transduced region was performed by GFP fluorescence or by hemagglutinin immunostaining (expression of CYP46A1 transgene). The primary antibodies used are the following: rat anti-HA (1:400; Sigma), rabbit anti-DARPP32 (1:500; SantaCruz) and mouse anti-HTT (EM48) (1:1000; Millipore), rabbit anti-SREBP2 (1:200, Abcam), mouse anti-bassoon (1:400, Abcam), rabbit anti-GluR1 (1:400, Millipore), rabbit anti-LC3 (1:400, Sigma), rabbit anti-ApoE (1:1000; Abcam), mouse anti-NeuN (1:500; Millipore), rabbit anti-VGLUT1 (1:400, a kind gift from Dr. S. El-Mestikawi), mouse anti p-ERK (1:500, cell signaling). The secondary antibodies used are

the following: anti-rat Alexa Fluor 488, anti-rabbit cy3, anti-mouse cy3, anti-mouse cy5 (all at 1:500, Jackson Laboratories).

Image acquisition and analysis

For immunohistochemistry, image stacks were taken using a confocal laser scanning microscope (SP5, Leica Microsystems), with a pinhole aperture set to 1 Airy unit. Stack of confocal images were done using a x40 oil objective, with a 1,6 µm z-interval (DARPP32 and EM48 analysis), or a x63 oil objective, with a 1 µm z-interval (SREBP2 and LC3 analysis). The excitation wavelength and emission range were 488 and 500-550nm for GFP and alexa-488, 561 and 570-620nm for cy3, 633 and 640-700nm for cy5. Laser intensity and detector gain were constant for all images of the same analysis. All images were done in the transduced area and all analyses were performed on maximum projection of confocal stack using Fiji software. For each analysis 3 to 5 mice were used (3 for homozygous groups and 5 for wild type and heterozygous groups). DARPP32-stained neurons were manually traced and SPN area was quantified using Fiji software. For each condition, 100 DARPP32 positive neurons were analyzed in two representative slices. For aggregates counting, 3 representative slices were analyzed per animal. EM48-stained images were segmented using the same global threshold and quantified using Fiji software. For SREBP2 analysis, 2 representative slices were analyzed per animal. A macro was created in Fiji software to locate the nuclei in the Hoechst channel and then to measure in the SREBP2 channel the fluorescence intensity into the nuclei. For LC3 quantification, in 2 representative slices per animal, a global threshold was defined for LC3 spots detection, and the number of these spots was counted using Fiji software. For the quantification of GluR1 and bassoon colocalization the density is the number of objects normalized for a cube of 10micron side and 4 image stacks of 60x60 micron size and 5-micron depth were taken in each hemisphere.

Cholesterol and oxysterol measurements

Cholesterol and oxysterol analysis was performed using 'gold standard' methods (79) in order to minimize the formation of autoxidation artefacts. Briefly, mouse striatal tissue samples were weighed and homogenized with a TissueLyser II apparatus (Qiagen) in a 500 ml solution containing butylated hydroxytoluene (BHT, 50 mg/ml) and EDTA (0.5 M). At this point, a mix of internal standards was added [epicoprostanol, 2H7-7-lathosterol, 2H6-desmosterol, 2H6-lanosterol and 2H7-24(R/S)-hydroxycholesterol] (Avanti Polar Lipids). Alkaline hydrolysis was performed under Ar using 0.35 M ethanolic KOH for 2h at room temperature (RT). After neutralization of the solution with phosphoric acid, sterols were extracted in chloroform. The lower phase was collected, dried under a stream of nitrogen and the residue was dissolved in toluene. Oxysterols were then separated from the cholesterol and its precursors on a 100 mg Isolute silica cartridge (Biotage); cholesterol was eluted in

0.5% propan-2-ol in hexane followed by oxysterols in 30% propan-2-ol in hexane. The sterol and oxysterol fractions were independently silylated with Regisil_ + 10% TMCS [bis(trimethylsilyl) trifluoroacetamide + 10% trimethylchlorosilane] (Regis technologies) as described previously (80). The trimethylsilylether derivatives of sterols and oxysterols were separated by gas chromatography (Hewlett-Packard 6890 series) in a medium polarity capillary column RTX-65 (65% diphenyl 35% dimethyl polysiloxane, length 30 m, diameter 0.32 mm, film thickness 0.25 mm; Restesk). The mass spectrometer (Agilent 5975 inert XL) in series with the gas chromatography was set up for detection of positive ions. Ions were produced in the electron impact mode at 70 eV. They were identified by the fragmentogram in the scanning mode and quantified by selective monitoring of the specific ions after normalization and calibration with the appropriate internal and external standards [epicoprostanol m/z 370, 2H7-7-lathosterol m/z 465, 2H6-desmosterol m/z 358, 2H6-lanosterol m/z 504, 2H7-24(R/S)-hydroxycholesterol m/z 553, cholesterol m/z 329, 7-lathosterol m/z, 7-dehydrocholesterol m/z 325, 8-dehydrocholesterol m/z 325, desmosterol m/z 343, lanosterol m/z 393 and 24(R/S)-hydroxycholesterol m/z 413].

RNA extraction and LightCycler real time polymerase chain reaction

Mice were perfused with ice cold PBS, the striata were rapidly extracted on ice and put on cryotubes to be snap frozen in liquid nitrogen and were stored at -80°C until RNA isolation. Samples were homogenized in QIAzol reagent (Qiagen) and RNA isolation was performed with miRNeasy Mini kit (Qiagen) according to manufacturer's instructions. RNA yields were measured using a NanoDrop 2000 (ThermoScientific). Reverse transcription was performed with RevertAid First Strand cDNA synthesis kit (ThermoScientific). Quantitative real-time PCR reactions were performed using LightCycler480 SYBR-Green I Master according to manufacturer's protocol and run on LightCycler480 (Roche Diagnostics). The cycle threshold values were calculated automatically by LightCycler480 SW 1.5 software with default parameters. Expression of hypoxanthine guanine phosphoribosyltransferase 1 (Hprt1) transcript was used to normalize the cDNA amount, all groups were then normalized to the wild type group. For primer sequences see the Supplementary material.

RNA-sequencing study

Messenger RNA isolation and sequencing. Mice were perfused with ice cold PBS, the striata were rapidly extracted on ice and put on cryotubes to be snap frozen in liquid nitrogen and were stored at -80°C until RNA isolation. Samples were homogenized in QIAzol reagent (Qiagen) and RNA isolation was performed with miRNeasy Mini kit (Qiagen) according to manufacturer's instructions. Each group, WT-GFP, HET-GFP and HET-CYP46A1, was composed of 5 mice. The preparation and sequencing of mRNA libraries was performed by the sequencing platform of the "Institut du Cerveau et de la Moelle" (ICM)

at the Pitié-Salpétrière hospital (Paris, France). Messenger RNA libraries were prepared using standard protocols from Illumina, using the kit Truseq Stranded mRNA LT (Illumina) and sequenced with the Illumina HiSeq Genome Analyzer.

Analysis of RNA-seq data. The raw sequencing reads were pre-processed in order to discard both adapter sequences and low-quality reads using the Trimmomatic. The filtered reads were then mapped to the mouse reference genome mm10 (UCSC 2013 release) by using HISAT2 (83). Read distribution were calculated by using the featureCounts tool (84). To generate the log fold-change values (LFC), we used DESeq2 available as an R package in Bioconductor (www.bioconductor.org). The ratio used to generate LFC values is the ratio between zQ175 mice injected with CYP46A1 and zQ175 mice injected with GFP and the ratio between zQ175 mice injected with GFP and wild-type mice injected with GFP. To generate the networks that describe the effects of mHtt expression in zQ175 mice compared to wild-type mice and that of CYP41A expression in zQ175 mice compared to untreated mice, we performed spectral decomposition of the RNA-seq signal (LFC values) against the probabilistic functional network Mousenet v2 as previously described (32, 85, 86). Briefly, this approach maps entire gene expression datasets onto Mousenet v2 in order to identify sub-networks of closely-deregulated genes, reducing the risk for false positives and false negatives in raw gene expression data and highlighting bio-topological essentiality and centrality in these data. To assess the specificity of the sub-networks generated by using spectral decomposition of the signal, we generated artificially-permuted datasets by randomly permuting the pairs of LFC values from the original LFC distribution. Under this scheme, the global distribution of LFC values in permuted datasets remains the same compared to the original data. The number of permuted genes was set from 10% to 100% by incremental step of 10%. For each permutation, we constructed the corresponding sub-networks and compared them to the original sub-networks by assessing the number of edges in common between original and permuted sub-networks. This permutation analyzes indicated that the sub-networks generated using Mousenet v2 for spectral decomposition of the signal are specific to the RNA-seq data sets analyzed herein (data, pt shown). To explore the biological content of the network signatures obtained for the effects of mHtt and CYP46A1 on gene expression, we used STRING (https://string-db.org/) analyzes (87) using high confidence settings (STRING confidence score > 0.7, 100 neighbors allowed on the first shell, information only from Data mining, Databases and Experiments), corresponding to the most informative GO annotations (Biological processes, KEGG pathways) as supported by a minimal number of nodes set to N > 9 and a P value < 10^{-6}. These analyzes were complemented with pubmed searches. These analyzes were also complemented by Connectivity-Map (CMap) 02 analysis (https://portals.broadinstitute.org/cmap/) (88). as performed for the red class (*de novo* effects) of genes specifically deregulated by CYP46A1 expression, using CMap scores and

guidelines for data interpretation. The class and mode of action of Cmap hits was assessed using the KEGG drug database (http://www.genome.jp/kegg/drug/).

Data availability. RNA-seq data obtained in the striatum of zQ175 mice are available at GEO: **GEOXXXX.**

Code availability. The source code developed for performing spectral decomposition of the signal (SDS), written using Python, is available upon email request to C.N. (christian.neri@inserm.fr).

Dendrite labeling, image acquisition for dendritic spines, 3D dendrite analysis and 3D measurements of synaptic elements density

Dendrite labeling. Dendrite spines were labeled in brain sections from perfused mice using the Diolistic technique. Briefly, 50 mg of tungsten beads were mixed with 3 mg of solid red DiI (3,3'-Dioctadecyloxacarbocyanine Perchlorate) dissolved in methylene chloride. Cartridges were obtained by coating the beads on the inner surface of a Teflon tube pretreated with polyvinylpyrrolidone. Helium gas pressure was applied with a genegun device to project the beads out of the cartridge onto the brain section. The beads were delivered through a 3-micron pore-size filter to avoid bead clusters. Then, the sections were kept in PBS at RT for at least 2h and mounted in Prolong Gold.

Image acquisition. Image stacks were taken using a confocal laser scanning microscope (SP5, Leica) equipped with a 1.4 NA objective (oil immersion, Leica) with a pinhole aperture set to 1 Airy unit, pixel size of 60 nm and z-step of 200 nm. The excitation wavelength and emission range were 561 and 570–620 nm for DiI. Metrology measurements were regularly performed using fluorescent beads to confirm proper laser alignment, laser power and field homogeneity using the ImageJ-based MetroloJ plugin. Deconvolution with experimental point spread function from fluorescent beads using a maximum likelihood estimation algorithm was performed with Huygens software (Scientific Volume Imaging).

Image analysis. Neuronstudio software was used to reconstruct the dendrite and detect dendritic spines. When necessary, manual correction was applied. Image analysis of synaptic markers was performed in 3D with the software ImageJ, using custom-written macros calling functions of the plugin 3DImageSuite. Image segmentation was based on 3D analysis of intensity distribution centered on local maxima. The segmentation output was an image in which all voxels of each object have a specific intensity value. Object-based co-localization was performed with segmented images, by computing the intensity values within 3D region of interest of objects of one channel in the other channel. For measurement of object density, an image mask was used to exclude regions corresponding to soma.

Brain slice preparation and patch-clamp recordings

Horizontal cortico-striatal brain slices (350 µm) were prepared from 6-7-month-old mice C57BL/6 (WT, WT injected bilaterally with GFP, zQ175 injected bilaterally with GFP in one hemisphere and GFP-CYP in the other hemisphere). Experiments were performed in accordance with the guidelines of the local animal welfare committee (Center for Interdisciplinary Research in Biology Ethics Committee) and the EU (directive 2010/63/EU). Animals were anaesthetized with isoflurane and decapitated. Then slices were prepared using 7000SM2 vibrating microtome (Campden Instruments, UK) in ice-cold solution (125 mM NaCl, 2.5 mM KCl, 25 mM glucose 25 mM NaHCO3, 1.25 mM NaH2PO4, 2 mM CaCl2, 1 mM MgCl2, 1 mM pyruvic acid, bubbled with 95% O2/5% CO2 and osmolarity adjusted to 295 ± 5 mOsm). Slices were incubated the same solution at 34°C for one hour and then kept at RT. The slices were then transferred to the recording chamber and continuously perfused with the same solution at 34°C. GFP-positive MSNs within GFP injection site were visualized and verified for the expression of GFP with LED excitation (470 nm, XLED1 X-Cite) under Olympus BX51WI microscope (Olympus, Rungis, France), with a 60x/1.00 water-immersion objective. For whole-cell recordings pipettes with 6-8 MΩ resistance were filled with the solution (in mM): 122 K-gluconate, 13 KCl, 10 HEPES, 10 phosphocreatine, 4 Mg-ATP, 0.3 Na-GTP, 0.3 EGTA (adjusted to pH 7.35 with KOH). Cellular excitability was measured in current-clamp mode by 500ms steps of current injections from -300 to +500 pA with step of 20 pA. Evoked and spontaneous excitatory postsynaptic currents (sEPSCs) were measure in presence of picrotoxin (50 µM). To assess the paired-pulse short-term plasticity we applied cortical stimulation with a bipolar electrode (Phymep, Paris, France) placed in layer 5 of the somatosensory cortex and applied stimulation at 25, 50, 100, 250, 500 ms ISI. Electrical stimulations were monophasic, at constant current (ISO-Flex stimulator, AMPI, Jerusalem, Israel). Currents were adjusted to evoke 50-200 pA EPSCs. The series resistance was usually <20 MΩ, and data were discarded if it changed by more than 20% during the recording. Signals were amplified using with EPC10-2 amplifiers (HEKA Elektronik, Lambrecht, Germany). All recordings were performed at 34°C, using a temperature control system (Bath-controller V, Luigs & Neumann, Ratingen, Germany) and slices were continuously perfused with extracellular solution, at a rate of 2 ml/min. Recordings were filtered at 10 kHz and sampled at 20 kHz, with the Patchmaster v2x32 program (HEKA Elektronik). Picrotoxin (50 µM) (Sigma) was dissolved in ethanol and then added in the external solution at a final concentration of ethanol of 0.01%.

Primary neuronal culture in microfluidic devices

Microfluidic fabrication. The microfluidic chambers were produced as previously described (81). The upper (cortical) and the synaptic chamber were coated with Poly-D-lysin (0.5mg/ml) while a mix of poly-D-lysin (0.5mg/ml) + laminin (10g/ml) was used to coat the lower (striatal) chamber. The coating

was performed overnight at 4°C. The microfluidic chambers were carefully washed 3 times with growing medium (Neurobasal medium supplemented with 2% B27, 2mM Glutamax, and 1% penicillin/streptomycin) and placed at 37°C before neurons were plated.

Primary neuronal culture. Cortical and striatal neurons were dissected from E15.5 *Hdh*$^{CAG140/+}$ mice embryos, then the neurons were chemically digested with a papain and cysteine, incubated with trypsin inhibitor solutions, and finally mechanically dissociated. Then, neurons were re-suspended in growing medium and then plated in the chamber with a final density of ~7000 cells/mm^2. After addition of growing medium in the synaptic chamber, cortical neurons were carefully plated in the upper chamber followed by striatal neurons in the lower chamber. Neurons were placed in the incubator for at least 3h, then all compartments were gently filled with growing medium.

Constructs, plasmids, and lentiviruses. Neurons were infected at early stages (DIV 0 to DIV 2) and for 48h with lentiviruses (LV) and adeno-associated viruses (AAV). For this study, we used the following constructs: LV.CMV.BDNF-mCh, LV.Syn.TrkB-mCh, AAVrh10-GFP and AAVrh10-CYP46A1-HA. The equivalent of 10^5 of LV particles and 10^9 of AAV particles were used to transduce the cortical or striatal neurons in their respective chambers.

Live-cell imaging. An inverted microscope (Axio Observer, Zeiss) coupled to a spinning-disk confocal system (CSU-W1-T3, Yokogawa) connected to wide field electron-multiplying CCD camera (ProEM$^+$1024, Princeton Instrument) was used to perform live-cell recordings. The cultures were maintained at 37 °C and 5% CO_2 all along the process. Images were taken every 200 ms for 30 s for BDNF-mCh and TrkB-mCh trafficking, using a ×63 oil-immersion objective (1.46 NA).

Kymograph analysis. KymoToolBox plugin for ImageJ (82) was used to generate the kymographs from live-cell video-acquisition of BDNF-mCh and TrkB-mCh vesicles traffic. BDNF-mCh and TrkB-mCh, kymographs were generated with a length of 100µm (x-axis) and a total time of 30s (y-axis), to extract the following parameters:

Anterograde velocity

$$\mathrm{Vma}(\mu\mathrm{m/s}) = \frac{\text{Anterograde Distance } (\mu\mathrm{m})}{\text{Time } (\mathrm{s})}$$

Retrograde velocity

$$\mathrm{Vmr}(\mu\mathrm{m/s}) = \frac{\text{Retrograde Distance } (\mu\mathrm{m})}{\text{Time } (\mathrm{s})}$$

Number of anterograde vesicles per 100 µm

$$\mathrm{Na} = \frac{\mathrm{na}}{\text{Axon length}(100\mu\mathrm{m})}$$

Number of retrograde vesicles per 100 µm

$$\mathrm{Nr} = \frac{\mathrm{nr}}{\text{Axon length}(100\mu\mathrm{m})}$$

Linear Flow Rate $\mathrm{Q}(\mu\,\mathrm{m/s}) = |\mathrm{Vma}| * \mathrm{na} + |\mathrm{Vmr}| * \mathrm{nr}$

Net Flux $\mathrm{D}(\mu\,\mathrm{m/s}) = \mathrm{Vma} * \mathrm{na} - \mathrm{Vmr} * \mathrm{nr}$

A minimum threshold of 0.12µm/s has been used to consider the vesicle motile. For each condition, at least 6 chambers from 3 independent cultures were used and a minimum of 40 axons or dendrites were analyzed (n = number of axons/dendrites).

Stimulation of cortical neurons, phospho-ERK immunostaining of striatal neurons, imaging and quantification. Cortical neurons were stimulated for 15 min at 37°C using Glycine/Strychnine solution (HEPES 25 mM pH 7.5, NaCl 124 mM, KCl 3 mM, $CaCl_2$ 2 mM, Glucose 10 mM, Glycine 200 µM, Strychnine 1 µM). Then, striatal neurons were fixed with a PFA/Sucrose solution (4%/4% in PBS) for 20 min at room temperature (RT), rinsed three times with PBS and incubated with a blocking solution (BSA 1%, normal goat serum 2%, Triton X-100 0.1%) for 1h at RT. Next, striatal neurons were incubated overnight at 4°C with primary antibodies directed against phospho-ERK (Cell Signaling, #9106, 1:400) and finally with the appropriate fluorescent secondary antibody for 1h at RT. Phospho-ERK immunostaining was imaged in the striatal chamber, using an inverted microscope (Axio Observer, Zeiss) connected to wide field electron-multiplying CCD camera (ProEM^{+}1024, Princeton Instrument) with a ×20 objective (0.8 NA). ImageJ software was used to count the number of pERK positive neurons. The percentage of pERK-positive neurons represent the total number of pERK positive neurons reported to the total number of neurons, determine by using a DAPI staining, this for each field. Each condition was tested using at least 2 chambers from 3 independent cultures. In each chamber, at least 3 fields were analyzed (n = number of fields).

Statistical analysis. For vesicles and endosomes trafficking, Mann and Whitney test was used.

Cultures of striatal neurons, transfection, sterol and inhibitors treatment and aggregate quantification

Primary striatal neurons were dissected from E14 embryos from pregnant Swiss mice (Janvier) as previously described (89, 90). At DIV7, transient transfection of striatal cells was performed with LipofectamineTM 2000 (Invitrogen). Green fluorescent protein (GFP)-tagged constructs encoding the first exon of human HTT containing 103 (103Q-HTT) continuous CAA or CAG repeats were provided by the Huntington's Disease Foundation Resource Bank, UCLA, USA. The human *cyp46A1* cDNA was tagged with the hemagglutinin (HA) epitope (CYP46A1-HA). Lanosterol or desmosterol (1 µM in dimethyl sulphoxide, Avanti Polar Lipids) was added for 48h in the cell culture medium just after transfection. Inhibitor treatment with chloroquine (30µM, Sigma) or MG132 (10µM, Sigma) was performed 24h after transfection and cells were fixed with 4% PFA 4% sucrose 24h after treatment. Cover slips were mounted using ProLong Gold antifade reagent with DAPI to stain the nuclei (ThermoFischer). Aggregates were manually quantified based on GFP fluorescence, using a fluorescence microscope (Leica, DM4000B) with a x40 objective.

Electron microscopy

Mice were overdosed with sodium pentobarbital and perfused transcardially with 0.9% saline solution followed by 4% paraformaldehyde (PFA) and 0.5% glutaraldehyde solution diluted in 0.1 M phosphate buffer pH 7.4 (PB; pH 7.4). The brains were removed from skull and post-fixed with the same fixative solution overnight at 4°C. Six coronal sections (50 µm thick) containing the striatum were cut using a vibratome (Leica VT1000S). Sections were post-fixed for 1h at RT in 2% osmium tetroxide diluted in PB, dehydrated and embedded with Epon 812 (Epoxy -Embedding Kit, Sigma Aldrich) between two silicone-coated glass slides. Dorsal striatum areas were selected mounted on supports constituted by gelatin capsules filled with polymerized resin. Then, ultrathin sections (70 nm) were cut and collected into copper mesh grids for observation. Observations were made in STEM mode in a Field Emission SEM GeminiSEM 500 (Zeiss) operating at 20kV with a 20-µm aperture. Transmitted electrons are collected in bright field mode with the STEM detector located beneath the sample.

Immunoblotting

Mouse tissues and striatal cells were homogenized as previously described (78). Primary antibody rabbit polyclonal anti-CYP46A1 (1:1000, Abcam), mouse monoclonal anti-b-tubulin (1:5000, Sigma), mouse monoclonal anti-MW1 (1:500, developmental studies hybridoma bank) were revealed with appropriate anti-mouse or anti-rabbit peroxidase conjugated secondary antibodies (1:5000, Dutscher) and the ECL chemiluminescent reaction (Pierce).

Statistical analysis

Statistical analysis was performed with GraphPad Prism 6 software. All data are represented as mean ±SEM. For behavioral studies, genotype and treatment effect were evaluated with a two-way ANOVA analysis with time and treatment as independent factors. For immunohistochemistry one-way ANOVA with Bonferroni correction was used, or when appropriate, two-way ANOVA with Bonferroni correction. Statistical significance for RNA quantification was evaluated using a one-way ANOVA followed by Tukey's *post hoc* test. Lipidomic experiments were analyzed using a multiple unpaired t-test corrected for multiple comparisons using the Holm-Sidak method. Multivariate data analysis (OPLS-DA) were achieved with SIMCA 15 software (Umetrics). For patch-clamp recordings, data were analyzed with custom made software in Python 3.0 and averaged in MS Excel (Microsoft, USA). sPSCs were identified using a semi-automated amplitude threshold-based detection software (Mini Analysis 6.0.7 Program, Synaptosoft, Fort Lee, NJ, USA) and were visually confirmed. Statistical analysis one- or three-way ANOVA test with Bonferroni's correction was performed as appropriate with Prism 5.02 software (San Diego, CA, USA).

Results

CYP46A1 improves behavioral and neuropathological phenotype in zQ175 mice

zQ175 is a knock-in mouse model of Huntington's disease with a humanized exon 1 containing an expansion of 190 CAG. This knock-in model, and more particularly zQ175 heterozygous mice, closely recapitulates the genetic context of Huntington's disease patients, where the mutation is mono-allelic. In these mice, behavioral and neuronal abnormalities appear more progressively than in transgenic mice, with robust motor abnormalities starting at 30 weeks (7-8 months) of age (Menalled *et al.*, 2012).

We compared cyp46a1 mRNA levels at 3, 7 and 12 months, in the striatum and cerebral cortex of zQ175 heterozygous (HET) and homozygous (HOMO), compared to WT mice (Figure S1A-I). While no significant difference was observed at 3 months (Figure S1A), we found a significant decrease of cyp46a1 mRNA levels in the striatum, but not in the cerebral cortex, of HET and HOMO mice, at 7 months of age (Figure S1B), along with a decrease of CYP46A1 protein in the striatum of these mice (Figure S1D). At 12 months, mRNA and protein levels significantly decreased in both striatum and cortex of HET and HOMO mice when compared to WT (Figure S1C, E, F).

In order to restore CYP46A1 expression levels in the striatum of zQ175 mice, we bilaterally injected AAVrh10 encoding CYP46A1 with an HA tag, in the striatum of 4-months-old zQ175 mice (Figure 1A), i.e. prior to the age-at-onset of behavioral alterations. As controls, we used WT and zQ175 (HET and HOMO) mice with bilateral injection of an AAVrh10 carrying a GFP transgene (WT-GFP; HET-GFP and HOMO-GFP). Cyp46a1 mRNA levels were rescued in CYP46A1-HA injected-mice (Figure S2A). Body weight loss, which is a progressive and characteristic symptom of Huntington's disease, was not rescued by CYP46A1 in HET- GFP and HOMO-GFP mice (Figure S3B-C). Motor performances were regularly assessed from 7- to 11 months (Figures B-G). Locomotor activity (Figure 1B-C), rearing (Figure 1D-E) and latency to fall in the rotarod test (Figure 1F-G) progressively declined in HET-GFP and HOMO-GFP mice when compared to WT-GFP mice. At 11 months of age, HET-GFP and HOMO-GFP mice exhibited a strong impairment in locomotor activity and rearing, which were restored by CYP46A1 (Figure 1B-E). In the rotarod test, CYP46A1 showed a trend towards improvement in HET mice and a significant restoration in HOMO mice (Figure 1F-G).

The neuropathological signature of Huntington's disease is a prominent striatal atrophy. It precedes neuronal loss and can be readily evaluated by measuring the surface area of DARPP32-expressing neurons, as DARPP32 is a marker of striatal projection neurons (SPNs). At 12 months of age, as compared to WT-GFP, HET- and HOMO-GFP neurons showed neuronal atrophy, as indicated by a smaller area of DARPP32 immunostaining in SPNs (Figure 1H-I). This atrophy was significantly improved

in HET-CYP- and HOMO-CYP- expressing neurons (Figure 1H-I). The presence of intracellular inclusions commonly consists in the accumulation of mHTT in aggregates, a hallmark of Huntington's disease. Aggregate numbers and areas were significantly reduced in HET- and HOMO-CYP mice when compared to HET- and HOMO-GFP mice (Figure 1J-K). Altogether these data demonstrate that CYP46A1 improves behavioral performance of zQ175 mice, and positively impacts on neuronal protection.

CYP46A1 regulates cholesterol homeostasis in zQ175 mice

Cholesterol metabolism was measured from WT-GFP, HET-GFP and HET-CYP46A1 mice at 12 months of age, after the behavioral experiments (Figure 2A-C). The specific sterol profile was altered in HET-GFP mice when compared to WT-GFP, and was improved in HET-CYP mice (Figure 2A-B). The score plot of OPLS-DA (Orthogonal Projections to Latent Structures-Discriminant Analysis) exhibited the segregation of the 3 groups of mice. Looking at the first component t1, HET-GFP mice were located in the left-hand panel at the opposite direction of WT-GFP and HET-CYP animals. The sterol biochemical signature of WT-GFP and HET-GFP showed a high degree of dissimilarity and CYP46A1 restored the cholesterol pathway to approximate WT phenotype (Figure 2A-B). Levels of lathosterol, which constitute a direct upstream sterol in the cholesterol biosynthesis pathway (Kandutsch-Russel pathway), were significantly reduced in HET-GFP when compared to WT-GFP mice and were restored by CYP46A1 (Figure 2C). In contrast, levels of lanosterol, the first tetracyclic sterol molecule of cholesterol pathway, were not different between HET-GFP and WT-GFP mice. Of interest, CYP46A1 induced a strong increase of lathosterol, desmosterol and lanosterol, the surrogate markers of cholesterol synthesis (Leoni and Caccia, 2014) (Figure 2C). We also studied the two main metabolites of cholesterol degradation and found that CYP46A1 increased levels of 24S-OHC, but not 27-OHC. In a striking contrast, the total cholesterol concentration was similar in WT-GFP, HET-GFP and HET-CYP mice.

We then studied the role of CYP46A1 in the cholesterogenic pathway at the transcriptional level. CYP46A1 restoration in HET mice lead to a significant increase of *Hmgcor*, *Fdft1*, *Cyp51*, *Dhcr24*, *Dhcr7* and *Apoe* mRNA levels, when compared to HET-GFP mice and lead to a trend of increase of *Srebp2* with no modification of the endogenous *Cyp46a1* (Figure 2D). We further examined nuclear expression levels of SREBP2, a key transcriptional factor which regulates several enzymes in the cholesterol pathway. In the striatum, the mean intensity in the nucleus was strongly decreased in HET-GFP mice compared to WT-GFP and CYP46A1 restored SREBP2 expression in the nucleus of heterozygous mice (Figure 2; E-F). This result is associated with an increase of the major cholesterol efflux protein, ApoE, which transports cholesterol from astrocytes to neurons (Figure S3).

CYP46A1 significantly modifies the striatal transcriptome and compensates for the effects of mHTT on mRNA levels in zQ175 mice

We hypothesized that neuroprotection mediated by CYP46A1 might reflect a global effect on transcription. Transcriptional dysregulation is a major event occurring early in Huntington's disease pathogenesis that underlies multiple neuronal dysfunction and neurodegeneration (Augood et al., 1996; Cha et al, 2000). In zQ175 mice, striatal gene deregulation is highly significant at 6-10 months of age, when these mice develop major symptoms. This notably translates in the CAG repeat- and age-dependent deregulation of several genes that are important to establish neuronal identity and to maintain synaptic transmission (Langfelder *et al.*, 2016). An RNA-seq study was performed in the striatum of 12-month old WT-GFP, HET-GFP and HET-CYP46A1 mice. Data were subjected to network-based analysis using spectral decomposition of RNA-seq signals (Tourette *et al.*, 2014) against MouseNet v2, followed by biological content analysis using STRING v10.5 analysis (https://string-db.org/) and complemented with testing for correlations with gene expression patterns of small compounds and drugs using Connectivity-Map (CMap) 02 analysis (see Methods). Interestingly, the gene expression network signature of HET-CYP46A1 mice showed that CYP46A1 expression significantly modified the striatal transcriptome of zQ175 mice (Figure 3, Table S4). Modification of gene transcription by CYP46A1 includes both genes down-regulations and up-regulations (Figure 3B, left and right panel respectively). First, CYP46A1 restored normal expression levels of striatal genes dysregulated by mHtt, including genes known to have a role in neurotransmission, synaptic activity and RNA processing (Figure 3B, upper panel: see green gene nodes). Second, CYP46A1 induced a strong up-regulation of genes associated with Toll-like receptor signaling, cytoskeleton dynamics and immune response, which might correspond to protective effects (Figure 3B: see yellow gene nodes, right panel) Finally, de novo up-regulation of genes associated with phagosome, proteasome and regulation of innate immune response was clearly induced by CYP46A1 (Figure 3B: see red gene nodes, right panel). To a lesser extent, de novo down-regulation of genes associated with small RNA metabolism and neuronal apoptosis was observed (Figure 3B: see red gene nodes, left panel). Pattern recognition using CMap 02 analysis indicated that the latter class of effects is related to cell protective compounds and drugs such as anti-inflammatory compound (Fisetin, Zomepirac), neuroprotective agents (Mitoxantrone, Antazoline), antioxidant (Esculetin), anti-depressive drugs (Pizotifen) as indicated by the top 50 highest ranked positively correlated small compounds and drugs (Milhaud *et al.*, 2003; Fox, 2006; Sarantos *et al.*, 2012; Wang *et al.*, 2012; Watanabe *et al.*, 2018) (Table S4). These results show that the protective effects of CYP46A1 on behavioral and cellular phenotypes may be associated with a better homeostasis of transcriptional regulation. Together, these data strongly suggest that CYP46A1 may tip the balance towards a proper expression of genes associated with neurotransmission in the

striatum, correcting for the alterations induced by mHTT expression, while potentially modifying autophagy and inflammation via regulators of innate immunity.

CYP46A1 improves cortico-striatal connectivity and synaptic transmission

The aforementioned data led us to explore the role of CYP46A1 in synaptic transmission and cortico-striatal connectivity. A proper supply of cholesterol is critical for neurite formation and maintenance of synapses (Heacock *et al.*, 1984; Mauch *et al.*, 2001) and dendritic spine degeneration, synaptic loss, altered neurotransmission occur early in Huntington's disease mouse models (Leoni and Caccia, 2015).

Dendritic spines were analyzed from striatal neurons in WT, HET and HOMO mice at 12 months (Figure 4A). Spine density was decreased in both HET-GFP and HOMO-GFP striatal neurons, with a density twice lower in HOMO-GFP mice when compared to WT-GFP (Figure 4B). CYP46A1 significantly restored spine density in both HET-CYP and HOMO-CYP mice, with a full restoration in HET-CYP mice (Figure 4B). Glutamatergic synapse density, measured using double immunolabeling of Bassoon (a marker of the active presynaptic zone), and the post-synaptic receptor GluR1 (an AMPA glutamatergic receptor subunit expressed in SPN) (Figure 4C), was strongly decreased in HET-GFP and HOMO-GFP mice at 7 months of age (Figure 4D) and restored by CYP46A1 (Figure 4D). Density of boutons from cortical afferents, immunolabeled with vesicular transporter of glutamate 1 (VGLUT1), remained unchanged in HET-GFP and HOMO-GFP mice, including upon CYP46A1 treatment (Figure S5 A-B). However, the number of presynaptic boutons (VGLUT1 positive) with multiple active zones (Bassoon) was significantly increased by CYP46A1 in the HOMO-CYP mice (Figure 4E-F), suggesting that the increase of glutamatergic synapses induced by CYP46A1 is dependent on presynaptic remodeling.

We tested whether CYP46A1 impacts the membrane properties of SPNs and synaptic transmission in cortico-striatal slices (Figure 4G) from HOMO mice at 7 months of age. Whole-cell recordings of SPNs located in the area of injection from zQ175 (HOMO-GFP and HOMO-CYP) and control (WT and WT-GFP) was performed (Figure 4G). When zQ175 was compared to WT mice, we observed increased excitability (Figure 4H1-2), decreased rheobase (Figure 4I) and increased input resistance (Figure 4J), in line with previous reports (Heikkinen *et al.*, 2012; Indersmitten *et al.*, 2015). We did not observe differences between WT and WT-GFP as well as in between HOMO-GFP and HOMO-CYP mice for excitability, rheobase and input resistance. Next, we compared the resting membrane potential and observed a depolarization in HOMO-GFP versus WT-GFP, when there was no significant difference between other groups (Figure S5C). The half-width of APs was not different between WT versus WT GFP and HOMO-GFP versus HOMO-CYP but increased between WT and zQ175 mice (Figure S5D). The threshold of generation of action potential did not differ between groups (Figure S5E). Paired-pulse ratio (PPR) experiments (Figure S5F1) displayed a larger depression in WT compared to zQ175 animals

and CYP46A1 did not have significant effect on PPR (Figure S5F2). We analyzed the spontaneous excitatory currents (sEPSCs) (Figure 4K1) and observed a decrease in frequency of sEPSCs in HOMO-GFP compared to WT and WT-GFP. Interestingly, sEPSCs frequency in HOMO-CYP was increased compare to HOMO-GFP and was similar to WT-GFP (Figure 4K2). Regarding sEPSC amplitude, an increase between WT and zQ175 animals was observed, without noticeable effect of CYP46A1 (Figure 4L). In conclusion, CYP46A1 injection in zQ175 mice was able to specifically rescue sEPSCs frequency, which is potentially related to the increase of synaptic contacts with multiple active zones (see Figure 4E-F).

CYP46A1 improves vesicles and endosomes trafficking

To further explore the role of CYP46A1 in cortico-striatal connectivity, we studied Brain Derived Neurotrophic Factor (BDNF) support at cortico-striatal synapses, which is defective in Huntington's disease (Plotkin and Surmeier, 2015). We investigated the effect of CYP46A1 overexpression on BDNF axonal transport in cortical neurons from the knock-in Huntington's disease mouse model CAG140. To this end, we took advantage of microfluidic devices allowing reconstituting WT or Huntington's disease cortico-striatal connections (Figure 5A). At DIV7, cortical neurons connect with striatal neurons and reconstitute a cortico-striatal circuit (Virlogeux *et al.*, 2018b). Cortical neurons were transduced with lentiviruses expressing a functional mCherry-tagged BDNF and with AAVrh10 expressing GFP (as a control) or HA-tagged CYP46A1 (Figure 5B). Axonal transport of BDNF was measured within single isolated cortical axons by spinning confocal microscopy and the generated kymographs were analyzed. CYP46A1 overexpression significantly increased anterograde and retrograde mean velocities of BDNF vesicles as well as the number of BDNF vesicles moving in the anterograde direction (Figure 5C). The increase in BDNF vesicular velocities and the increased number of vesicles resulted in a significant effect on the global linear flow rate of BDNF vesicle trafficking in axons (Figure 5C). Together, these results suggest that CYP46A1 tips the balance towards improving BDNF transport in the axons of cortical neurons.

Upon release by cortical synapses, BDNF binds to tropomyosin-related kinase receptor B (TrkB). Previous studies have shown that trafficking of TrkB endosomes in striatal dendrites is altered in Huntington's disease context (Liot *et al.*, 2013; Virlogeux *et al.*, 2018b). Therefore, we investigated whether CYP46A1 overexpression can improve the trafficking of TrkB signaling endosomes in striatal dendrites of postsynaptic striatal neurons within the Huntington's disease cortico-striatal network. Striatal neurons were transduced with lentiviruses expressing a functional mCherry-tagged TrkB and with AAVrh10 expressing GFP (as a control) or HA-tagged CYP46A1 (Figure 5D). Kymograph analyses were performed at DIV 7. We observed a significant improvement of the mean velocities in both

inward and outward directions in striatal neurons (Figure 5E), suggesting that CYP46A1 improved TrkB endosome trafficking in striatal dendrites. CYP46A1 has no significant effect on the number of signaling endosomes or on the linear flow rate. Finally, we investigated the consequences of CYP46A1 overexpression on post-synaptic signaling, using ERK phosphorylation as a read-out for striatal response to cortical stimulation. Both cortical and striatal neurons were transduced with AAVrh10 expressing GFP (as a control) or HA-tagged. Following glycine/strychnine treatment on cortical neurons, we observed a significant increase in the number of phospho-ERK-immuno-positive striatal neurons after CYP46A1 overexpression compared to control (Figure 5F-G). Thus, in addition to increasing the presynaptic and postsynaptic trafficking of components of the BDNF-TrkB signaling, CYP46A1 overexpression improves dramatically the functioning of the whole cortico-striatal Huntington's disease circuitry.

Clearance of aggregates, autophagy and proteasome machineries are improved by CYP46A1, lanosterol and desmosterol.

An important observation from the transcriptomic study, was the de novo upregulation of genes associated with autophagosome and proteasome, which are known to be dysregulated in Huntington's disease (Bennett *et al.*, 2005; Martinez-Vicente *et al.*, 2010), with, as a consequence, a lack of clearance of unfolded, aggregated mHTT. CYP46A1 induced a strong diminution of mHTT aggregates in the striatum (see Figure 1G-H). To investigate a possible regulation of autophagosome and proteasome machinery in CYP46A1-mediated clearance of aggregates, we used primary cultures of striatal neurons that express the first exon of HTT with 103 CAG repeats (103Q-HTT) (Figure 6A). In these cells, co-expression of CYP46A1 and 103Q-HTT reduced the number of transfected neurons with aggregates (-50%) (Figure 6B-C). When treated with selective inhibitors of the proteasome (MG132) or the autophagosome (Chloroquine) machinery, the clearance of aggregates induced by CYP46A1 was fully reversed (Figure 6B-C). We next tested the sterols increased by CYP46A1 *in vivo*, lanosterol and desmosterol (see Figure 2A), which significantly reduced (-20%) aggregate formation (Figure 6C-D). Similarly, to CYP46A1, the clearance of aggregates induced by lanosterol and desmosterol was reversed by MG132 and Chloroquine.

To study autophagy *in vivo*, we analyzed the expression of LC3 (microtubule associated protein light chain 3), which is essential for the formation of autophagosomes. The amount of LC3-II (phospholipid conjugated form) correlates with autophagosomes formation (Kabeya *et al.*, 2000; Tanida *et al.*, 2004). In HET-GFP mice, we found an accumulation of LC3 puncti compared to WT mice and restoration of normal density of LC3 puncta in HET-CYP mice, associated to an increase of the size LC3 puncta with CYP46A1 (Figure 6E-F). Ultrastructural study of autophagy vacuoles allowed us to investigate the

features of autophagosomes (Figure 6 H-I). Analysis by electron microscopy in HET-GFP mice, revealed a marked presence of large vacuoles (0.5-0.9 µm of diameter) compatible with autophagosomes. The most abundant type of vacuoles identifiable in the cytosol of heterozygous cells exhibited amorphous and low electron dense content, suggesting that they were empty of cytosolic content (Figure 6H). Those vacuoles were closely associated, on their cytosolic side, with smaller vesicular dense-electron structures suggesting lysosomes (0.2-0.3 µm of diameter) (Figure 6H). Analysis of ultrathin sections from dorsal striatum of HET-CYP46A1 mice also showed some empty vacuoles (0.5-0.6 µm of diameter), but larger vacuoles (1.2-1.3 µm of diameter) with electron dense content (Figure 6I). These data suggest that the accumulation of empty vacuoles observed in the striatum of zQ175 mice, is reversed by CYP46A1, with a better ability to load their cargo and fuse with lysosomes to degrade their content. In agreement with this observation, mHTT level was significantly decreased in HET-CYP46A1 mice suggesting a better clearance of unfolded protein (Figure S6).

Discussion

In this study, we show that restoring the cholesterol degradation enzyme, CYP46A1, in the striatum of zQ175 mice alleviates Huntington's disease phenotype through cholesterol metabolism regulation. Importantly, CYP46A1 broadly impacts the transcriptomic signature related to major pathways strongly altered in Huntington's disease, including synaptic transmission, vesicular transport and unfolded protein metabolism. We further demonstrate that, by a cascade of events implicating cholesterol metabolism, CYP46A1 compensates for important dysfunctions induced by mHTT, including cortico-striatal synaptic connectivity and activity, along with BDNF cortical axonal transport and trafficking of striatal TrkB endosomes. Finally, we show that CYP46A1, and cholesterol precursors (lanosterol and desmosterol) which are positively regulated by CYP46A1, have an efficient role in promoting aggregate clearance, via the autophagosome and proteasome machineries.

CYP46A1 restoration had a strong impact on cholesterol metabolism by increasing both cholesterol precursor levels (lathosterol, lanosterol and desmosterol) and 24S-OHC, the product of cholesterol degradation. In the adult brain, cholesterol is mainly synthesized by astrocytes, via the Bloch pathway, with desmosterol as cholesterol precursor. In neurons, the main cholesterol pathway is the Kandutsch Russel pathway, with lathosterol as cholesterol precursor (Nieweg *et al.*, 2009). This pathway is altered in Huntington's disease, with a striking lathosterol decrease in zQ175 (Shankaran *et al.*, 2017). Since CYP46A1 restoration promoted production of both lathosterol and desmosterol, we can hypothesize that cholesterol synthesis was reactivated in both astrocytes and neurons.

Interestingly, mRNAs encoding cholesterogenic enzymes (Hmgcor, cyp51, dhrc24, dhcr7) were increased by CYP46A1, an effect that could depend on activation of SREBP2, a sensor of cholesterol levels, which can regulate transcription of cholesterogenic enzymes upon its nuclear translocation (Brown and Goldstein, 1997). Accordingly, we found that nuclear expression of SREBP2 was increased by CYP46A1. CYP46A1-mediated regulation of cholesterol metabolism can also occur via production of 24S-OHC and desmosterol, which are ligands of Liver X receptors (LXRs) (Lehmann *et al.*, 1997; Yang *et al.*, 2006; Spann *et al.*, 2012). LXRs positively regulate transcription of ApoE lipoproteins (Abildayeva *et al.*, 2006) that are cargo proteins for cholesterol transport from astrocytes to neurons (Boyles *et al.*, 1985; Pitas *et al.*, 1987). In Huntington's disease, astrocytes produce less ApoE, thus lowering cholesterol support to neurons (Valenza *et al.*, 2010, 2015). Thus, ApoE increase suggests that besides regulation of cholesterol metabolism, CYP46A1 also positively impacts the transport of cholesterol from astrocytes to neurons. Therefore, our study unravels the mechanisms underlying CYP46A1-mediated regulation of cholesterol homeostasis, via production of 24S-OHC, regulation of the

cholesterol biosynthesis pathways in both neurons and astrocytes, along with an increased cholesterol transport (see Figure 7).

As previously described in several Huntington's disease knock-in mice (Ament *et al.*, 2017), we confirmed deregulation of gene expression in the striatum of zQ175 mice. Importantly, CYP46A1 was able to significantly modify this striatal transcriptome, via mechanisms need to be further explored. In Huntington's disease, the global down-regulation of gene expression is associated to the sequestration of key transcriptional activators, such as TBP, CBP and Sp1 into nuclear mHTT aggregates (Nucifora *et al.*, 2001; Li *et al.*, 2002; Schaffar *et al.*, 2004). Therefore, a possible mechanism to explain the transcriptional correction mediated by CYP46A1 in zQ175 mice could involve aggregate clearance, allowing transcription factors to be more available to regulate the expression of their targets. Gene compensation noticeably applied to genes associated with neurotransmission, synaptic activity, the proteasome and autophagy related gene regulation. The increase in proteasome-related gene expression could potentiate the clearance of aggregates induced by CYP46A1, along with lanosterol and desmosterol (see below). Intriguingly, our data also showed that CYP46A1 modulates the expression of several genes involved in pathways that regulate innate immunity such as complement and toll-like receptor pathways. When CYP46A1 transcriptional signature is compared to the gene expression patterns of small compounds and drugs it is correlated to anti-inflammatory compound and neuroprotective agents (see Table S4 for CMap analysis). Moreover, 24S-OHC and desmosterol can activate Liver X Receptors (LXR), leading to anti-inflammatory responses (Ghisletti *et al.*, 2007; Spann *et al.*, 2012). We content that CYP46A1 expression could also promote neuroimmune mechanisms that protects against cytotoxicity either directly, in neurons, or indirectly, through non-cell autonomous mechanisms involving glial cells, an issue that remains to be addressed.

Synaptic dysfunctions have been widely described in Huntington's disease mouse models (Raymond, 2017), and a significant decrease in spine density has been shown at 7 and 12 months in zQ175 mice, along with altered excitatory and inhibitory inputs in SPN (Indersmitten *et al.*, 2015; Rothe *et al.*, 2015). In line with these data, we observed reduced glutamatergic connectivity as well as increased excitability and input resistance in these mice, which could serve as a compensatory mechanism to lower cortico-striatal transmission. CYP46A1 delivery in the striatum of zQ175 mice improved glutamatergic connectivity at 7 months and spine density at 12 months. In addition, the lowered frequency of sEPSC observed in zQ175 mice was rescued by CYP46A1 expression. The increase in probability of spontaneous release at glutamatergic synapses is in line with the observed increase of synapses with multiple active zones, indicating that, CYP46A1 would tend to normalize altered glutamatergic transmission in Huntington's disease by regulating both pre- and post-synaptic events.

Increased levels of presynaptic proteins have been observed in mice overexpressing CYP46A1 (Maioli *et al.*, 2013), while knock-out mice for cyp46A1 exhibited alterations of protein phosphorylation related to synaptic vesicles and neurotransmission (Mast *et al.*, 2017). *In vitro*, CYP46A1 overexpression is also associated with an increase in dendritic protrusions and an enrichment in synaptic proteins (Moutinho *et al.*, 2016). Finally, as a positive allosteric modulator of NMDA receptors, 24S-OHC could potentiate NMDAR-mediated EPSC (Paul *et al.*, 2013).

One of the important pathways involved in Huntington's disease striatal degeneration is the defect in BDNF/TrkB signaling. Huntingtin protein is involved in the microtubule-dependent transport of BDNF in cortical neurons along microtubules, whereas mHTT impairs this transport (Gauthier *et al.*, 2004). After release, BDNF binds on SPN to the TrkB receptor, which dimerizes and is internalized into endosomes. These endosomes are transported from the dendrites to the soma, where TrkB triggers survival signaling (Zhang *et al.*, 2000). Silencing HTT reduces vesicular transport of TrkB in striatal neurons and the polyQ expansion in mHTT alters the binding of TrkB-containing vesicles to microtubules and reduces transport (Liot *et al.*, 2013). We show that both BDNF and TrkB transport in Huntington's disease neurons are improved by CYP46A1 restoration. Cholesterol depletion can promote endosome motility by suppressing the association of endosomes containing lipid rafts with Rab7 GTPase and promotes their association with Rab4 GTPase (Chen *et al.*, 2008). Cholesterol depletion also blocks internalization via caveolae and clathrin-coated pits (Subtil *et al.*, 1999), and its turnover could thus facilitate the transport of endosomes and TrkB internalization.

Restoration of CYP46A1 in the striatum of zQ175 mice, produced a strong clearance of aggregates, one of the main neuropathological landmarks in Huntington's disease. The precursors of cholesterol, lanosterol and desmosterol were also described to favor aggregate clearance in other neurodegenerative diseases. Lanosterol treatment *in vitro*, decreased aggregation in different cell models of neurodegenerative diseases (SOD1, α-synuclein, ataxin-3, mHTT) via induced expression of co-chaperone C terminus of Hsc70-interacting protein (CHIP) and elevated autophagy (Upadhyay *et al.*, 2018). In the context of cataracts caused by a mutation in the lanosterol synthase enzyme, treatment with lanosterol significantly decreased protein aggregation (Zhao *et al.*, 2015). In the present study, we show that treatment with lanosterol, desmosterol and CYP46A1, *in vitro*, decreased aggregate formation in striatal neurons expressing the first exon of mHTT. Inhibition of proteasome (MG132) or autophagy (chloroquine) counteracted lanosterol, desmosterol and CYP46A1 clearing effects, suggesting that these two major proteolytic systems are involved in the beneficial effect of CYP46A1 on the clearance of mHTT aggregates. In Huntington's disease, the proteasome system is less efficient *in vitro* and in patient tissues (Seo *et al.*, 2004; Hunter *et al.*, 2007). Autophagy is also affected

in Huntington's disease, with a defect in cargo loading, autophagosome trafficking and accumulation of autophagosome because of a decreased fusion with lysosome (del Toro *et al.*, 2009; Martinez-Vicente *et al.*, 2010; Wong and Holzbaur, 2014). Accumulation of autophagosomes directly induces cellular toxicity, and this process may be implicated in the pathogenesis of Huntington's disease (Button *et al.*, 2017). Because cholesterol is important for endosome formation, acting on cholesterol turnover could also improve autophagosome formation and recycling. It should be noted that clustering of dynein into cholesterol domains on late phagosomes facilitates their directed transport into lysosomes (Rai *et al.*, 2016). Electron microscopy revealed an accumulation of autophagosome with empty vacuoles in HET-GFP zQ175 mice as previously observed in ^{111}Qhtt knock-in mice (Martinez-Vicente *et al.*, 2010). CYP46A1 restoration in HET zQ175 mice favored the autophagosome activity, a cellular event that plays a critical role for clearance of unfolded proteins, and neuronal survival.

In conclusion, our data put forth a comprehensive model in which regulating striatal cholesterol metabolism by means of CYP46A1 delivery has multiple beneficial effects in the context of Huntington's disease (Figure 7). Cholesterol metabolism regulation and neuroprotection provided by CYP46A1 relied on a wide transcriptomic signature, regulation of synaptic connectivity and activity along with endosomal trafficking and aggregate clearance. Given the pivotal role of cholesterol metabolism in the brain, this strategy could be a promising avenue for other neurodegenerative diseases such as Alzheimer's disease (AD) where CYP46A1 has been shown to be beneficial in AD mice (Hudry *et al.*, 2010; Burlot *et al.*, 2015; Djelti *et al.*, 2015).

Author contributions

J.C. and S.B. conceived the project, designed the experiments, analyzed the data and wrote the manuscript. RK designed the experiments, performed the experiments, analyzed the data, wrote the manuscript. P.V. and N.C. conceived the experiments. N.H., K.P., C.M., G.D., L.D., E.P., W.C., S.S.N., V.M., performed experiments and analyzed their respective data. A.L. analyzed GC/MS experiments and wrote the paper. L.V. designed, realized, analyzed electrophysiology data and wrote the paper. F.S. designed, realized and analyzed the experiments related to microfluidic devices and wrote the paper. C.N. designed network-based analysis of RNA-seq data, analyzed the data and wrote the manuscript. All authors read and commented on the manuscript.

Acknowledgements

We thank Christophe Antoniewski and ARTBio facility for RNAseq analysis and the vectorology platform (Inserm U1089, Nantes, France) for the production of AAV vectors.

Fundings

This work was supported by Agence Nationale pour la Recherche (ANR) grants “13-BSV1-022-01” (JC, SB and FS), « 14-CE35-0027-01 » and « 15-JPWG-0003-05 » (F.S.), Dopaciumcity and Mopla (L.V.), Fondation Groupama « Vaincre les Maladies Rares » (JC, SB), Association Française pour les Myopathies (SB), Centre National pour la Recherche Scientifique (CNRS) (J.C., C.N.), Institut National pour la Santé et la Recherche Médicale (INSERM) (J.C., C.N.) and Sorbonne Université, Faculté des Sciences et Ingénierie (C.N., J.C., S.B.), the CHDI fondation (S.S.N., C.N.). FS was supported by NeuroCoG in the framework of the “Investissements d’avenir” program (ANR-15-IDEX-02). F.S. laboratory is member of the Grenoble Center of Excellence in Neurodegeneration (GREEN). C.N. laboratory is member and lead facilitator of the working group "Systems modeling" of the European Huntington's Disease Network (EHDN).

Competing interests

The clinical application of gene therapy approach for CYP46A1 delivery in Huntington's Disease is protected by the published patent filed in Europe and the United States, PCT/EP2011/068033 and WO2012049314A1, respectively. This does not alter our adherence to Journal of clinical Investigation policies on sharing data and materials. NC is a founding shareholder of Brain Vectis, a biotech company, which develops CYP46A1 gene therapy for neurodegenerative diseases. The company did not have any role in study design, data collection and analysis, decision to publish or preparation of the manuscript. JC, NC and SB declare that they received consultancy benefits from the company, for their scientific advice.

Figure 1

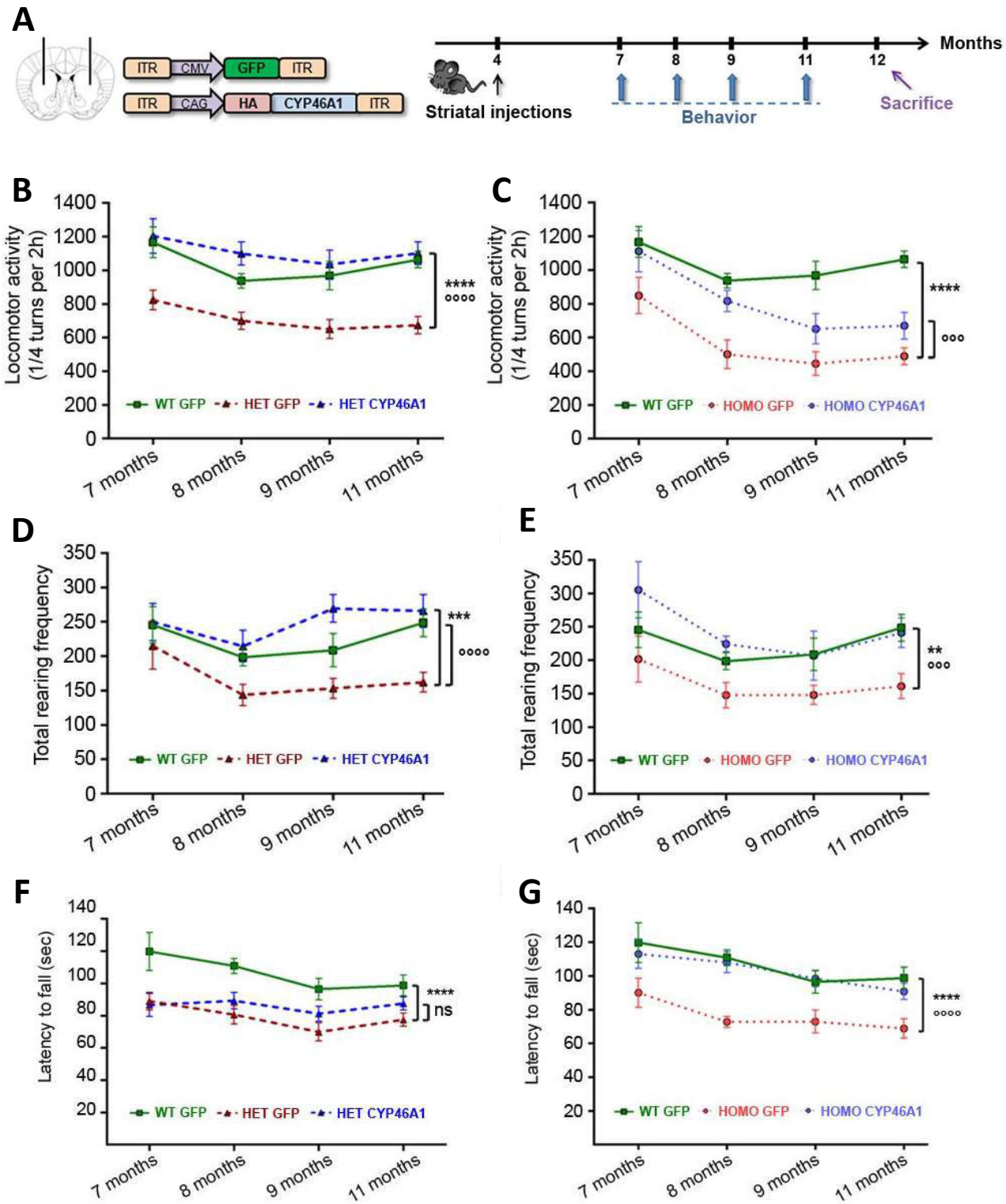
A
ITR
CMV
GFP
ITR
ITR
CAG
HA
CYP46A1
ITR
Striatal injections
4
7
8
9
11
12
Months
Behavior
Sacrifice
B
Locomotor activity (1/4 turns per 2h)
WT GFP
HET GFP
HET CYP46A1
7 months
8 months
9 months
11 months
****
oooo
C
Locomotor activity (1/4 turns per 2h)
WT GFP
HOMO GFP
HOMO CYP46A1
****
ooo
D
Total rearing frequency
***
oooo
E
Total rearing frequency
**
ooo
F
Latency to fall (sec)
****
ns
G
Latency to fall (sec)
****
oooo

Figure 1

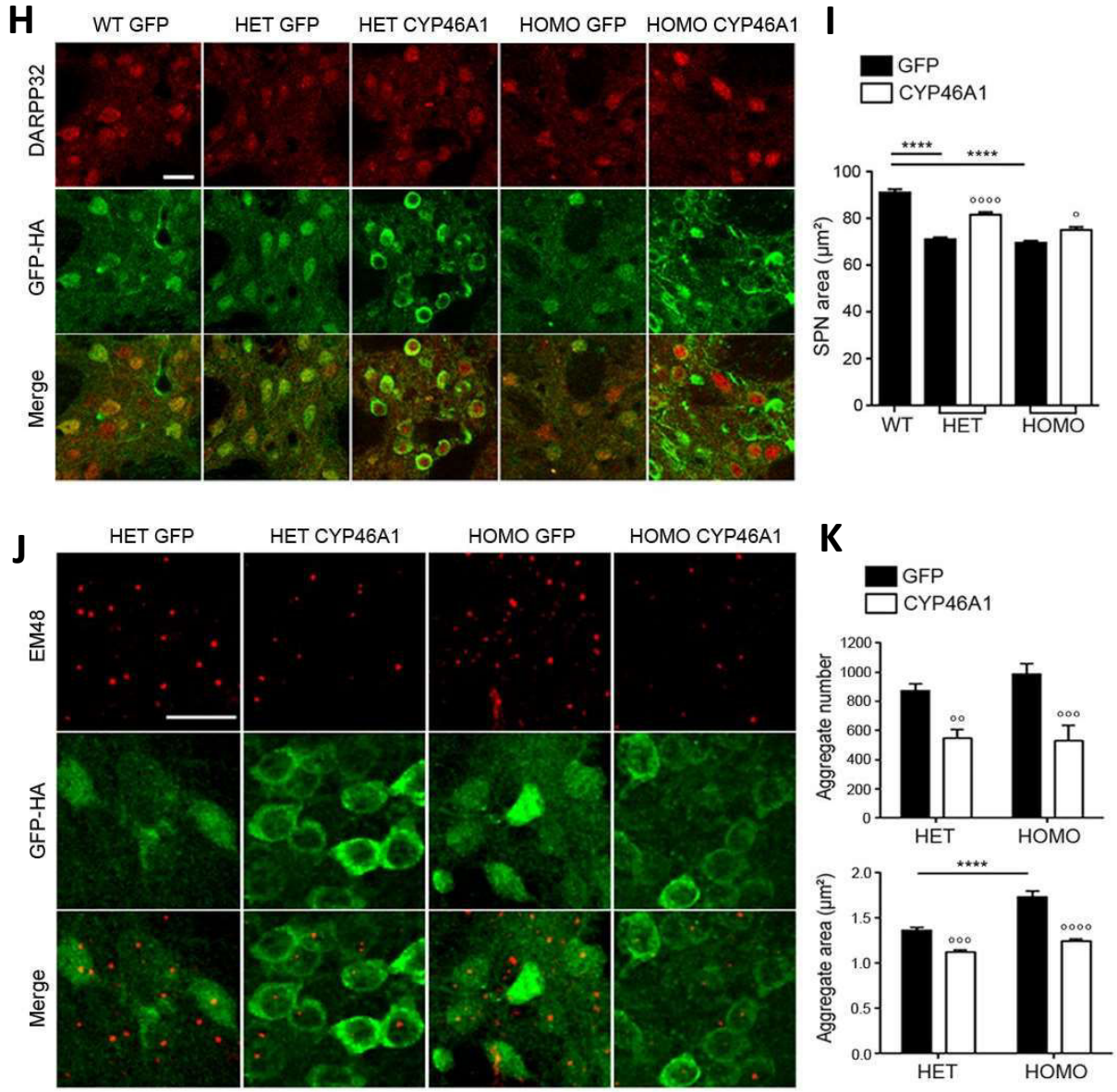
H
WT GFP
HET GFP
HET CYP46A1
HOMO GFP
HOMO CYP46A1
DARPP32
GFP-HA
Merge
I
GFP
CYP46A1
SPN area (µm²)
WT
HET
HOMO
J
HET GFP
HET CYP46A1
HOMO GFP
HOMO CYP46A1
EM48
GFP-HA
Merge
K
GFP
CYP46A1
Aggregate number
Aggregate area (µm²)
HET
HOMO

Figure 1. Striatal expression of CYP46A1 improves behavioral and neuropathological phenotypes in zQ175 mice. (**A**) Experimental set-up for the striatal expression of CYP46A1 and time frame of the phenotypic assessments. (**B-G**) Locomotor performances were measured in wild-type mice injected with AAV-GFP (WT-GFP), heterozygous and homozygous mice injected with GFP or CYP46A1 (HET-GFP, HET-CYP46A1, left panels; HOMO-GFP, HOMO-CYP46A1, right panels). (**B-C**) Locomotor activity assessed in a circular corridor. (**D-E**) Rearing frequency measured in actimeter boxes. (**F-G**) Latency to fall evaluated with a rotarod apparatus. (**B-E**) n = 10 for WT-GFP, n = 16-18 for HET-GFP and HET-CYP46A1, respectively, n = 6 for HOMO-GFP and HOMO-CYP46A1 mice. (**F-G**) n = 12 for WT-GFP, n = 20 for HET-GFP and HET-CYP46A1, n = 8 for HOMO-GFP and HOMO-CYP46A1 mice. (**B-G**) Data are represented as mean ± SEM, Statistical analysis: two-way ANOVA repeated measures. (**H-K**) Sections from dorsal striata of 12-month-old mice were immunostained for DARPP32 (**H-I**) or EM48 (**J-K**) along with hemagglutinin (HA). (**H**) Illustration of DARPP32 immunostaining (red) in the infected areas (green) as depicted by GFP labeling or HA immunostaining (CYP46A1 panels). Scale bar 20 µm. (**I**) Quantification of striatal projection neurons (SPN) area, 100 DARPP32-positive SPNs were measured per animal (**J**) Double immunostaining with EM48 (red) and HA (green) antibodies. Scale bar 20 µm. (**K**) Quantification of aggregate number and area. (**H-K**) n = 3-5 per group. Data are represented as mean ±SEM. Statistical analysis: one-way ANOVA (**I**) and two-way ANOVA (**K**) followed by Bonferroni's post hoc test. (**B-K**) Genotype main effect (WT vs HET or HOMO GFP): **p<0.01, ***p<0.001, ****p<0.0001. Treatment main effect (GFP vs CYP46A1): °p<0.05, °°p<0.01, °°°p<0.001, **°°°°**p<0.0001, ns: not significant.

Figure 2

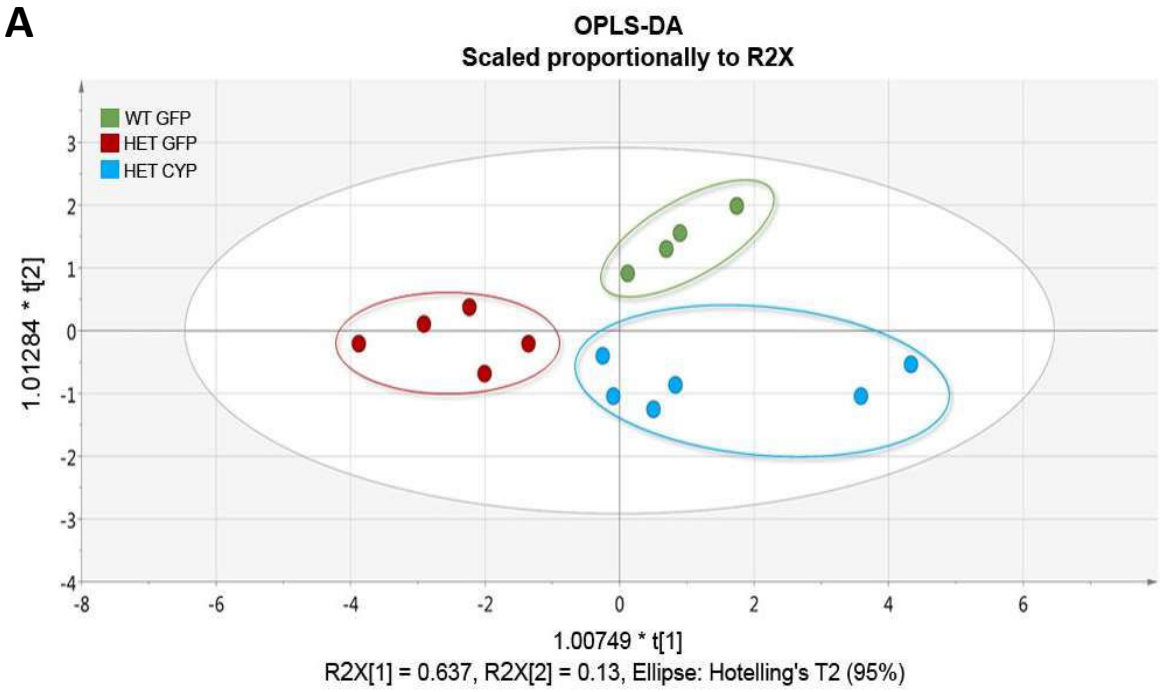
A
OPLS-DA
Scaled proportionally to R2X
WT GFP
HET GFP
HET CYP
1.01284 * t[2]
1.00749 * t[1]
R2X[1] = 0.637, R2X[2] = 0.13, Ellipse: Hotelling's T2 (95%)

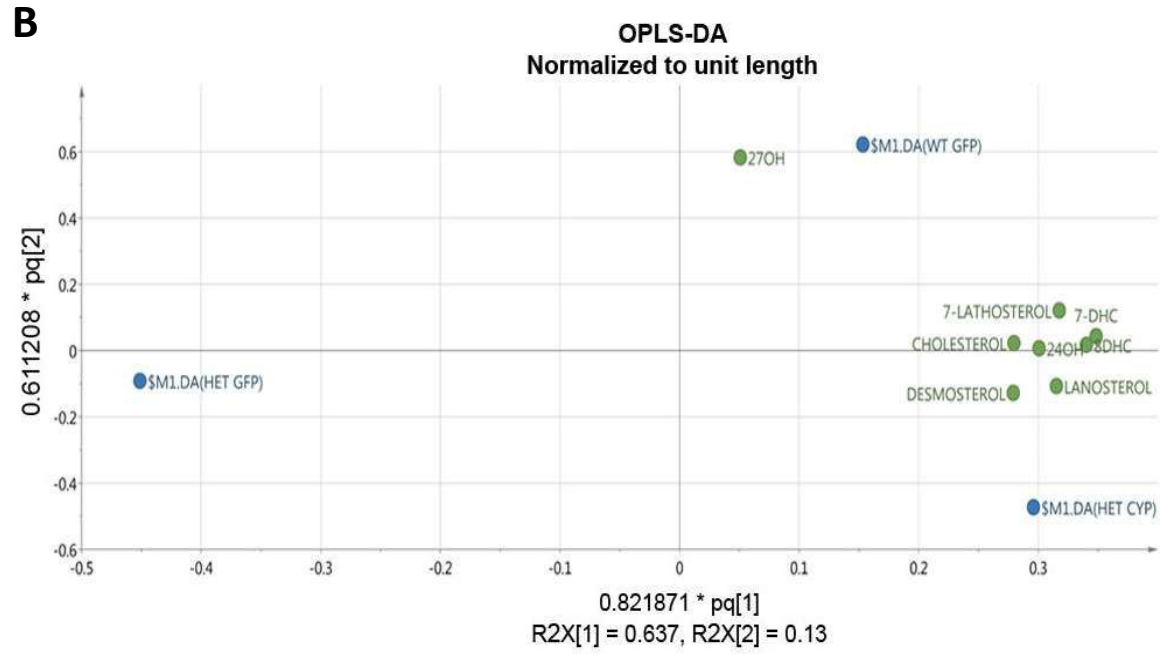
B
OPLS-DA
Normalized to unit length
27OH
$M1.DA(WT GFP)
7-LATHOSTEROL
7-DHC
CHOLESTEROL
24OH
DESMOSTEROL
LANOSTEROL
$M1.DA(HET GFP)
$M1.DA(HET CYP)
0.611208 * pq[2]
0.821871 * pq[1]
R2X[1] = 0.637, R2X[2] = 0.13

Figure 2

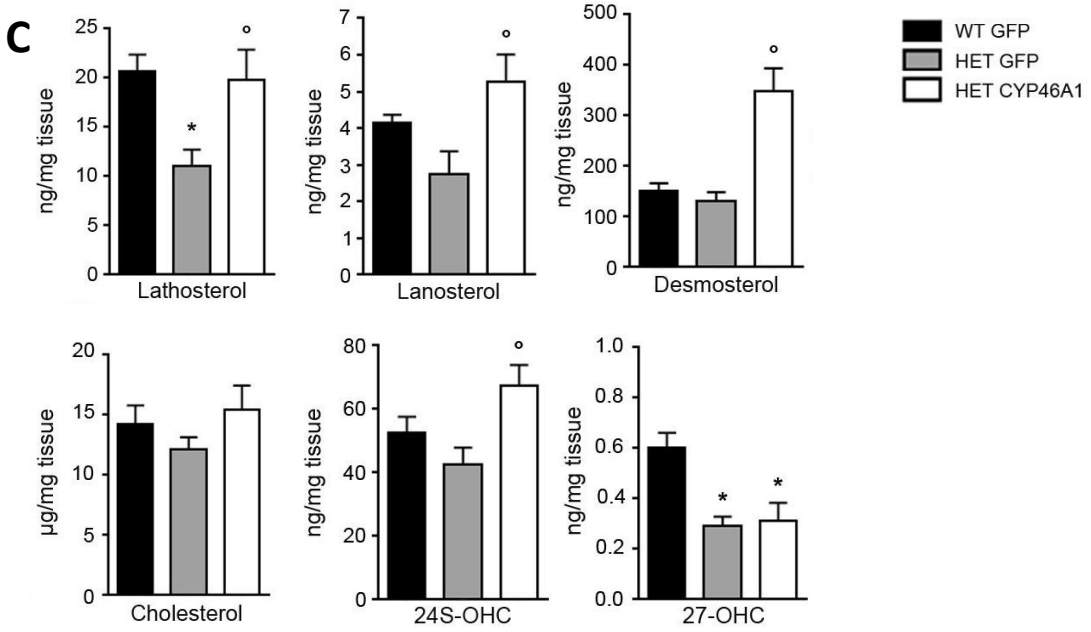
C
WT GFP
HET GFP
HET CYP46A1
ng/mg tissue
Lathosterol
Lanosterol
Desmosterol
µg/mg tissue
Cholesterol
24S-OHC
27-OHC

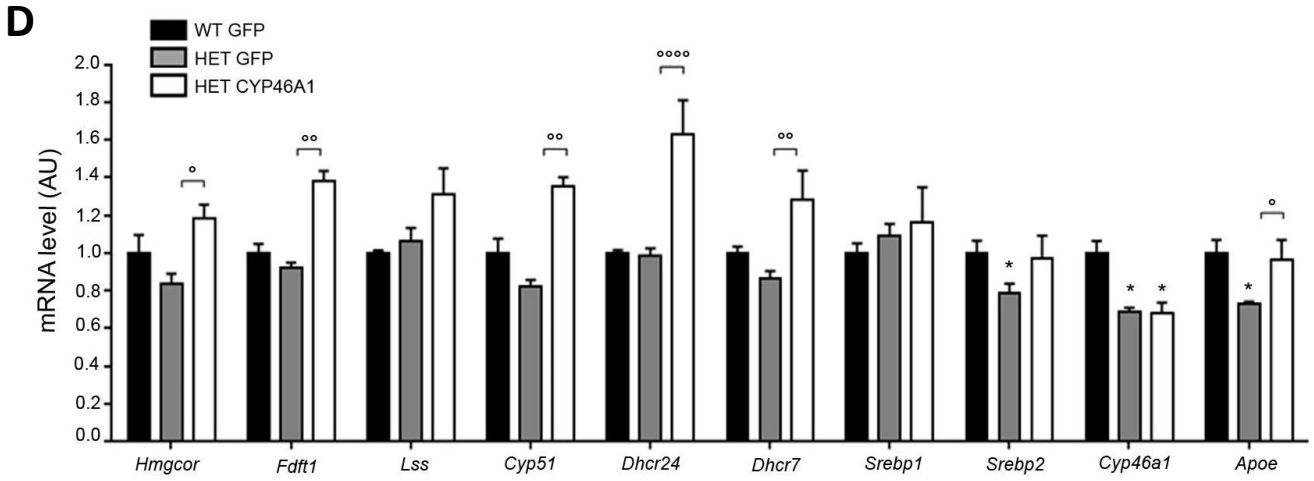
D
WT GFP
HET GFP
HET CYP46A1
mRNA level (AU)
Hmgcor
Fdft1
Lss
Cyp51
Dhcr24
Dhcr7
Srebp1
Srebp2
Cyp46a1
Apoe

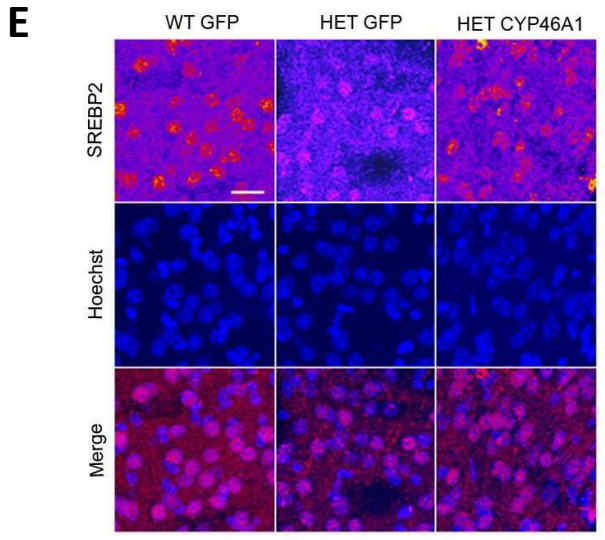
E
WT GFP
HET GFP
HET CYP46A1
SREBP2
Hoechst
Merge

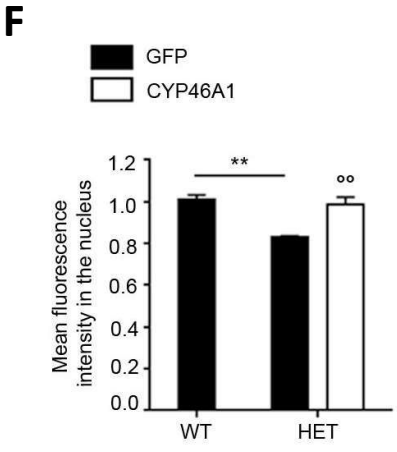
F
GFP
CYP46A1
Mean fluorescence intensity in the nucleus
WT
HET

Figure 2. Regulation of cholesterol homeostasis by CYP46A1 expression in the striatum of zQ175 mice. (**A-B**) OPLS-DA score plot and load plot for the overview model including three groups (WT-GFP (green dots), HET-GFP (red dots) and HET-CYP (blue dots)). The model consists of two predictive component (p1,p2) shown in the figure and two orthogonal components (not shown). t[1] = scores for predictive component 1, t [2] = scores for predictive component 2. Explained variation of each components: R2Xp1 = 0.637; R2Xp2 = 0.13. Goodness of prediction Q2cum = 0.642. The ellipse shows the 95% confidence interval using Hotelling T2 statistics. (**C**) Sterol and oxysterols levels were measured by GC-MS in striatal extracts of 12 months-old WT-GFP, HET-GFP and HET-CYP46A1 zQ175 mice. Data are represented as mean ± SEM (n = 4 for WT n = 5-6 for HET). Statistical analysis: Multiple t Test, (**D**) mRNA was extracted from the striatum of 12 months-old WT-GFP, HET-GFP and HET-CYP46A1 mice. mRNA levels were normalized to *Hprt* housekeeping gene. Data are represented as mean ± SEM (n = 5-6 per group). Statistical analysis: one-way ANOVA followed by Tukey's post hoc test. (**E**) Section from dorsal striatum of 12-month-old mice. Double immunostaining with SREBP2 (red) and HA (green) antibodies. Scale bar 20 µm. (**F**) Quantification of nuclear SREBP2 fluorescence intensity. Data are represented as mean ± SEM, n = 5 per group. Statistical analysis: one-way ANOVA followed by Bonferroni's post hoc test. (**C-F**) Genotype main effect: *p<0.05, **p<0.01 Treatment main effect: °p<0.05, °°p<0.01, °°°°p<0.0001

Figure 3

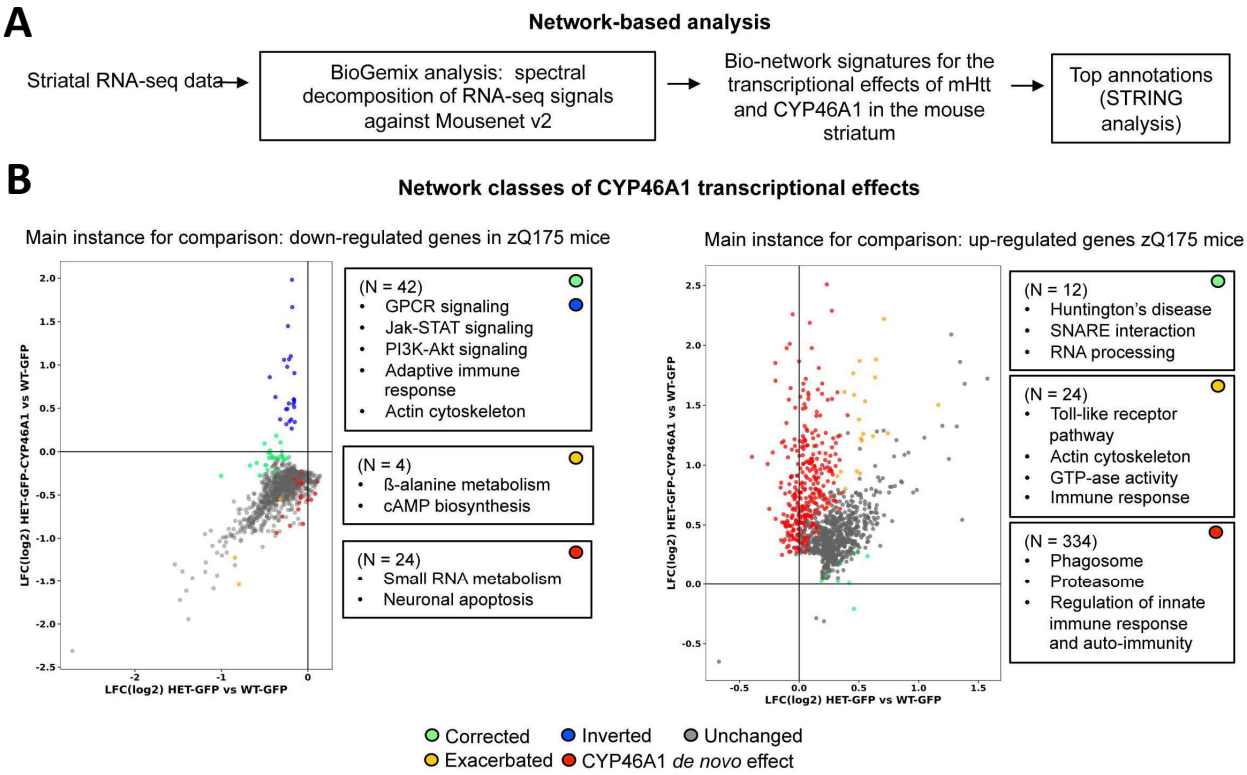

Figure 3. **Network signatures for the transcriptional effects of restoring CYP46A1 expression in the striatum of zQ175 mice.** (**A**) Overview of network-based analysis for assessing the biological significance of RNA-seq data. (**B**) Network profiles for the transcriptional effects of CYP46A1 expression in zQ175 mice. These profiles show the effects of CYP46A1 on the gene expression in zQ175 mice. The left panel shows LFC of down-regulated gene nodes in zQ175 mice and their corresponding LFCs in HET-GFP;CYP46A1 mice as well as the gene nodes that are down-regulated in the HET-GFP;CYP46A1 mice and that are not deregulated by mHtt in zQ175 mice. The right panel shows the LFC of up-regulated genes in zQ175 mice and their corresponding LFCs in the HET-GFP; CYP46A1 mice as well as the gene nodes that are up-regulated in HET-GFP-CYP46A1 mice and that are not deregulated by mHtt in zQ175 mice. In both panels, the green label indicates the gene nodes that are corrected back to normal by CYP46A1 expression. The blue label indicates the gene nodes for which showing an inverted effect meaning the genes which are inversely deregulated in the HET-GFP;CYP46A1 mice compared to zQ175 mice. The grey label indicates the gene nodes that are deregulated by mHtt and unchanged upon CYP46A1 expression. The orange label indicates the genes whose deregulation by mHtt is exacerbated by CYP46A1 expression. The red label indicates the *de novo* effects with CYP46A1 expression. The annotations shown in both panels result from STRING analyzes using high confidence settings and retaining the most informative GO annotations (Biological processes, KEGG pathways) as supported by a minimal number of nodes set to N > 9 and a *P* value < 10^{-6}.

Figure 4

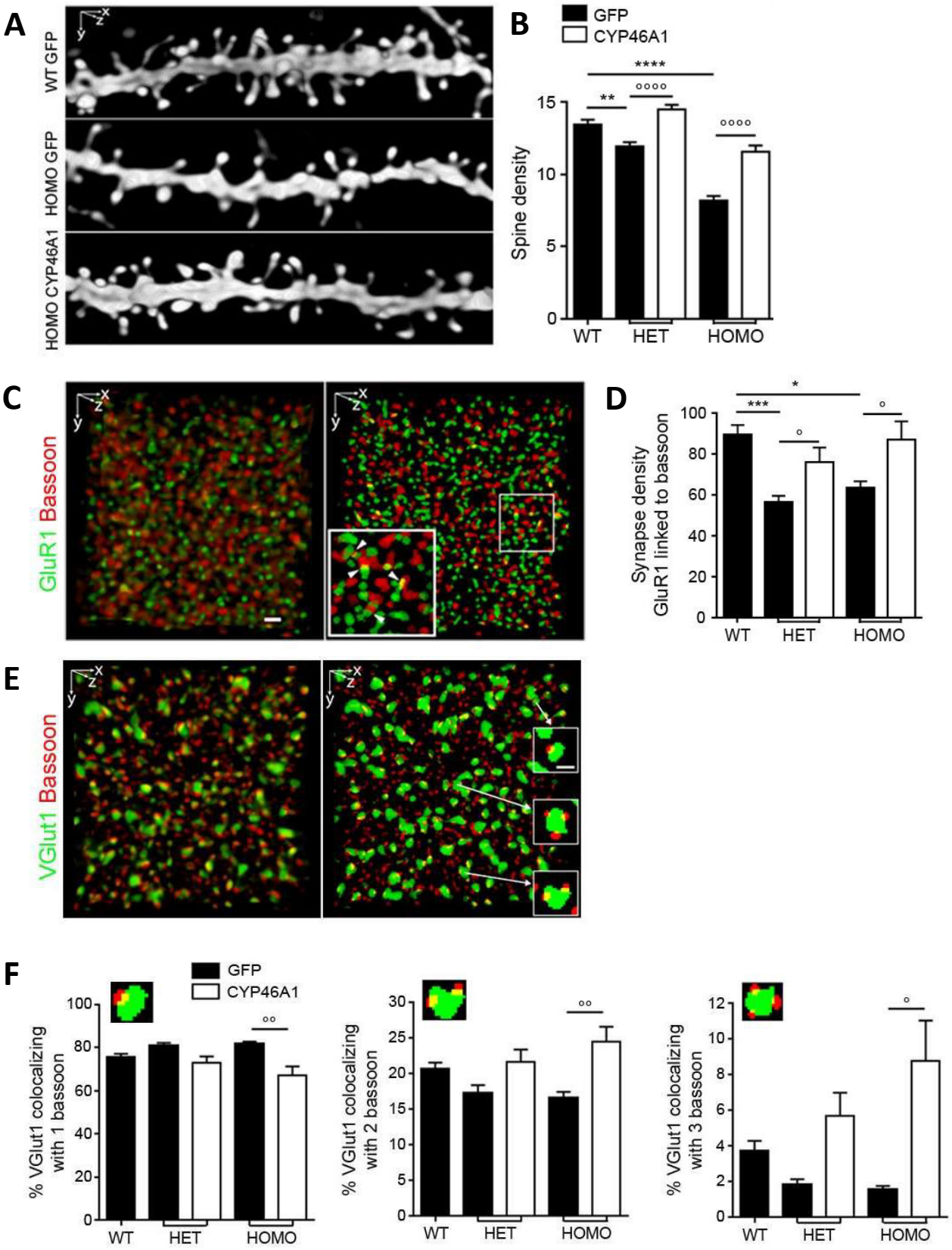
A
WT GFP
HOMO GFP
HOMO CYP46A1
B
GFP
CYP46A1
Spine density
WT
HET
HOMO
C
GluR1 Bassoon
D
Synapse density GluR1 linked to bassoon
E
VGlut1 Bassoon
F
% VGlut1 colocalizing with 1 bassoon
% VGlut1 colocalizing with 2 bassoon
% VGlut1 colocalizing with 3 bassoon

Figure 4

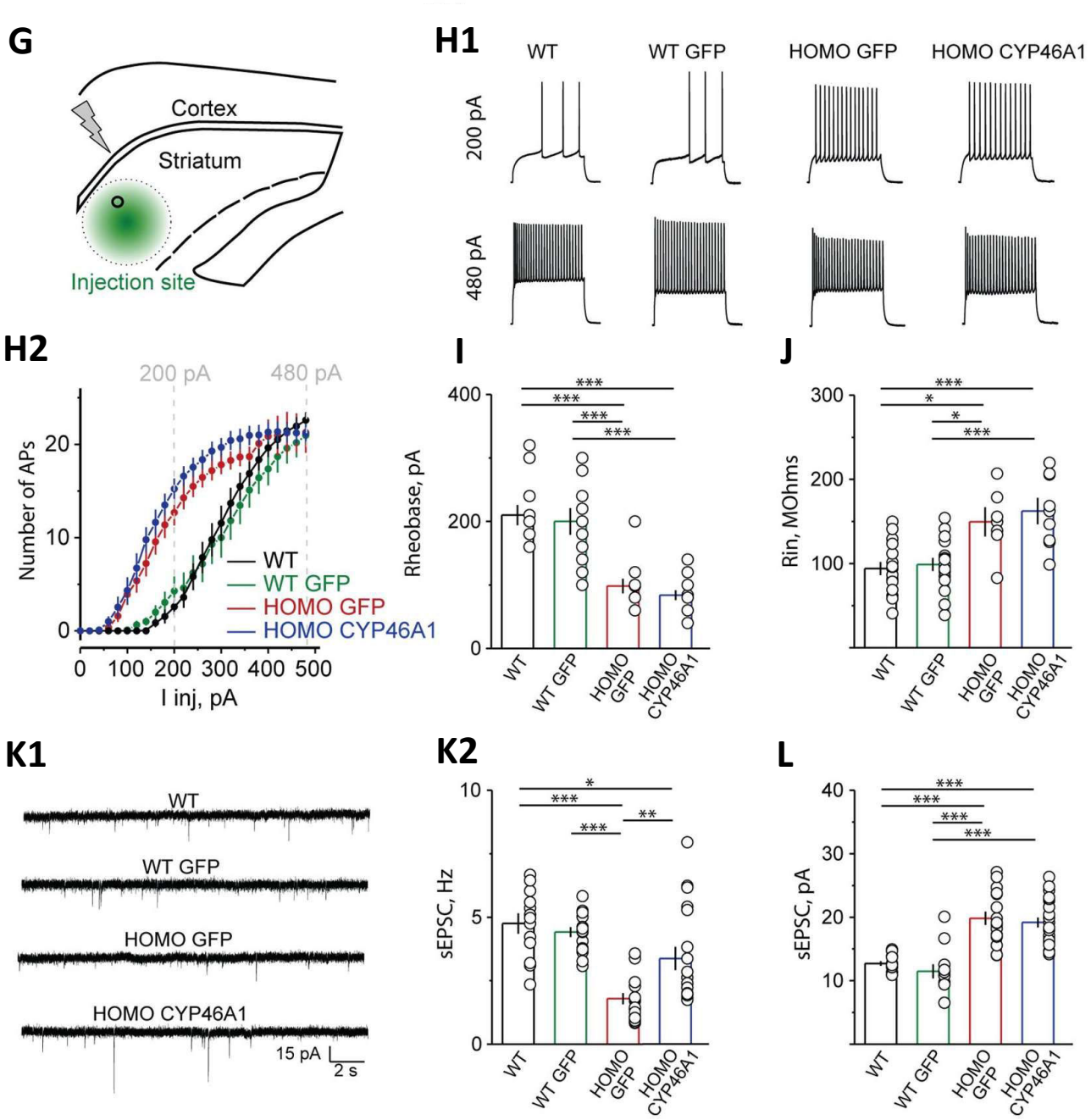
G
Cortex
Striatum
Injection site
H1
WT
WT GFP
HOMO GFP
HOMO CYP46A1
200 pA
480 pA
H2
200 pA
480 pA
Number of APs
I inj, pA
WT
WT GFP
HOMO GFP
HOMO CYP46A1
I
Rheobase, pA
J
Rin, MOhms
K1
WT
WT GFP
HOMO GFP
HOMO CYP46A1
15 pA
2 s
K2
sEPSC, Hz
L
sEPSC, pA

Figure 4. Improvement of glutamatergic connectivity with CYP46A1. (**A-D**) Sections from the dorsal striatum of 12-month-old (**A-B**) and 7-month-old (**C-D**) wild type and zQ175 mice. (**A**) Three-dimensional (3D) volume rendering of dendrites labeled by DiI. (**B**) Spine density is defined as the number of spines normalized for 10micron length of dendrite. n = 10 to 15 dendrites from N = 3 to 5 mice for each condition. Data are represented as mean ±SEM. Statistical analysis: one-way ANOVA followed by Bonferroni's post hoc test. (**C**) Double immunostaining with GluR1 (green) and bassoon (red) antibodies. 3D volume rendering of deconvolved and segmented image stacks. Scale bar 1µm. (**D**) Quantification of GluR1 and bassoon colocalization. The density is the number of objects normalized for a cube of 10micron side. (**E**) Double immunostaining with VGlut1 (green) and Bassoon (red) antibodies. 3D volume rendering of deconvolved (left), and segmented (right) image stack. Scale bar 0.5 µm. (**F**) Quantification of VGlut1 colocalizing with one, two or three Bassoon elements. (**C-F**) n = 3 mice of each genotype. Data are represented as mean ±SEM. Statistical analysis: two-way ANOVA followed by Bonferroni's post hoc test. (**A-F**) Genotype main effect: **p*<0.05, ***p*<0.01, ****p*<0.001, *****p*<0.0001, Treatment main effect: °*p*<0.05, °°*p*<0.01, °°°°*p*<0.0001 (**G-L**) Membrane properties of SPNs and synaptic transmission at cortico-striatal synapses in WT and zQ175 mice. (**G**) Scheme of the experimental set-up and the injection site in cortico-striatal slices. (**H1**) Representative action potentials (APs) triggered by somatic current injections (200 and 480 pA) in WT, WT-GFP, HOMO-GFP and HOMO-CYP mice. (**H2**) SPN excitability (n=11). one-way ANOVA with Bonferroni's correction *p<0.05, **p<0.01, **p<0.001, ***p<0.0001. (**I**) Rheobase (WT n=12, WT-GFP n=12, HOMO-GFP/CYP n=12/15) (**J**) Input resistance of SPNs (WT, n=16, WT-GFP, n=16, HOMO-GFP/CYP, n=6/8) (**K1**) Representative spontaneous excitatory currents (sEPSCs) in SPNs (**K2**) sEPSC frequency in SPNs (HOMO-GFP/CYP n=18). (**I-K2**) *p<0.05, **p<0.01, ***p<0.001 (**L**) sEPSC amplitude in SPNs. Statistical analysis: three-way ANOVA with Bonferroni's correction, p<0.0001

Figure 5

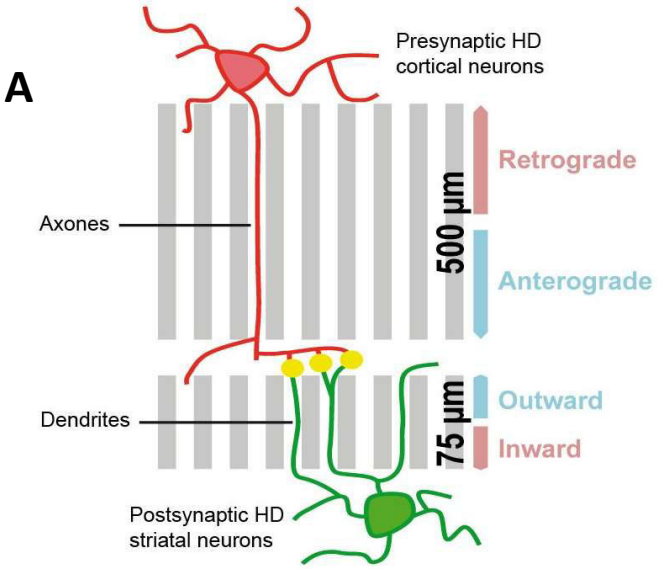
A
Presynaptic HD
cortical neurons
Axones
500 µm
Retrograde
Anterograde
Dendrites
75 µm
Outward
Inward
Postsynaptic HD
striatal neurons

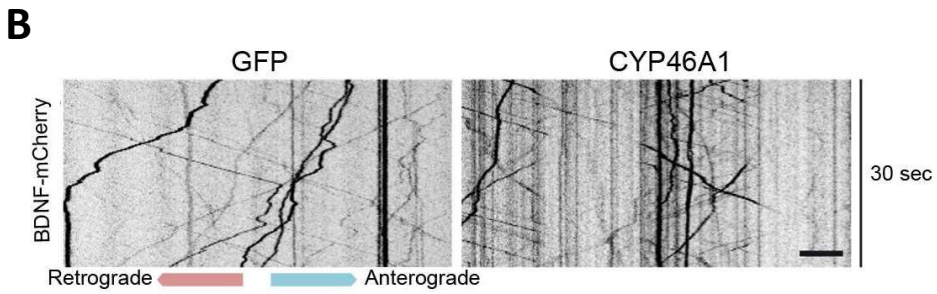
B
GFP
CYP46A1
BDNF-mCherry
30 sec
Retrograde
Anterograde

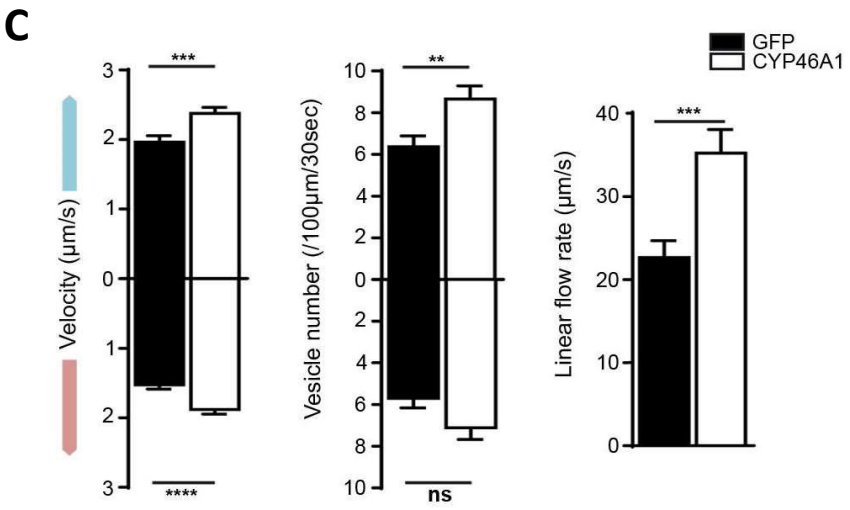
C
GFP
CYP46A1
Velocity (µm/s)
***
****
Vesicle number (/100µm/30sec)
**
ns
Linear flow rate (µm/s)
***

Figure 5

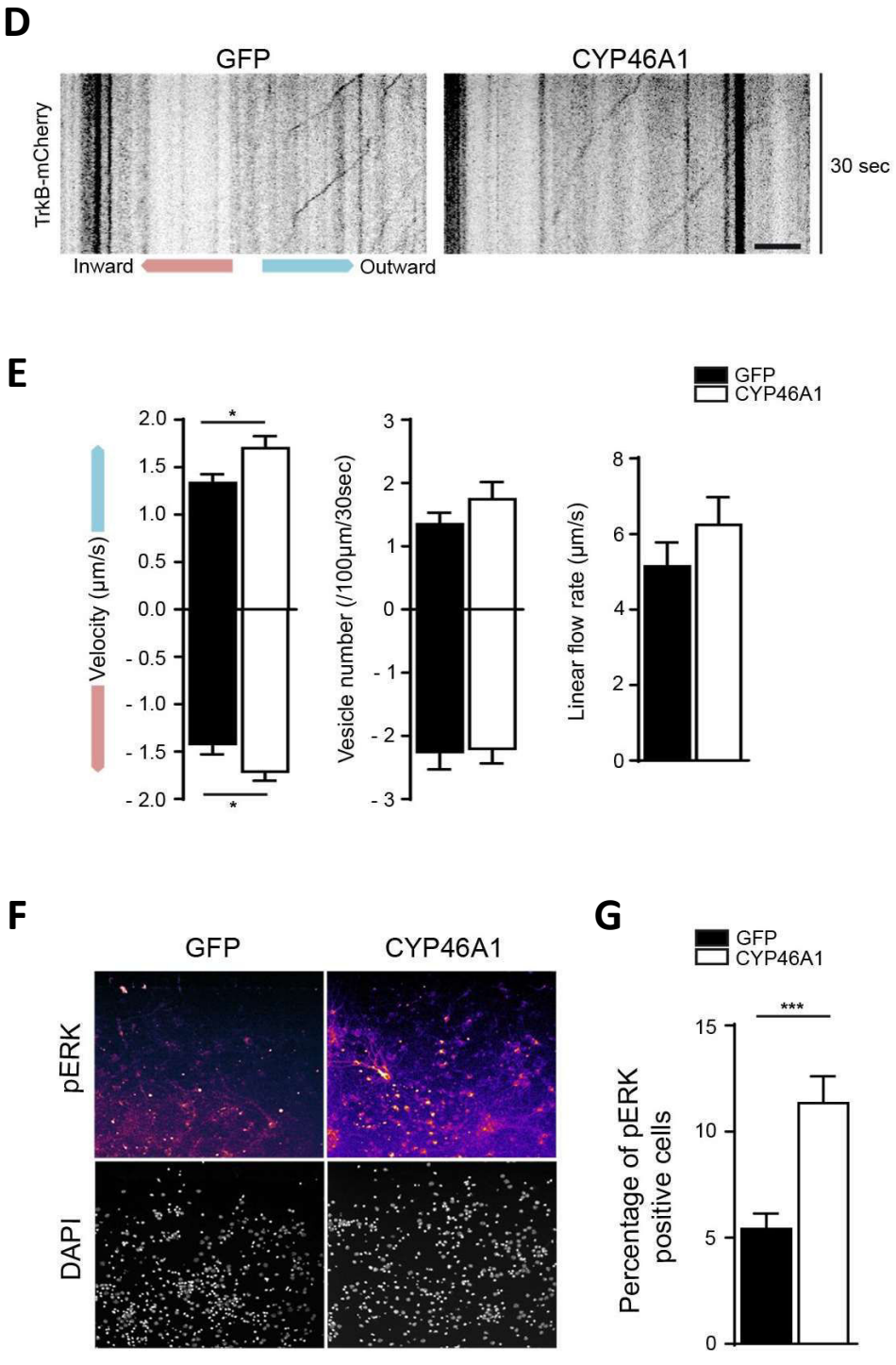
D
GFP
CYP46A1
TrkB-mCherry
30 sec
Inward
Outward
E
GFP
CYP46A1
Velocity (µm/s)
2.0
1.5
1.0
0.5
0.0
- 0.5
- 1.0
- 1.5
- 2.0
*
*
Vesicle number (/100µm/30sec)
3
2
1
0
- 1
- 2
- 3
Linear flow rate (µm/s)
8
6
4
2
0
F
GFP
CYP46A1
pERK
DAPI
G
GFP
CYP46A1
***
Percentage of pERK positive cells
15
10
5
0

Figure 5. CYP46A1 overexpression improves axonal BDNF vesicles trafficking in Huntington' disease cortical neurons and postsynaptic dynamics in Huntington' disease striatal neurons. (**A**) Outline showing the 3-compartments microfluidic device used to reconstruct the cortico-striatal networks *in vitro*. (**B**) Representative kymographs of axonal transport of BDNF-mCherry vesicles obtained in *Hdh*$^{CAG140/+}$ (HD) cortical neurons treated with AAV-GFP or with AAV-CYP46A1 at DIV 7. Scale bar, 10 µm. (**C**) Kinetics analysis of BDNF vesicles transport in axons. Data are represented as mean ± SEM (n≥65 axons). (**D**) Representative kymographs of dendritic transport of TrkB-mCherry obtained in HD striatal neurons treated with AAV-GFP or with AAV-CYP46A1 at DIV7. Scale bar, 10 µm. (**E**) Kinetics analysis of TrkB vesicles transport in dendrites. Data are represented as mean ± SEM (n≥40 dendrites). (**F**) Representative images of pERK immunofluorescence in striatal neurons at DIV12 after Glycine/Strychnine stimulation of cortical neurons. Cortical and striatal neurons were treated with either AAV-GFP or AVV-CYP46A1. Scale bars, 100 µm. (**G**) Percentage of pERK-positive cells of after cortical stimulation. Data are represented as mean ± SEM (n≥40 fields). (**B-G**) Statistical analysis: Mann and Whitney test. CYP46A1 overexpression effect: **p*<0.05, ***p*<0.01, ****p*<0.001, *****p*<0.0001.

Figure 6

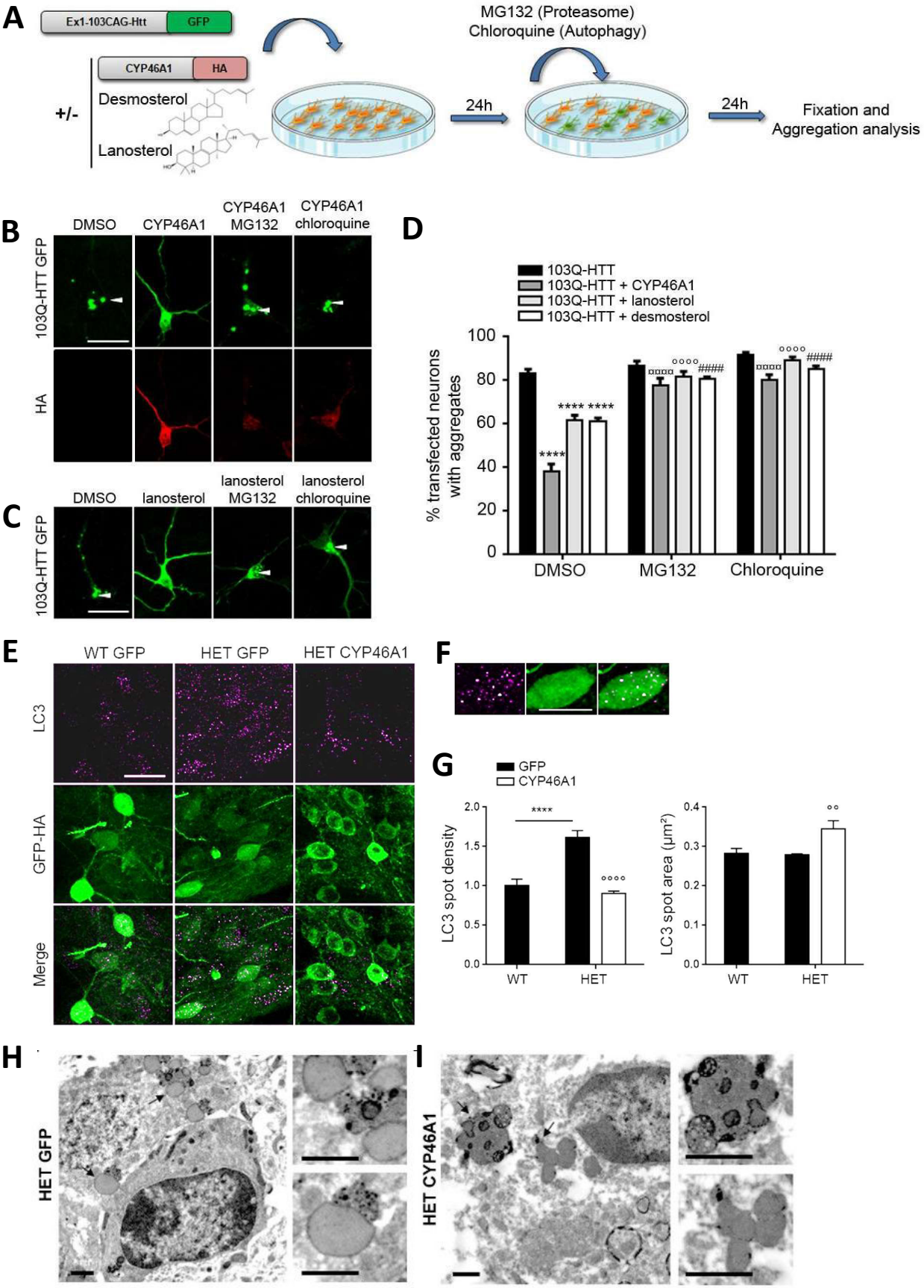
A
Ex1-103CAG-Htt
GFP
CYP46A1
HA
+/-
Desmosterol
Lanosterol
MG132 (Proteasome)
Chloroquine (Autophagy)
24h
24h
Fixation and
Aggregation analysis
B
DMSO
CYP46A1
CYP46A1
MG132
CYP46A1
chloroquine
103Q-HTT GFP
HA
C
DMSO
lanosterol
lanosterol
MG132
lanosterol
chloroquine
103Q-HTT GFP
D
103Q-HTT
103Q-HTT + CYP46A1
103Q-HTT + lanosterol
103Q-HTT + desmosterol
% transfected neurons
with aggregates
DMSO
MG132
Chloroquine
E
WT GFP
HET GFP
HET CYP46A1
LC3
GFP-HA
Merge
F
G
GFP
CYP46A1
LC3 spot density
LC3 spot area (µm²)
WT
HET
H
HET GFP
I
HET CYP46A1

Figure 6. The aggregate load decrease induced by CYP46A1 expression is associated with an improvement of proteasome and autophagy processes. (**A**) Striatal neurons were transfected with plasmids coding for 103Q-HTT and were either co-transfected with CYP46A1 or treated with lanosterol (1 µM) or desmosterol (1 µM). After 24h, cells were treated with proteasome inhibitor (MG132, 10 µM) or autophagy inhibitor (Chloroquine, 30 µM) for 24h. (**B-C**) GFP staining of 103Q-HTT (green) co-labelled with HA (red). Aggregates are pointed with white arrows. Scale bar 20 µm. (**D**) Quantification of aggregates based on GFP fluorescence. Data are represented as mean ±SEM (n = 100 transfected neurons per condition and per experiment). (**E-F**) Section from dorsal striatum of 12-month-old WT, HET and HOMO zQ175 mice. Double immunostaining with LC3 (red) and HA (green) antibodies (**E**), with a zoom on one cell from the HET-GFP section (**F**) Scale bar 20 µm. (**G**) Quantification of LC3 spots and area. (**B-G**) Data are represented as mean ±SEM. Statistical analysis: two-way ANOVA (**D**) and one-way ANOVA (**G**) followed by Bonferroni's post hoc. (**D**) CYP46A1, lanosterol and desmosterol effect: ****p<0.0001, inhibitor treatment effect: °°°°p<0.0001, ####p<0.0001, ¤¤¤¤p<0.0001. (**G**) Genotype main effect: ****p<0.0001, Treatment main effect: °°p<0.01, °°°°p<0.0001. (**H-I**) Electron micrographs of dorsal striatum of 12-month-old HET zQ175 mice (n = 4-5). Scale bar 1 µm (**H**) Higher magnification fields show clear content of the cytosolic large vacuoles. (**I**) Higher magnification fields show electron dense content inside some cytosolic large vacuoles.

Figure 7

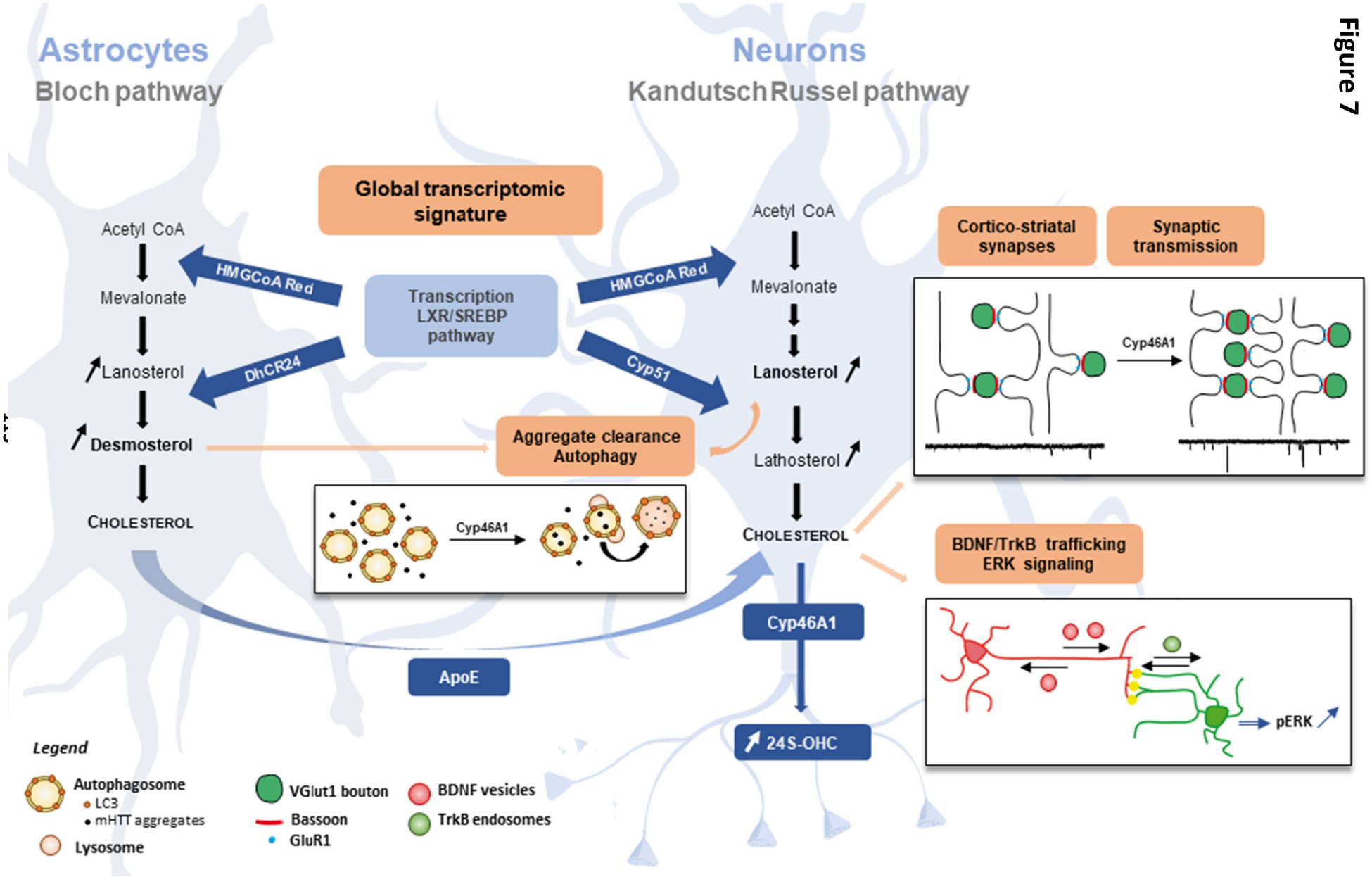
Astrocytes
Bloch pathway
Neurons
Kandutsch Russel pathway
Global transcriptomic signature
Acetyl CoA
Mevalonate
Lanosterol
Desmosterol
CHOLESTEROL
HMGCoA Red
DhCR24
Transcription LXR/SREBP pathway
HMGCoA Red
Cyp51
Aggregate clearance Autophagy
Cyp46A1
ApoE
Acetyl CoA
Mevalonate
Lanosterol
Lathosterol
CHOLESTEROL
Cyp46A1
24S-OHC
Cortico-striatal synapses
Synaptic transmission
Cyp46A1
BDNF/TrkB trafficking ERK signaling
pERK
Legend
Autophagosome
LC3
mHTT aggregates
Lysosome
VGlut1 bouton
Bassoon
GluR1
BDNF vesicles
TrkB endosomes

Figure 7. Schematic representation of cellular and molecular events involved in CYP46A1-mediated neuroprotection in Huntington' disease. Restoration of CYP46A1 in neuronal cells increases 24S-OHC the product of cholesterol degradation (blue). As a ligand of LXR 24S-OHC exerts a transcriptional control (blue) on cholesterogenic enzyme genes and ApoE (blue). It results in increased levels of lanosterol and desmosterol in astrocytes (Bloch pathway), along with lanosterol and lathosterol in neurons (Kandutsch Russel pathway). CYP46A1 strongly impacts on the transcriptional signature, with regulation of synaptic connectivity and autophagy/proteasome machineries (orange). As a consequence, a global restoration of cholesterol metabolism and transcriptomic signature exerts a beneficial control onto multiple cellular targets in a Huntington's disease context (orange). It includes restoration of cortico-striatal connectivity, synaptic transmission, BDNF/TrkB trafficking and activation of the pro-survival ERK signaling pathway (**See also Figure S7**). CYP46A1-induced production of lanosterol and desmosterol leads to a clearance of aggregates via the autophagosome and proteasome machineries (orange). Altogether, these data put forth a comprehensive model for CYP46A1-mediated neuroprotection in Huntington's disease.

Figure S1. Related to Figure 1

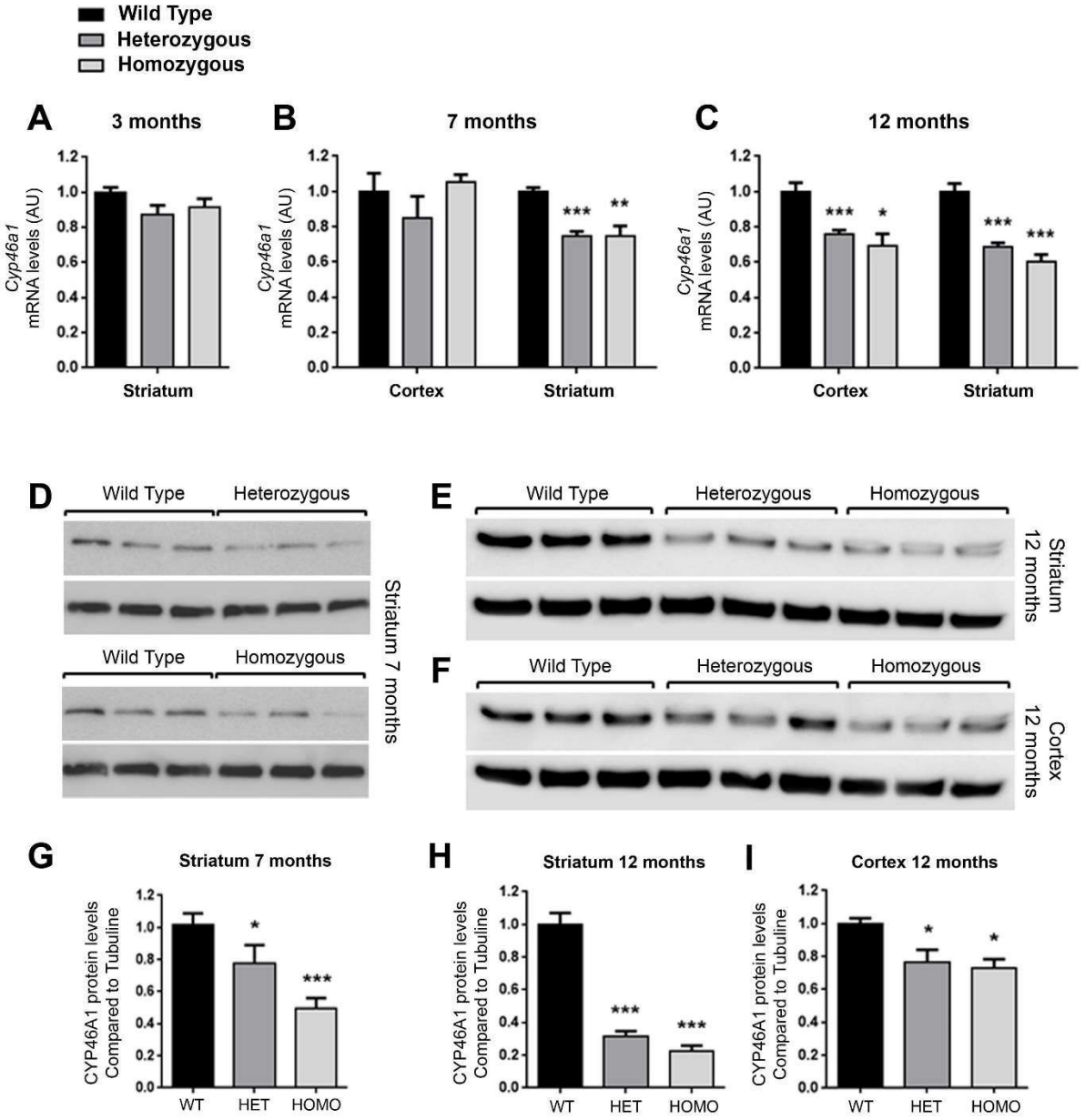

Figure S1. Expression levels of cyp46A1 mRNA and CYP46A1 protein are decreased in the cortex and striatum of zQ175 mice. Relative mouse endogenous *cyp46A1* mRNA levels (**A-C**) were measured by qPCR from cortex and striatum extracts from wild type (WT) and zQ175 mice (HET and HOMO) at different ages. Levels of *cyp46A1* mRNA were analyzed at 3-month-old (**A**), 7 months old (**B**) and 12-month-old (**C**) using *hprt* as housekeeping gene. (**D-F**) Striatum extracts from WT and zQ175 mice (HET and HOMO) at 7 months (**D**) and 12 months (**E**) and cortex extracts from WT and zQ175 mice (HET and HOMO) at 12 months (**F**) were processed for western blotting with antibodies directed against CYP46A1 and β-tubulin. (**G-I**) Quantification of CYP46A1 protein levels normalized to β-tubulin from western blots. Data are represented as mean ± SEM (n = 3-6 per group). Statistical analysis: unpaired Student's t-test *P<0.05; **P<0.01; ***P<0.001.

Figure S2. Related to Figure 1

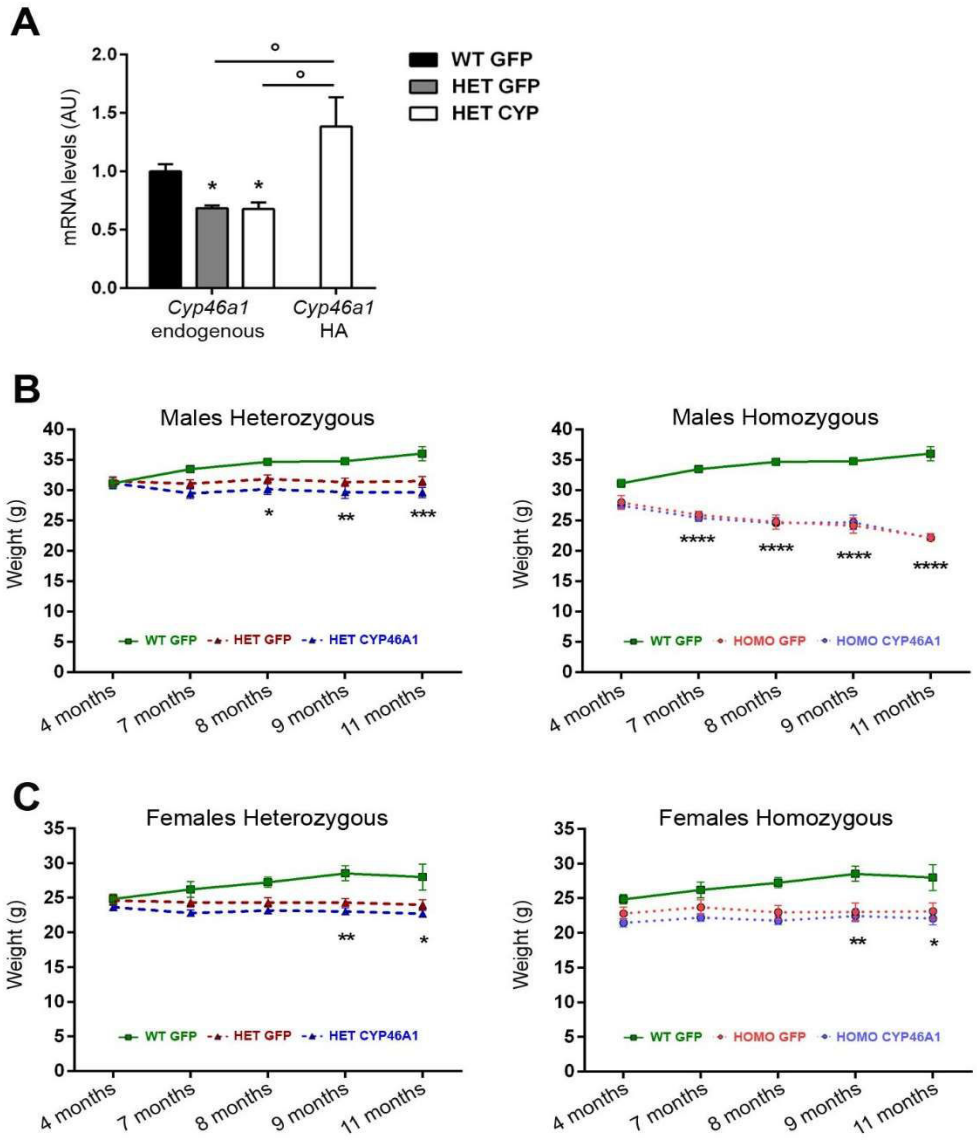

Figure S2. Restoration of CYP46A1 expression after injection of AAVrh10-CYP46A1 and its effect on average body weight as a function of age, genotype and condition. (**A**) Mouse endogenous *cyp46A1* and human *cyp46a1-HA* mRNA levels were measured by qPCR from striatum extracts from wild type (WT) and heterozygous mice (HET) at 12-month-old. Data are represented as mean ± SEM (n=5-6). Statistical analysis: one-way ANOVA followed by Tukey's post hoc test. *P<0.05, °P<0.05 (**B-C**) Mice were injected at 4-month-old with AAVrh10.GFP (GFP) or AAVrh10.CYP46A1 (CYP46A1) and were weighed once a month. Average body weight in males (**B**) and females (**C**). Data are represented as mean ± SEM; males: WT GFP (n=10), HET GFP (n=14), HET CYP4 (n=11), HOMO GFP (n=5), HOMO CYP46 (n=4); females: WT GFP (n=5), HET GFP (n=12), HTZ CYP46 (n=17), HOMO GFP and CYP46 (n=5). Statistical analysis: two-way ANOVA repeated measures with Bonferroni's post-test. Genotype main effect: *P<0.05, **P<0.01, ***P<0.001. Treatment main effect (GFP vs CYP46A1): not significant.

Figure S3. Related to Figure 2

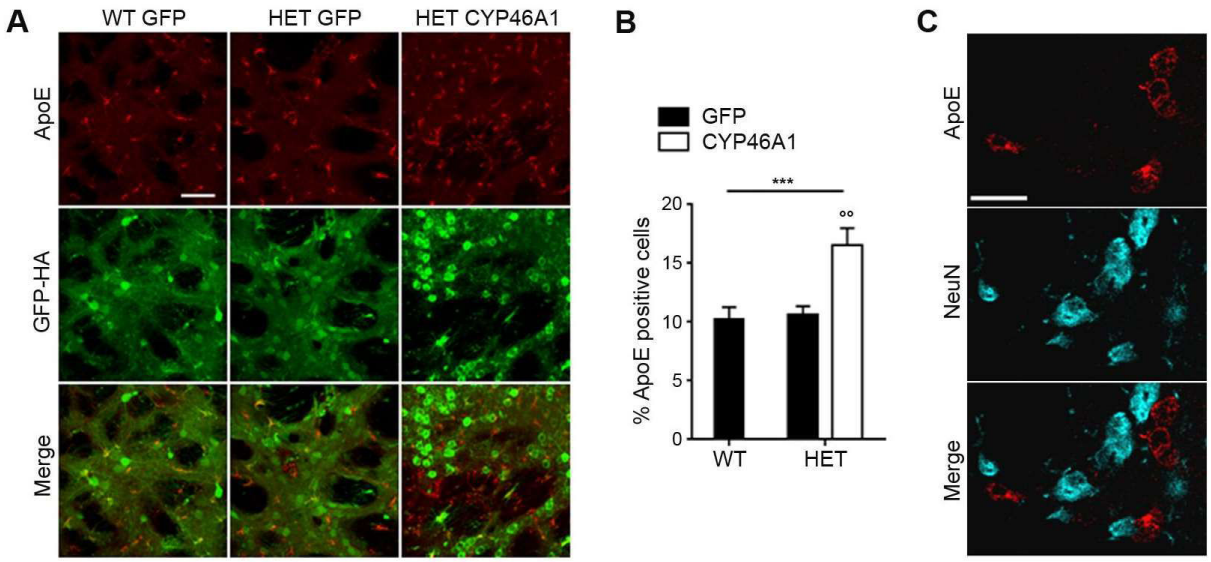

Figure S3. CYP46A1 increases APOE expression in non-neuronal cells. Section from dorsal striatum of 12-month-old WT and HET zQ175 mice. (**A**) Double immunostaining with ApoE (red) and HA (green) antibodies. Scale bar 50µm. (**B**) Quantification of ApoE positive cells. Data are represented as mean ± SEM, n = 5 per group. Statistical analysis: one-way ANOVA followed by Bonferroni's post hoc test. Genotype main effect: ***p<0.001, Treatment main effect: °°p<0.01. (**C**) Double immunostaining with ApoE (red) and NeuN (blue) antibodies. Scale bar 20µm.

Table S4. Related to Figure 3

CMap name	Enrichment	Drug/compound type	Mode of action
dexverapamil	0,963	Vasodilator agent	Calcium channel blocker
3-aminobenzamide	0,878	Neuroprotective agent	Poly(ADP-ribose) polymerase inhibitor
exemestane	0,872	Antineoplastic agent	Aromatase inhibitor
demecolcine	0,862	Antineoplastic agent	Tubulin modulator
4,5-dianilinophthalimide	0,853	Neuroprotective agent	Tyrosine kinase inhibitor
fisetin	0,829	Anti-Inflammatory agent - Antioxidant	Cyclin-dependent protein serine - Inhibits mTOR pathway
albendazole	0,815	Anti-Infective agent	Tubulin modulator
camptothecin	0,813	Antineoplastic agent	Topoisomerase I inhibitor
alexidine	0,809	Antimicrobial agent	ATPase proton transport modulator
irinotecan	0,803	Antineoplastic agent	Topoisomerase I inhibitor
doxorubicin	0,802	Antibiotic, Antineoplastic agent	Topoisomerase II inhibitor
corticosterone	0,786	Anti-Inflammatory agent	Activation of steroid nuclear receptors
procarbazine	0,78	Antineoplastic agent	Alkylating agent
esculetin	0,775	Antioxidant	Mitochondria modulation
atropine methonitrate	0,754	Parasympatholitic agent	Cholinergic antagonist
pizotifen	0,752	Antidepressive agent	Serotonin antagonist
mitoxantrone	0,747	Antineoplastic agent	Topoisomerase II inhibitor
adrenosterone	0,742	Steroid hormone	Activation androgenic receptors
nimesulide	0,725	Anti-Inflammatory agent	Cyclooxygenase inhibitor
ethosuximide	0,724	Anti-epileptic	Voltage dependent T-type calcium channel inhibitor
mepacrine	0,724	Antiparasitic agent	Phospholipase A2 inhibitor
tranylcypromine	0,717	Antidepressive agent	Monoamine oxidase inhibitor
octopamine	0,715	Vasoconstrictor agent	Adrenergic alpha agonist
gefitinib	0,713	Antineoplastic agent	Tyrosine kinase inhibitor
fendiline	0,711	Cardiovascular agent	Calcium channel blocker
helveticoside	0,704	Antiviral agent	
dirithromycin	0,703	Antibacterial agent	rRNA inhibition
zomepirac	0,696	Anti-Inflammatory agent	Cyclooxygenase inhibitor
tyrphostin AG-825	0,679	Antineoplastic agent	Tyrosine kinase inhibitor
celastrol	0,678	Neuroprotective agent	Antioxidant-Anti-Inflammatory agent
milrinone	0,674	Vasodilator agent	Phosphodiesterase 3 inhibitor
quinostatin	0,672	Antiproliferative agent	mTOR inhibitor
DL-thiorphan	0,671	Protease inhibitor	Prevent degradation of enkephalins

menadione	0,669	Vitamin	cofactor for gamma-carboxylases
homochlorcyclizine	0,663	Antihitaminic	Histamine H1 receptor antagonist
diperodon	0,662	Anaestetic	Sodium ion transmembrane transport
blebbistatin	0,662	Cytosqueleton modulation	Myosin II inhibitor
ketanserin	0,653	Antihypertensive agent	Serotonin antagonist (5-HT2 receptor)
altretamine	0,652	Antineoplastic agent	Alkylating agent
nortriptyline	0,648	Antidepressive agent	Noradrenaline and serotonin reuptake inhibitor
lysergol	0,648	Antipsychotic agent	5-Hydroxytryptamine receptor
rottlerin	0,646	Antioxidant	Uncoupler mitochondrial oxidative phosphorylation
butoconazole	0,637	Antifungal agent	Inhibits conversion of lanosterol in ergosterol
H-7	0,637	Enzyme inhibitor	Protein kinase C inhibitor
mycophenolic acid	0,637	Antibiotic, Antineoplastic agent	Inhibition of inosine monophosphate dehydrogenase
mefloquine	0,63	Antiparasitic agent	Inhibition of autophagocytosis (similar to chloroquine)
florfenicol	0,63	Antibacterial agent	
antazoline	0,624	Antihitaminic	Histamine H1 receptor antagonist
(-)-catechin	0,62	Antioxidant	Flavonoid biosynthesis
trazodone	0,619	Antidepressive, anti-anxiety agent	Serotonin uptake inhibitor (5-HT2 receptor)

Neuroprotective agent	9
Neurologic treatment	6
Antioxidant	3
Anti-Inflammatory agent	5
Antiviral/bacterial/parasitic	9
Antineoplastic agent	9
Calcium channel modulator	2

Table S4. Connectivity Map analysis (CMap) of gene expression patterns for the 50 small compounds and drugs highly correlated with transcriptome modification by CYP46A1 in zQ175 mice. CMap analysis was performed for the genes specifically regulated by CYP46A1. The hits were ranked using the CMap score 'Enrichment', for which values between +1 and -1 represent the relative strength of a given transcriptional signature related to CYP46A1 induced signature in zQ175 mice.

Figure S5. Related to Figure 4

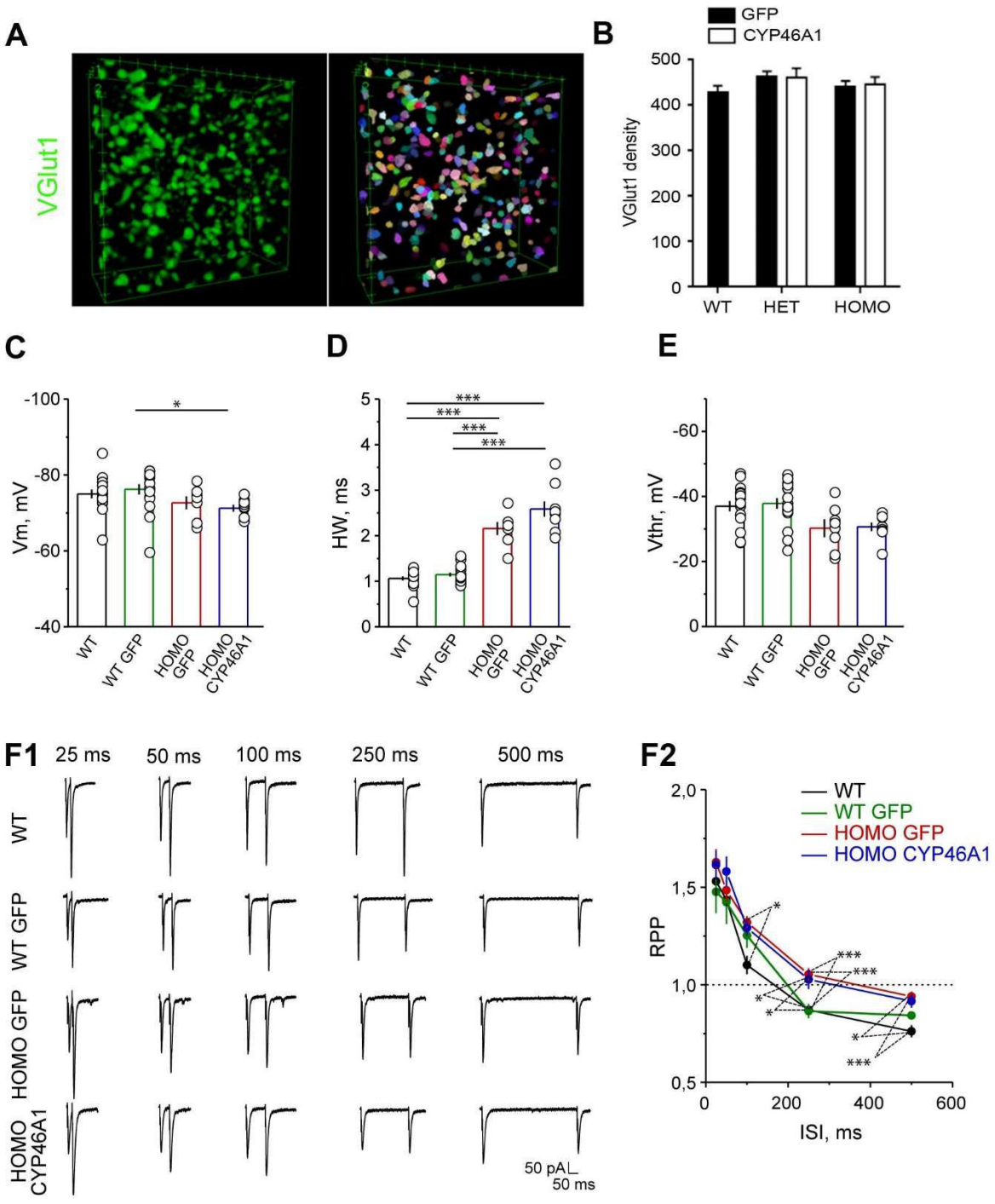

Figure S5. VGlut1 density and membrane properties of SPNs and paired-pulse ratio at cortico-striatal synapses in WT and zQ175 mice (**A-B**) Dorso-striatal sections of 7-month-old WT, HET and HOMO zQ175 mice. (**A**) 3D volume rendering of deconvolved image stack of VGlut1 3D surface rendering showing the output of the image segmentation. Each VGLUT1 boutons is assigned with a different color. Scale 1µm (**B**) Quantification of VGlut1 density. Data are represented as mean ± SEM. Statistical analysis: two-way ANOVA (not significant). (**C**) Resting membrane potential of SPNs in WT, WT-GFP, HOMO-GFP and HOMO-CYP mice. (**D**) Half-width of action potentials of SPNs in zQ175 mice were larger compared to WT mice. (**E**) The threshold of action potentials of SPNs in WT and zQ175 mice was not different after the injection of saline or CYP46A1. (**F1**) Representative traces of evoked EPSCs by cortical stimulation in SPNs for different inter-spike intervals (ISI, 25, 50, 100, 250, 500 ms) in WT, WT-GFP, HOMO-GFP and HOMO-CYP mice. (**F2**) The paired-pulse ratios of evoked EPSCs by cortical stimulation in SPNs in WT and zQ175 mice were not different at short intervals (ISI, 25, 50, 100ms) after the injection of saline or CYP46A1. WT mice displayed stronger depression at longer ISI (250, 500 ms) compared to ZQ175 mice after the injection of saline or CYP46A1. Statistical analysis: one-way ANOVA with Bonferroni's correction. *p<0.05, **p<0.01, **p<0.001.

Figure S6. Related to Figure 6

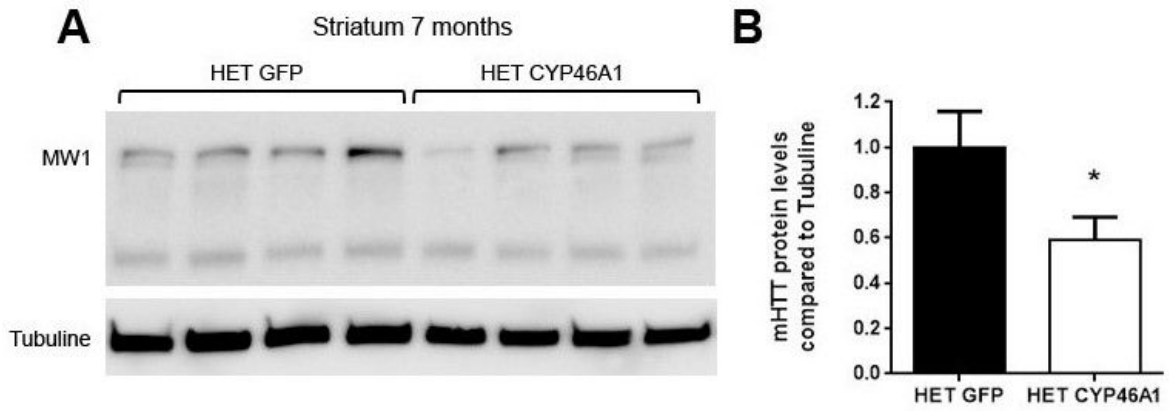

Figure S6. Expression levels of mHTT are decreased in the striatum of zQ175 mice after CYP46A1 injection. (**A**) Striatum extracts from WT and heterozygous zQ175 mice (HET) at 7 months were processed for western blotting with antibodies directed against MW1 (for mHTT) and β-tubulin. (**B**) Quantification of MW1 protein levels normalized to β-tubulin from western blots. Data are represented as mean ± SEM (n = 4 per group). Statistical analysis: Mann-Whitney test *P<0.05

Figure S7. Related to Figure 7

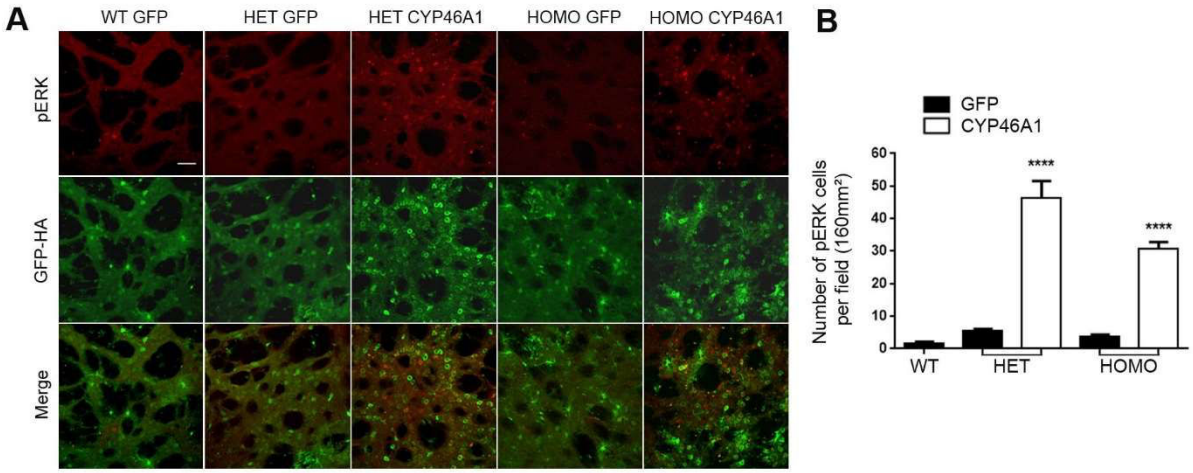

Figure S7. CYP46A1 induces ERK phosphorylation in vivo. Section from dorsal striatum of 12-month-old WT, HET and HOMO zQ175 mice. (**A**) Double immunostaining with pERK (red) and HA (green) antibodies. Scale bar 50µm. (**B**) Quantification of pERK positive cells. Data are represented as mean ± SEM, n = 5 per group. Statistical analysis: one-way ANOVA followed by Bonferroni's post hoc test. ****p<0.0001

References

Abildayeva K, Jansen PJ, Hirsch-Reinshagen V, Bloks VW, Bakker AHF, Ramaekers FCS, et al. 24(S)-Hydroxycholesterol Participates in a Liver X Receptor-controlled Pathway in Astrocytes That Regulates Apolipoprotein E-mediated Cholesterol Efflux. J. Biol. Chem. 2006; 281: 12799–12808.

Ament SA, Pearl JR, Grindeland A, St Claire J, Earls JC, Kovalenko M, et al. High resolution time-course mapping of early transcriptomic, molecular and cellular phenotypes in Huntington's disease CAG knock-in mice across multiple genetic backgrounds. Hum. Mol. Genet. 2017; 26: 913–922.

Aylward EH, Codori AM, Rosenblatt A, Sherr M, Brandt J, Stine OC, et al. Rate of caudate atrophy in presymptomatic and symptomatic stages of Huntington's disease. Mov. Disord. 2000; 15: 552–560.

Bennett EJ, Bence NF, Jayakumar R, Kopito RR. Global impairment of the ubiquitin-proteasome system by nuclear or cytoplasmic protein aggregates precedes inclusion body formation. Mol. Cell 2005; 17: 351–365.

Boussicault L, Alves S, Lamazière A, Planques A, Heck N, Moumné L, et al. CYP46A1, the rate-limiting enzyme for cholesterol degradation, is neuroprotective in Huntington's disease. Brain J. Neurol. 2016; 139: 953–970.

Boyles JK, Pitas RE, Wilson E, Mahley RW, Taylor JM. Apolipoprotein E associated with astrocytic glia of the central nervous system and with nonmyelinating glia of the peripheral nervous system. J. Clin. Invest. 1985; 76: 1501–1513.

Brown MS, Goldstein JL. The SREBP pathway: regulation of cholesterol metabolism by proteolysis of a membrane-bound transcription factor. Cell 1997; 89: 331–340.

Burlot M-A, Braudeau J, Michaelsen-Preusse K, Potier B, Ayciriex S, Varin J, et al. Cholesterol 24-hydroxylase defect is implicated in memory impairments associated with Alzheimer-like Tau pathology. Hum. Mol. Genet. 2015; 24: 5965–5976.

Button RW, Roberts SL, Willis TL, Hanemann CO, Luo S. Accumulation of autophagosomes confers cytotoxicity. J. Biol. Chem. 2017; 292: 13599–13614.

Charvin D, Vanhoutte P, Pagès C, Borrelli E, Borelli E, Caboche J. Unraveling a role for dopamine in Huntington's disease: the dual role of reactive oxygen species and D2 receptor stimulation. Proc. Natl. Acad. Sci. U. S. A. 2005; 102: 12218–12223.

Chen H, Yang J, Low PS, Cheng J-X. Cholesterol level regulates endosome motility via Rab proteins. Biophys. J. 2008; 94: 1508–1520.

Chevy F, Humbert L, Wolf C. Sterol profiling of amniotic fluid: a routine method for the detection of distal cholesterol synthesis deficit. Prenat. Diagn. 2005; 25: 1000–1006.

Cui L, Jeong H, Borovecki F, Parkhurst CN, Tanese N, Krainc D. Transcriptional repression of PGC-1alpha by mutant huntingtin leads to mitochondrial dysfunction and neurodegeneration. Cell 2006; 127: 59–69.

Deyts C, Galan-Rodriguez B, Martin E, Bouveyron N, Roze E, Charvin D, et al. Dopamine D2 receptor stimulation potentiates PolyQ-Huntingtin-induced mouse striatal neuron dysfunctions via Rho/ROCK-II activation. PloS One 2009; 4: e8287.

Djelti F, Braudeau J, Hudry E, Dhenain M, Varin J, Bièche I, et al. CYP46A1 inhibition, brain cholesterol accumulation and neurodegeneration pave the way for Alzheimer's disease. Brain J. Neurol. 2015; 138: 2383–2398.

Dzeletovic S, Breuer O, Lund E, Diczfalusy U. Determination of cholesterol oxidation products in human plasma by isotope dilution-mass spectrometry. Anal. Biochem. 1995; 225: 73–80.

Fan Q-W, Yu W, Gong J-S, Zou K, Sawamura N, Senda T, et al. Cholesterol-dependent modulation of dendrite outgrowth and microtubule stability in cultured neurons. J. Neurochem. 2002; 80: 178–190.

Fox EJ. Management of worsening multiple sclerosis with mitoxantrone: a review. Clin. Ther. 2006; 28: 461–474.

Gauthier LR, Charrin BC, Borrell-Pagès M, Dompierre JP, Rangone H, Cordelières FP, et al. Huntingtin controls neurotrophic support and survival of neurons by enhancing BDNF vesicular transport along microtubules. Cell 2004; 118: 127–138.

Ghisletti S, Huang W, Ogawa S, Pascual G, Lin M-E, Willson TM, et al. Parallel SUMOylation-dependent pathways mediate gene- and signal-specific transrepression by LXRs and PPARgamma. Mol. Cell 2007; 25: 57–70.

Goritz C, Mauch DH, Pfrieger FW. Multiple mechanisms mediate cholesterol-induced synaptogenesis in a CNS neuron. Mol. Cell. Neurosci. 2005; 29: 190–201.

Heacock AM, Klinger PD, Seguin EB, Agranoff BW. Cholesterol synthesis and nerve regeneration. J. Neurochem. 1984; 42: 987–993.

Heikkinen T, Lehtimäki K, Vartiainen N, Puoliväli J, Hendricks SJ, Glaser JR, et al. Characterization of neurophysiological and behavioral changes, MRI brain volumetry and 1H MRS in zQ175 knock-in mouse model of Huntington's disease. PloS One 2012; 7: e50717.

Hudry E, Van Dam D, Kulik W, De Deyn PP, Stet FS, Ahouansou O, et al. Adeno-associated virus gene therapy with cholesterol 24-hydroxylase reduces the amyloid pathology before or after the onset of amyloid plaques in mouse models of Alzheimer's disease. Mol. Ther. J. Am. Soc. Gene Ther. 2010; 18: 44–53.

Hunter JM, Lesort M, Johnson GVW. Ubiquitin-proteasome system alterations in a striatal cell model of Huntington's disease. J. Neurosci. Res. 2007; 85: 1774–1788.

Indersmitten T, Tran CH, Cepeda C, Levine MS. Altered excitatory and inhibitory inputs to striatal medium-sized spiny neurons and cortical pyramidal neurons in the Q175 mouse model of Huntington's disease. J. Neurophysiol. 2015; 113: 2953–2966.

Kabeya Y, Mizushima N, Ueno T, Yamamoto A, Kirisako T, Noda T, et al. LC3, a mammalian homologue of yeast Apg8p, is localized in autophagosome membranes after processing. EMBO J. 2000; 19: 5720–5728.

Karasinska JM, Hayden MR. Cholesterol metabolism in Huntington disease. Nat. Rev. Neurol. 2011; 7: 561–572.

Kim D, Langmead B, Salzberg SL. HISAT: a fast spliced aligner with low memory requirements. Nat. Methods 2015; 12: 357–360.

Korade Z, Kenworthy AK. Lipid rafts, cholesterol, and the brain. Neuropharmacology 2008; 55: 1265–1273.

Kreilaus F, Spiro AS, McLean CA, Garner B, Jenner AM. Evidence for altered cholesterol metabolism in Huntington's disease post mortem brain tissue. Neuropathol. Appl. Neurobiol. 2016; 42: 535–546.

Langfelder P, Cantle JP, Chatzopoulou D, Wang N, Gao F, Al-Ramahi I, et al. Integrated genomics and proteomics define huntingtin CAG length-dependent networks in mice. Nat. Neurosci. 2016; 19: 623–633.

Lehmann JM, Kliewer SA, Moore LB, Smith-Oliver TA, Oliver BB, Su J-L, et al. Activation of the Nuclear Receptor LXR by Oxysterols Defines a New Hormone Response Pathway. J. Biol. Chem. 1997; 272: 3137–3140.

Lejeune F-X, Mesrob L, Parmentier F, Bicep C, Vazquez-Manrique RP, Parker JA, et al. Large-scale functional RNAi screen in C. elegans identifies genes that regulate the dysfunction of mutant polyglutamine neurons. BMC Genomics 2012; 13: 91.

Leoni V, Caccia C. The impairment of cholesterol metabolism in Huntington disease. Biochim. Biophys. Acta 2015; 1851: 1095–1105.

Leoni V, Long JD, Mills JA, Di Donato S, Paulsen JS, PREDICT-HD study group. Plasma 24S-hydroxycholesterol correlation with markers of Huntington disease progression. Neurobiol. Dis. 2013; 55: 37–43.

Leoni V, Mariotti C, Tabrizi SJ, Valenza M, Wild EJ, Henley SMD, et al. Plasma 24S-hydroxycholesterol and caudate MRI in pre-manifest and early Huntington's disease. Brain J. Neurol. 2008; 131: 2851–2859.

Li H, Li SH, Yu ZX, Shelbourne P, Li XJ. Huntingtin aggregate-associated axonal degeneration is an early pathological event in Huntington's disease mice. J. Neurosci. Off. J. Soc. Neurosci. 2001; 21: 8473–8481.

Li S-H, Cheng AL, Zhou H, Lam S, Rao M, Li H, et al. Interaction of Huntington disease protein with transcriptional activator Sp1. Mol. Cell. Biol. 2002; 22: 1277–1287.

Liao Y, Smyth GK, Shi W. featureCounts: an efficient general purpose program for assigning sequence reads to genomic features. Bioinformatics 2014; 30: 923–930.

Liot G, Zala D, Pla P, Mottet G, Piel M, Saudou F. Mutant Huntingtin alters retrograde transport of TrkB receptors in striatal dendrites. J. Neurosci. Off. J. Soc. Neurosci. 2013; 33: 6298–6309.

Lund EG, Guileyardo JM, Russell DW. cDNA cloning of cholesterol 24-hydroxylase, a mediator of cholesterol homeostasis in the brain. Proc. Natl. Acad. Sci. U. S. A. 1999; 96: 7238–7243.

MacDonald ME, Ambrose CM, Duyao MP, Myers RH, Lin C, Srinidhi L, et al. A novel gene containing a trinucleotide repeat that is expanded and unstable on Huntington's disease chromosomes. Cell 1993; 72: 971–983.

Maioli S, Båvner A, Ali Z, Heverin M, Ismail M-A-M, Puerta E, et al. Is it possible to improve memory function by upregulation of the cholesterol 24S-hydroxylase (CYP46A1) in the brain? PloS One 2013; 8: e68534.

Martinez-Vicente M, Talloczy Z, Wong E, Tang G, Koga H, Kaushik S, et al. Cargo recognition failure is responsible for inefficient autophagy in Huntington's disease. Nat. Neurosci. 2010; 13: 567–576.

Mast N, Lin JB, Anderson KW, Bjorkhem I, Pikuleva IA. Transcriptional and post-translational changes in the brain of mice deficient in cholesterol removal mediated by cytochrome P450 46A1 (CYP46A1). PloS One 2017; 12: e0187168.

Mauch DH, Nägler K, Schumacher S, Göritz C, Müller EC, Otto A, et al. CNS synaptogenesis promoted by glia-derived cholesterol. Science 2001; 294: 1354–1357.

Menalled LB, Kudwa AE, Miller S, Fitzpatrick J, Watson-Johnson J, Keating N, et al. Comprehensive behavioral and molecular characterization of a new knock-in mouse model of Huntington's disease: zQ175. PloS One 2012; 7: e49838.

Milhaud D, Rondouin G, Lerner-Natoli M, Bockaert J, Lafon-Cazal M. Neuroprotective activity of antazoline against neuronal damage induced by limbic status epilepticus. Neuroscience 2003; 120: 475–484.

Milnerwood AJ, Raymond LA. Early synaptic pathophysiology in neurodegeneration: insights from Huntington's disease. Trends Neurosci. 2010; 33: 513–523.

Moumné L, Betuing S, Caboche J. Multiple Aspects of Gene Dysregulation in Huntington's Disease. Front. Neurol. 2013; 4: 127.

Moutinho M, Nunes MJ, Correia JC, Gama MJ, Castro-Caldas M, Cedazo-Minguez A, et al. Neuronal cholesterol metabolism increases dendritic outgrowth and synaptic markers via a concerted action of GGTase-I and Trk. Sci. Rep. 2016; 6: 30928.

Nieweg K, Schaller H, Pfrieger FW. Marked differences in cholesterol synthesis between neurons and glial cells from postnatal rats. J. Neurochem. 2009; 109: 125–134.

Nucifora FC, Sasaki M, Peters MF, Huang H, Cooper JK, Yamada M, et al. Interference by huntingtin and atrophin-1 with cbp-mediated transcription leading to cellular toxicity. Science 2001; 291: 2423–2428.

Paul SM, Doherty JJ, Robichaud AJ, Belfort GM, Chow BY, Hammond RS, et al. The major brain cholesterol metabolite 24(S)-hydroxycholesterol is a potent allosteric modulator of N-methyl-D-aspartate receptors. J. Neurosci. Off. J. Soc. Neurosci. 2013; 33: 17290–17300.

Pfrieger FW. Role of cholesterol in synapse formation and function. Biochim. Biophys. Acta 2003; 1610: 271–280.

Pitas RE, Boyles JK, Lee SH, Hui D, Weisgraber KH. Lipoproteins and their receptors in the central nervous system. Characterization of the lipoproteins in cerebrospinal fluid and identification of apolipoprotein B,E(LDL) receptors in the brain. J. Biol. Chem. 1987; 262: 14352–14360.

Plotkin JL, Surmeier DJ. Corticostriatal synaptic adaptations in Huntington's disease. Curr. Opin. Neurobiol. 2015; 33: 53–62.

Rai A, Pathak D, Thakur S, Singh S, Dubey AK, Mallik R. Dynein Clusters into Lipid Microdomains on Phagosomes to Drive Rapid Transport toward Lysosomes. Cell 2016; 164: 722–734.

Rapaport F, Zinovyev A, Dutreix M, Barillot E, Vert J-P. Classification of microarray data using gene networks. BMC Bioinformatics 2007; 8: 35.

Raymond LA. Striatal synaptic dysfunction and altered calcium regulation in Huntington disease. Biochem. Biophys. Res. Commun. 2017; 483: 1051–1062.

Rothe T, Deliano M, Wójtowicz AM, Dvorzhak A, Harnack D, Paul S, et al. Pathological gamma oscillations, impaired dopamine release, synapse loss and reduced dynamic range of unitary glutamatergic synaptic transmission in the striatum of hypokinetic Q175 Huntington mice. Neuroscience 2015; 311: 519–538.

Roze E, Betuing S, Deyts C, Marcon E, Brami-Cherrier K, Pagès C, et al. Mitogen- and stress-activated protein kinase-1 deficiency is involved in expanded-huntingtin-induced transcriptional dysregulation and striatal death. FASEB J. Off. Publ. Fed. Am. Soc. Exp. Biol. 2008; 22: 1083–1093.

Sarantos MR, Papanikolaou T, Ellerby LM, Hughes RE. Pizotifen Activates ERK and Provides Neuroprotection in vitro and in vivo in Models of Huntington's Disease. J. Huntingt. Dis. 2012; 1: 195–210.

Schaffar G, Breuer P, Boteva R, Behrends C, Tzvetkov N, Strippel N, et al. Cellular toxicity of polyglutamine expansion proteins: mechanism of transcription factor deactivation. Mol. Cell 2004; 15: 95–105.

Seo H, Sonntag K-C, Isacson O. Generalized brain and skin proteasome inhibition in Huntington's disease. Ann. Neurol. 2004; 56: 319–328.

Shankaran M, Di Paolo E, Leoni V, Caccia C, Ferrari Bardile C, Mohammed H, et al. Early and brain region-specific decrease of de novo cholesterol biosynthesis in Huntington's disease: A cross-validation study in Q175 knock-in mice. Neurobiol. Dis. 2017; 98: 66–76.

Sipione S, Rigamonti D, Valenza M, Zuccato C, Conti L, Pritchard J, et al. Early transcriptional profiles in huntingtin-inducible striatal cells by microarray analyses. Hum. Mol. Genet. 2002; 11: 1953–1965.

Spann NJ, Garmire LX, McDonald JG, Myers DS, Milne SB, Shibata N, et al. Regulated accumulation of desmosterol integrates macrophage lipid metabolism and inflammatory responses. Cell 2012; 151: 138–152.

Subramanian A, Narayan R, Corsello SM, Peck DD, Natoli TE, Lu X, et al. A Next Generation Connectivity Map: L1000 Platform and the First 1,000,000 Profiles. Cell 2017; 171: 1437-1452.e17.

Subtil A, Gaidarov I, Kobylarz K, Lampson MA, Keen JH, McGraw TE. Acute cholesterol depletion inhibits clathrin-coated pit budding. Proc. Natl. Acad. Sci. U. S. A. 1999; 96: 6775–6780.

Szklarczyk D, Morris JH, Cook H, Kuhn M, Wyder S, Simonovic M, et al. The STRING database in 2017: quality-controlled protein-protein association networks, made broadly accessible. Nucleic Acids Res. 2017; 45: D362–D368.

Tanida I, Ueno T, Kominami E. LC3 conjugation system in mammalian autophagy. Int. J. Biochem. Cell Biol. 2004; 36: 2503–2518.

del Toro D, Alberch J, Lázaro-Diéguez F, Martín-Ibáñez R, Xifró X, Egea G, et al. Mutant huntingtin impairs post-Golgi trafficking to lysosomes by delocalizing optineurin/Rab8 complex from the Golgi apparatus. Mol. Biol. Cell 2009; 20: 1478–1492.

Tourette C, Farina F, Vazquez-Manrique RP, Orfila A-M, Voisin J, Hernandez S, et al. The Wnt receptor Ryk reduces neuronal and cell survival capacity by repressing FOXO activity during the early phases of mutant huntingtin pathogenicity. PLoS Biol. 2014; 12: e1001895.

Tsunemi T, Ashe TD, Morrison BE, Soriano KR, Au J, Roque RAV, et al. PGC-1α rescues Huntington's disease proteotoxicity by preventing oxidative stress and promoting TFEB function. Sci. Transl. Med. 2012; 4: 142ra97.

Upadhyay A, Amanullah A, Mishra R, Kumar A, Mishra A. Lanosterol Suppresses the Aggregation and Cytotoxicity of Misfolded Proteins Linked with Neurodegenerative Diseases. Mol. Neurobiol. 2018; 55: 1169–1182.

Valenza M, Cattaneo E. Emerging roles for cholesterol in Huntington's disease. Trends Neurosci. 2011; 34: 474–486.

Valenza M, Leoni V, Karasinska JM, Petricca L, Fan J, Carroll J, et al. Cholesterol defect is marked across multiple rodent models of Huntington's disease and is manifest in astrocytes. J. Neurosci. Off. J. Soc. Neurosci. 2010; 30: 10844–10850.

Valenza M, Marullo M, Di Paolo E, Cesana E, Zuccato C, Biella G, et al. Disruption of astrocyte-neuron cholesterol cross talk affects neuronal function in Huntington's disease. Cell Death Differ. 2015; 22: 690–702.

Virlogeux A, Moutaux E, Christaller W, Genoux A, Bruyère J, Fino E, et al. Reconstituting Corticostriatal Network on-a-Chip Reveals the Contribution of the Presynaptic Compartment to Huntington's Disease. Cell Rep. 2018a; 22: 110–122.

Virlogeux A, Moutaux E, Christaller W, Genoux A, Bruyère J, Fino E, et al. Reconstituting Corticostriatal Network on-a-Chip Reveals the Contribution of the Presynaptic Compartment to Huntington's Disease. Cell Rep. 2018b; 22: 110–122.

Wang C, Pei A, Chen J, Yu H, Sun M-L, Liu C-F, et al. A natural coumarin derivative esculetin offers neuroprotection on cerebral ischemia/reperfusion injury in mice. J. Neurochem. 2012; 121: 1007–1013.

Watanabe R, Kurose T, Morishige Y, Fujimori K. Protective Effects of Fisetin Against 6-OHDA-Induced Apoptosis by Activation of PI3K-Akt Signaling in Human Neuroblastoma SH-SY5Y Cells. Neurochem. Res. 2018; 43: 488–499.

Wong YC, Holzbaur ELF. The regulation of autophagosome dynamics by huntingtin and HAP1 is disrupted by expression of mutant huntingtin, leading to defective cargo degradation. J. Neurosci. Off. J. Soc. Neurosci. 2014; 34: 1293–1305.

Yang C, McDonald JG, Patel A, Zhang Y, Umetani M, Xu F, et al. Sterol intermediates from cholesterol biosynthetic pathway as liver X receptor ligands. J. Biol. Chem. 2006; 281: 27816–27826.

Zala D, Hinckelmann MV, Yu H, Lyra Da Cunha MM, Liot G, Cordelières FP, et al. Vesicular glycolysis provides on-board energy for fast axonal transport. Cell 2013; 152: 479–491.

Zhang Y, Moheban DB, Conway BR, Bhattacharyya A, Segal RA. Cell surface Trk receptors mediate NGF-induced survival while internalized receptors regulate NGF-induced differentiation. J. Neurosci. Off. J. Soc. Neurosci. 2000; 20: 5671–5678.

Zhao L, Chen X-J, Zhu J, Xi Y-B, Yang X, Hu L-D, et al. Lanosterol reverses protein aggregation in cataracts. Nature 2015; 523: 607–611.

Zuccato C, Tartari M, Crotti A, Goffredo D, Valenza M, Conti L, et al. Huntingtin interacts with REST/NRSF to modulate the transcription of NRSE-controlled neuronal genes. Nat. Genet. 2003; 35: 76–83.

Paper 2 – Profiling gene expression and cholesterol metabolism in purified neurons and astrocytes from mouse tissue using Fluorescence-Activated Cell sorting

Profiling gene expression and cholesterol metabolism in purified neurons and astrocytes from mouse tissue using Fluorescence-Activated Cell sorting

Introduction

Cholesterol is a major component of the CNS, with a tightly regulated metabolism (Zhang and Liu, 2015). Cholesterol exerts key functions as a structural component of membranes, myelin sheaths but also through its precursors, which are biologically active. Glia-neuron interactions are critical for maintaining the normal function and survival of neurons in the brain (Barros et al., 2018). More specifically, it is now well established that cholesterol metabolism and turn-over depend on a crosstalk between astrocytes and neurons (Nieweg et al., 2009). Cholesterol cannot cross the blood brain barrier (Jeske and Dietschy, 1980) and the main origin for newly synthesized cholesterol depends on astrocytes in the adult brain (Saher and Stumpf, 2015). Cholesterol is then transported to neurons via ApoE lipoproteins (Pitas et al., 1987). Cholesterol turn-over depends on CYP46A1, the neuronal rate-limiting enzyme for cholesterol degradation (Lund et al., 1999). Disturbed cholesterol metabolism has been described in neurodegenerative diseases, such as Alzheimer's and Huntington's disease (Martín et al., 2014). However, it remains to be known whether and how cholesterol metabolism is controlled in these pathological conditions. In particular it remains to be established whether neuronal/astrocyte normal functions for cholesterol metabolism are maintained. In line with this, we recently showed that neuronal restoration of CYP461, produced a large restoration of transcriptomic and sterol profiles (Kacher et al., under review).

To specifically address this, we set up in the present study a methodology based on fluorescence-activated cell sorting (FACS) for the isolation of neurons and astrocytes from the striatum. Stereotaxic striatal injections in mice were performed with an AAV5. gfaBC1D.dtTomato which targets astrocytes, and a neuronal AAVrh10.CMV.GFP alone or co-injected with a neuronal AAVrh10.CAG.CYP46A1. Striatal cells were enzymatically and mechanically dissociated followed by analysis and sorting using FACS. The cell viability and quality of RNA were optimized after cell sorting. Moreover, cell sorting was validated using qPCR analysis of neuronal and astrocytic target genes, showing a cell-specific enrichment. Therefore, this method will be a useful tool for further studies in HD mice.

Methods

Experimental models

Mice were housed in groups of 2 to 5 with access to food and water *ad libitum* and kept at a constant temperature (19-22 °C) and humidity (40-50%) on a 12:12 h light/dark cycle. All experimental procedures were performed in authorized establishments in strict accordance with the recommendations of the European Community (86/609/EEC) and the French National Committee (2010/63) for care and use of laboratory animals under the supervision of authorized investigators (permission (#01435.02 to J. Caboche and S. Betuing). The male wild type mice C57BL/6J were obtained from Charles River Laboratories. The local ethics committee approved the experiments.

Production and stereotaxic injection of AAVrh10.CMV.GFP, AAV5.gfaBC1D.dtTomato and AAVrh10.CAG.CYP46A1

AAVrh10.CMV.GFP and AAVrh10.CAG.CYP46A1-HA vectors were produced and purified by Atlantic Gene therapies (Inserm U1089, Nantes, France). AAV5.gfaBC1D.dtTomato vector was produced and purified by Penn Vector Core (University of Pennsylvania). Viral constructs for AAVrh10.CMV.GFP contains the expression cassette consisting of the GFP sequence, driven by a CMV/β-actin hybrid promoter surrounded by inverted terminal repeats of AAV2. Viral constructs for AAVrh10.CAG.CYP46A1-HA contains the expression cassette consisting of the human CYP46A1 sequence driven by a CAG promoter surrounded by inverted terminal repeats of AAV2. Viral constructs for AAV5.gfaBC1D.dtTomato contain the expression cassette consisting on dt-Tomato driven by a gfaABC1D promoter surrounded by inverted terminal repeats of AAV5. The mice were injected at 4 months at the following stereotaxic coordinates: 1.5 mm or 0.86 mm rostral to the bregma, 1.5 mm or 2 mm lateral to midline (respectively) and 3.25 mm ventral to the skull surface. The rate of injection was 0,2 µl/min with a total volume of 2 µl per striatum (equivalent to 3.10^9 genomic particles).

Immunohistochemistry

Mice were deeply anaesthetized by intraperitoneal injection of sodium pentobarbital 250 mg/kg (Sanofi). Intracardiac perfusion of 4% paraformaldehyde in 0.1 M Na2HPO4/NaH2PO4 buffer, pH 7.5 was performed and brains were post-fixed overnight in the same solution at 4°C. Coronal brain sections (30 µm) were done using a vibratome in 0.1 M Na2HPO4/NaH2PO4 buffer. Free-floating sections were permeabilized and blocked with 5% NGS (normal goat serum) 0,2% triton in TBS (Tris-Buffered Saline) for 2h at RT. Sections were then incubated with primary antibody rat anti-HA (1:400; Sigma) in 5% NGS in TBS overnight. The sections were incubated in secondary antibody anti-rat cy5 (1:500, Jackson

Laboratories) in 1% NGS in TBS for 2h at RT. Sections were then mounted under cover slips in ProLong Gold antifade reagent (ThermoFischer).

Image acquisition and analysis

For immunohistochemistry, image stacks were taken using a confocal laser scanning microscope (SP5, Leica Microsystems), with a pinhole aperture set to 1 Airy unit. Stack of confocal images were done using a x40 oil objective, with a 1,6 µm z-interval. The excitation wavelength and emission range were 488 and 500-550nm for GFP, 561 and 570-620nm for tomato, 633 and 640-700nm for cy5. Laser intensity and detector gain were constant for all images of the same analysis. All images were done in the transduced area and all analyses were performed on maximum projection of confocal stack using Fiji software. For each analysis 5 mice were used.

Dissociation of brain tissue and purification of single cell suspension

Mice were sacrificed 2 months after injection by decapitation and the striatum was dissected on ice. For tissue dissociation the Neural Tissue Dissociation Kit was used (Miltenyi Biotec), followed by a removal of myelin debris using Myelin Removal Beads II (Miltenyi Biotec). Briefly, the tissue was cut in pre-warmed papain solution and incubated with agitation at 37°C. After 15 min of incubation, the tissue is mechanically dissociated using large diameter fire polished Pasteur pipette. The suspension is then incubated 10 min followed by mechanical dissociation with medium diameter fire polished Pasteur pipette. The suspension is incubated 10 min followed by mechanical dissociation with small diameter fire polished Pasteur pipette. Large debris were removed by filtration through a 70 µm filter (Sigma) and the cell suspension was then centrifuged 10 min at 500 g. The pellet was resuspended in PBS 0.5% BSA and the appropriate volume of Myelin Removal Beads was added. After 15 min of incubation at 4°C, the cells were washed with PBS 0.5% BSA and centrifuged 10 min at 500 g. The pellet was resuspended in PBS 0.5% BSA and the cell suspension was passed through LS columns in the magnetic field of a MACS separator (Miltenyi Biotec). The collected cells were centrifuged 10 min at 500 g at 4° C and resuspended in HBSS without phenol (Sigma) for cell sorting.

Cell sorting

A FACS Aria II (BD Biosciences) instrument was used for cell sorting. The following controls were used: non-injected mouse (control without fluorescence), AAVrh10.CMV.GFP injected mouse and AAV5.gfaBC1D.tdTomato injected mouse. Cell population was identified based on forward scattering (FSC) and side scattering (SSC) properties. Gating based on FSC width was used to select only single cells. Fluorescent positive cells were selected based on gating for FITC positive cells (GFP expressing

cells) and PE-Texas Red positive cells (tdTomato expressing cells). Cells were sorted in low binding tubes in 30 µL of HBSS without phenol (Sigma).

RNA extraction and preparation of amplified cDNA

Sorted cells were homogenized in Trizol LS (ThermoFischer) and stored at – 80° C until RNA extraction. RNA isolation was performed with RNeasy Micro kit (Qiagen) according to manufacturer's instructions, with a DNAse treatment step. RNA quality was evaluated using RNA HighSens Chip (Experion, BioRad). Preparation of amplified cDNA was done using the Ovation PicoSL WTA System V2 (NuGEN) according to manufacturer's instructions. It is based on three main steps: generation of first strand cDNA, generation of DNA/RNA double strand cDNA and amplification. Finally, a purification of cDNA was performed using MinElute Reaction Cleanup Kit (Qiagen) according to manufacturer's instructions. cDNA purity and concentration were measured with a Nanodrop 2000 (ThermoScientific).

LightCycler real time polymerase chain reaction

Quantitative real-time PCR reactions were performed using LightCycler480 SYBR-Green I Master according to manufacturer's protocol and run on LightCycler480 (Roche Diagnostics). The cycle threshold values were calculated automatically by LightCycler480 SW 1.5 software with default parameters. Gene expression was quantified using specific primers (see table). *Hprt1* was used as a control for the cDNA levels.

Gene	Forward sequence	Reverse sequence
darpp32	5' CACCCAAGTCGAAGAGACC 3'	5' TCCTCCTCATCATCCTCCTG 3'
3pgdh	5' AATTGGAAGAGAGGTGGCCA 3'	5' GCACACCTTTCTTGCACTGA 3'
s100b	5' AAAGTGATGGAGACGCTGGA 3'	5' CTTTGCTGTGCCTCCTCTTG 3'
iba1	5' GACAGACTGCCAGCCTAAGA 3'	5' TTTGGACGGCAGATCCTCAT 3'
dhcr7	5' AGACATTTGGGCCAAGACAC 3'	5' AACCTGGCAGAAATCTGTGG 3'
dhcr24	5' ATCTGCCCTGTTGCTACTGT 3'	5'CAAGGCAGAAGGACCTCAGA 3'
cyp46a1	5' TCCTCTCCTGTTCAGCACC 3'	5'CAGCTTGGCCATGACAACT 3'
abca1	5' ACCCGCTGTATGGAAGGAAA 3'	5' TCTGAAGGATGTCTGCGGTT 3'
apoe	5' GATCAGCTCGAGTGGCAAAG 3'	5' TAGTGTCCTCCATCAGTGCC 3'
hprt1	5' TTGCTCGAGATGTCATGAAGGA 3'	5'AGCAGGTCAGCAAAGAACTTATAG 3'

Statistical analysis

Statistical analysis was performed with GraphPad Prism 6 software. All data are represented as mean ±SEM. A Mann-Whitney test was performed for qPCR analysis of markers in neurons versus astrocytes.

Results

Virus expression validation

The three viruses AAV5.GfaABC1D.tdTomato, AAVrh10.CMV.GFP and AAVrh10.CAG.CYP46A1.HA were co-injected in the striatum of wild type mice (**Figure 1A**). The expression of the three transgenes, tdTomato, GFP, CYP46A1-HA, was analyzed from striatal slices. GFP and tdTomato fluorophore were already visible by fluorescence microscopy and an immunohistochemistry was performed against CYP46A1 tag HA (**Figure 1B**). A large number of GFP positive cells (84.8%) colocalize with CYP46A1 expressing cells. Only 4.4% of GFP positive cells colocalized with dtTomato expressing cells, and 4.23% of dtTomato positive cells colocalize with CYP46A1 expressing cells (**Figure 1C**). Therefore, CYP46A1 cells are mainly co-expressed with GFP positive cells which mainly exclude astrocytes (tdTomato expressing cells).

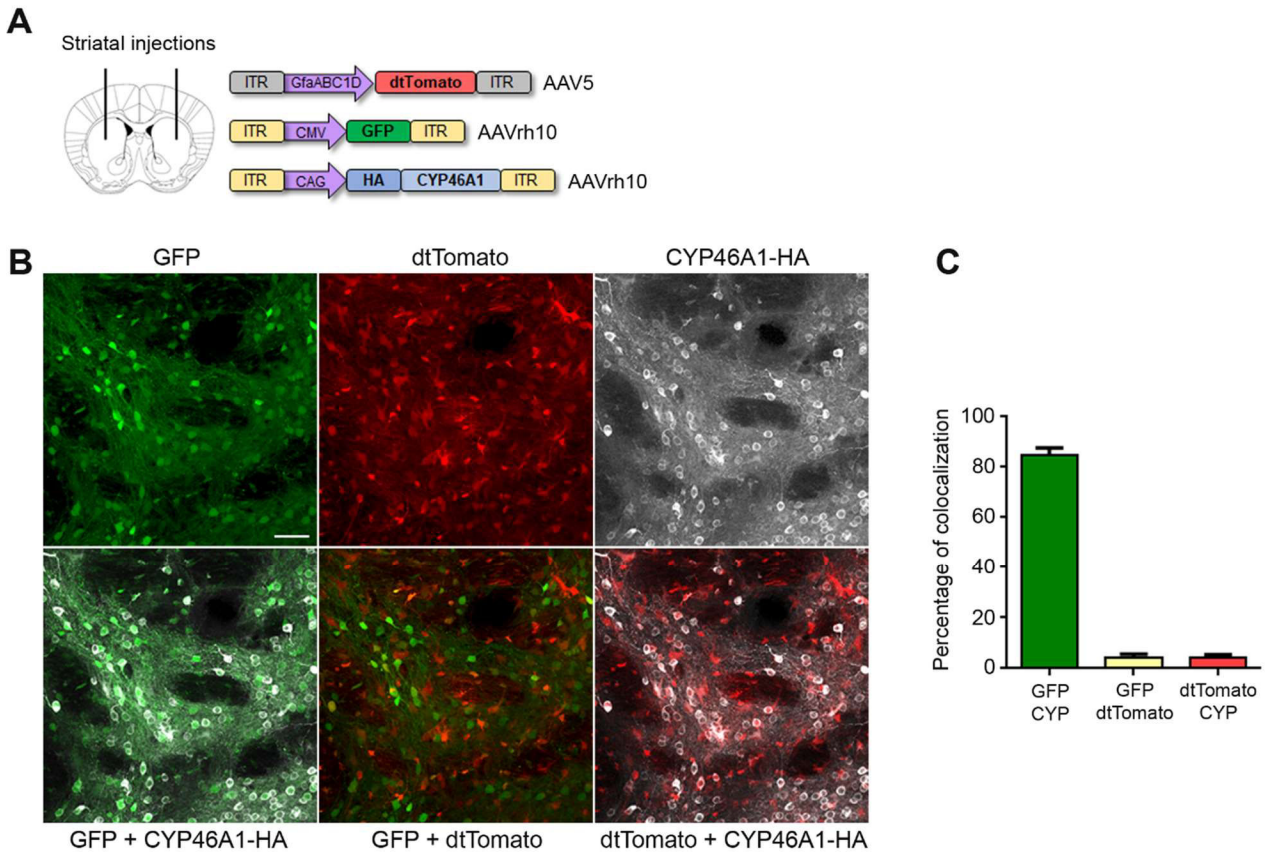

Figure 1. Expression of AAVrh10.CYP46A1, AAVrh10.GFP and AAV5.dtTomato following stereotaxic injection within the striatum of the mice. (**A**) Scheme of the viruses injected in the striatum of the mice (**B**) CYP46A1 transgene is tagged with a Hemagglutinin (HA) tag and stained with a HA antibody. GFP and Tomato staining are relative to AAVrh10.CMV.GFP and AAV5.gfaBC1D.dtTomato expression. Merged pictures show a good co-localization of AAVrh10.CMV.GFP and AAVrh10.CAG.CYP46A1 transgenes. Note the specific labelling of tdTomato in astrocytes. Scale bar: 50µm (**C**) Percentage of colocalization between the expressed proteins. Data are represented as mean ±SEM, n=4 animals.

Cell sorting set up

WT mice were injected with AAV5.gaBC1D.dtTomato, which targets astrocytes, and an AAVrh10.CMV.GFP which targets neurons. Four weeks post-injection, the striata were extracted and cells were dissociated after papain incubation followed by myelin removal using magnetic beads. This last step is crucial to overcome the stressful effect of cell sorting and to favor cell viability. Indeed, when myelin-containing neural tissue is dissociated, large quantities of myelin debris are generated, which could considerably impair cell sorting and cell viability. Depletion of myelin debris from single-cell suspensions is an important step to improve cell separation and purity after cell sorting (Orre et al., 2014). Indeed, myelin debris can interfere with the sorting, it can reduce the speed and efficiency of the sorting, therefore reducing the total yield of cells after sorting. Myelin debris also have high autofluorescence properties that can interfere with the FACS analysis.

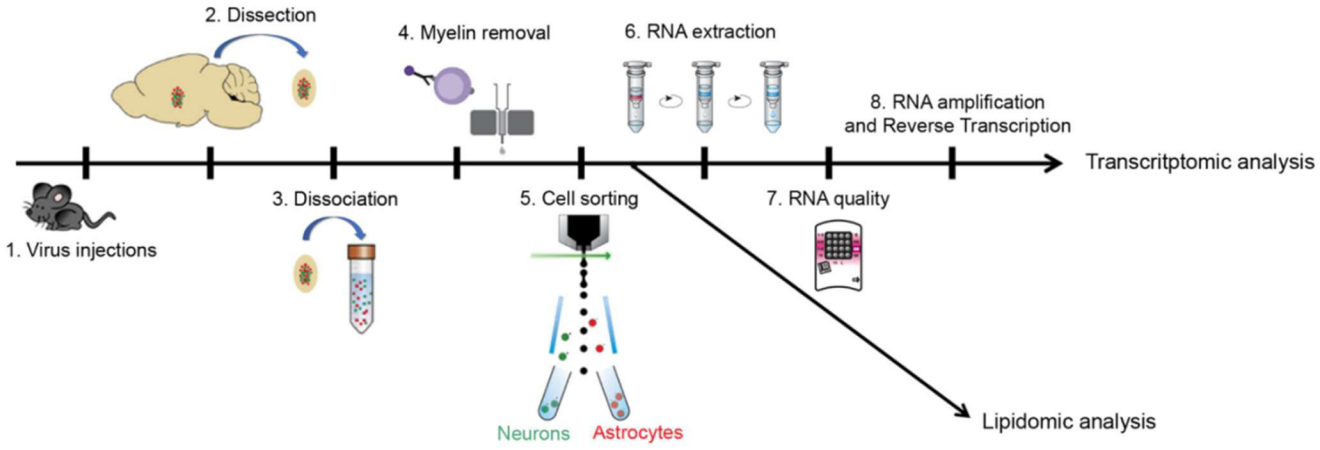

Figure 2. Illustration of the different steps of the protocol. The striata are dissected (2) then incubated at 37°C in a papain solution, associated to mechanical dissociations with fire polished Pasteur pipettes (3). Then, the myelin removal step is realized using antibodies coupled to magnetic beads, after incubation with these antibodies, the cell suspension is put on magnetic columns which will retain the antibodies associated to the myelin debris (4). After cell sorting (5), RNA extraction is performed using columns adapted for small quantities (6) and RNA quality is analyzed using microchips (7). The quantity of RNA retrieved requires a step of RNA amplification coupled with reverse transcription (8). For the lipidomic analysis by GC-MS the protocol stops after cell sorting.

Validation of cell integrity after sorting

We validated cell viability after cell sorting. Determination of cell viability is critical after cell sorting especially for adult neurons and astrocytes isolated from mature brains. In addition, detection of dead cells in a cell suspension is important in order to exclude them from the analysis. Dead cells can generate artifacts in the analysis following cell sorting. One method to assess cell viability is through the use of dye exclusion. Living cells have intact membranes that exclude a variety of dyes that easily penetrate the damaged, permeable membranes of non-viable cells. Propidium iodide (PI) is a membrane permeant dye that is generally excluded from viable cells. It binds to double stranded DNA by intercalating between base pairs. Annexin V is commonly used to detect apoptotic cells thanks to its ability to bind to phosphatidylserine, a marker of apoptosis when it is present on the outer leaflet of the plasma membrane. The combination of these two markers allows us to distinguish dead cells (necrotic cells) from dying cells (apoptotic cells). Incubation of cells with PI and Annexin V staining was followed by cell analysis. The stained cells were analysed by flow cytometry, measuring the fluorescence emission at 530 nm (FITC) for Annexin V and 575 nm (PE-Texas Red) for PI (**Figure 3C-D**). The population separate into three groups: live cells showing no fluorescence (Q3); apoptotic cells showing green fluorescence only (Q4) and dead cells showing both red and green fluorescence (Q1+Q2) (**Figure 3E**). Percentage of PI positive cells measured with FACS showed a low percentage of cells labelled with PI (3%) which corresponds to dead cells. Very few cells are labelled with Annexin V (0.3%) meaning most of the cells are not apoptotic. Thus, this protocol allows to maintain a high percentage of living cells (96.8%) which is absolutely require for the goal of the study (**Figure 3F**).

The second crucial criteria for transcriptomic analysis after cell sorting was to validate RNA quality of sorted cell. RNA extraction after cell sorting was followed by electrophoresis on microchips to determine integrity of 18S and 28S ribosomal RNA (Experion, RNA HighSens analysis, Biorad). This analysis is recommended for RNA purity and concentration at picogram levels. Electrophoresis of RNA from cells before sorting showed, as expected, 28S and 18S RNA. The first lower band in the electropherogram corresponds to the marker, which is incorporated into the loading buffer and is used for alignment to the RNA ladder. The results showed in neurons and astrocytes samples the two most prominent bands, which represent 18S and 28S ribosomal RNA. RNA quality control showed a well preserved 28S and 18S RNA in neuron and astrocyte samples after cell sorting (**Figure 4**).

Overall, the cell dissociation protocol used preserved neurons and astrocytes from cell death and RNA degradation. This protocol will allow the sorting of several thousands of neurons and astrocytes to quantify sterol/oxysterols and to establish transcriptomic signature in each cell type.

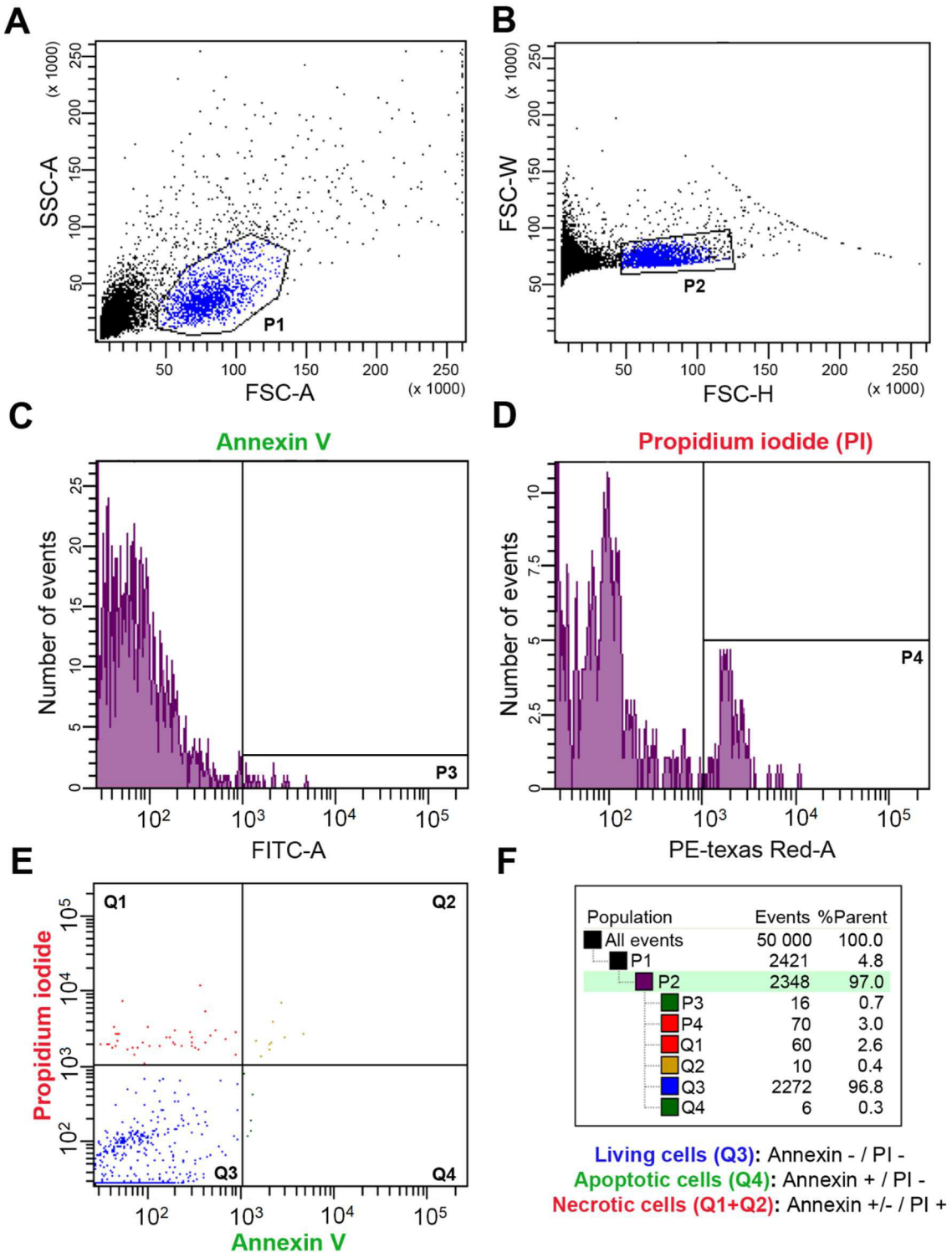

Figure 3. Annexin V and Propidium iodide (PI) detection on dissociated cells. Striata were dissected and dissociated. The single cell suspension was labeled with PI and Annexin V and analyzed with the cytometer. (**A**) Cells are selected by forward and side scatter profiles. (**B**) Single cells are selected by forward scatter profile. (**C-D**) Labeled events are displayed in a fluorescence scattergram for Annexin V (**C**), and PI in (**D**) with in P3 Annexin V positive cells and in P4 PI positive cells. The double labelling events are displayed in (**E**) The Q3 population is considered to be the living cell population (no labelling). (**F**) Quantification of each cell population: the total analyzed cells are 2348, among them, 16 are labelled with Annexin V and 70 with PI.

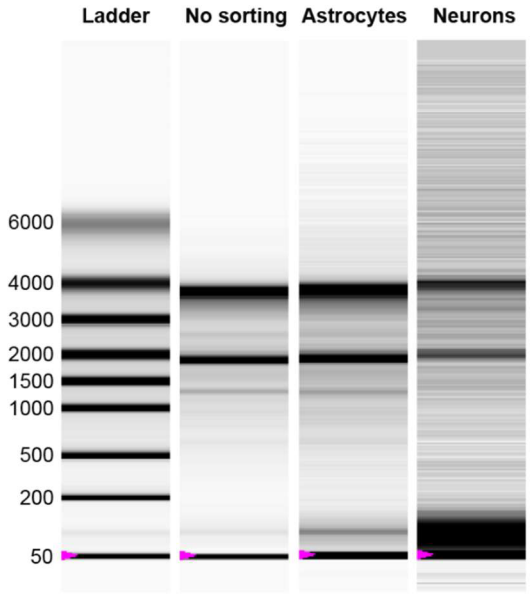

Figure 4. RNA integrity before and after cell sorting. AAVrh10.CMV.GFP and AAV5.gfaBC1D.dtTomato were injected within the striatum of WT mouse. After mouse sacrifice, brains were extracted followed by striata dissection and cell dissociation. RNA extraction was performed before and after cell sorting. RNA purity and quality in each sample was achieved through electrophoresis on microchips. The reference ladder is on the left. Two main bands are visible after RNA extraction: the 18S and 28S ribosomal RNA.

FACS analysis

The cell suspension was analysed with the cytometer. The lasers allow to collect data on the size and complexity of the cells according to the FSC-A (forward scatter area) and SSC-A (side scatter area) as well as the dye specific fluorescence (**Figure 5A**). A first window called P1 was created based on the FSC-A and SSC-A scattergram to exclude debris and aggregated cells (**Figure 5B**). Non-fluorescent cells were first analyzed to determine the window of positive fluorescence P3 for GFP positive cells and P4 for tdTomato positive cells (**Figure 5C**), then the injected samples were analysed for fluorescence (**Figure 5C**). Note in **C**. GFP positive cells that are related to AAVrh10.CMV.GFP expression in striatal neurons and the tdTomato positive cells that are related to AAV5.dtTomato expression in striatal astrocytes. On average, GFP and tdTomato positive cells represent 5% of the total population selected in **B**. After establishing the windows, cell sorting is performed according to the charge attributed to GFP positive cells or tdTomato positive cells, which allows a specific sorting of neurons versus astrocytes (**Figure 5A**). GFP positive cells and tdTomato positive cells are then resuspended either in Trizol LS for RNA extraction or in HBSS medium for GC-MS analysis.

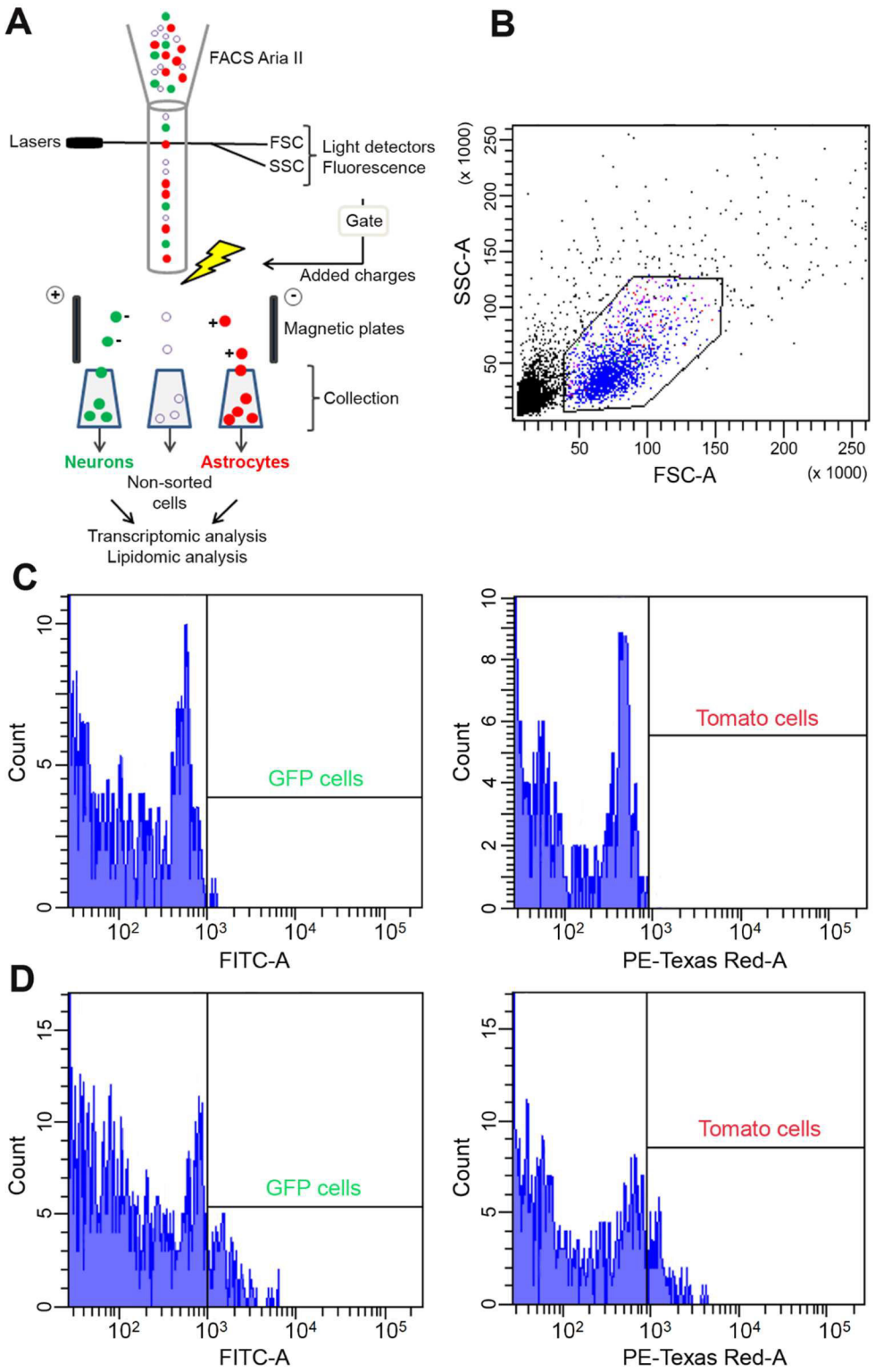

Figure 5. Fluorescence activated cell sorting of neurons (GFP) and astrocytes (Tomato). (**A**) The single cell suspension is analyzed with the cytometer. Each particle is called an event and each event is indicated by a dot in the graph (called scattergram). Droplets containing events of interest can be programmed to receive an electric charge as they leave the flow cell. Magnetic plates direct the charged droplets and sort them into positive or negative sample tubes. **(B)** Cells are selected by forward and side scatter profiles. The cluster of events blue dots corresponds to the events that are considered as single living cells. (**D-C**) Labeled events are displayed in a fluorescence scattergram. (**C**) Fluorescence gates are established on non-injected mice**.** (**D**) Injected mice with tdTomato and GFP.

Analysis of molecular markers

We next investigated the purity of sorted cell using neuronal or astrocytic gene markers analyzed by RT-qPCR. After reverse transcription of the mRNA from the sorted cells and amplification of the resulting cDNA, qPCRs were performed using specific neuronal and astrocyte primers. Expression level of striatal neuron marker *darpp32* is enriched in the sorted neurons (GFP positive cells) compared to astrocytes (tdTomato positive cells) (**Figure 6A**). Expression levels of astrocytic markers *3pgdh* and *s100β* are enriched in the sorted astrocytes compared to neurons (**Figure 6B-C**). A microglial marker, *iba1* was used as negative control, and was not expressed neither in neurons nor in astrocytes (**Figure 6D**). Cholesterol synthesis enzymes *dhcr7* and *dhcr24* have a tendency of enrichment in astrocytes (**Figure 6E-F**), whereas the cholesterol degradation enzyme *cyp46a1* expression is enriched in neurons (**Figure 6G**). Expression of *apoe* and *abca1*, which are involved in the transport of cholesterol, supposedly from astrocytes to neurons, is enriched in astrocytes, although not significantly for *apoe* (**Figure 6H-I**). Altogether, we confirmed the specific cell sorting of neurons versus astrocytes with enrichment of neuronal markers in the sorted neurons (*darpp32*) and enrichment of astrocytic marker (*3pgdh and s100b*) in sorted astrocytes (**Figure 6J-K**). We showed in these cells a specific enrichment of the cholesterol degradation enzymes in neurons; and of sterol synthesis enzymes (*dhcr7* and *dhcr24*) and cholesterol transport genes (*apoe* and *abca1*) in astrocytes (**Figure 6J-K**). Overall, we validated the FACS procedure to purify neurons and astrocytes from adult mouse striatum in order to perform transcriptomic and lipidomic analysis.

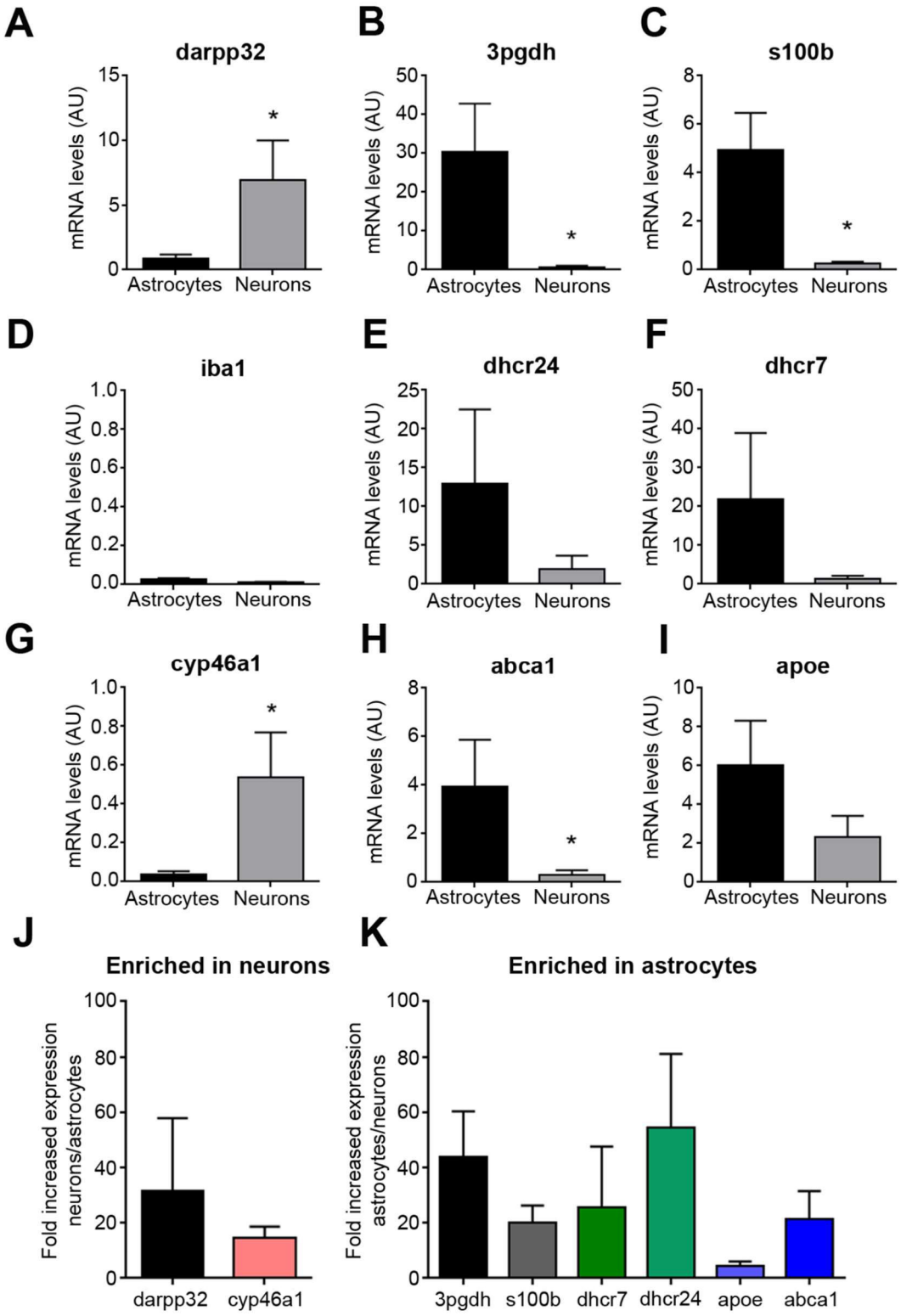

Figure 6. Specific gene expression in the sorted neurons and astrocytes. (**A-C**) Markers of neurons (*darpp32*) and astrocytes (*3pgdh and s100b*). (**D-H**) Markers of cholesterol metabolism: degradation (*cyp46a1*), synthesis (*dhcr7* and *dhcr24*) and transport (apoe and abca1). (**I**) Microglial marker. (**J**) Markers enriched in neurons, neuronal expression divided by astrocytic expression. (**K**) Markers enriched in astrocytes, astrocytic expression divided by neuronal expression. (**A-K**) Data are represented as mean ±SEM, n=3 animals. Statistical analysis: Mann-Whitney test, **p*<0.05.

Discussion

We developed and validated a rapid and quantitative FACS procedure for purifying neurons and astrocytes from adult mouse striatum. The ability to separate cells based on fluorophore expression (GFP in neurons and tdTomato in astrocytes) and not on antibody labelling, is an important advantage since it shortens the time for cell preparation. We have adapted the cell dissociation procedure to preserve astrocytes and neurons viability and RNA integrity after cell sorting. We validated the purity of the sorted cells with neuronal and astrocytic markers and we confirmed the specific segregation of cholesterol related genes in neurons and astrocytes, as demonstrated in the RNAseq study from purified cells from the mouse cortex (Zhang et al., 2014). Having this procedure in hands, the next step will be to determine transcriptomic and lipidomic signature in purified neurons and astrocytes from wild type and HD mouse model.

Lipidomic analysis in neurons versus astrocytes (sterols, oxysterols and fatty acids profiling) will be then performed by isotope dilution/mass spectrometry analysis (Collaboration with Dr V. Leoni, Italy) operating in SIM mode with deuterium labeled internal standard for each compound. Peak integration will be performed manually, and metabolites will be quantified from analyses against internal standards using standard curves for the listed sterols and oxysterols: i) cholesterol ii) cholesterol precursors: lathosterol, lanosterol, desmosterol iii) oxysterols: 24S-OHC (CYP46A1 product), 27-OHC and 25-OHC iii) campesterol and β-sitosterol as markers of cholesterol uptake from the circulation iv) cellular fatty acid profile to study structural modification of membranes and lipid metabolism.

For the second aspect of the study, transcriptomic signature will be investigated using RNAseq. The preparation and sequencing of mRNA libraries will be performed by the sequencing platform of the "Institut du Cerveau et de la Moelle épinière" at the Pitié-Salpêtrière hospital (Paris, France). Messenger RNA libraries will be prepared using standard protocols from Illumina, using the kit Truseq Stranded mRNA LT (Illumina) and sequenced with the Illumina HiSeq Genome Analyzer. Data will be subjected to network-based analysis using spectral decomposition of RNA-seq signals (Tourette et al., 2014) against MouseNet v2, followed by biological content analysis using STRING v10.5 analysis**.**

Previous groups have already performed transcriptome studies of one or more purified cell types in the brain (Gokce et al., 2016; Guez-Barber et al., 2012; Srinivasan et al., 2016) but to our knowledge no data has yet been published in the context of HD. Regarding lipidomic studies, no dataset that allows direct comparison of sterols and oxysterols contents across astrocytes and neurons from *in vivo* samples is available. Understanding striatum dysfunction in HD requires an understanding of how neurons, astrocytes and other glial cells interact in a dynamic environment.

In the context of studying CYP46A1 neuroprotection in HD, it will be important to understand the specific regulations mediated by neuronal expression of CYP46A1 in both neurons and astrocytes. Thus, this protocol will allow us to answer to this question. For the lipidomic analysis, the major limitation of GC/MS quantification within sorted astrocytes and neurons is the number of cells that we can collect after cell sorting, the limit to quantify sterols and oxysterols being 500 000 cells. Therefore, we will need to pool the striata of several mice to get enough cells for GC/MS studies.

Overall, deciphering how CYP46A1 neuronal expression could modulate neuronal and astrocytic transcription processes as well as cholesterol homeostasis will be crucial in the perspective of developing a therapy targeting CYP46A1 in HD.

References

Barros, L.F., Brown, A., and Swanson, R.A. (2018). Glia in brain energy metabolism: A perspective. Glia *66*, 1134–1137.

Gokce, O., Stanley, G.M., Treutlein, B., Neff, N.F., Camp, J.G., Malenka, R.C., Rothwell, P.E., Fuccillo, M.V., Südhof, T.C., and Quake, S.R. (2016). Cellular Taxonomy of the Mouse Striatum as Revealed by Single-Cell RNA-Seq. Cell Rep.

Guez-Barber, D., Fanous, S., Harvey, B.K., Zhang, Y., Lehrmann, E., Becker, K.G., Picciotto, M.R., and Hope, B.T. (2012). FACS purification of immunolabeled cell types from adult rat brain. J. Neurosci. Methods *203*, 10–18.

Jeske, D.J., and Dietschy, J.M. (1980). Regulation of rates of cholesterol synthesis in vivo in the liver and carcass of the rat measured using [3H]water. J. Lipid Res. *21*, 364–376.

Lund, E.G., Guileyardo, J.M., and Russell, D.W. (1999). cDNA cloning of cholesterol 24-hydroxylase, a mediator of cholesterol homeostasis in the brain. Proc. Natl. Acad. Sci. U.S.A. *96*, 7238–7243.

Martín, M.G., Pfrieger, F., and Dotti, C.G. (2014). Cholesterol in brain disease: sometimes determinant and frequently implicated. EMBO Reports *15*, 1036–1052.

Nieweg, K., Schaller, H., and Pfrieger, F.W. (2009). Marked differences in cholesterol synthesis between neurons and glial cells from postnatal rats. J. Neurochem. *109*, 125–134.

Orre, M., Kamphuis, W., Osborn, L.M., Melief, J., Kooijman, L., Huitinga, I., Klooster, J., Bossers, K., and Hol, E.M. (2014). Acute isolation and transcriptome characterization of cortical astrocytes and microglia from young and aged mice. Neurobiol. Aging *35*, 1–14.

Pitas, R.E., Boyles, J.K., Lee, S.H., Hui, D., and Weisgraber, K.H. (1987). Lipoproteins and their receptors in the central nervous system. Characterization of the lipoproteins in cerebrospinal fluid and identification of apolipoprotein B,E(LDL) receptors in the brain. J. Biol. Chem. *262*, 14352–14360.

Saher, G., and Stumpf, S.K. (2015). Cholesterol in myelin biogenesis and hypomyelinating disorders. Biochim. Biophys. Acta *1851*, 1083–1094.

Srinivasan, K., Friedman, B.A., Larson, J.L., Lauffer, B.E., Goldstein, L.D., Appling, L.L., Borneo, J., Poon, C., Ho, T., Cai, F., et al. (2016). Untangling the brain's neuroinflammatory and neurodegenerative transcriptional responses. Nat Commun *7*, 11295.

Tourette, C., Farina, F., Vazquez-Manrique, R.P., Orfila, A.-M., Voisin, J., Hernandez, S., Offner, N., Parker, J.A., Menet, S., Kim, J., et al. (2014). The Wnt receptor Ryk reduces neuronal and cell survival capacity by repressing FOXO activity during the early phases of mutant huntingtin pathogenicity. PLoS Biol. *12*, e1001895.

Zhang, J., and Liu, Q. (2015). Cholesterol metabolism and homeostasis in the brain. Protein Cell *6*, 254–264.

Zhang, Y., Chen, K., Sloan, S.A., Bennett, M.L., Scholze, A.R., O'Keeffe, S., Phatnani, H.P., Guarnieri, P., Caneda, C., Ruderisch, N., et al. (2014). An RNA-Sequencing Transcriptome and Splicing Database of Glia, Neurons, and Vascular Cells of the Cerebral Cortex. J Neurosci *34*, 11929–11947.

DISCUSSION AND PERSPECTIVES

CYP46A1 restoration is neuroprotective and compensate for HD phenotype

Huntington's disease is associated with multiple dysregulations leading progressively to neurodegeneration. Cholesterol metabolism is one of the altered processes in HD and is involved in many essential cellular functions. By restoring the expression of the cholesterol degradation enzyme, CYP46A1, in the striatum of zQ175 mice, we showed that cholesterol metabolism is enhanced, with not only an increase of cholesterol degradation but also an increase of cholesterol precursors content and cholesterol transport. These changes in cholesterol metabolism are associated with an improvement of HD phenotype in the zQ175 mice. Importantly, CYP46A1 broadly impacts the transcriptomic signature related to major pathways strongly altered in HD, including synaptic transmission, vesicular transport and unfolded protein metabolism. This new transcriptomic signature showed a global compensation of altered functions in HD through a stimulation of cholesterol metabolism. We demonstrated that CYP46A1 compensates for important dysfunctions induced by mHTT, especially cortico-striatal synaptic connectivity and activity, along with axonal transport of BDNF from cortical to striatal neurons and trafficking of TrkB endosomes on striatal dendrites. Interestingly, we showed that CYP46A1, and the cholesterol precursors lanosterol and desmosterol, which are increased by CYP46A1 restoration, have a positive role in promoting aggregate clearance, via autophagy and the proteasome system. Overall, these improvements lead to a better motor behavior in the zQ175 mice. Therefore, CYP46A1 appear like an interesting therapeutic target as a neuroprotective strategy for HD.

CYP46A1 improves cholesterol homeostasis

CYP46A1 restoration in the zQ175 mice increased cholesterol precursor levels, mainly lathosterol, lanosterol and desmosterol, and the product of cholesterol degradation, the 24S-OHC. In the adult brain, activation of the Bloch pathway in astrocytes is the main source of cholesterol synthesis, through desmosterol production; in neurons, the Kandutsch Russel pathway is dominant, with lathosterol as one of the precursors (Nieweg et al., 2009). Since CYP46A1 restoration promoted the production of both lathosterol and desmosterol, we can hypothesize that cholesterol synthesis was stimulated in both astrocytes and neurons. Furthermore, expression of synthesis enzymes was increased by CYP46A1, an effect that could depend on the cholesterol sensor SREBP2 (Brown and Goldstein, 1997). Accordingly, we found an increase of SREBP2 nuclear localisation after CYP46A1 injection. LXR activation by 24S-OHC and desmosterol could also be implicated (Lehmann et al., 1997; Spann et al., 2012), by positively regulating the transcription of ApoE in astrocytes (Abildayeva et al., 2006),

potentially favoring cholesterol transport in lipoproteins from astrocytes to neurons (Boyles et al., 1985). CYP46A1 expression restored ApoE expression, which is decreased in HD (Valenza et al., 2010, 2015a). In our study, CYP46A1 restoration in neurons increased ApoE expression in non-neuronal cells, suggesting a global activation of cholesterol transport from astrocytes to neurons. Therefore, our study supports an original mechanism underlying CYP46A1-mediated regulation of cholesterol homeostasis via an autocrine regulation in neurons, and a potentially paracrine regulation in astrocytes, that could explain the increased ApoE expression and thus regulation of cholesterol transport. ApoE related pathways could be interesting to study in the context of a neuroprotective strategy. Indeed, ApoE lipoproteins can attenuate inflammation by inhibiting cytokine expression and favoring M2 macrophage phenotype over the pro-inflammatory stage (Vitali et al., 2014). It was also shown that ApoE containing lipoproteins protect from apoptosis by binding to LRP1, initiating a signaling pathway that leads to the activation of protein kinase Cδ (PKCδ) and inhibition of the pro-apoptotic glycogen synthase kinase 3β (GSK3β), without needing lipoprotein internalization. ApoE containing lipoproteins also attenuates neuronal death caused by oxidative stress (Hayashi et al., 2009). ApoER2, which is another receptor for ApoE, is involved in the maintenance of efficient synaptic plasticity, dendritic remodeling (Petit-Turcotte et al., 2005) and organization of the presynaptic dendritic spine density (Dumanis et al., 2011).

CYP46A1 restoration induces a specific transcriptional signature

We confirmed a large striatal transcriptional dysregulation in the zQ175 mice, as previously described in HD knock-in mice (Ament et al., 2017), with a deep down-regulation of genes involved in glutamatergic signaling and synapse functions. We showed that CYP46A1 is able to compensate some of the gene alterations in the striatum of zQ175 mice, which noticeably applies to genes associated with neurotransmission, synaptic activity and autophagy. The transcriptional modifications mediated by CYP46A1 could involve the aggregate clearance observed in the zQ175 mice, allowing more available transcription factors. Indeed, sequestration of key transcriptional activators, such as TBP, CBP and Sp1 into mHTT aggregates was previously described in HD (Nucifora et al., 2001; Schaffar et al., 2004). Intriguingly, CYP46A1 expression modulates the expression of genes involved in pathways that regulate innate immunity such as complement pathways and toll-like receptor pathways, which are known to induce autophagy (Delgado et al., 2008). Interestingly, CYP46A1 transcriptional signature is correlated to the gene expression patterns of anti-inflammatory compound and neuroprotective agents. Anti-inflammatory responses could also be the consequence of LXR activation by the 24S-OHC and desmosterol (Ghisletti et al., 2007; Spann et al., 2012). In HD, increased production of pro-inflammatory molecules has been implicated in the neurodegenerative processes, by cell-autonomous action of the mHTT on microglia and also over-activation of microglia and astrocytes by signals received

from degenerating neurons (Crotti and Glass, 2015). Therefore, a stimulation of anti-inflammatory pathways by CYP46A1 expression may then promote protective neuro-immune mechanisms against cytotoxicity either directly, in neurons, or indirectly, through non-cell autonomous mechanisms involving glial cells.

CYP46A1 favors synapse connectivity

Neurotransmission and synaptic connectivity is altered in several HD models, in the zQ175 mice a significant decrease in spine density is observed, along with altered excitatory and inhibitory inputs in SPN (Indersmitten et al., 2015; Rothe et al., 2015). After expression of CYP46A1 in the striatum of zQ175 mice, spine density was increased at late stages, the number of glutamatergic connections between bassoon and GluR1 was improved early in the course of the study, and was associated to an increased number of VLUGT1 connected to bassoon, which together could mean an increased number of active zones. To study the functionality of these improved connections we analyzed the electrophysiologic properties that could be modified with CYP46A1. In homozygous zQ175 mice, we observed alterations in membrane properties, increased excitability and input resistance of SPN, in agreement with previous studies (Heikkinen et al., 2012; Indersmitten et al., 2015). This increased excitability can serve as a compensatory mechanism to lower cortico-striatal transmission in zQ175 mice. We show larger amplitude and lower sEPSCs frequency, such changes agree with lower number of spines observed in zQ175 mice. CYP46A1 restoration specifically rescued sEPSCs frequency and therefore the probability of spontaneous release at glutamatergic synapses, which is in accordance with the observed increase of synapses with multiple active zones. Therefore, CYP46A1 tend to normalize altered glutamatergic transmission in the zQ175 mice. To understand these regulations, one should consider that cholesterol is an essential component of the membrane, with a leading role in synapse dynamic. Indeed, cholesterol is a major component of lipid rafts in dendrites, organizing the signaling domains at the synapse, interacting for example with AMPA receptors (Hering et al., 2003). Moreover, cholesterol turnover by CYP46A1 is induced during excitatory neurotransmission (Sodero et al., 2012). Synaptic plasticity was not studied here; however, it should be noted that CYP46A1 contribution to synaptic plasticity was previously described and might participate in CYP46A1 mediated neuroprotection. Knock-out mice for *cyp46A1* exhibited severe learning deficiencies and long-term potentiation (LTP) decrease (Kotti et al., 2006) as well as alterations of protein phosphorylation related to synaptic vesicles and neurotransmission (Shank3, Slc, Syn1, Bsn) (Mast et al., 2017a). On the other hand, mice overexpressing CYP46A1 showed an enhanced spatial memory, along with an increased level of post-synaptic proteins (PSD95, NMDAR1) and presynaptic proteins (synapsin, synaptophysin) (Maioli et al., 2013). *In vitro*, CYP46A1 overexpression is also associated with an increase of dendritic protrusions, an enrichment in synaptic proteins (Shank3, PSD95,

synaptophysin), through geranylgeranyl transferase-I (GGTase-I) prenylation activity (Moutinho et al., 2016b). Finally, the product of cholesterol degradation by CYP46A1, the 24S-OHC may participate in synaptic plasticity, as a positive allosteric modulator of NMDA receptors (Paul et al., 2013).

CYP46A1 increases BDNF vesicles and TrkB endosomes trafficking

Defect in BDNF/TrkB signaling is a major event involved in HD striatal degeneration. Striatal neurons rely on cortical delivery of BDNF for their survival (Altar et al., 1997; Baquet et al., 2004). However, mHTT impairs the transport of BDNF along cortical neurons microtubules (Gauthier et al., 2004). After release, BDNF binds to TrkB receptors, which dimerizes and are internalized into endosomes. These endosomes are transported from to the soma to triggers survival signaling (Zhang et al., 2000), but the mHTT polyQ alters TrkB-endosomes binding to microtubules, reducing their transport (Liot et al., 2013). In a microfluidic system reconstituting the cortico-striatal connections, we showed that BDNF and TrkB transport in HD neurons are increased after CYP46A1 restoration. This increase could be due to the role of cholesterol in endosomes formation and motility. Indeed, cholesterol domains on endosome can regulate the recruitment of motor proteins, by regulating the interaction between Rab7 interacting lysosomal protein (RILP) and oxysterol binding protein related protein 1L (ORP1L), which are necessary to load dynein onto the cargo (Johansson et al., 2007; Jordens et al., 2001). Moreover, cholesterol depletion can promote endosome motility towards the plus end of microtubules by suppressing the association of endosomes containing lipid rafts with Rab7 GTPase and promotes their association with Rab4 GTPase (Chen et al., 2008). Cholesterol turnover could thus facilitate the transport of vesicles. Here we studied BDNF and TrkB transport, but modulation of cholesterol levels can also modulate TrkB activity. Indeed, a loss of cholesterol content correlates with an increase of TrkB activity (Martin et al., 2008), on the contrary, CYP46A1 knock-down lead to a decrease of TrkB activity along with an increase of apoptosis (Martin et al., 2011b). Moreover, when CYP46A1 is overexpressed *in vivo* and *in vitro*, TrkB phosphorylation is increased (Moutinho et al., 2016b). Because TrkB activity is associated with activation of pro-survival pathways, an increase of its activation by CYP46A1 could also participate to the neuroprotection.

CYP46A1 expression is associated to an enhanced aggregate clearance

CYP46A1 restoration is associated to a strong clearance of aggregates in the zQ175 mice, as well as in the transgenic R6/2 mouse model (Boussicault et al., 2016) and decreased aggregate accumulation in an Alzheimer disease mouse model (Hudry et al., 2010). Cholesterol precursors were also described to favor aggregate clearance. Lanosterol treatment *in vitro*, decreased aggregation in different cell models of neurodegenerative diseases (SOD1, α-synuclein, ataxin-3, mHTT) (Upadhyay et al., 2018). In our study, treatment with lanosterol, desmosterol and CYP46A1 *in vitro* decreased aggregate

formation in mHTT expressing cells, in a mechanism dependent on the proteasome and autophagy machineries. In HD, autophagy is altered with a defect in cargo loading, autophagosome trafficking and accumulation of autophagosome because of a decreased fusion with lysosome (Martinez-Vicente et al., 2010; del Toro et al., 2009; Wong and Holzbaur, 2014). Accumulation of autophagosomes directly induces cellular toxicity, and may be implicated in HD pathogenesis (Button et al., 2017). In our study, lanosterol could participate to an enhancement of autophagy. Indeed, it has been shown that lanosterol treatment decreases aberrant aggregation via induced expression of co-chaperone C terminus of Hsc70-interacting protein (CHIP) and increases autophagy (Upadhyay et al., 2018). Because cholesterol is important for endosome formation, increasing cholesterol turnover could then improve autophagosome formation and recycling. It should be noted that clustering of dynein into cholesterol domains on late phagosomes facilitates their directed transport into lysosomes (Rai et al., 2016). Electron microscopy revealed an accumulation of empty autophagosomes in zQ175 mice, as previously observed in the HdhQ111 knock-in mice (Martinez-Vicente et al., 2010) and with CYP46A1 restoration empty autophagosomes are decreased, instead autophagosomes fuse more with lysosomes. Therefore, CYP46A1 favors a more efficient autophagosome activity that can participate to neuronal survival.

In vitro, we studied autophagy on mice primary neuronal cultures, to go further it would be interesting to use isogenic human iPSCs and differentiate them into neurons and astrocytes. First cholesterol metabolism defects would need to be confirmed in these cells. Then, autophagic flux, autophagosome load and mHTT levels could be assessed, with or without CYP46A1 expression and with or without sterol (lanosterol and desmosterol) treatment. The autophagic flux assessed in these cells could help to understand how cholesterol signaling might drive mHTT clearance, especially by integrating the study of autophagy in astrocytes.

Overall, we showed that regulating cholesterol metabolism through gene therapy involving CYP46A1 has a therapeutic potential for alleviating HD symptoms by reinstating striatal homeostasis. Given the pivotal role of cholesterol metabolism in the brain homeostasis and function, this strategy could have a promising potential for other neurodegenerative diseases such as Alzheimer's disease, where CYP46A1 was shown to be beneficial in mouse models (Burlot et al., 2015; Djelti et al., 2015; Hudry et al., 2010).

Study of the cell specific regulations induced by CYP46A1

A better understanding of the cell-type-specific mechanisms underlying the dysregulation of brain cholesterol signaling is needed in order to identify a solid basis for developing an efficient neuroprotective strategy in HD. To do so during my PhD I set up a protocol to separate neurons and astrocytes and study their specific regulations.

Transcriptomic and lipidomic profiles in astrocytes versus neurons

Brain cholesterol synthesis mostly relies on astrocytes whereas neurons catabolize cholesterol *via* CYP46A1 activity and production of 24S-OHC. Astrocyte dysfunction is an important component of HD pathogenesis (Faideau et al., 2010; Shin et al., 2005). However, the specific contribution of cholesterol signaling in striatal astrocytes *versus* neurons in an HD context remains poorly understood. During my PhD, I set up a fluorescence-activated cell sorting (FACS) protocol based on neuronal expression of GFP and astrocytic expression of tdTomato using adeno-associated-viral vectors (AAVs). Specific neuronal and astrocytic markers allowed the validation of the cell sorting of neurons and astrocytes. Moreover, genes involved in cholesterol metabolism were analyzed and showed an enrichment of synthesis enzymes and transport genes in astrocytes versus an enrichment of *cyp46a1* in neurons. Pre-symptomatic zQ175 knock-in mice were injected at 4 months with AAVs encoding for these cell-specific fluorescent proteins along with the AAVrh10.CAG.CYP46A1, which has a neuronal tropism. Striatal cell dissociation and cells sorting was realized at 7 months. Astrocytes expressing tdTomato and neurons expressing GFP alone or with CYP46A1 will be analyzed for their lipidomic profile using mass spectrometry and for their transcriptomic signature using RNAseq. In futur projects, it would be very interesting to extend this study to other cell types such as oligodendrocytes, which are the major pool of cholesterol in the brain, and microglia which are essential for the immune responses in the brain. Moreover, a separation between the different neuronal populations of the striatum would give a more precise idea of the specific neuronal regulation, especially to distinguish between the neurons expressing the D1R and the neurons expressing the D2R, which have a specific temporal pattern of degeneration in HD. Some interesting studies have already shown the rich cell diversity in the striatum (Gokce et al., 2016) and the cell specific gene regulations in the brain (Orre et al., 2014; Srinivasan et al., 2016).

Impact of reactive astrocyte on CYP46A1 neuroprotection

Some studies have suggested that handling of toxic proteins is more efficient in astrocytes than in neurons, with a more active Ubiquitin Proteasome System in glial cells compared to neurons (Tydlacka et al., 2008). In Alzheimer's disease, it was shown that astrocytes are able to internalize amyloid

plaques and Aβ peptides by phagocytosis or receptor mediated internalization (Thal, 2012). In pathological cases, astrocytes could thus participate to the clearance of aggregated proteins. Specific molecular tools were developed to block astrocyte reactivity in the mouse brain (Ben Haim et al., 2015; Ceyzériat et al., 2018), namely viral-vector-mediated expression of SOCS3, an inhibitor of the JAK-STAT3 pathway, a key regulator of astrocyte reactivity (Ceyzériat et al., 2016). Blocking astrocyte reactivity in a mouse model of HD, by overexpression of SOCS3, significantly promotes the formation of mHTT aggregates (Ben Haim et al., 2015), suggesting that reactive astrocytes contribute to aggregate clearance in HD. We observed that CYP46A1 expression in neurons leads to an astrocyte reactivity in the striatum of zQ175 mice. To evaluate how the prevention of astrocyte reactivity may impact the beneficial effects of CYP46A1, preliminary experiments were performed using SOCS3 to block astrocyte reactivity (collaboration with Dr C. Escartin, MirCen, Fontenay aux Roses, France). SOCS3 efficiently prevents CYP46A1-induced astrocyte reactivity in zQ175 mice and increases the number of mHTT aggregates, counteracting CYP46A1 effect on aggregate clearance (data not shown). Thus, it would be interesting to go deeper into the role of reactive astrocytes in CYP46A1-mediated neuroprotection.

Exploring CYP46A1 compensatory mechanisms

Cell stress compensation mechanisms are key to neuronal function and survival in HD; CYP46A1 and sterol modulation could act as compensation mechanisms on stress response and cell survival mechanisms.

Excitotoxicity has been largely studied in HD (Parsons and Raymond, 2014) and is one of the mechanisms leading to neuronal toxicity. More specifically, neurons expressing mHTT have an increased localization of extra-synaptic NMDA-R containing the GluN2B subunit, which in HD models is associated to apoptosis (Milnerwood et al., 2010, 2012). Studies have shown that expression of mHTT increases the localization of NMDA-R in lipid rafts, which participates to the NMDA-mediated excitotoxicity (del Toro et al., 2010). Interestingly, lowering cholesterol levels is protective against NMDA-mediated excitotoxicity and is associated to a redistribution of NMDA-R subunits in lipid rafts (Abulrob et al., 2005; Ponce et al., 2008; del Toro et al., 2010). Therefore, we hypothesized that regulation of cholesterol metabolism by CYP46A1 expression might act on excitotoxicity, potentially by a mechanism involving a redistribution of GluN2B subunits in lipid rafts. In a recent study I participated to (Boussicault et al., 2018), see appendix 1, we showed that CYP46A1 is neuroprotective against NMDA induced excitotoxicity, in neurons expressing the 82Q-mHTT and in YAC128 cultured neurons. The study of lipid raft in the 82Q-mHTT model showed an increase of cholesterol content in lipid rafts, associated to an increased localization of GluN2B subunits in these lipid raft. CYP46A1 expression in cultured neurons showed a global decrease of cholesterol, but more specifically a

decrease in lipid raft. However, this decrease in cholesterol content was not associated to a modification of GluN2B localization in lipid rafts; and when expressed in 82Q-mHTT expressing neurons, CYP46A1 was not able to decrease cholesterol in lipid rafts. Thus, CYP46A1 exhibits neuroprotective effects against NMDA-induced excitotoxicity, but the mechanisms underlying this protection are not dependent on a relocalization of GluN2B subunits in lipid rafts. First, it would be interesting to study this mechanism *in vivo,* to have interactions between all the cell types, especially with astrocytes which are essential for cholesterol metabolism and also for the regulation of glutamatergic neurotransmission (Rothstein et al., 1996). Then, other mechanisms could be explored such as TrkB activation, which is associated to CYP46A1 overexpression (Moutinho et al., 2016b). We could also consider the regulation of GSK3β, which is highly associated to lipid rafts and is increased in HD, triggering apoptosis (Valencia et al., 2010).

DNA damage repair is another key survival mechanism that may be altered in HD (Maiuri et al., 2017). The transcriptomic study on the zQ175 mice showed an effect of CYP46A1 on the expression of genes from the PARP family, which are involved in DNA repair processes (Amé et al., 2004). Preliminary data showed that cell cycle regulators are central in computer models of HD molecular processes in mouse models and in human iPSC/NSC, along with increased double strand breaks and DNA damage repair alteration. Therefore, it could be interesting to assess the influence of CYP46A1 expression and sterols on the dynamics of DNA repair on iPSCs from HD patients.

Related pathway in cholesterol metabolism: LXR pathways and neuroprotection

Since the cholesterol catabolite, 24S-OHC, binds to Liver X Receptors (LXR), a family of nuclear receptors with important transcriptional activities in neurons and astrocytes (Lehmann et al., 1997), we hypothesized that part of CYP46A1 neuroprotective effect arise from the activation of LXRs. This hypothesis is supported by transcriptional activation of LXR target genes by CYP46A1 in the zQ175 mice and the deficiency of LXR activity in HD models (Futter et al., 2009). In line of these data, it would be interesting to study in HD knock-in mice the specific role of LXR downstream to CYP46A1.

LXR activation and regulation of pathways of interest in HD

Defect of myelination has been clearly described in HD, with an early white matter degeneration (Bartzokis et al., 2007; Bohanna et al., 2011) and a specific deleterious effect of mHTT on oligodendrocytes (Huang et al., 2015; Xiang et al., 2011). Thus, because LXRs have critical roles in oligodendrocytes, a special interest should be given to the study of myelination in the contest of LXR activation. Indeed, the use of LXR agonist is able to stimulate oligodendrocytes differentiation (Meffre et al., 2015) and mediates cholesterol efflux from oligodendrocytes (Nelissen et al., 2012). LXR agonist

was also able to stimulate remyelination in organotypic slices that had experienced demyelinating lesions (Meffre et al., 2015).

LXRs also have an established role in the regulation of inflammation in peripheral macrophages, through both their repressive activity and their transcriptional activation (Spann and Glass, 2013). In the brain, the main cells responsible for immune responses are microglia. It was shown that LXRs exhibit similar repressive activities in microglia (Saijo et al., 2013) by regulating the activity of microglial phagocytic receptors such as the tyrosine kinase MerTK, which, in the context of Alzheimer's disease promotes the clearance of amyloid β plaques (Savage et al., 2015). LXR activation was also able to inhibit the nitric oxide synthase 2, inducible expression and nitric oxide production in activated microglia, which is a pro-inflammatory enzyme (Secor McVoy et al., 2015). A modulation of inflammation by limiting the pro-inflammatory activity of microglia using LXR agonist could then have interesting neuroprotective effect in HD.

Involvement of LXR in CYP46A1 neuroprotection

We showed that CYP46A1 expression strongly impacts striatal gene regulation in HD knock-in mice, which is strongly altered in HD. In particular, CYP46A1 regulates the transcription LXR targets such as *apoE* and *cyp51* in zQ175 mice, suggesting that CYP46A1 induces LXR activity, potentially through the production of 24S-OHC. There are two LXRs isoforms, LXRα and LXRβ, that could be studied in astrocytes and neurons, using the zQ175 mice. For instance, specific invalidation of LXR could give us insights into their role in HD. Several conditional mouse models for LXRs are available: the LXRαloxP/loxP and LXRβloxP/loxP mice. Homozygous zQ175 mice could be bred with LXRαloxP/loxP and LXRβloxP/loxP mice to create heterozygous zQ175 mice with genetic invalidation of LXR α or β. Intra-striatal injections of AAVs carrying the cre recombinase transgene under cell-specific promotor (synapsin.CRE to target neurons or gfaABC1D.CRE to target astrocytes) in the zQ175+/- LoxP/LoxP mice would allow a specific ablation of LXRs either in neurons or in astrocytes. Preclinical assessment could then be performed to evaluated locomotor behavior, neuropathology and regulation of cholesterol metabolism. This study would then answer the question of LXR role in HD pathogenesis.

Investigation of therapeutic strategies with new LXR agonists

The use of LXR agonists as a potential therapeutic strategy for neurodegenerative diseases including HD has been previously proposed (Moutinho et al., 2018). However, commercialized compounds suffer from side effects due to the expression of LXRs in peripheral organs. New LXRα or β agonists have been designed and synthesized in order to avoid these side effects (Marinozzi et al., 2017). We validated the activity of these agonists on HD striatal primary neurons, on the transcription of genes involved in

cholesterol metabolism such as *abca1*, *apoe*, *hmgcor* and *fdft1*. Preliminary data support their beneficial effects on HD striatal primary neurons on cell survival and aggregate clearance (data not shown). It would be interesting to study the impacts of these new ligands *in vivo*, either by systemic injection or local striatal administrations in zQ175 mice. This study would give more knowledge on the use of small molecule like LXR modulators in the development of a therapy for HD.

Concluding remarks

The study of global neuroprotective strategies in HD is of particular interest to delay disease onset and slow down the disease progression. The team showed that targeting cholesterol metabolism, by restoring CYP46A1 expression in the striatum of HD models is neuroprotective; in models with a fast progression of HD phenotype like the R6/2 mice (Boussicault et al., 2016) and also in more progressive models, like the zQ175 mice (Kacher et al., under review). CYP46A1 delivery in striatal neurons using AAVs is currently under clinical consideration for several neurodegenerative diseases, including HD (Boussicault et al., 2016) and Alzheimer's disease (Hudry et al., 2010). The clinical development of such a strategy needs a better knowledge of CYP46A1 neuroprotection and sterol signalling through a detailed analysis of lipidomic and transcriptomic signatures and cell protective mechanisms, in both astrocytes and neurons in an HD context. Beyond the scope of HD, a follow-up of this project will also bring important breakthrough on cholesterol metabolism and associated cell-specific signalling, which remains poorly understood despite its fundamental role in brain homeostasis.

REFERENCES

Abad-Rodriguez, J., Ledesma, M.D., Craessaerts, K., Perga, S., Medina, M., Delacourte, A., Dingwall, C., Strooper, B.D., and Dotti, C.G. (2004). Neuronal membrane cholesterol loss enhances amyloid peptide generation. J Cell Biol *167*, 953–960.

Abildayeva, K., Jansen, P.J., Hirsch-Reinshagen, V., Bloks, V.W., Bakker, A.H.F., Ramaekers, F.C.S., Vente, J. de, Groen, A.K., Cheryl L. Wellington, Kuipers, F., et al. (2006). 24(S)-Hydroxycholesterol Participates in a Liver X Receptor-controlled Pathway in Astrocytes That Regulates Apolipoprotein E-mediated Cholesterol Efflux. J. Biol. Chem. *281*, 12799–12808.

Abulrob, A., Tauskela, J.S., Mealing, G., Brunette, E., Faid, K., and Stanimirovic, D. (2005). Protection by cholesterol-extracting cyclodextrins: a role for N-methyl-D-aspartate receptor redistribution. J. Neurochem. *92*, 1477–1486.

Adachi, Y., and Nakashima, K. (1999). [Population genetic study of Huntington's disease--prevalence and founder's effect in the San-in area, western Japan]. Nihon Rinsho Jpn. J. Clin. Med. *57*, 900–904.

Allinquant, B., Clamagirand, C., and Potier, M.-C. (2014). Role of cholesterol metabolism in the pathogenesis of Alzheimer's disease. Curr. Opin. Clin. Nutr. Metab. Care *17*, 319–323.

Altar, C.A., Cai, N., Bliven, T., Juhasz, M., Conner, J.M., Acheson, A.L., Lindsay, R.M., and Wiegand, S.J. (1997). Anterograde transport of brain-derived neurotrophic factor and its role in the brain. Nature *389*, 856–860.

Amé, J.-C., Spenlehauer, C., and de Murcia, G. (2004). The PARP superfamily. BioEssays News Rev. Mol. Cell. Dev. Biol. *26*, 882–893.

Ament, S.A., Pearl, J.R., Grindeland, A., St Claire, J., Earls, J.C., Kovalenko, M., Gillis, T., Mysore, J., Gusella, J.F., Lee, J.-M., et al. (2017). High resolution time-course mapping of early transcriptomic, molecular and cellular phenotypes in Huntington's disease CAG knock-in mice across multiple genetic backgrounds. Hum. Mol. Genet. *26*, 913–922.

Anderson, A.N., Roncaroli, F., Hodges, A., Deprez, M., and Turkheimer, F.E. (2008). Chromosomal profiles of gene expression in Huntington's disease. Brain J. Neurol. *131*, 381–388.

Anderson, K.W., Mast, N., Hudgens, J.W., Lin, J.B., Turko, I.V., and Pikuleva, I.A. (2016). Mapping of the Allosteric Site in Cholesterol Hydroxylase CYP46A1 for Efavirenz, a Drug That Stimulates Enzyme Activity. J. Biol. Chem. *291*, 11876–11886.

Andersson, M., Elmberger, P.G., Edlund, C., Kristensson, K., and Dallner, G. (1990). Rates of cholesterol, ubiquinone, dolichol and dolichyl-P biosynthesis in rat brain slices. FEBS Lett. *269*, 15–18.

André, V.M., Cepeda, C., and Levine, M.S. (2010). Dopamine and Glutamate in Huntington's Disease: A Balancing Act. CNS Neurosci. Ther. *16*, 163–178.

Andrew, S.E., Goldberg, Y.P., Kremer, B., Telenius, H., Theilmann, J., Adam, S., Starr, E., Squitieri, F., Lin, B., and Kalchman, M.A. (1993). The relationship between trinucleotide (CAG) repeat length and clinical features of Huntington's disease. Nat. Genet. *4*, 398–403.

Aono, M., Lee, Y., Grant, E.R., Zivin, R.A., Pearlstein, R.D., Warner, D.S., Bennett, E.R., and Laskowitz, D.T. (2002). Apolipoprotein E protects against NMDA excitotoxicity. Neurobiol. Dis. *11*, 214–220.

Aqul, A., Liu, B., Ramirez, C.M., Pieper, A.A., Estill, S.J., Burns, D.K., Liu, B., Repa, J.J., Turley, S.D., and Dietschy, J.M. (2011). Unesterified Cholesterol Accumulation in Late Endosomes/Lysosomes Causes Neurodegeneration and Is Prevented by Driving Cholesterol Export from This Compartment. J. Neurosci. *31*, 9404–9413.

Arenas, F., Garcia-Ruiz, C., and Fernandez-Checa, J.C. (2017). Intracellular Cholesterol Trafficking and Impact in Neurodegeneration. Front. Mol. Neurosci. *10*.

Arnulf, I., Nielsen, J., Lohmann, E., Schiefer, J., Schieffer, J., Wild, E., Jennum, P., Konofal, E., Walker, M., Oudiette, D., et al. (2008). Rapid eye movement sleep disturbances in Huntington disease. Arch. Neurol. *65*, 482–488.

Arrasate, M., Mitra, S., Schweitzer, E.S., Segal, M.R., and Finkbeiner, S. (2004). Inclusion body formation reduces levels of mutant huntingtin and the risk of neuronal death. Nature *431*, 805–810.

Arzberger, T., Krampfl, K., Leimgruber, S., and Weindl, A. (1997). Changes of NMDA receptor subunit (NR1, NR2B) and glutamate transporter (GLT1) mRNA expression in Huntington's disease--an in situ hybridization study. J. Neuropathol. Exp. Neurol. *56*, 440–454.

Ashkenazi, A., Bento, C.F., Ricketts, T., Vicinanza, M., Siddiqi, F., Pavel, M., Squitieri, F., Hardenberg, M.C., Imarisio, S., Menzies, F.M., et al. (2017). Polyglutamine tracts regulate beclin 1-dependent autophagy. Nature *545*, 108–111.

Atwal, R.S., Xia, J., Pinchev, D., Taylor, J., Epand, R.M., and Truant, R. (2007). Huntingtin has a membrane association signal that can modulate huntingtin aggregation, nuclear entry and toxicity. Hum. Mol. Genet. *16*, 2600–2615.

Augood, S.J., Faull, R.L., Love, D.R., and Emson, P.C. (1996). Reduction in enkephalin and substance P messenger RNA in the striatum of early grade Huntington's disease: a detailed cellular in situ hybridization study. Neuroscience *72*, 1023–1036.

Augood, S.J., Faull, R.L., and Emson, P.C. (1997). Dopamine D1 and D2 receptor gene expression in the striatum in Huntington's disease. Ann. Neurol. *42*, 215–221.

Bañez-Coronel, M., Porta, S., Kagerbauer, B., Mateu-Huertas, E., Pantano, L., Ferrer, I., Guzmán, M., Estivill, X., and Martí, E. (2012). A pathogenic mechanism in Huntington's disease involves small CAG-repeated RNAs with neurotoxic activity. PLoS Genet. *8*, e1002481.

Bañez-Coronel, M., Ayhan, F., Tarabochia, A.D., Zu, T., Perez, B.A., Tusi, S.K., Pletnikova, O., Borchelt, D.R., Ross, C.A., Margolis, R.L., et al. (2015). RAN Translation in Huntington Disease. Neuron *88*, 667–677.

Baquet, Z.C., Gorski, J.A., and Jones, K.R. (2004). Early striatal dendrite deficits followed by neuron loss with advanced age in the absence of anterograde cortical brain-derived neurotrophic factor. J. Neurosci. Off. J. Soc. Neurosci. *24*, 4250–4258.

Barbero-Camps, E., Roca-Agujetas, V., Bartolessis, I., Dios, C. de, Fernández-Checa, J.C., Marí, M., Morales, A., Hartmann, T., and Colell, A. (2018). Cholesterol impairs autophagy-mediated clearance of amyloid beta while promoting its secretion. Autophagy *14*, 1129–1154.

Barnat, M., Le Friec, J., Benstaali, C., and Humbert, S. (2017). Huntingtin-Mediated Multipolar-Bipolar Transition of Newborn Cortical Neurons Is Critical for Their Postnatal Neuronal Morphology. Neuron *93*, 99–114.

Bartzokis, G., Lu, P.H., Tishler, T.A., Fong, S.M., Oluwadara, B., Finn, J.P., Huang, D., Bordelon, Y., Mintz, J., and Perlman, S. (2007). Myelin breakdown and iron changes in Huntington's disease: pathogenesis and treatment implications. Neurochem. Res. *32*, 1655–1664.

Bates, G. (2003). Huntingtin aggregation and toxicity in Huntington's disease. The Lancet *361*, 1642–1644.

Beal, M.F., Kowall, N.W., Ellison, D.W., Mazurek, M.F., Swartz, K.J., and Martin, J.B. (1986). Replication of the neurochemical characteristics of Huntington's disease by quinolinic acid. Nature *321*, 168–171.

Behrens, P.F., Franz, P., Woodman, B., Lindenberg, K.S., and Landwehrmeyer, G.B. (2002). Impaired glutamate transport and glutamate-glutamine cycling: downstream effects of the Huntington mutation. Brain J. Neurol. *125*, 1908–1922.

Ben Haim, L., Ceyzériat, K., Carrillo-de Sauvage, M.A., Aubry, F., Auregan, G., Guillermier, M., Ruiz, M., Petit, F., Houitte, D., Faivre, E., et al. (2015). The JAK/STAT3 pathway is a common inducer of astrocyte reactivity in Alzheimer's and Huntington's diseases. J. Neurosci. Off. J. Soc. Neurosci. *35*, 2817–2829.

Benchoua, A., Trioulier, Y., Zala, D., Gaillard, M.-C., Lefort, N., Dufour, N., Saudou, F., Elalouf, J.-M., Hirsch, E., Hantraye, P., et al. (2006). Involvement of Mitochondrial Complex II Defects in Neuronal Death Produced by N-Terminus Fragment of Mutated Huntingtin. Mol. Biol. Cell *17*, 1652–1663.

Benn, C.L., Sun, T., Sadri-Vakili, G., McFarland, K.N., DiRocco, D.P., Yohrling, G.J., Clark, T.W., Bouzou, B., and Cha, J.-H.J. (2008). Huntingtin modulates transcription, occupies gene promoters in vivo, and binds directly to DNA in a polyglutamine-dependent manner. J. Neurosci. Off. J. Soc. Neurosci. *28*, 10720–10733.

Bennett, E.J., Shaler, T.A., Woodman, B., Ryu, K.-Y., Zaitseva, T.S., Becker, C.H., Bates, G.P., Schulman, H., and Kopito, R.R. (2007). Global changes to the ubiquitin system in Huntington's disease. Nature *448*, 704–708.

Björkhem, I., and Meaney, S. (2004). Brain Cholesterol: Long Secret Life Behind a Barrier. Arterioscler. Thromb. Vasc. Biol.

Björkhem, I., Lövgren-Sandblom, A., Leoni, V., Meaney, S., Brodin, L., Salveson, L., Winge, K., Pålhagen, S., and Svenningsson, P. (2013). Oxysterols and Parkinson's disease: Evidence that levels of 24S-hydroxycholesterol in cerebrospinal fluid correlates with the duration of the disease. Neurosci. Lett. *555*, 102–105.

Bjørkøy, G., Lamark, T., Brech, A., Outzen, H., Perander, M., Øvervatn, A., Stenmark, H., and Johansen, T. (2005). p62/SQSTM1 forms protein aggregates degraded by autophagy and has a protective effect on huntingtin-induced cell death. J. Cell Biol. *171*, 603–614.

Björkqvist, M., Wild, E.J., Thiele, J., Silvestroni, A., Andre, R., Lahiri, N., Raibon, E., Lee, R.V., Benn, C.L., Soulet, D., et al. (2008). A novel pathogenic pathway of immune activation detectable before clinical onset in Huntington's disease. J. Exp. Med. *205*, 1869–1877.

Blalock, E.M., Chen, K.-C., Sharrow, K., Herman, J.P., Porter, N.M., Foster, T.C., and Landfield, P.W. (2003). Gene microarrays in hippocampal aging: statistical profiling identifies novel processes correlated with cognitive impairment. J. Neurosci. Off. J. Soc. Neurosci. *23*, 3807–3819.

Bogdanovic, N., Bretillon, L., Lund, E.G., Diczfalusy, U., Lannfelt, L., Winblad, B., Russell, D.W., and Björkhem, I. (2001). On the turnover of brain cholesterol in patients with Alzheimer's disease.

Abnormal induction of the cholesterol-catabolic enzyme CYP46 in glial cells. Neurosci. Lett. *314*, 45–48.

Bohanna, I., Georgiou-Karistianis, N., Sritharan, A., Asadi, H., Johnston, L., Churchyard, A., and Egan, G. (2011). Diffusion tensor imaging in Huntington's disease reveals distinct patterns of white matter degeneration associated with motor and cognitive deficits. Brain Imaging Behav. *5*, 171–180.

Boussicault, L., Hérard, A.-S., Calingasan, N., Petit, F., Malgorn, C., Merienne, N., Jan, C., Gaillard, M.-C., Lerchundi, R., Barros, L.F., et al. (2014). Impaired brain energy metabolism in the BACHD mouse model of Huntington's disease: critical role of astrocyte-neuron interactions. J. Cereb. Blood Flow Metab. Off. J. Int. Soc. Cereb. Blood Flow Metab. *34*, 1500–1510.

Boussicault, L., Alves, S., Lamazière, A., Planques, A., Heck, N., Moumné, L., Despres, G., Bolte, S., Hu, A., Pagès, C., et al. (2016). CYP46A1, the rate-limiting enzyme for cholesterol degradation, is neuroprotective in Huntington's disease. Brain J. Neurol. *139*, 953–970.

Boussicault, L., Kacher, R., Lamazière, A., Vanhoutte, P., Caboche, J., Betuing, S., and Potier, M.-C. (2018). CYP46A1 protects against NMDA-mediated excitotoxicity in Huntington's disease: Analysis of lipid raft content. Biochimie.

Boutell, J.M., Thomas, P., Neal, J.W., Weston, V.J., Duce, J., Harper, P.S., and Jones, A.L. (1999). Aberrant interactions of transcriptional repressor proteins with the Huntington's disease gene product, huntingtin. Hum. Mol. Genet. *8*, 1647–1655.

Boyles, J.K., Pitas, R.E., Wilson, E., Mahley, R.W., and Taylor, J.M. (1985). Apolipoprotein E associated with astrocytic glia of the central nervous system and with nonmyelinating glia of the peripheral nervous system. J. Clin. Invest. *76*, 1501–1513.

Brachet, A., Norwood, S., Brouwers, J.F., Palomer, E., Helms, J.B., Dotti, C.G., and Esteban, J.A. (2015). LTP-triggered cholesterol redistribution activates Cdc42 and drives AMPA receptor synaptic delivery. J. Cell Biol. *208*, 791–806.

Bradford, J., Shin, J.-Y., Roberts, M., Wang, C.-E., Li, X.-J., and Li, S. (2009). Expression of mutant huntingtin in mouse brain astrocytes causes age-dependent neurological symptoms. Proc. Natl. Acad. Sci. U. S. A. *106*, 22480–22485.

Bretillon, L., Lütjohann, D., Ståhle, L., Widhe, T., Bindl, L., Eggertsen, G., Diczfalusy, U., and Björkhem, I. (2000a). Plasma levels of 24S-hydroxycholesterol reflect the balance between cerebral production and hepatic metabolism and are inversely related to body surface. J. Lipid Res. *41*, 840–845.

Bretillon, L., Sidén, Å., Wahlund, L.-O., Lütjohann, D., Minthon, L., Crisby, M., Hillert, J., Groth, C.-G., Diczfalusy, U., and Björkhem, I. (2000b). Plasma levels of 24S-hydroxycholesterol in patients with neurological diseases. Neurosci. Lett. *293*, 87–90.

Bretillon, L., Diczfalusy, U., Björkhem, I., Maire, M.A., Martine, L., Joffre, C., Acar, N., Bron, A., and Creuzot-Garcher, C. (2007). Cholesterol-24S-hydroxylase (CYP46A1) is specifically expressed in neurons of the neural retina. Curr. Eye Res. *32*, 361–366.

Breuer, O., and Björkhem, I. (1995). Use of an 18O2 Inhalation Technique and Mass Isotopomer Distribution Analysis to Study Oxygenation of Cholesterol in Rat EVIDENCE FOR IN VIVO FORMATION OF 7-OXO-, 7β-HYDROXY-, 24-HYDROXY-, AND 25-HYDROXYCHOLESTEROL. J. Biol. Chem. *270*, 20278–20284.

Brouillet, E., Jenkins, B.G., Hyman, B.T., Ferrante, R.J., Kowall, N.W., Srivastava, R., Roy, D.S., Rosen, B.R., and Beal, M.F. (1993). Age-dependent vulnerability of the striatum to the mitochondrial toxin 3-nitropropionic acid. J. Neurochem. *60*, 356–359.

Brouillet, E., Hantraye, P., Ferrante, R.J., Dolan, R., Leroy-Willig, A., Kowall, N.W., and Beal, M.F. (1995). Chronic mitochondrial energy impairment produces selective striatal degeneration and abnormal choreiform movements in primates. Proc. Natl. Acad. Sci. *92*, 7105–7109.

Brown, M.S., and Goldstein, J.L. (1997). The SREBP pathway: regulation of cholesterol metabolism by proteolysis of a membrane-bound transcription factor. Cell *89*, 331–340.

Brown, J., Theisler, C., Silberman, S., Magnuson, D., Gottardi-Littell, N., Lee, J.M., Yager, D., Crowley, J., Sambamurti, K., Rahman, M.M., et al. (2004). Differential Expression of Cholesterol Hydroxylases in Alzheimer's Disease. J. Biol. Chem. *279*, 34674–34681.

Browne, S.E., Bowling, A.C., Macgarvey, U., Baik, M.J., Berger, S.C., Muquit, M.M.K., Bird, E.D., and Beal, M.F. (1997). Oxidative damage and metabolic dysfunction in Huntington's disease: Selective vulnerability of the basal ganglia. Ann. Neurol. *41*, 646–653.

Brustovetsky, N., LaFrance, R., Purl, K.J., Brustovetsky, T., Keene, C.D., Low, W.C., and Dubinsky, J.M. (2005). Age-Dependent Changes in the Calcium Sensitivity of Striatal Mitochondria in Mouse Models of Huntington's Disease. J. Neurochem. *93*, 1361–1370.

van der Burg, J.M.M., Björkqvist, M., and Brundin, P. (2009). Beyond the brain: widespread pathology in Huntington's disease. Lancet Neurol. *8*, 765–774.

Burlot, M.-A., Braudeau, J., Michaelsen-Preusse, K., Potier, B., Ayciriex, S., Varin, J., Gautier, B., Djelti, F., Audrain, M., Dauphinot, L., et al. (2015). Cholesterol 24-hydroxylase defect is implicated in memory impairments associated with Alzheimer-like Tau pathology. Hum. Mol. Genet. *24*, 5965–5976.

Butchbach, M.E.R., Tian, G., Guo, H., and Lin, C.-L.G. (2004). Association of excitatory amino acid transporters, especially EAAT2, with cholesterol-rich lipid raft microdomains: importance for excitatory amino acid transporter localization and function. J. Biol. Chem. *279*, 34388–34396.

Button, R.W., Roberts, S.L., Willis, T.L., Hanemann, C.O., and Luo, S. (2017). Accumulation of autophagosomes confers cytotoxicity. J. Biol. Chem. *292*, 13599–13614.

Camacho, M., Barker, R.A., and Mason, S.L. (2018). Apathy in Huntington's Disease: A Review of the Current Conceptualization. J. Alzheimers Dis. Park. *8*, 1–9.

Cankar, K., Melik, Z., Kobal, J., and Starc, V. (2018). Evidence of cardiac electrical remodeling in patients with Huntington disease. Brain Behav. *8*, e01077.

Caron, N.S., Dorsey, E.R., and Hayden, M.R. (2018). Therapeutic approaches to Huntington disease: from the bench to the clinic. Nat. Rev. Drug Discov. *17*, 729–750.

Carpenter, M.B., Nakano, K., and Kim, R. (1976). Nigrothalamic projections in the monkey demonstrated by autoradiographic technics. J. Comp. Neurol. *165*, 401–415.

Cartagena, C.M., Ahmed, F., Burns, M.P., Pajoohesh-Ganji, A., Pak, D.T., Faden, A.I., and Rebeck, G.W. (2008). Cortical Injury Increases Cholesterol 24S Hydroxylase (Cyp46) Levels in the Rat Brain. J. Neurotrauma *25*, 1087–1098.

Carty, N., Berson, N., Tillack, K., Thiede, C., Scholz, D., Kottig, K., Sedaghat, Y., Gabrysiak, C., Yohrling, G., von der Kammer, H., et al. (2015). Characterization of HTT inclusion size, location, and timing in the zQ175 mouse model of Huntington's disease: an in vivo high-content imaging study. PloS One *10*, e0123527.

Caviston, J.P., Zajac, A.L., Tokito, M., Holzbaur, E.L.F., and Steinberg, G. (2010). Huntingtin coordinates the dynein-mediated dynamic positioning of endosomes and lysosomes. Mol. Biol. Cell *22*, 478–492.

Ceyzériat, K., Abjean, L., Carrillo-de Sauvage, M.-A., Ben Haim, L., and Escartin, C. (2016). The complex STATes of astrocyte reactivity: How are they controlled by the JAK-STAT3 pathway? Neuroscience *330*, 205–218.

Ceyzériat, K., Ben Haim, L., Denizot, A., Pommier, D., Matos, M., Guillemaud, O., Palomares, M.-A., Abjean, L., Petit, F., Gipchtein, P., et al. (2018). Modulation of astrocyte reactivity improves functional deficits in mouse models of Alzheimer's disease. Acta Neuropathol. Commun. *6*.

Cha, J.-H.J. (2007). Transcriptional signatures in Huntington's disease. Prog. Neurobiol. *83*, 228–248.

Chali, F., Djelti, F., Eugene, E., Valderrama, M., Marquer, C., Aubourg, P., Duykaerts, C., Miles, R., Cartier, N., and Navarro, V. (2015). Inhibiting cholesterol degradation induces neuronal sclerosis and epileptic activity in mouse hippocampus. Eur. J. Neurosci. *41*, 1345–1355.

Chalmers, K.A., Culpan, D., Kehoe, P.G., Wilcock, G.K., Hughes, A., and Love, S. (2004). APOE promoter, ACE1 and CYP46 polymorphisms and beta-amyloid in Alzheimer's disease. Neuroreport *15*, 95–98.

Chang, D.T.W., Rintoul, G.L., Pandipati, S., and Reynolds, I.J. (2006). Mutant huntingtin aggregates impair mitochondrial movement and trafficking in cortical neurons. Neurobiol. Dis. *22*, 388–400.

Chang, T.-Y., Li, B.-L., Chang, C.C.Y., and Urano, Y. (2009). Acyl-coenzyme A:cholesterol acyltransferases. Am. J. Physiol. - Endocrinol. Metab. *297*, E1–E9.

Chen, Z., and Rand, R.P. (1997). The influence of cholesterol on phospholipid membrane curvature and bending elasticity. Biophys. J. *73*, 267–276.

Chen, H., Yang, J., Low, P.S., and Cheng, J.-X. (2008). Cholesterol level regulates endosome motility via Rab proteins. Biophys. J. *94*, 1508–1520.

Chen, J., Zhang, X., Kusumo, H., Costa, L.G., and Guizzetti, M. (2013). Cholesterol efflux is differentially regulated in neurons and astrocytes: implications for brain cholesterol homeostasis. Biochim. Biophys. Acta *1831*, 263–275.

Choo, Y.S., Johnson, G.V.W., MacDonald, M., Detloff, P.J., and Lesort, M. (2004). Mutant huntingtin directly increases susceptibility of mitochondria to the calcium-induced permeability transition and cytochrome c release. Hum. Mol. Genet. *13*, 1407–1420.

Churchward, M.A., Rogasevskaia, T., Höfgen, J., Bau, J., and Coorssen, J.R. (2005). Cholesterol facilitates the native mechanism of Ca2+-triggered membrane fusion. J. Cell Sci. *118*, 4833–4848.

Cicchetti, F., and Parent, A. (1996). Striatal interneurons in Huntington's disease: selective increase in the density of calretinin-immunoreactive medium-sized neurons. Mov. Disord. Off. J. Mov. Disord. Soc. *11*, 619–626.

Coarelli, G., Diallo, A., Thion, M.S., Rinaldi, D., Calvas, F., Boukbiza, O.L., Tataru, A., Charles, P., Tranchant, C., Marelli, C., et al. (2017). Low cancer prevalence in polyglutamine expansion diseases. Neurology *88*, 1114–1119.

Colin, E., Zala, D., Liot, G., Rangone, H., Borrell-Pagès, M., Li, X.-J., Saudou, F., and Humbert, S. (2008). Huntingtin phosphorylation acts as a molecular switch for anterograde/retrograde transport in neurons. EMBO J. *27*, 2124–2134.

Conaco, C., Otto, S., Han, J.-J., and Mandel, G. (2006). Reciprocal actions of REST and a microRNA promote neuronal identity. Proc. Natl. Acad. Sci. *103*, 2422–2427.

Costa, V., and Scorrano, L. (2012). Shaping the role of mitochondria in the pathogenesis of Huntington's disease. EMBO J. *31*, 1853–1864.

Coyle, J.T., and Schwarcz, R. (1976). Lesion of striatal neurones with kainic acid provides a model for Huntington's chorea. Nature *263*, 244–246.

Craufurd, D., and Snowden, J. Neuropsychological and neuropsychiatric aspects of Huntington's Disease.

Crawford, H.E., Hobbs, N.Z., Keogh, R., Langbehn, D.R., Frost, C., Johnson, H., Landwehrmeyer, B., Reilmann, R., Craufurd, D., Stout, J.C., et al. (2013). Corpus callosal atrophy in premanifest and early Huntington's disease. J. Huntingt. Dis. *2*, 517–526.

Crook, Z.R., and Housman, D. (2011). Huntington's disease: can mice lead the way to treatment? Neuron *69*, 423–435.

Crotti, A., and Glass, C.K. (2015). The choreography of neuroinflammation in Huntington's disease. Trends Immunol. *36*, 364–373.

Crotti, A., Benner, C., Kerman, B.E., Gosselin, D., Lagier-Tourenne, C., Zuccato, C., Cattaneo, E., Gage, F.H., Cleveland, D.W., and Glass, C.K. (2014). Mutant Huntingtin promotes autonomous microglia activation via myeloid lineage-determining factors. Nat. Neurosci. *17*, 513–521.

Cudkowicz, M., and Kowall, N.W. (1990). Degeneration of pyramidal projection neurons in Huntington's disease cortex. Ann. Neurol. *27*, 200–204.

Cui, L., Jeong, H., Borovecki, F., Parkhurst, C.N., Tanese, N., and Krainc, D. (2006). Transcriptional Repression of PGC-1α by Mutant Huntingtin Leads to Mitochondrial Dysfunction and Neurodegeneration. Cell *127*, 59–69.

Damiano, M., Diguet, E., Malgorn, C., D'Aurelio, M., Galvan, L., Petit, F., Benhaim, L., Guillermier, M., Houitte, D., Dufour, N., et al. (2013). A role of mitochondrial complex II defects in genetic models of Huntington's disease expressing N-terminal fragments of mutant huntingtin. Hum. Mol. Genet. *22*, 3869–3882.

Davies, S.W., Turmaine, M., Cozens, B.A., DiFiglia, M., Sharp, A.H., Ross, C.A., Scherzinger, E., Wanker, E.E., Mangiarini, L., and Bates, G.P. (1997). Formation of Neuronal Intranuclear Inclusions Underlies the Neurological Dysfunction in Mice Transgenic for the HD Mutation. Cell *90*, 537–548.

Davison, A.N. (1965). Brain sterol metabolism. Adv. Lipid Res. *3*, 171–196.

Déglon, N. (2017). Chapter 9 - From huntingtin gene to Huntington's disease-altering strategies. In Disease-Modifying Targets in Neurodegenerative Disorders, V. Baekelandt, and E. Lobbestael, eds. (Academic Press), pp. 251–276.

Déglon, N., and Hantraye, P. (2005). Viral vectors as tools to model and treat neurodegenerative disorders. J. Gene Med. *7*, 530–539.

Delgado, M.A., Elmaoued, R.A., Davis, A.S., Kyei, G., and Deretic, V. (2008). Toll-like receptors control autophagy. EMBO J. *27*, 1110–1121.

Delint-Ramirez, I., Fernández, E., Bayés, A., Kicsi, E., Komiyama, N.H., and Grant, S.G.N. (2010). In vivo composition of NMDA receptor signaling complexes differs between membrane subdomains and is modulated by PSD-95 and PSD-93. J. Neurosci. Off. J. Soc. Neurosci. *30*, 8162–8170.

Desai, P., DeKosky, S.T., and Kamboh, M.I. (2002). Genetic variation in the cholesterol 24-hydroxylase (CYP46) gene and the risk of Alzheimer's disease. Neurosci. Lett. *328*, 9–12.

Destainville, N., Schmidt, T.H., and Lang, T. (2016). Chapter Two - Where Biology Meets Physics—A Converging View on Membrane Microdomain Dynamics. In Current Topics in Membranes, V. Bennett, ed. (Academic Press), pp. 27–65.

Dhar, A.K., Teng, J.I., and Smith, L.L. (1973). BIOSYNTHESIS OF CHOLEST-5-ENE-3β, 24-DIOL (CEREBROSTEROL) BY BOVINE CEREBRAL CORTICAL MICROSOMES1. J. Neurochem. *21*, 51–60.

Dickey, A.S., Pineda, V.V., Tsunemi, T., Liu, P.P., Miranda, H.C., Gilmore-Hall, S.K., Lomas, N., Sampat, K.R., Buttgereit, A., Torres, M.-J.M., et al. (2016). PPAR-δ is repressed in Huntington's disease, is required for normal neuronal function and can be targeted therapeutically. Nat. Med. *22*, 37–45.

Diczfalusy, U., Olofsson, K.E., Carlsson, A.-M., Gong, M., Golenbock, D.T., Rooyackers, O., Fläring, U., and Björkbacka, H. (2009). Marked upregulation of cholesterol 25-hydroxylase expression by lipopolysaccharide. J. Lipid Res. *50*, 2258–2264.

Didiot, M.-C., Ferguson, C.M., Ly, S., Coles, A.H., Smith, A.O., Bicknell, A.A., Hall, L.M., Sapp, E., Echeverria, D., Pai, A.A., et al. (2018). Nuclear Localization of Huntingtin mRNA Is Specific to Cells of Neuronal Origin. Cell Rep. *24*, 2553-2560.e5.

Dietschy, J.M. (2009). Central nervous system: cholesterol turnover, brain development and neurodegeneration. Biol. Chem. *390*, 287–293.

Dietschy, J.M., and Turley, S.D. (2004). Thematic review series: brain Lipids. Cholesterol metabolism in the central nervous system during early development and in the mature animal. J. Lipid Res. *45*, 1375–1397.

DiFiglia, M., Sapp, E., Chase, K., Schwarz, C., Meloni, A., Young, C., Martin, E., Vonsattel, J.-P., Carraway, R., Reeves, S.A., et al. (1995). Huntingtin is a cytoplasmic protein associated with vesicles in human and rat brain neurons. Neuron *14*, 1075–1081.

DiFiglia, M., Sapp, E., Chase, K.O., Davies, S.W., Bates, G.P., Vonsattel, J.P., and Aronin, N. (1997). Aggregation of Huntingtin in Neuronal Intranuclear Inclusions and Dystrophic Neurites in Brain. Science *277*, 1990–1993.

DiFiglia, M., Sena-Esteves, M., Chase, K., Sapp, E., Pfister, E., Sass, M., Yoder, J., Reeves, P., Pandey, R.K., Rajeev, K.G., et al. (2007). Therapeutic silencing of mutant huntingtin with siRNA attenuates

striatal and cortical neuropathology and behavioral deficits. Proc. Natl. Acad. Sci. U. S. A. *104*, 17204–17209.

Djelti, F., Braudeau, J., Hudry, E., Dhenain, M., Varin, J., Bièche, I., Marquer, C., Chali, F., Ayciriex, S., Auzeil, N., et al. (2015). CYP46A1 inhibition, brain cholesterol accumulation and neurodegeneration pave the way for Alzheimer's disease. Brain *138*, 2383–2398.

Doria, M., Maugest, L., Moreau, T., Lizard, G., and Vejux, A. (2016). Contribution of cholesterol and oxysterols to the pathophysiology of Parkinson's disease. Free Radic. Biol. Med. *101*, 393–400.

Dumanis, S.B., Cha, H.-J., Song, J.M., Trotter, J.H., Spitzer, M., Lee, J.-Y., Weeber, E.J., Turner, R.S., Pak, D.T.S., Rebeck, G.W., et al. (2011). ApoE receptor 2 regulates synapse and dendritic spine formation. PloS One *6*, e17203.

Dunah, A.W., Jeong, H., Griffin, A., Kim, Y.-M., Standaert, D.G., Hersch, S.M., Mouradian, M.M., Young, A.B., Tanese, N., and Krainc, D. (2002). Sp1 and TAFII130 Transcriptional Activity Disrupted in Early Huntington's Disease. Science *296*, 2238–2243.

Duyao, M., Ambrose, C., Myers, R., Novelletto, A., Persichetti, F., Frontali, M., Folstein, S., Ross, C., Franz, M., and Abbott, M. (1993). Trinucleotide repeat length instability and age of onset in Huntington's disease. Nat. Genet. *4*, 387–392.

Duyao, M.P., Auerbach, A.B., Ryan, A., Persichetti, F., Barnes, G.T., McNeil, S.M., Ge, P., Vonsattel, J.P., Gusella, J.F., and Joyner, A.L. (1995). Inactivation of the mouse Huntington's disease gene homolog Hdh. Science *269*, 407–410.

Dzeletovic, S., Breuer, O., Lund, E., and Diczfalusy, U. (1995). Determination of cholesterol oxidation products in human plasma by isotope dilution-mass spectrometry. Anal. Biochem. *225*, 73–80.

Eckmann, J., Clemens, L.E., Eckert, S.H., Hagl, S., Yu-Taeger, L., Bordet, T., Pruss, R.M., Muller, W.E., Leuner, K., Nguyen, H.P., et al. (2014). Mitochondrial Membrane Fluidity is Consistently Increased in Different Models of Huntington Disease: Restorative Effects of Olesoxime. Mol. Neurobiol. *50*, 107–118.

El-Daher, M.-T., Hangen, E., Bruyère, J., Poizat, G., Al-Ramahi, I., Pardo, R., Bourg, N., Souquere, S., Mayet, C., Pierron, G., et al. (2015). Huntingtin proteolysis releases non-polyQ fragments that cause toxicity through dynamin 1 dysregulation. EMBO J. *34*, 2255–2271.

Elias, S., Thion, M.S., Yu, H., Sousa, C.M., Lasgi, C., Morin, X., and Humbert, S. (2014). Huntingtin regulates mammary stem cell division and differentiation. Stem Cell Rep. *2*, 491–506.

Engelender, S., Sharp, A.H., Colomer, V., Tokito, M.K., Lanahan, A., Worley, P., Holzbaur, E.L.F., and Ross, C.A. (1997). Huntingtin-associated Protein 1 (HAP1) Interacts with the p150Glued Bubunit of Dynactin. Hum. Mol. Genet. *6*, 2205–2212.

Faideau, M., Kim, J., Cormier, K., Gilmore, R., Welch, M., Auregan, G., Dufour, N., Guillermier, M., Brouillet, E., Hantraye, P., et al. (2010). In vivo expression of polyglutamine-expanded huntingtin by mouse striatal astrocytes impairs glutamate transport: a correlation with Huntington's disease subjects. Hum. Mol. Genet. *19*, 3053–3067.

Falush, D., Almqvist, E.W., Brinkmann, R.R., Iwasa, Y., and Hayden, M.R. (2001). Measurement of mutational flow implies both a high new-mutation rate for Huntington disease and substantial underascertainment of late-onset cases. Am. J. Hum. Genet. *68*, 373–385.

Fantini, J., and Barrantes, F.J. (2013). How cholesterol interacts with membrane proteins: an exploration of cholesterol-binding sites including CRAC, CARC, and tilted domains. Front. Physiol. *4*, 31.

Farrer, L.A., Cupples, L.A., Haines, J.L., Hyman, B., Kukull, W.A., Mayeux, R., Myers, R.H., Pericak-Vance, M.A., Risch, N., and van Duijn, C.M. (1997). Effects of age, sex, and ethnicity on the association between apolipoprotein E genotype and Alzheimer disease. A meta-analysis. APOE and Alzheimer Disease Meta Analysis Consortium. JAMA *278*, 1349–1356.

Feng, Z., Jin, S., Zupnick, A., Hoh, J., Stanchina, E. de, Lowe, S., Prives, C., and Levine, A.J. (2006). p53 tumor suppressor protein regulates the levels of huntingtin gene expression. Oncogene *25*, 1–7.

Ferrante, R.J., Kubilus, J.K., Lee, J., Ryu, H., Beesen, A., Zucker, B., Smith, K., Kowall, N.W., Ratan, R.R., Luthi-Carter, R., et al. (2003). Histone deacetylase inhibition by sodium butyrate chemotherapy ameliorates the neurodegenerative phenotype in Huntington's disease mice. J. Neurosci. Off. J. Soc. Neurosci. *23*, 9418–9427.

Ferris, H.A., Perry, R.J., Moreira, G.V., Shulman, G.I., Horton, J.D., and Kahn, C.R. (2017). Loss of astrocyte cholesterol synthesis disrupts neuronal function and alters whole-body metabolism. Proc. Natl. Acad. Sci. U. S. A. *114*, 1189–1194.

Fester, L., Zhou, L., Bütow, A., Huber, C., von Lossow, R., Prange-Kiel, J., Jarry, H., and Rune, G.M. (2009). Cholesterol-promoted synaptogenesis requires the conversion of cholesterol to estradiol in the hippocampus. Hippocampus *19*, 692–705.

Fisher, E.R., and Hayden, M.R. (2014). Multisource ascertainment of Huntington disease in Canada: prevalence and population at risk. Mov. Disord. Off. J. Mov. Disord. Soc. *29*, 105–114.

Fourgeux, C., Martine, L., Björkhem, I., Diczfalusy, U., Joffre, C., Acar, N., Creuzot-Garcher, C., Bron, A., and Bretillon, L. (2009). Primary Open-Angle Glaucoma: Association with Cholesterol 24S-Hydroxylase (CYP46A1) Gene Polymorphism and Plasma 24-Hydroxycholesterol Levels. Invest. Ophthalmol. Vis. Sci. *50*, 5712–5717.

Fourgeux, C., Martine, L., Pasquis, B., Maire, M.-A., Acar, N., Creuzot-Garcher, C., Bron, A., and Bretillon, L. (2012). Steady-state levels of retinal 24S-hydroxycholesterol are maintained by glial cells intervention after elevation of intraocular pressure in the rat. Acta Ophthalmol. (Copenh.) *90*, e560–e567.

Fourgeux, C., Martine, L., Acar, N., Bron, A.M., Creuzot-Garcher, C.P., and Bretillon, L. (2014). In vivo consequences of cholesterol-24S-hydroxylase (CYP46A1) inhibition by voriconazole on cholesterol homeostasis and function in the rat retina. Biochem. Biophys. Res. Commun. *446*, 775–781.

Fraldi, A., Annunziata, F., Lombardi, A., Kaiser, H.-J., Medina, D.L., Spampanato, C., Fedele, A.O., Polishchuk, R., Sorrentino, N.C., Simons, K., et al. (2010). Lysosomal fusion and SNARE function are impaired by cholesterol accumulation in lysosomal storage disorders. EMBO J. *29*, 3607–3620.

Frank, C., Giammarioli, A.M., Pepponi, R., Fiorentini, C., and Rufini, S. (2004). Cholesterol perturbing agents inhibit NMDA-dependent calcium influx in rat hippocampal primary culture. FEBS Lett. *566*, 25–29.

Fu, B.Y., Ma, S.L., Tang, N.L.S., Tam, C.W.C., Lui, V.W.C., Chiu, H.F.K., and Lam, L.C.W. (2009). Cholesterol 24-hydroxylase (CYP46A1) polymorphisms are associated with faster cognitive deterioration in Chinese older persons: a two-year follow up study. Int. J. Geriatr. Psychiatry *24*, 921–926.

Fumagalli, R., and Paoletti, R. (1963). The identification and significance of desmosterol in the developing human and animal brain. Life Sci. *2*, 291–295.

Fusco, F.R., Chen, Q., Lamoreaux, W.J., Figueredo-Cardenas, G., Jiao, Y., Coffman, J.A., Surmeier, D.J., Honig, M.G., Carlock, L.R., and Reiner, A. (1999). Cellular localization of huntingtin in striatal and cortical neurons in rats: lack of correlation with neuronal vulnerability in Huntington's disease. J. Neurosci. Off. J. Soc. Neurosci. *19*, 1189–1202.

Futter, M., Diekmann, H., Schoenmakers, E., Sadiq, O., Chatterjee, K., and Rubinsztein, D.C. (2009). Wild-type but not mutant huntingtin modulates the transcriptional activity of liver X receptors. J. Med. Genet. *46*, 438–446.

Gafni, J., and Ellerby, L.M. (2002). Calpain activation in Huntington's disease. J. Neurosci. Off. J. Soc. Neurosci. *22*, 4842–4849.

Galvan, L., André, V.M., Wang, E.A., Cepeda, C., and Levine, M.S. (2012). Functional Differences Between Direct and Indirect Striatal Output Pathways in Huntington's Disease. J. Huntingt. Dis. *1*, 17–25.

Gao, X., Campbell, W.A., Chaibva, M., Jain, P., Leslie, A.E., Frey, S.L., and Legleiter, J. (2016). Cholesterol Modifies Huntingtin Binding to, Disruption of, and Aggregation on Lipid Membranes. Biochemistry *55*, 92–102.

Gauthier, L.R., Charrin, B.C., Borrell-Pagès, M., Dompierre, J.P., Rangone, H., Cordelières, F.P., De Mey, J., MacDonald, M.E., Lessmann, V., Humbert, S., et al. (2004). Huntingtin controls neurotrophic support and survival of neurons by enhancing BDNF vesicular transport along microtubules. Cell *118*, 127–138.

Gaylor, J.L. (2002). Membrane-Bound Enzymes of Cholesterol Synthesis from Lanosterol. Biochem. Biophys. Res. Commun. *292*, 1139–1146.

Genetic Modifiers of Huntington's Disease (GeM-HD) Consortium (2015). Identification of Genetic Factors that Modify Clinical Onset of Huntington's Disease. Cell *162*, 516–526.

Ghisletti, S., Huang, W., Ogawa, S., Pascual, G., Lin, M.-E., Willson, T.M., Rosenfeld, M.G., and Glass, C.K. (2007). Parallel SUMOylation-dependent pathways mediate gene- and signal-specific transrepression by LXRs and PPARgamma. Mol. Cell *25*, 57–70.

Gil, C., Soler-Jover, A., Blasi, J., and Aguilera, J. (2005). Synaptic proteins and SNARE complexes are localized in lipid rafts from rat brain synaptosomes. Biochem. Biophys. Res. Commun. *329*, 117–124.

Gimpl, G., Burger, K., and Fahrenholz, F. (1997). Cholesterol as Modulator of Receptor Function. Biochemistry *36*, 10959–10974.

Gladding, C.M., Sepers, M.D., Xu, J., Zhang, L.Y.J., Milnerwood, A.J., Lombroso, P.J., and Raymond, L.A. (2012). Calpain and STriatal-Enriched protein tyrosine phosphatase (STEP) activation contribute to extrasynaptic NMDA receptor localization in a Huntington's disease mouse model. Hum. Mol. Genet. *21*, 3739–3752.

Glass, M., Dragunow, M., and Faull, R.L. (2000). The pattern of neurodegeneration in Huntington's disease: a comparative study of cannabinoid, dopamine, adenosine and GABA(A) receptor alterations in the human basal ganglia in Huntington's disease. Neuroscience *97*, 505–519.

Godin, J.D., Colombo, K., Molina-Calavita, M., Keryer, G., Zala, D., Charrin, B.C., Dietrich, P., Volvert, M.-L., Guillemot, F., Dragatsis, I., et al. (2010). Huntingtin is required for mitotic spindle orientation and mammalian neurogenesis. Neuron *67*, 392–406.

Gokce, O., Stanley, G.M., Treutlein, B., Neff, N.F., Camp, J.G., Malenka, R.C., Rothwell, P.E., Fuccillo, M.V., Südhof, T.C., and Quake, S.R. (2016). Cellular Taxonomy of the Mouse Striatum as Revealed by Single-Cell RNA-Seq. Cell Rep.

Goldstein, J.L., and Brown, M.S. (1990). Regulation of the mevalonate pathway. Nature *343*, 425–430.

Gonzalez-Alegre, P., and Afifi, A.K. (2006). Clinical characteristics of childhood-onset (juvenile) Huntington disease: report of 12 patients and review of the literature. J. Child Neurol. *21*, 223–229.

Goodman, D.S., Avigan, J., and Wilson, H. (1962). THE *IN VITRO* METABOLISM OF DESMOSTEROL WITH ADRENAL AND LIVER PREPARATIONS. J. Clin. Invest. *41*, 2135–2141.

Goritz, C., Mauch, D.H., and Pfrieger, F.W. (2005). Multiple mechanisms mediate cholesterol-induced synaptogenesis in a CNS neuron. Mol. Cell. Neurosci. *29*, 190–201.

Gourfinkel-An, I., Cancel, G., Trottier, Y., Devys, D., Tora, L., Lutz, Y., Imbert, G., Saudou, F., Stevanin, G., Agid, Y., et al. (1997). Differential distribution of the normal and mutated forms of huntingtin in the human brain. Ann. Neurol. *42*, 712–719.

Govek, E.-E., Newey, S.E., and Aelst, L.V. (2005). The role of the Rho GTPases in neuronal development. Genes Dev. *19*, 1–49.

Govek, E.-E., Hatten, M.E., and Aelst, L.V. (2011). The role of Rho GTPase proteins in CNS neuronal migration. Dev. Neurobiol. *71*, 528–553.

Grafton, S.T., Mazziotta, J.C., Pahl, J.J., St George-Hyslop, P., Haines, J.L., Gusella, J., Hoffman, J.M., Baxter, L.R., and Phelps, M.E. (1992). Serial changes of cerebral glucose metabolism and caudate size in persons at risk for Huntington's disease. Arch. Neurol. *49*, 1161–1167.

Graham, R.K., Deng, Y., Slow, E.J., Haigh, B., Bissada, N., Lu, G., Pearson, J., Shehadeh, J., Bertram, L., Murphy, Z., et al. (2006). Cleavage at the Caspase-6 Site Is Required for Neuronal Dysfunction and Degeneration Due to Mutant Huntingtin. Cell *125*, 1179–1191.

Guo, Q., Bin Huang, null, Cheng, J., Seefelder, M., Engler, T., Pfeifer, G., Oeckl, P., Otto, M., Moser, F., Maurer, M., et al. (2018). The cryo-electron microscopy structure of huntingtin. Nature *555*, 117–120.

Gusella, J.F., Wexler, N.S., Conneally, P.M., Naylor, S.L., Anderson, M.A., Tanzi, R.E., Watkins, P.C., Ottina, K., Wallace, M.R., and Sakaguchi, A.Y. (1983). A polymorphic DNA marker genetically linked to Huntington's disease. Nature *306*, 234–238.

Gutekunst, C.A., Levey, A.I., Heilman, C.J., Whaley, W.L., Yi, H., Nash, N.R., Rees, H.D., Madden, J.J., and Hersch, S.M. (1995). Identification and localization of huntingtin in brain and human lymphoblastoid cell lines with anti-fusion protein antibodies. Proc. Natl. Acad. Sci. *92*, 8710–8714.

Gutekunst, C.-A., Li, S.-H., Yi, H., Mulroy, J.S., Kuemmerle, S., Jones, R., Rye, D., Ferrante, R.J., Hersch, S.M., and Li, X.-J. (1999). Nuclear and Neuropil Aggregates in Huntington's Disease: Relationship to Neuropathology. J. Neurosci. *19*, 2522–2534.

Halford, R.W., and Russell, D.W. (2009). Reduction of cholesterol synthesis in the mouse brain does not affect amyloid formation in Alzheimer's disease, but does extend lifespan. Proc. Natl. Acad. Sci. *106*, 3502–3506.

Hall, A., and Lalli, G. (2010). Rho and Ras GTPases in Axon Growth, Guidance, and Branching. Cold Spring Harb. Perspect. Biol. *2*, a001818.

Han, I., You, Y., Kordower, J.H., Brady, S.T., and Morfini, G.A. (2010). Differential vulnerability of neurons in Huntington's disease: the role of cell type-specific features. J. Neurochem. *113*, 1073–1091.

Hannedouche, S., Zhang, J., Yi, T., Shen, W., Nguyen, D., Pereira, J.P., Guerini, D., Baumgarten, B.U., Roggo, S., Wen, B., et al. (2011). Oxysterols direct immune cell migration via EBI2. Nature *475*, 524–527.

Hardingham, G.E., and Bading, H. (2010). Synaptic versus extrasynaptic NMDA receptor signalling: implications for neurodegenerative disorders. Nat. Rev. Neurosci. *11*, 682–696.

Harjes, P., and Wanker, E.E. (2003). The hunt for huntingtin function: interaction partners tell many different stories. Trends Biochem. Sci. *28*, 425–433.

Hattula, K., and Peränen, J. (2000). FIP-2, a coiled-coil protein, links Huntingtin to Rab8 and modulates cellular morphogenesis. Curr. Biol. *10*, 1603–1606.

Hayashi, H., Campenot, R.B., Vance, D.E., and Vance, J.E. (2009). Protection of neurons from apoptosis by apolipoprotein E-containing lipoproteins does not require lipoprotein uptake and involves activation of phospholipase Cgamma1 and inhibition of calcineurin. J. Biol. Chem. *284*, 29605–29613.

HD iPSC Consortium (2012). Induced pluripotent stem cells from patients with Huntington's disease show CAG-repeat-expansion-associated phenotypes. Cell Stem Cell *11*, 264–278.

He, X., Jenner, A.M., Ong, W.-Y., Farooqui, A.A., and Patel, S.C. (2006). Lovastatin Modulates Increased Cholesterol and Oxysterol Levels and Has a Neuroprotective Effect on Rat Hippocampal Neurons After Kainate Injury. J. Neuropathol. Exp. Neurol. *65*, 652–663.

He, X., Zhang, Z., Zhang, J., Zhou, Y., Wu, C., Tang, M., and Hong, Z. (2012). An Intronic CYP46A1 Polymorphism Is Associated with Alzheimer Disease in a Chinese Han Population. J. Mol. Neurosci. *47*, 514–518.

Head, B.P., Patel, H.H., Tsutsumi, Y.M., Hu, Y., Mejia, T., Mora, R.C., Insel, P.A., Roth, D.M., Drummond, J.C., and Patel, P.M. (2008). Caveolin-1 expression is essential for N-methyl-D-aspartate receptor-mediated Src and extracellular signal-regulated kinase 1/2 activation and protection of primary neurons from ischemic cell death. FASEB J. Off. Publ. Fed. Am. Soc. Exp. Biol. *22*, 828–840.

Head, B.P., Peart, J.N., Panneerselvam, M., Yokoyama, T., Pearn, M.L., Niesman, I.R., Bonds, J.A., Schilling, J.M., Miyanohara, A., Headrick, J., et al. (2010). Loss of caveolin-1 accelerates neurodegeneration and aging. PloS One *5*, e15697.

Hedreen, J.C., Peyser, C.E., Folstein, S.E., and Ross, C.A. (1991). Neuronal loss in layers V and VI of cerebral cortex in Huntington's disease. Neurosci. Lett. *133*, 257–261.

Heikkinen, T., Lehtimäki, K., Vartiainen, N., Puoliväli, J., Hendricks, S.J., Glaser, J.R., Bradaia, A., Wadel, K., Touller, C., Kontkanen, O., et al. (2012). Characterization of neurophysiological and behavioral

changes, MRI brain volumetry and 1H MRS in zQ175 knock-in mouse model of Huntington's disease. PloS One *7*, e50717.

Hering, H., Lin, C.-C., and Sheng, M. (2003). Lipid rafts in the maintenance of synapses, dendritic spines, and surface AMPA receptor stability. J. Neurosci. Off. J. Soc. Neurosci. *23*, 3262–3271.

Hering, T., Kojer, K., Birth, N., Hallitsch, J., Taanman, J.-W., and Orth, M. (2017). Mitochondrial cristae remodelling is associated with disrupted OPA1 oligomerisation in the Huntington's disease R6/2 fragment model. Exp. Neurol. *288*, 167–175.

Herz, J., and Chen, Y. (2006). Reelin, lipoprotein receptors and synaptic plasticity. Nat. Rev. Neurosci. *7*, 850–859.

Heverin, M., Bogdanovic, N., Lütjohann, D., Bayer, T., Pikuleva, I., Bretillon, L., Diczfalusy, U., Winblad, B., and Björkhem, I. (2004). Changes in the levels of cerebral and extracerebral sterols in the brain of patients with Alzheimer's disease. J. Lipid Res. *45*, 186–193.

Hodgson, J.G., Agopyan, N., Gutekunst, C.A., Leavitt, B.R., LePiane, F., Singaraja, R., Smith, D.J., Bissada, N., McCutcheon, K., Nasir, J., et al. (1999). A YAC mouse model for Huntington's disease with full-length mutant huntingtin, cytoplasmic toxicity, and selective striatal neurodegeneration. Neuron *23*, 181–192.

Holmans, P.A., Massey, T.H., and Jones, L. (2017). Genetic modifiers of Mendelian disease: Huntington's disease and the trinucleotide repeat disorders. Hum. Mol. Genet. *26*, R83–R90.

Holzmann, C., Schmidt, T., Thiel, G., Epplen, J.T., and Riess, O. (2001). Functional characterization of the human Huntington's disease gene promoter. Mol. Brain Res. *92*, 85–97.

Horton, J.D., Goldstein, J.L., and Brown, M.S. (2002). SREBPs: activators of the complete program of cholesterol and fatty acid synthesis in the liver. J. Clin. Invest. *109*, 1125–1131.

Hou, Q., Huang, Y., Amato, S., Snyder, S.H., Huganir, R.L., and Man, H.-Y. (2008). Regulation of AMPA receptor localization in lipid rafts. Mol. Cell. Neurosci. *38*, 213–223.

Huang, B., Wei, W., Wang, G., Gaertig, M.A., Feng, Y., Wang, W., Li, X.-J., and Li, S. (2015). Mutant huntingtin downregulates myelin regulatory factor-mediated myelin gene expression and affects mature oligodendrocytes. Neuron *85*, 1212–1226.

Huang, N., Erie, C., Lu, M.L., and Wei, J. (2018). Aberrant subcellular localization of SQSTM1/p62 contributes to increased vulnerability to proteotoxic stress recovery in Huntington's disease. Mol. Cell. Neurosci. *88*, 43–52.

Huang, Y.-N., Lin, C.-I., Liao, H., Liu, C.-Y., Chen, Y.-H., Chiu, W.-C., and Lin, S.-H. (2016). Cholesterol overload induces apoptosis in SH-SY5Y human neuroblastoma cells through the up regulation of flotillin-2 in the lipid raft and the activation of BDNF/Trkb signaling. Neuroscience *328*, 201–209.

Huang, Y.-W.A., Zhou, B., Wernig, M., and Südhof, T.C. (2017). ApoE2, ApoE3, and ApoE4 Differentially Stimulate APP Transcription and Aβ Secretion. Cell *168*, 427-441.e21.

Hudry, E., Van Dam, D., Kulik, W., De Deyn, P.P., Stet, F.S., Ahouansou, O., Benraiss, A., Delacourte, A., Bougnères, P., Aubourg, P., et al. (2010). Adeno-associated Virus Gene Therapy With Cholesterol 24-Hydroxylase Reduces the Amyloid Pathology Before or After the Onset of Amyloid Plaques in Mouse Models of Alzheimer's Disease. Mol. Ther. *18*, 44–53.

Hunter, J.M., Lesort, M., and Johnson, G.V.W. (2007). Ubiquitin-proteasome system alterations in a striatal cell model of Huntington's disease. J. Neurosci. Res. *85*, 1774–1788.

Hwang, S., Disatnik, M.-H., and Mochly-Rosen, D. (2015). Impaired GAPDH-induced mitophagy contributes to the pathology of Huntington's disease. EMBO Mol. Med. *7*, 1307–1326.

Iannilli, F., Sodero, A.O., Ledesma, M.D., and Dotti, C.G. (2011). Oxidative stress activates the pro-survival TrkA pathway through membrane cholesterol loss. Neurobiol. Aging *32*, 1033–1042.

Ignatius, M.J., Gebicke-Härter, P.J., Skene, J.H., Schilling, J.W., Weisgraber, K.H., Mahley, R.W., and Shooter, E.M. (1986). Expression of apolipoprotein E during nerve degeneration and regeneration. Proc. Natl. Acad. Sci. U. S. A. *83*, 1125–1129.

Indersmitten, T., Tran, C.H., Cepeda, C., and Levine, M.S. (2015). Altered excitatory and inhibitory inputs to striatal medium-sized spiny neurons and cortical pyramidal neurons in the Q175 mouse model of Huntington's disease. J. Neurophysiol. *113*, 2953–2966.

Ito, A., Hong, C., Rong, X., Zhu, X., Tarling, E.J., Hedde, P.N., Gratton, E., Parks, J., and Tontonoz, P. (2015). LXRs link metabolism to inflammation through Abca1-dependent regulation of membrane composition and TLR signaling. ELife *4*, e08009.

Jacobsen, J.C., Bawden, C.S., Rudiger, S.R., McLaughlan, C.J., Reid, S.J., Waldvogel, H.J., MacDonald, M.E., Gusella, J.F., Walker, S.K., Kelly, J.M., et al. (2010). An ovine transgenic Huntington's disease model. Hum. Mol. Genet. *19*, 1873–1882.

Jang, J., Park, S., Hur, H.J., Cho, H.J., Hwang, I., Kang, Y.P., Im, I., Lee, H., Lee, E., Yang, W., et al. (2016). 25-hydroxycholesterol contributes to cerebral inflammation of X-linked adrenoleukodystrophy through activation of the NLRP3 inflammasome. Nat. Commun. *7*, 13129.

Jang, M., Lee, S.E., and Cho, I.-H. (2018). Adeno-Associated Viral Vector Serotype DJ-Mediated Overexpression of N171-82Q-Mutant Huntingtin in the Striatum of Juvenile Mice Is a New Model for Huntington's Disease. Front. Cell. Neurosci. *12*, 157.

Jansen, A.H.P., Hal, M. van, Kelder, I.C. op den, Meier, R.T., Ruiter, A.-A. de, Schut, M.H., Smith, D.L., Grit, C., Brouwer, N., Kamphuis, W., et al. (2017). Frequency of nuclear mutant huntingtin inclusion formation in neurons and glia is cell-type-specific. Glia *65*, 50–61.

Jayaraman, M., Kodali, R., Sahoo, B., Thakur, A.K., Mayasundari, A., Mishra, R., Peterson, C.B., and Wetzel, R. (2012). Slow amyloid nucleation via α-helix-rich oligomeric intermediates in short polyglutamine-containing huntingtin fragments. J. Mol. Biol. *415*, 881–899.

Jeske, D.J., and Dietschy, J.M. (1980). Regulation of rates of cholesterol synthesis in vivo in the liver and carcass of the rat measured using [3H]water. J. Lipid Res. *21*, 364–376.

Jia, F., Liu, Z., Song, N., Du, X., Xie, J., and Jiang, H. (2016). The association between CYP46A1 rs4900442 polymorphism and the risk of Alzheimer's disease: A meta-analysis. Neurosci. Lett. *620*, 83–87.

Jiang, R., Diaz-Castro, B., Looger, L.L., and Khakh, B.S. (2016). Dysfunctional Calcium and Glutamate Signaling in Striatal Astrocytes from Huntington's Disease Model Mice. J. Neurosci. Off. J. Soc. Neurosci. *36*, 3453–3470.

Johansson, A., Katzov, H., Zetterberg, H., Feuk, L., Johansson, B., Bogdanovic, N., Andreasen, N., Lenhard, B., Brookes, A.J., Pedersen, N.L., et al. (2004). Variants of CYP46A1 may interact with age and APOE to influence CSF Abeta42 levels in Alzheimer's disease. Hum. Genet. *114*, 581–587.

Johansson, M., Rocha, N., Zwart, W., Jordens, I., Janssen, L., Kuijl, C., Olkkonen, V.M., and Neefjes, J. (2007). Activation of endosomal dynein motors by stepwise assembly of Rab7-RILP-p150Glued, ORP1L, and the receptor betalll spectrin. J. Cell Biol. *176*, 459–471.

Jordens, I., Fernandez-Borja, M., Marsman, M., Dusseljee, S., Janssen, L., Calafat, J., Janssen, H., Wubbolts, R., and Neefjes, J. (2001). The Rab7 effector protein RILP controls lysosomal transport by inducing the recruitment of dynein-dynactin motors. Curr. Biol. CB *11*, 1680–1685.

Jurevics, H., and Morell, P. (1995). Cholesterol for Synthesis of Myelin Is Made Locally, Not Imported into Brain. J. Neurochem. *64*, 895–901.

Kant, R. van der, Fish, A., Janssen, L., Janssen, H., Krom, S., Ho, N., Brummelkamp, T., Carette, J., Rocha, N., and Neefjes, J. (2013). Late endosomal transport and tethering are coupled processes controlled by RILP and the cholesterol sensor ORP1L. J Cell Sci *126*, 3462–3474.

Kasimov, M.R., Fatkhrakhmanova, M.R., Mukhutdinova, K.A., and Petrov, A.M. (2017). 24S-Hydroxycholesterol enhances synaptic vesicle cycling in the mouse neuromuscular junction: Implication of glutamate NMDA receptors and nitric oxide. Neuropharmacology *117*, 61–73.

Kegel, K.B., Meloni, A.R., Yi, Y., Kim, Y.J., Doyle, E., Cuiffo, B.G., Sapp, E., Wang, Y., Qin, Z.-H., Chen, J.D., et al. (2002). Huntingtin Is Present in the Nucleus, Interacts with the Transcriptional Corepressor C-terminal Binding Protein, and Represses Transcription. J. Biol. Chem. *277*, 7466–7476.

Kim, Y.J., Yi, Y., Sapp, E., Wang, Y., Cuiffo, B., Kegel, K.B., Qin, Z.H., Aronin, N., and DiFiglia, M. (2001). Caspase 3-cleaved N-terminal fragments of wild-type and mutant huntingtin are present in normal and Huntington's disease brains, associate with membranes, and undergo calpain-dependent proteolysis. Proc. Natl. Acad. Sci. U. S. A. *98*, 12784–12789.

Koga, H., Kaushik, S., and Cuervo, A.M. (2010). Altered lipid content inhibits autophagic vesicular fusion. FASEB J. *24*, 3052–3065.

Kölsch, H., Lütjohann, D., Ludwig, M., Schulte, A., Ptok, U., Jessen, F., von Bergmann, K., Rao, M.L., Maier, W., and Heun, R. (2002). Polymorphism in the cholesterol 24S-hydroxylase gene is associated with Alzheimer's disease. Mol. Psychiatry *7*, 899–902.

Kölsch, H., Heun, R., Kerksiek, A., Bergmann, K. v., Maier, W., and Lütjohann, D. (2004). Altered levels of plasma 24S- and 27-hydroxycholesterol in demented patients. Neurosci. Lett. *368*, 303–308.

Korinek, M., Vyklicky, V., Borovska, J., Lichnerova, K., Kaniakova, M., Krausova, B., Krusek, J., Balik, A., Smejkalova, T., Horak, M., et al. (2015). Cholesterol modulates open probability and desensitization of NMDA receptors. J. Physiol. *593*, 2279–2293.

Koseoglu, S., Love, S.A., and Haynes, C.L. (2011). Cholesterol effects on vesicle pools in chromaffin cells revealed by carbon-fiber microelectrode amperometry. Anal. Bioanal. Chem. *400*, 2963.

Kotti, T., Head, D.D., McKenna, C.E., and Russell, D.W. (2008). Biphasic requirement for geranylgeraniol in hippocampal long-term potentiation. Proc. Natl. Acad. Sci. *105*, 11394–11399.

Kotti, T.J., Ramirez, D.M.O., Pfeiffer, B.E., Huber, K.M., and Russell, D.W. (2006). Brain cholesterol turnover required for geranylgeraniol production and learning in mice. Proc. Natl. Acad. Sci. *103*, 3869–3874.

Koudinov, A.R., and Koudinova, N.V. (2005). Cholesterol homeostasis failure as a unifying cause of synaptic degeneration. J. Neurol. Sci. *229–230*, 233–240.

Kraft, A.D., Kaltenbach, L.S., Lo, D.C., and Harry, G.J. (2012). Activated microglia proliferate at neurites of mutant huntingtin-expressing neurons. Neurobiol. Aging *33*, 621.e17-33.

Kreilaus, F., Spiro, A.S., Hannan, A.J., Garner, B., and Jenner, A.M. (2015). Brain Cholesterol Synthesis and Metabolism is Progressively Disturbed in the R6/1 Mouse Model of Huntington's Disease: A Targeted GC-MS/MS Sterol Analysis. J. Huntingt. Dis. *4*, 305–318.

Kreilaus, F., Spiro, A.S., McLean, C.A., Garner, B., and Jenner, A.M. (2016). Evidence for altered cholesterol metabolism in Huntington's disease post mortem brain tissue. Neuropathol. Appl. Neurobiol. *42*, 535–546.

Kuhn, A., Goldstein, D.R., Hodges, A., Strand, A.D., Sengstag, T., Kooperberg, C., Becanovic, K., Pouladi, M.A., Sathasivam, K., Cha, J.-H.J., et al. (2007). Mutant huntingtin's effects on striatal gene expression in mice recapitulate changes observed in human Huntington's disease brain and do not differ with mutant huntingtin length or wild-type huntingtin dosage. Hum. Mol. Genet. *16*, 1845–1861.

Küppenbender, K.D., Standaert, D.G., Feuerstein, T.J., Penney, J.B., Young, A.B., and Landwehrmeyer, G.B. (2000). Expression of NMDA receptor subunit mRNAs in neurochemically identified projection and interneurons in the human striatum. J. Comp. Neurol. *419*, 407–421.

Lai, C.-L., Liou, L.-M., Liu, C.-K., Yang, Y.-H., and Lin, R.-T. (2014). Effects of metabolic syndrome, apolipoprotein E, and CYP46 on cognition among Taiwanese Chinese. Kaohsiung J. Med. Sci. *30*, 343–349.

Lakk, M., Vazquez-Chona, F., Yarishkin, O., and Križaj, D. (2018). Dyslipidemia modulates Müller glial sensing and transduction of ambient information. Neural Regen. Res. *13*, 207–210.

Landwehrmeyer, G.B., McNeil, S.M., Dure, L.S., Ge, P., Aizawa, H., Huang, Q., Ambrose, C.M., Duyao, M.P., Bird, E.D., and Bonilla, E. (1995). Huntington's disease gene: regional and cellular expression in brain of normal and affected individuals. Ann. Neurol. *37*, 218–230.

Lang, T. (2007). SNARE proteins and 'membrane rafts.' J. Physiol. *585*, 693–698.

Lange, H., Thörner, G., Hopf, A., and Schröder, K.F. (1976). Morphometric studies of the neuropathological changes in choreatic diseases. J. Neurol. Sci. *28*, 401–425.

Langfelder, P., Cantle, J.P., Chatzopoulou, D., Wang, N., Gao, F., Al-Ramahi, I., Lu, X.-H., Ramos, E.M., El-Zein, K., Zhao, Y., et al. (2016). Integrated genomics and proteomics define huntingtin CAG length-dependent networks in mice. Nat. Neurosci. *19*, 623–633.

Leavitt, B.R., van Raamsdonk, J.M., Shehadeh, J., Fernandes, H., Murphy, Z., Graham, R.K., Wellington, C.L., Raymond, L.A., and Hayden, M.R. (2006). Wild-type huntingtin protects neurons from excitotoxicity. J. Neurochem. *96*, 1121–1129.

Lee, J.-M., Gillis, T., Mysore, J.S., Ramos, E.M., Myers, R.H., Hayden, M.R., Morrison, P.J., Nance, M., Ross, C.A., Margolis, R.L., et al. (2012a). Common SNP-Based Haplotype Analysis of the 4p16.3 Huntington Disease Gene Region. Am. J. Hum. Genet. *90*, 434–444.

Lee, J.-M., Ramos, E.M., Lee, J.-H., Gillis, T., Mysore, J.S., Hayden, M.R., Warby, S.C., Morrison, P., Nance, M., Ross, C.A., et al. (2012b). CAG repeat expansion in Huntington disease determines age at onset in a fully dominant fashion. Neurology *78*, 690–695.

Lee, J.-M., Chao, M.J., Harold, D., Abu Elneel, K., Gillis, T., Holmans, P., Jones, L., Orth, M., Myers, R.H., Kwak, S., et al. (2017). A modifier of Huntington's disease onset at the MLH1 locus. Hum. Mol. Genet. *26*, 3859–3867.

Lee, S.-T., Chu, K., Im, W.-S., Yoon, H.-J., Im, J.-Y., Park, J.-E., Park, K.-H., Jung, K.-H., Lee, S.K., Kim, M., et al. (2011). Altered microRNA regulation in Huntington's disease models. Exp. Neurol. *227*, 172–179.

Legleiter, J., Mitchell, E., Lotz, G.P., Sapp, E., Ng, C., DiFiglia, M., Thompson, L.M., and Muchowski, P.J. (2010). Mutant huntingtin fragments form oligomers in a polyglutamine length-dependent manner in vitro and in vivo. J. Biol. Chem. *285*, 14777–14790.

Lehmann, J.M., Kliewer, S.A., Moore, L.B., Smith-Oliver, T.A., Oliver, B.B., Su, J.-L., Sundseth, S.S., Winegar, D.A., Blanchard, D.E., Spencer, T.A., et al. (1997). Activation of the Nuclear Receptor LXR by Oxysterols Defines a New Hormone Response Pathway. J. Biol. Chem. *272*, 3137–3140.

Leitman, J., Ulrich Hartl, F., and Lederkremer, G.Z. (2013). Soluble forms of polyQ-expanded huntingtin rather than large aggregates cause endoplasmic reticulum stress. Nat. Commun. *4*, 2753.

Leoni, V., Masterman, T., Patel, P., Meaney, S., Diczfalusy, U., and Björkhem, I. (2003). Side chain oxidized oxysterols in cerebrospinal fluid and the integrity of blood-brain and blood-cerebrospinal fluid barriers. J. Lipid Res. *44*, 793–799.

Leoni, V., Mariotti, C., Tabrizi, S.J., Valenza, M., Wild, E.J., Henley, S.M.D., Hobbs, N.Z., Mandelli, M.L., Grisoli, M., Björkhem, I., et al. (2008). Plasma 24S-hydroxycholesterol and caudate MRI in pre-manifest and early Huntington's disease. Brain J. Neurol. *131*, 2851–2859.

Leoni, V., Mariotti, C., Nanetti, L., Salvatore, E., Squitieri, F., Bentivoglio, A.R., Bandettini di Poggio, M., Bandettini Del Poggio, M., Piacentini, S., Monza, D., et al. (2011). Whole body cholesterol metabolism is impaired in Huntington's disease. Neurosci. Lett. *494*, 245–249.

Leoni, V., Long, J.D., Mills, J.A., Di Donato, S., Paulsen, J.S., and PREDICT-HD study group (2013). Plasma 24S-hydroxycholesterol correlation with markers of Huntington disease progression. Neurobiol. Dis. *55*, 37–43.

Li, S.-H., Cheng, A.L., Zhou, H., Lam, S., Rao, M., Li, H., and Li, X.-J. (2002). Interaction of Huntington disease protein with transcriptional activator Sp1. Mol. Cell. Biol. *22*, 1277–1287.

Li, X., Sapp, E., Valencia, A., Kegel, K.B., Qin, Z.-H., Alexander, J., Masso, N., Reeves, P., Ritch, J.J., Zeitlin, S., et al. (2008). A function of huntingtin in guanine nucleotide exchange on Rab11. Neuroreport *19*, 1643–1647.

Liao, G., Yao, Y., Liu, J., Yu, Z., Cheung, S., Xie, A., Liang, X., and Bi, X. (2007). Cholesterol Accumulation Is Associated with Lysosomal Dysfunction and Autophagic Stress in Npc1−/− Mouse Brain. Am. J. Pathol. *171*, 962–975.

Liddelow, S.A., Guttenplan, K.A., Clarke, L.E., Bennett, F.C., Bohlen, C.J., Schirmer, L., Bennett, M.L., Münch, A.E., Chung, W.-S., Peterson, T.C., et al. (2017). Neurotoxic reactive astrocytes are induced by activated microglia. Nature *541*, 481–487.

Li-Hawkins, J., Lund, E.G., Bronson, A.D., and Russell, D.W. (2000). Expression Cloning of an Oxysterol 7α-Hydroxylase Selective for 24-Hydroxycholesterol. J. Biol. Chem. *275*, 16543–16549.

Lin, B., Rommens, J.M., Graham, R.K., Kalchman, M., MacDonald, H., Nasir, J., Delaney, A., Goldberg, Y.P., and Hayden, M.R. (1993). Differential 3' polyadenylation of the Huntington disease gene results in two mRNA species with variable tissue expression. Hum. Mol. Genet. *2*, 1541–1545.

Lin, C.H., Tallaksen-Greene, S., Chien, W.M., Cearley, J.A., Jackson, W.S., Crouse, A.B., Ren, S., Li, X.J., Albin, R.L., and Detloff, P.J. (2001). Neurological abnormalities in a knock-in mouse model of Huntington's disease. Hum. Mol. Genet. *10*, 137–144.

Lin, J.B., Sene, A., Santeford, A., Fujiwara, H., Sidhu, R., Ligon, M.M., Shankar, V.A., Ban, N., Mysorekar, I.U., Ory, D.S., et al. (2018a). Oxysterol Signatures Distinguish Age-Related Macular Degeneration from Physiologic Aging. EBioMedicine *32*, 9–20.

Lin, Y.-T., Seo, J., Gao, F., Feldman, H.M., Wen, H.-L., Penney, J., Cam, H.P., Gjoneska, E., Raja, W.K., Cheng, J., et al. (2018b). APOE4 Causes Widespread Molecular and Cellular Alterations Associated with Alzheimer's Disease Phenotypes in Human iPSC-Derived Brain Cell Types. Neuron *98*, 1141-1154.e7.

Linetti, A., Fratangeli, A., Taverna, E., Valnegri, P., Francolini, M., Cappello, V., Matteoli, M., Passafaro, M., and Rosa, P. (2010). Cholesterol reduction impairs exocytosis of synaptic vesicles. J. Cell Sci. *123*, 595–605.

Lingwood, D., and Simons, K. (2010). Lipid Rafts As a Membrane-Organizing Principle. Science *327*, 46–50.

Liot, G., Bossy, B., Lubitz, S., Kushnareva, Y., Sejbuk, N., and Bossy-Wetzel, E. (2009). Complex II inhibition by 3-NP causes mitochondrial fragmentation and neuronal cell death via an NMDA- and ROS-dependent pathway. Cell Death Differ. *16*, 899–909.

Liot, G., Zala, D., Pla, P., Mottet, G., Piel, M., and Saudou, F. (2013). Mutant Huntingtin alters retrograde transport of TrkB receptors in striatal dendrites. J. Neurosci. Off. J. Soc. Neurosci. *33*, 6298–6309.

Liu, W., Chaurette, J., Pfister, E.L., Kennington, L.A., Chase, K.O., Bullock, J., Vonsattel, J.P.G., Faull, R.L.M., Macdonald, D., DiFiglia, M., et al. (2013). Increased Steady-State Mutant Huntingtin mRNA in Huntington's Disease Brain. J. Huntingt. Dis. *2*, 491–500.

Loh, D.H., Kudo, T., Truong, D., Wu, Y., and Colwell, C.S. (2013). The Q175 mouse model of Huntington's disease shows gene dosage- and age-related decline in circadian rhythms of activity and sleep. PloS One *8*, e69993.

Lund, E.G., Guileyardo, J.M., and Russell, D.W. (1999). cDNA cloning of cholesterol 24-hydroxylase, a mediator of cholesterol homeostasis in the brain. Proc. Natl. Acad. Sci. U. S. A. *96*, 7238–7243.

Lund, E.G., Xie, C., Kotti, T., Turley, S.D., Dietschy, J.M., and Russell, D.W. (2003). Knockout of the Cholesterol 24-Hydroxylase Gene in Mice Reveals a Brain-specific Mechanism of Cholesterol Turnover. J. Biol. Chem. *278*, 22980–22988.

Lunkes, A., Lindenberg, K.S., Ben-Haïem, L., Weber, C., Devys, D., Landwehrmeyer, G.B., Mandel, J.-L., and Trottier, Y. (2002). Proteases acting on mutant huntingtin generate cleaved products that differentially build up cytoplasmic and nuclear inclusions. Mol. Cell *10*, 259–269.

Luthi-Carter, R., Taylor, D.M., Pallos, J., Lambert, E., Amore, A., Parker, A., Moffitt, H., Smith, D.L., Runne, H., Gokce, O., et al. (2010). SIRT2 inhibition achieves neuroprotection by decreasing sterol biosynthesis. Proc. Natl. Acad. Sci. U. S. A. *107*, 7927–7932.

Lütjohann, D., Breuer, O., Ahlborg, G., Nennesmo, I., Sidén, A., Diczfalusy, U., and Björkhem, I. (1996). Cholesterol homeostasis in human brain: evidence for an age-dependent flux of 24S-hydroxycholesterol from the brain into the circulation. Proc. Natl. Acad. Sci. *93*, 9799–9804.

Lütjohann, D., Papassotiropoulos, A., Björkhem, I., Locatelli, S., Bagli, M., Oehring, R.D., Schlegel, U., Jessen, F., Rao, M.L., von Bergmann, K., et al. (2000). Plasma 24S-hydroxycholesterol (cerebrosterol) is increased in Alzheimer and vascular demented patients. J. Lipid Res. *41*, 195–198.

Ma, Q., Yang, J., Li, T., Milner, T.A., and Hempstead, B.L. (2015). Selective reduction of striatal mature BDNF without induction of proBDNF in the zQ175 mouse model of Huntington's disease. Neurobiol. Dis. *82*, 466–477.

MacDonald, M.E., Ambrose, C.M., Duyao, M.P., Myers, R.H., Lin, C., Srinidhi, L., Barnes, G., Taylor, S.A., James, M., Groot, N., et al. (1993). A novel gene containing a trinucleotide repeat that is expanded and unstable on Huntington's disease chromosomes. Cell *72*, 971–983.

Maioli, S., Båvner, A., Ali, Z., Heverin, M., Ismail, M.-A.-M., Puerta, E., Olin, M., Saeed, A., Shafaati, M., Parini, P., et al. (2013). Is It Possible to Improve Memory Function by Upregulation of the Cholesterol 24S-Hydroxylase (CYP46A1) in the Brain? PLOS ONE *8*, e68534.

Maiuri, T., Mocle, A.J., Hung, C.L., Xia, J., van Roon-Mom, W.M.C., and Truant, R. (2017). Huntingtin is a scaffolding protein in the ATM oxidative DNA damage response complex. Hum. Mol. Genet. *26*, 395–406.

Mangiarini, L., Sathasivam, K., Seller, M., Cozens, B., Harper, A., Hetherington, C., Lawton, M., Trottier, Y., Lehrach, H., Davies, S.W., et al. (1996). Exon 1 of the HD gene with an expanded CAG repeat is sufficient to cause a progressive neurological phenotype in transgenic mice. Cell *87*, 493–506.

Marcora, E., Gowan, K., and Lee, J.E. (2003). Stimulation of NeuroD activity by huntingtin and huntingtin-associated proteins HAP1 and MLK2. Proc. Natl. Acad. Sci. *100*, 9578–9583.

Marinozzi, M., Castro Navas, F.F., Maggioni, D., Carosati, E., Bocci, G., Carloncelli, M., Giorgi, G., Cruciani, G., Fontana, R., and Russo, V. (2017). Side-Chain Modified Ergosterol and Stigmasterol Derivatives as Liver X Receptor Agonists. J. Med. Chem. *60*, 6548–6562.

Martin, D.D.O., Ladha, S., Ehrnhoefer, D.E., and Hayden, M.R. (2015). Autophagy in Huntington disease and huntingtin in autophagy. Trends Neurosci. *38*, 26–35.

Martin, E., Betuing, S., Pagès, C., Cambon, K., Auregan, G., Deglon, N., Roze, E., and Caboche, J. (2011a). Mitogen- and stress-activated protein kinase 1-induced neuroprotection in Huntington's disease: role on chromatin remodeling at the PGC-1-alpha promoter. Hum. Mol. Genet. *20*, 2422–2434.

Martin, M.G., Perga, S., Trovò, L., Rasola, A., Holm, P., Rantamäki, T., Harkany, T., Castrén, E., Chiara, F., and Dotti, C.G. (2008). Cholesterol loss enhances TrkB signaling in hippocampal neurons aging in vitro. Mol. Biol. Cell *19*, 2101–2112.

Martin, M.G., Trovò, L., Perga, S., Sadowska, A., Rasola, A., Chiara, F., and Dotti, C.G. (2011b). Cyp46-mediated cholesterol loss promotes survival in stressed hippocampal neurons. Neurobiol. Aging *32*, 933–943.

Martín, M.G., Pfrieger, F., and Dotti, C.G. (2014). Cholesterol in brain disease: sometimes determinant and frequently implicated. EMBO Rep. *15*, 1036–1052.

Martin, M.G., Ahmed, T., Korovaichuk, A., Venero, C., Menchón, S.A., Salas, I., Munck, S., Herreras, O., Balschun, D., and Dotti, C.G. (2014). Constitutive hippocampal cholesterol loss underlies poor cognition in old rodents. EMBO Mol. Med. *6*, 902–917.

Martindale, D., Hackam, A., Wieczorek, A., Ellerby, L., Wellington, C., McCutcheon, K., Singaraja, R., Kazemi-Esfarjani, P., Devon, R., Kim, S.U., et al. (1998). Length of huntingtin and its polyglutamine tract influences localization and frequency of intracellular aggregates. Nat. Genet. *18*, 150–154.

Martínez-Turrillas, R., Puerta, E., Chowdhury, D., Marco, S., Watanabe, M., Aguirre, N., and Pérez-Otaño, I. (2012). The NMDA receptor subunit GluN3A protects against 3-nitroproprionic-induced striatal lesions via inhibition of calpain activation. Neurobiol. Dis. *48*, 290–298.

Martinez-Vicente, M., Talloczy, Z., Wong, E., Tang, G., Koga, H., Kaushik, S., de Vries, R., Arias, E., Harris, S., Sulzer, D., et al. (2010). Cargo recognition failure is responsible for inefficient autophagy in Huntington's disease. Nat. Neurosci. *13*, 567–576.

Marullo, M., Valenza, M., Leoni, V., Caccia, C., Scarlatti, C., De Mario, A., Zuccato, C., Di Donato, S., Carafoli, E., and Cattaneo, E. (2012). Pitfalls in the detection of cholesterol in Huntington's disease models. PLoS Curr. *4*.

Marwarha, G., and Ghribi, O. (2015). Does the oxysterol 27-hydroxycholesterol underlie Alzheimer's disease-Parkinson's disease overlap? Exp. Gerontol. *68*, 13–18.

Mast, N., Norcross, R., Andersson, U., Shou, M., Nakayama, K., Bjorkhem, I., and Pikuleva, I.A. (2003). Broad substrate specificity of human cytochrome P450 46A1 which initiates cholesterol degradation in the brain. Biochemistry *42*, 14284–14292.

Mast, N., White, M.A., Bjorkhem, I., Johnson, E.F., Stout, C.D., and Pikuleva, I.A. (2008). Crystal structures of substrate-bound and substrate-free cytochrome P450 46A1, the principal cholesterol hydroxylase in the brain. Proc. Natl. Acad. Sci. U. S. A. *105*, 9546–9551.

Mast, N., Linger, M., Clark, M., Wiseman, J., Stout, C.D., and Pikuleva, I.A. (2012). In silico and intuitive predictions of CYP46A1 inhibition by marketed drugs with subsequent enzyme crystallization in complex with fluvoxamine. Mol. Pharmacol. *82*, 824–834.

Mast, N., Li, Y., Linger, M., Clark, M., Wiseman, J., and Pikuleva, I.A. (2014). Pharmacologic Stimulation of Cytochrome P450 46A1 and Cerebral Cholesterol Turnover in Mice. J. Biol. Chem. *289*, 3529–3538.

Mast, N., Lin, J.B., Anderson, K.W., Bjorkhem, I., and Pikuleva, I.A. (2017a). Transcriptional and post-translational changes in the brain of mice deficient in cholesterol removal mediated by cytochrome P450 46A1 (CYP46A1). PloS One *12*, e0187168.

Mast, N., Saadane, A., Valencia-Olvera, A., Constans, J., Maxfield, E., Arakawa, H., Li, Y., Landreth, G., and Pikuleva, I.A. (2017b). Cholesterol-metabolizing enzyme cytochrome P450 46A1 as a pharmacologic target for Alzheimer's disease. Neuropharmacology *123*, 465–476.

McGill, J.K., and Beal, M.F. (2006). PGC-1alpha, a new therapeutic target in Huntington's disease? Cell *127*, 465–468.

McGuire, J.R., Rong, J., Li, S.-H., and Li, X.-J. (2006). Interaction of Huntingtin-associated Protein-1 with Kinesin Light Chain IMPLICATIONS IN INTRACELLULAR TRAFFICKING IN NEURONS. J. Biol. Chem. *281*, 3552–3559.

Meaney, S., Lütjohann, D., Diczfalusy, U., and Björkhem, I. (2000). Formation of oxysterols from different pools of cholesterol as studied by stable isotope technique: cerebral origin of most circulating 24S-hydroxycholesterol in rats, but not in mice. Biochim. Biophys. Acta *1486*, 293–298.

van Meer, G., Voelker, D.R., and Feigenson, G.W. (2008). Membrane lipids: where they are and how they behave. Nat. Rev. Mol. Cell Biol. *9*, 112–124.

Meffre, D., Shackleford, G., Hichor, M., Gorgievski, V., Tzavara, E.T., Trousson, A., Ghoumari, A.M., Deboux, C., Oumesmar, B.N., Liere, P., et al. (2015). Liver X receptors alpha and beta promote myelination and remyelination in the cerebellum. Proc. Natl. Acad. Sci. *112*, 7587–7592.

Mehrotra, A., Sood, A., and Sandhir, R. (2015). Mitochondrial modulators improve lipid composition and attenuate memory deficits in experimental model of Huntington's disease. Mol. Cell. Biochem. *410*, 281–292.

Meljon, A., Wang, Y., and Griffiths, W.J. (2014). Oxysterols in the brain of the cholesterol 24-hydroxylase knockout mouse. Biochem. Biophys. Res. Commun. *446*, 768–774.

Menalled, L.B., Sison, J.D., Dragatsis, I., Zeitlin, S., and Chesselet, M.-F. (2003). Time course of early motor and neuropathological anomalies in a knock-in mouse model of Huntington's disease with 140 CAG repeats. J. Comp. Neurol. *465*, 11–26.

Menalled, L.B., Kudwa, A.E., Miller, S., Fitzpatrick, J., Watson-Johnson, J., Keating, N., Ruiz, M., Mushlin, R., Alosio, W., McConnell, K., et al. (2012). Comprehensive behavioral and molecular characterization of a new knock-in mouse model of Huntington's disease: zQ175. PloS One *7*, e49838.

Milagre, I., Nunes, M.J., Gama, M.J., Silva, R.F., Pascussi, J.M., Lechner, M.C., and Rodrigues, E. (2008). Transcriptional regulation of the human CYP46A1 brain-specific expression by Sp transcription factors. J. Neurochem. *106*, 835–849.

Milagre, I., Nunes, M.J., Moutinho, M., Rivera, I., Fuso, A., Scarpa, S., Gama, M.J., and Rodrigues, E. (2010). Chromatin-modifying agents increase transcription of CYP46A1, a key player in brain cholesterol elimination. J. Alzheimers Dis. JAD *22*, 1209–1221.

Milagre, I., Nunes, M.J., Castro-Caldas, M., Moutinho, M., Gama, M.J., and Rodrigues, E. (2012a). Neuronal differentiation alters the ratio of Sp transcription factors recruited to the CYP46A1 promoter. J. Neurochem. *120*, 220–229.

Milagre, I., Olin, M., Nunes, M.J., Moutinho, M., Lövgren-Sandblom, A., Gama, M.J., Björkhem, I., and Rodrigues, E. (2012b). Marked change in the balance between CYP27A1 and CYP46A1 mediated elimination of cholesterol during differentiation of human neuronal cells. Neurochem. Int. *60*, 192–198.

Milakovic, T., Quintanilla, R.A., and Johnson, G.V.W. (2006). Mutant huntingtin expression induces mitochondrial calcium handling defects in clonal striatal cells: functional consequences. J. Biol. Chem. *281*, 34785–34795.

Milnerwood, A.J., Gladding, C.M., Pouladi, M.A., Kaufman, A.M., Hines, R.M., Boyd, J.D., Ko, R.W.Y., Vasuta, O.C., Graham, R.K., Hayden, M.R., et al. (2010). Early increase in extrasynaptic NMDA receptor signaling and expression contributes to phenotype onset in Huntington's disease mice. Neuron *65*, 178–190.

Milnerwood, A.J., Kaufman, A.M., Sepers, M.D., Gladding, C.M., Zhang, L., Wang, L., Fan, J., Coquinco, A., Qiao, J.Y., Lee, H., et al. (2012). Mitigation of augmented extrasynaptic NMDAR signaling and apoptosis in cortico-striatal co-cultures from Huntington's disease mice. Neurobiol. Dis. *48*, 40–51.

Mitter, D., Reisinger, C., Hinz, B., Hollmann, S., Yelamanchili, S.V., Treiber-Held, S., Ohm, T.G., Herrmann, A., and Ahnert-Hilger, G. (2003). The synaptophysin/synaptobrevin interaction critically depends on the cholesterol content. J. Neurochem. *84*, 35–42.

Mochel, F., Durant, B., Meng, X., O'Callaghan, J., Yu, H., Brouillet, E., Wheeler, V.C., Humbert, S., Schiffmann, R., and Durr, A. (2012). Early Alterations of Brain Cellular Energy Homeostasis in Huntington Disease Models. J. Biol. Chem. *287*, 1361–1370.

Modregger, J., DiProspero, N.A., Charles, V., Tagle, D.A., and Plomann, M. (2002). PACSIN 1 interacts with huntingtin and is absent from synaptic varicosities in presymptomatic Huntington's disease brains. Hum. Mol. Genet. *11*, 2547–2558.

Modregger, J., Schmidt, A.A., Ritter, B., Huttner, W.B., and Plomann, M. (2003). Characterization of Endophilin B1b, a Brain-specific Membrane-associated Lysophosphatidic Acid Acyl Transferase with Properties Distinct from Endophilin A1. J. Biol. Chem. *278*, 4160–4167.

de la Monte, S.M., Vonsattel, J.P., and Richardson, E.P. (1988). Morphometric demonstration of atrophic changes in the cerebral cortex, white matter, and neostriatum in Huntington's disease. J. Neuropathol. Exp. Neurol. *47*, 516–525.

Morales Jesús R., Ballesteros Iván, Deniz José Manuel, Hurtado Olivia, Vivancos José, Nombela Florentino, Lizasoain Ignacio, Castrillo Antonio, and Moro María A. (2008). Activation of Liver X Receptors Promotes Neuroprotection and Reduces Brain Inflammation in Experimental Stroke. Circulation *118*, 1450–1459.

Moutinho, M., Nunes, M.J., Gomes, A.Q., Gama, M.J., Cedazo-Minguez, A., Rodrigues, C.M.P., Björkhem, I., and Rodrigues, E. (2015). Cholesterol 24S-Hydroxylase Overexpression Inhibits the Liver X Receptor (LXR) Pathway by Activating Small Guanosine Triphosphate-Binding Proteins (sGTPases) in Neuronal Cells. Mol. Neurobiol. *51*, 1489–1503.

Moutinho, M., Nunes, M.J., and Rodrigues, E. (2016a). Cholesterol 24-hydroxylase: Brain cholesterol metabolism and beyond. Biochim. Biophys. Acta *1861*, 1911–1920.

Moutinho, M., Nunes, M.J., Correia, J.C., Gama, M.J., Castro-Caldas, M., Cedazo-Minguez, A., Rodrigues, C.M.P., Björkhem, I., Ruas, J.L., and Rodrigues, E. (2016b). Neuronal cholesterol metabolism increases dendritic outgrowth and synaptic markers via a concerted action of GGTase-I and Trk. Sci. Rep. *6*, 30928.

Moutinho, M., Codocedo, J.F., Puntambekar, S.S., and Landreth, G.E. (2018). Nuclear Receptors as Therapeutic Targets for Neurodegenerative Diseases: Lost in Translation. Annu. Rev. Pharmacol. Toxicol.

Muratore, M. (2013). Raman spectroscopy and partial least squares analysis in discrimination of peripheral cells affected by Huntington's disease. Anal. Chim. Acta *793*, 1–10.

Murray, D.H., and Tamm, L.K. (2009). Clustering of syntaxin-1A in model membranes is modulated by phosphatidylinositol 4,5-bisphosphate and cholesterol. Biochemistry *48*, 4617–4625.

Myers, R.H. (2004). Huntington's disease genetics. NeuroRx J. Am. Soc. Exp. Neurother. *1*, 255–262.

Nasir, J., Floresco, S.B., O'Kusky, J.R., Diewert, V.M., Richman, J.M., Zeisler, J., Borowski, A., Marth, J.D., Phillips, A.G., and Hayden, M.R. (1995). Targeted disruption of the Huntington's disease gene results in embryonic lethality and behavioral and morphological changes in heterozygotes. Cell *81*, 811–823.

Nelissen, K., Mulder, M., Smets, I., Timmermans, S., Smeets, K., Ameloot, M., and Hendriks, J.J.A. (2012). Liver X receptors regulate cholesterol homeostasis in oligodendrocytes. J. Neurosci. Res. *90*, 60–71.

Neueder, A., Landles, C., Ghosh, R., Howland, D., Myers, R.H., Faull, R.L.M., Tabrizi, S.J., and Bates, G.P. (2017). The pathogenic exon 1 HTT protein is produced by incomplete splicing in Huntington's disease patients. Sci. Rep. *7*, 1307.

Nieweg, K., Schaller, H., and Pfrieger, F.W. (2009). Marked differences in cholesterol synthesis between neurons and glial cells from postnatal rats. J. Neurochem. *109*, 125–134.

Nishimura, M., Yaguti, H., Yoshitsugu, H., Naito, S., and Satoh, T. (2003). Tissue distribution of mRNA expression of human cytochrome P450 isoforms assessed by high-sensitivity real-time reverse transcription PCR. Yakugaku Zasshi *123*, 369–375.

Nothdurfter, C., Tanasic, S., Di Benedetto, B., Uhr, M., Wagner, E.-M., Gilling, K.E., Parsons, C.G., Rein, T., Holsboer, F., Rupprecht, R., et al. (2013). Lipid raft integrity affects GABAA receptor, but not NMDA receptor modulation by psychopharmacological compounds. Int. J. Neuropsychopharmacol. *16*, 1361–1371.

Novak, M.J.U., and Tabrizi, S.J. (2010). Huntington's disease. BMJ *340*, c3109.

Nowaczyk, M.J.M., and Irons, M.B. (2012). Smith-Lemli-Opitz syndrome: phenotype, natural history, and epidemiology. Am. J. Med. Genet. C Semin. Med. Genet. *160C*, 250–262.

Nucifora, F.C., Sasaki, M., Peters, M.F., Huang, H., Cooper, J.K., Yamada, M., Takahashi, H., Tsuji, S., Troncoso, J., Dawson, V.L., et al. (2001). Interference by huntingtin and atrophin-1 with cbp-mediated transcription leading to cellular toxicity. Science *291*, 2423–2428.

Nunes, M.J., Milagre, I., Schnekenburger, M., Gama, M.J., Diederich, M., and Rodrigues, E. (2010). Sp proteins play a critical role in histone deacetylase inhibitor-mediated derepression of CYP46A1 gene transcription. J. Neurochem. *113*, 418–431.

Nunes, M.J., Moutinho, M., Milagre, I., Gama, M.J., and Rodrigues, E. (2012). Okadaic acid inhibits the trichostatin A-mediated increase of human CYP46A1 neuronal expression in a ERK1/2-Sp3-dependent pathway. J. Lipid Res. *53*, 1910–1919.

Nwaobi, S.E., Cuddapah, V.A., Patterson, K.C., Randolph, A.C., and Olsen, M.L. (2016). The role of glial-specific Kir4.1 in normal and pathological states of the CNS. Acta Neuropathol. (Berl.) *132*, 1–21.

Oakeshott, S., Port, R., Cummins-Sutphen, J., Berger, J., Watson-Johnson, J., Ramboz, S., Paterson, N., Kwak, S., Howland, D., and Brunner, D. (2012). A mixed fixed ratio/progressive ratio procedure reveals an apathy phenotype in the BAC HD and the z_Q175 KI mouse models of Huntington's disease. PLoS Curr. *4*, e4f972cffe82c0.

Ochaba, J., Lukacsovich, T., Csikos, G., Zheng, S., Margulis, J., Salazar, L., Mao, K., Lau, A.L., Yeung, S.Y., Humbert, S., et al. (2014). Potential function for the Huntingtin protein as a scaffold for selective autophagy. Proc. Natl. Acad. Sci. *111*, 16889–16894.

Ohyama, Y., Meaney, S., Heverin, M., Ekström, L., Brafman, A., Shafir, M., Andersson, U., Olin, M., Eggertsen, G., Diczfalusy, U., et al. (2006). Studies on the transcriptional regulation of cholesterol 24-hydroxylase (CYP46A1): marked insensitivity toward different regulatory axes. J. Biol. Chem. *281*, 3810–3820.

Okabe, A., Urano, Y., Itoh, S., Suda, N., Kotani, R., Nishimura, Y., Saito, Y., and Noguchi, N. (2013). Adaptive responses induced by 24S-hydroxycholesterol through liver X receptor pathway reduce 7-ketocholesterol-caused neuronal cell death. Redox Biol. *2*, 28–35.

Okamoto, S., Pouladi, M.A., Talantova, M., Yao, D., Xia, P., Ehrnhoefer, D.E., Zaidi, R., Clemente, A., Kaul, M., Graham, R.K., et al. (2009). Balance between synaptic versus extrasynaptic NMDA receptor activity influences inclusions and neurotoxicity of mutant huntingtin. Nat. Med. *15*, 1407–1413.

Orr, A.L., Li, S., Wang, C.-E., Li, H., Wang, J., Rong, J., Xu, X., Mastroberardino, P.G., Greenamyre, J.T., and Li, X.-J. (2008). N-Terminal Mutant Huntingtin Associates with Mitochondria and Impairs Mitochondrial Trafficking. J. Neurosci. *28*, 2783–2792.

Orre, M., Kamphuis, W., Osborn, L.M., Melief, J., Kooijman, L., Huitinga, I., Klooster, J., Bossers, K., and Hol, E.M. (2014). Acute isolation and transcriptome characterization of cortical astrocytes and microglia from young and aged mice. Neurobiol. Aging *35*, 1–14.

Pal, A., Severin, F., Lommer, B., Shevchenko, A., and Zerial, M. (2006). Huntingtin–HAP40 complex is a novel Rab5 effector that regulates early endosome motility and is up-regulated in Huntington's disease. J Cell Biol *172*, 605–618.

Palidwor, G.A., Shcherbinin, S., Huska, M.R., Rasko, T., Stelzl, U., Arumughan, A., Foulle, R., Porras, P., Sanchez-Pulido, L., Wanker, E.E., et al. (2009). Detection of alpha-rod protein repeats using a neural network and application to huntingtin. PLoS Comput. Biol. *5*, e1000304.

Panov, A.V., Gutekunst, C.-A., Leavitt, B.R., Hayden, M.R., Burke, J.R., Strittmatter, W.J., and Greenamyre, J.T. (2002). Early mitochondrial calcium defects in Huntington's disease are a direct effect of polyglutamines. Nat. Neurosci. *5*, 731–736.

Paoletti, P., Bellone, C., and Zhou, Q. (2013). NMDA receptor subunit diversity: impact on receptor properties, synaptic plasticity and disease. Nat. Rev. Neurosci. *14*, 383–400.

Papassotiropoulos, A., Streffer, J.R., Tsolaki, M., Schmid, S., Thal, D., Nicosia, F., Iakovidou, V., Maddalena, A., Lütjohann, D., Ghebremedhin, E., et al. (2003). Increased Brain β-Amyloid Load, Phosphorylated Tau, and Risk of Alzheimer Disease Associated With an Intronic CYP46 Polymorphism. Arch. Neurol. *60*, 29–35.

Papoutsi, M., Labuschagne, I., Tabrizi, S.J., and Stout, J.C. (2014). The cognitive burden in Huntington's disease: pathology, phenotype, and mechanisms of compensation. Mov. Disord. Off. J. Mov. Disord. Soc. *29*, 673–683.

Parker, J.A., Connolly, J.B., Wellington, C., Hayden, M., Dausset, J., and Neri, C. (2001). Expanded polyglutamines in Caenorhabditis elegans cause axonal abnormalities and severe dysfunction of PLM mechanosensory neurons without cell death. Proc. Natl. Acad. Sci. U. S. A. *98*, 13318–13323.

Parsons, M.P., and Raymond, L.A. (2014). Extrasynaptic NMDA receptor involvement in central nervous system disorders. Neuron *82*, 279–293.

Paul, S.M., Doherty, J.J., Robichaud, A.J., Belfort, G.M., Chow, B.Y., Hammond, R.S., Crawford, D.C., Linsenbardt, A.J., Shu, H.-J., Izumi, Y., et al. (2013). The Major Brain Cholesterol Metabolite 24(S)-Hydroxycholesterol Is a Potent Allosteric Modulator of N-Methyl-d-Aspartate Receptors. J. Neurosci. *33*, 17290–17300.

Paulsen, J.S., Ready, R.E., Hamilton, J.M., Mega, M.S., and Cummings, J.L. (2001). Neuropsychiatric aspects of Huntington's disease. J. Neurol. Neurosurg. Psychiatry *71*, 310–314.

Paulsen, J.S., Hoth, K.F., Nehl, C., and Stierman, L. (2005). Critical periods of suicide risk in Huntington's disease. Am. J. Psychiatry *162*, 725–731.

Pavese, N., Gerhard, A., Tai, Y.F., Ho, A.K., Turkheimer, F., Barker, R.A., Brooks, D.J., and Piccini, P. (2006). Microglial activation correlates with severity in Huntington disease: a clinical and PET study. Neurology *66*, 1638–1643.

Pellerin, L., and Magistretti, P.J. (1994). Glutamate uptake into astrocytes stimulates aerobic glycolysis: a mechanism coupling neuronal activity to glucose utilization. Proc. Natl. Acad. Sci. U. S. A. *91*, 10625–10629.

Peng, Q., Wu, B., Jiang, M., Jin, J., Hou, Z., Zheng, J., Zhang, J., and Duan, W. (2016). Characterization of Behavioral, Neuropathological, Brain Metabolic and Key Molecular Changes in zQ175 Knock-In Mouse Model of Huntington's Disease. PloS One *11*, e0148839.

Persichetti, F., Carlee, L., Faber, P.W., McNeil, S.M., Ambrose, C.M., Srinidhi, J., Anderson, M., Barnes, G.T., Gusella, J.F., and MacDonald, M.E. (1996). Differential Expression of Normal and Mutant Huntington's Disease Gene Alleles. Neurobiol. Dis. *3*, 183–190.

Perutz, M.F., Johnson, T., Suzuki, M., and Finch, J.T. (1994). Glutamine repeats as polar zippers: their possible role in inherited neurodegenerative diseases. Proc. Natl. Acad. Sci. *91*, 5355–5358.

Petit-Turcotte, C., Aumont, N., Beffert, U., Dea, D., Herz, J., and Poirier, J. (2005). The apoE receptor apoER2 is involved in the maintenance of efficient synaptic plasticity. Neurobiol. Aging *26*, 195–206.

Petrov, A.M., Kudryashova, K.E., Odnoshivkina, Y.G., and Zefirov, A.L. (2011). Cholesterol and lipid rafts in the plasma membrane of nerve terminal and membrane of synaptic vesicles. Neurochem. J. *5*, 13–19.

Pfrieger, F.W., and Ungerer, N. (2011). Cholesterol metabolism in neurons and astrocytes. Prog. Lipid Res. *50*, 357–371.

Pitas, R.E., Boyles, J.K., Lee, S.H., Foss, D., and Mahley, R.W. (1987). Astrocytes synthesize apolipoprotein E and metabolize apolipoprotein E-containing lipoproteins. Biochim. Biophys. Acta BBA - Lipids Lipid Metab. *917*, 148–161.

Poirier, M.A., Jiang, H., and Ross, C.A. (2005). A structure-based analysis of huntingtin mutant polyglutamine aggregation and toxicity: evidence for a compact beta-sheet structure. Hum. Mol. Genet. *14*, 765–774.

Ponce, J., de la Ossa, N.P., Hurtado, O., Millan, M., Arenillas, J.F., Dávalos, A., and Gasull, T. (2008). Simvastatin reduces the association of NMDA receptors to lipid rafts: a cholesterol-mediated effect in neuroprotection. Stroke *39*, 1269–1275.

Pouladi, M.A., Morton, A.J., and Hayden, M.R. (2013). Choosing an animal model for the study of Huntington's disease. Nat. Rev. Neurosci. *14*, 708–721.

Rahbek-Clemmensen, T., Lycas, M.D., Erlendsson, S., Eriksen, J., Apuschkin, M., Vilhardt, F., Jørgensen, T.N., Hansen, F.H., and Gether, U. (2017). Super-resolution microscopy reveals functional organization of dopamine transporters into cholesterol and neuronal activity-dependent nanodomains. Nat. Commun. *8*, 740.

Rai, A., Pathak, D., Thakur, S., Singh, S., Dubey, A.K., and Mallik, R. (2016). Dynein Clusters into Lipid Microdomains on Phagosomes to Drive Rapid Transport toward Lysosomes. Cell *164*, 722–734.

Ramirez, C.M., Liu, B., Aqul, A., Taylor, A.M., Repa, J.J., Turley, S.D., and Dietschy, J.M. (2011). Quantitative role of LAL, NPC2, and NPC1 in lysosomal cholesterol processing defined by genetic and pharmacological manipulations. J. Lipid Res. *52*, 688–698.

Ramirez, D.M.O., Andersson, S., and Russell, D.W. (2008). Neuronal expression and subcellular localization of cholesterol 24-hydroxylase in the mouse brain. J. Comp. Neurol. *507*, 1676–1693.

Ratovitski, T., Chighladze, E., Arbez, N., Boronina, T., Herbrich, S., Cole, R.N., and Ross, C.A. (2012). Huntingtin protein interactions altered by polyglutamine expansion as determined by quantitative proteomic analysis. Cell Cycle Georget. Tex *11*, 2006–2021.

Ravikumar, B., Vacher, C., Berger, Z., Davies, J.E., Luo, S., Oroz, L.G., Scaravilli, F., Easton, D.F., Duden, R., O'Kane, C.J., et al. (2004). Inhibition of mTOR induces autophagy and reduces toxicity of polyglutamine expansions in fly and mouse models of Huntington disease. Nat. Genet. *36*, 585–595.

Reed, E.R., Latourelle, J.C., Bockholt, J.H., Bregu, J., Smock, J., Paulsen, J.S., Myers, R.H., and PREDICT-HD CSF ancillary study investigators (2018). MicroRNAs in CSF as prodromal biomarkers for Huntington disease in the PREDICT-HD study. Neurology *90*, e264–e272.

Reiner, A., Albin, R.L., Anderson, K.D., D'Amato, C.J., Penney, J.B., and Young, A.B. (1988). Differential loss of striatal projection neurons in Huntington disease. Proc. Natl. Acad. Sci. U. S. A. *85*, 5733–5737.

Richfield, E.K., Maguire-Zeiss, K.A., Vonkeman, H.E., and Voorn, P. (1995). Preferential loss of preproenkephalin versus preprotachykinin neurons from the striatum of Huntington's disease patients. Ann. Neurol. *38*, 852–861.

Rigamonti, D., Sipione, S., Goffredo, D., Zuccato, C., Fossale, E., and Cattaneo, E. (2001). Huntingtin's Neuroprotective Activity Occurs via Inhibition of Procaspase-9 Processing. J. Biol. Chem. *276*, 14545–14548.

Ritch, J.J., Valencia, A., Alexander, J., Sapp, E., Gatune, L., Sangrey, G.R., Sinha, S., Scherber, C.M., Zeitlin, S., Sadri-Vakili, G., et al. (2012). Multiple phenotypes in Huntington disease mouse neural stem cells. Mol. Cell. Neurosci. *50*, 70–81.

Rodwell, V.W., Nordstrom, J.L., and Mitschelen, J.J. (1976). Regulation of HMG-CoA Reductase. In Advances in Lipid Research, R. Paoletti, and D. Kritchevsky, eds. (Elsevier), pp. 1–74.

Romero, E., Cha, G.-H., Verstreken, P., Ly, C.V., Hughes, R.E., Bellen, H.J., and Botas, J. (2008). Suppression of neurodegeneration and increased neurotransmission caused by expanded full-length huntingtin accumulating in the cytoplasm. Neuron *57*, 27–40.

Ross, C.A., Aylward, E.H., Wild, E.J., Langbehn, D.R., Long, J.D., Warner, J.H., Scahill, R.I., Leavitt, B.R., Stout, J.C., Paulsen, J.S., et al. (2014). Huntington disease: natural history, biomarkers and prospects for therapeutics. Nat. Rev. Neurol. *10*, 204–216.

Rothe, T., Deliano, M., Wójtowicz, A.M., Dvorzhak, A., Harnack, D., Paul, S., Vagner, T., Melnick, I., Stark, H., and Grantyn, R. (2015). Pathological gamma oscillations, impaired dopamine release, synapse loss and reduced dynamic range of unitary glutamatergic synaptic transmission in the striatum of hypokinetic Q175 Huntington mice. Neuroscience *311*, 519–538.

Rothstein, J.D., Dykes-Hoberg, M., Pardo, C.A., Bristol, L.A., Jin, L., Kuncl, R.W., Kanai, Y., Hediger, M.A., Wang, Y., Schielke, J.P., et al. (1996). Knockout of Glutamate Transporters Reveals a Major Role for Astroglial Transport in Excitotoxicity and Clearance of Glutamate. Neuron *16*, 675–686.

Roze, E., Betuing, S., Deyts, C., Marcon, E., Brami-Cherrier, K., Pagès, C., Humbert, S., Mérienne, K., and Caboche, J. (2008). Mitogen- and stress-activated protein kinase-1 deficiency is involved in expanded-huntingtin-induced transcriptional dysregulation and striatal death. FASEB J. Off. Publ. Fed. Am. Soc. Exp. Biol. *22*, 1083–1093.

Rubenstein, J.L.R., Smith, B.A., and McConnell, H.M. (1979). Lateral Diffusion in Binary Mixtures of Cholesterol and Phosphatidylcholines. Proc. Natl. Acad. Sci. U. S. A. *76*, 15–18.

Rubinsztein, D.C., Leggo, J., Coles, R., Almqvist, E., Biancalana, V., Cassiman, J.J., Chotai, K., Connarty, M., Crauford, D., Curtis, A., et al. (1996). Phenotypic characterization of individuals with 30-40 CAG repeats in the Huntington disease (HD) gene reveals HD cases with 36 repeats and apparently normal elderly individuals with 36-39 repeats. Am. J. Hum. Genet. *59*, 16–22.

Rui, Y.-N., Xu, Z., Patel, B., Chen, Z., Chen, D., Tito, A., David, G., Sun, Y., Stimming, E.F., Bellen, H.J., et al. (2015). Huntingtin functions as a scaffold for selective macroautophagy. Nat. Cell Biol. *17*, 262–275.

Russell, D.W., Halford, R.W., Ramirez, D.M.O., Shah, R., and Kotti, T. (2009). Cholesterol 24-hydroxylase: an enzyme of cholesterol turnover in the brain. Annu. Rev. Biochem. *78*, 1017–1040.

Ryu, H., Lee, J., Hagerty, S.W., Soh, B.Y., McAlpin, S.E., Cormier, K.A., Smith, K.M., and Ferrante, R.J. (2006). ESET/SETDB1 gene expression and histone H3 (K9) trimethylation in Huntington's disease. Proc. Natl. Acad. Sci. U. S. A. *103*, 19176–19181.

Saher, G., and Stumpf, S.K. (2015). Cholesterol in myelin biogenesis and hypomyelinating disorders. Biochim. Biophys. Acta *1851*, 1083–1094.

Saher, G., Brügger, B., Lappe-Siefke, C., Möbius, W., Tozawa, R., Wehr, M.C., Wieland, F., Ishibashi, S., and Nave, K.-A. (2005). High cholesterol level is essential for myelin membrane growth. Nat. Neurosci. *8*, 468–475.

Sahlender, D.A., Roberts, R.C., Arden, S.D., Spudich, G., Taylor, M.J., Luzio, J.P., Kendrick-Jones, J., and Buss, F. (2005). Optineurin links myosin VI to the Golgi complex and is involved in Golgi organization and exocytosis. J. Cell Biol. *169*, 285–295.

Saijo, K., Crotti, A., and Glass, C.K. (2013). Regulation of microglia activation and deactivation by nuclear receptors. Glia *61*, 104–111.

Samara, A., Galbiati, M., Luciani, P., Deledda, C., Messi, E., Peri, A., and Maggi, R. (2014). Altered expression of 3-betahydroxysterol delta-24-reductase/selective Alzheimer's disease indicator-1 gene in Huntington's disease models. J. Endocrinol. Invest. *37*, 729–737.

Sankaram, M.B., and Thompson, T.E. (1990). Modulation of phospholipid acyl chain order by cholesterol. A solid-state 2H nuclear magnetic resonance study. Biochemistry *29*, 10676–10684.

Sarkar, S., Carroll, B., Buganim, Y., Maetzel, D., Ng, A.H.M., Cassady, J.P., Cohen, M.A., Chakraborty, S., Wang, H., Spooner, E., et al. (2013). Impaired autophagy in the lipid-storage disorder Niemann-Pick type C1 disease. Cell Rep. *5*, 1302–1315.

Saudou, F., and Humbert, S. (2016). The Biology of Huntingtin. Neuron *89*, 910–926.

Saudou, F., Finkbeiner, S., Devys, D., and Greenberg, M.E. (1998). Huntingtin acts in the nucleus to induce apoptosis but death does not correlate with the formation of intranuclear inclusions. Cell *95*, 55–66.

Savage, J.C., Jay, T., Goduni, E., Quigley, C., Mariani, M.M., Malm, T., Ransohoff, R.M., Lamb, B.T., and Landreth, G.E. (2015). Nuclear Receptors License Phagocytosis by Trem2+ Myeloid Cells in Mouse Models of Alzheimer's Disease. J. Neurosci. *35*, 6532–6543.

Saxena, R., and Chattopadhyay, A. (2012). Membrane cholesterol stabilizes the human serotonin1A receptor. Biochim. Biophys. Acta BBA - Biomembr. *1818*, 2936–2942.

Scarpulla, R.C. (2008). Transcriptional Paradigms in Mammalian Mitochondrial Biogenesis and Function. Physiol. Rev. *88*, 611–638.

Schaefer, M.H., Fontaine, J.-F., Vinayagam, A., Porras, P., Wanker, E.E., and Andrade-Navarro, M.A. (2012). HIPPIE: Integrating Protein Interaction Networks with Experiment Based Quality Scores. PLOS ONE *7*, e31826.

Schaffar, G., Breuer, P., Boteva, R., Behrends, C., Tzvetkov, N., Strippel, N., Sakahira, H., Siegers, K., Hayer-Hartl, M., and Hartl, F.U. (2004). Cellular toxicity of polyglutamine expansion proteins: mechanism of transcription factor deactivation. Mol. Cell *15*, 95–105.

Schilling, G., Becher, M.W., Sharp, A.H., Jinnah, H.A., Duan, K., Kotzuk, J.A., Slunt, H.H., Ratovitski, T., Cooper, J.K., Jenkins, N.A., et al. (1999). Intranuclear inclusions and neuritic aggregates in transgenic mice expressing a mutant N-terminal fragment of huntingtin. Hum. Mol. Genet. *8*, 397–407.

Schipper-Krom, S., Juenemann, K., Jansen, A.H., Wiemhoefer, A., van den Nieuwendijk, R., Smith, D.L., Hink, M.A., Bates, G.P., Overkleeft, H., Ovaa, H., et al. (2014). Dynamic recruitment of active proteasomes into polyglutamine initiated inclusion bodies. FEBS Lett. *588*, 151–159.

Schönknecht, P., Lütjohann, D., Pantel, J., Bardenheuer, H., Hartmann, T., von Bergmann, K., Beyreuther, K., and Schröder, J. (2002). Cerebrospinal fluid 24S-hydroxycholesterol is increased in patients with Alzheimer's disease compared to healthy controls. Neurosci. Lett. *324*, 83–85.

Schulz, J.G., Bösel, J., Stoeckel, M., Megow, D., Dirnagl, U., and Endres, M. (2004). HMG-CoA reductase inhibition causes neurite loss by interfering with geranylgeranylpyrophosphate synthesis. J. Neurochem. *89*, 24–32.

Schumacher, M., Guennoun, R., Robert, F., Carelli, C., Gago, N., Ghoumari, A., Gonzalez Deniselle, M.C., Gonzalez, S.L., Ibanez, C., Labombarda, F., et al. (2004). Local synthesis and dual actions of

progesterone in the nervous system: neuroprotection and myelination. Growth Horm. IGF Res. Off. J. Growth Horm. Res. Soc. Int. IGF Res. Soc. *14 Suppl A*, S18-33.

Secor McVoy, J.R., Oughli, H.A., and Oh, U. (2015). Liver X receptor-dependent inhibition of microglial nitric oxide synthase 2. J. Neuroinflammation *12*, 27.

Senut, M.C., Suhr, S.T., Kaspar, B., and Gage, F.H. (2000). Intraneuronal aggregate formation and cell death after viral expression of expanded polyglutamine tracts in the adult rat brain. J. Neurosci. Off. J. Soc. Neurosci. *20*, 219–229.

Seo, H., Sonntag, K.-C., and Isacson, O. (2004). Generalized brain and skin proteasome inhibition in Huntington's disease. Ann. Neurol. *56*, 319–328.

Seong, I.S., Woda, J.M., Song, J.-J., Lloret, A., Abeyrathne, P.D., Woo, C.J., Gregory, G., Lee, J.-M., Wheeler, V.C., Walz, T., et al. (2010). Huntingtin facilitates polycomb repressive complex 2. Hum. Mol. Genet. *19*, 573–583.

Shafaati, M., O'Driscoll, R., Björkhem, I., and Meaney, S. (2009). Transcriptional regulation of cholesterol 24-hydroxylase by histone deacetylase inhibitors. Biochem. Biophys. Res. Commun. *378*, 689–694.

Shafaati, M., Mast, N., Beck, O., Nayef, R., Heo, G.Y., Björkhem-Bergman, L., Lütjohann, D., Björkhem, I., and Pikuleva, I.A. (2010). The antifungal drug voriconazole is an efficient inhibitor of brain cholesterol 24S-hydroxylase in vitro and in vivo. J. Lipid Res. *51*, 318–323.

Shafaati, M., Olin, M., Båvner, A., Pettersson, H., Rozell, B., Meaney, S., Parini, P., and Björkhem, I. (2011). Enhanced production of 24S-hydroxycholesterol is not sufficient to drive liver X receptor target genes in vivo. J. Intern. Med. *270*, 377–387.

Shankaran, M., Di Paolo, E., Leoni, V., Caccia, C., Ferrari Bardile, C., Mohammed, H., Di Donato, S., Kwak, S., Marchionini, D., Turner, S., et al. (2017). Early and brain region-specific decrease of de novo cholesterol biosynthesis in Huntington's disease: A cross-validation study in Q175 knock-in mice. Neurobiol. Dis. *98*, 66–76.

Sharp, A.H., Loev, S.J., Schilling, G., Li, S.-H., Li, X.-J., Bao, J., Wagster, M.V., Kotzuk, J.A., Steiner, J.P., Lo, A., et al. (1995). Widespread expression of Huntington's disease gene (IT15) protein product. Neuron *14*, 1065–1074.

Shibuya, K., Watanabe, T., Urano, Y., Takabe, W., Noguchi, N., and Kitagishi, H. (2016). Synthesis of 24(S)-hydroxycholesterol esters responsible for the induction of neuronal cell death. Bioorg. Med. Chem. *24*, 2559–2566.

Shimohata, T., Nakajima, T., Yamada, M., Uchida, C., Onodera, O., Naruse, S., Kimura, T., Koide, R., Nozaki, K., Sano, Y., et al. (2000). Expanded polyglutamine stretches interact with TAFII130, interfering with CREB-dependent transcription. Nat. Genet. *26*, 29–36.

Shin, J.-Y., Fang, Z.-H., Yu, Z.-X., Wang, C.-E., Li, S.-H., and Li, X.-J. (2005). Expression of mutant huntingtin in glial cells contributes to neuronal excitotoxicity. J. Cell Biol. *171*, 1001–1012.

Shirendeb, U., Reddy, A.P., Manczak, M., Calkins, M.J., Mao, P., Tagle, D.A., and Hemachandra Reddy, P. (2011). Abnormal mitochondrial dynamics, mitochondrial loss and mutant huntingtin oligomers in Huntington's disease: implications for selective neuronal damage. Hum. Mol. Genet. *20*, 1438–1455.

Shirendeb, U.P., Calkins, M.J., Manczak, M., Anekonda, V., Dufour, B., McBride, J.L., Mao, P., and Reddy, P.H. (2012). Mutant huntingtin's interaction with mitochondrial protein Drp1 impairs mitochondrial biogenesis and causes defective axonal transport and synaptic degeneration in Huntington's disease. Hum. Mol. Genet. *21*, 406–420.

Simons, K., and Ikonen, E. (2000). How Cells Handle Cholesterol. Science *290*, 1721–1726.

Simons, M., Krämer, E.-M., Thiele, C., Stoffel, W., and Trotter, J. (2000). Assembly of Myelin by Association of Proteolipid Protein with Cholesterol- and Galactosylceramide-Rich Membrane Domains. J Cell Biol *151*, 143–154.

Singhrao, S.K., Neal, J.W., Morgan, B.P., and Gasque, P. (1999). Increased complement biosynthesis by microglia and complement activation on neurons in Huntington's disease. Exp. Neurol. *159*, 362–376.

Sipione, S., Rigamonti, D., Valenza, M., Zuccato, C., Conti, L., Pritchard, J., Kooperberg, C., Olson, J.M., and Cattaneo, E. (2002). Early transcriptional profiles in huntingtin-inducible striatal cells by microarray analyses. Hum. Mol. Genet. *11*, 1953–1965.

Skene, D.J., Middleton, B., Fraser, C.K., Pennings, J.L.A., Kuchel, T.R., Rudiger, S.R., Bawden, C.S., and Morton, A.J. (2017). Metabolic profiling of presymptomatic Huntington's disease sheep reveals novel biomarkers. Sci. Rep. *7*, 43030.

Slow, E.J., van Raamsdonk, J., Rogers, D., Coleman, S.H., Graham, R.K., Deng, Y., Oh, R., Bissada, N., Hossain, S.M., Yang, Y.-Z., et al. (2003). Selective striatal neuronal loss in a YAC128 mouse model of Huntington disease. Hum. Mol. Genet. *12*, 1555–1567.

Slow, E.J., Graham, R.K., Osmand, A.P., Devon, R.S., Lu, G., Deng, Y., Pearson, J., Vaid, K., Bissada, N., Wetzel, R., et al. (2005). Absence of behavioral abnormalities and neurodegeneration in vivo despite widespread neuronal huntingtin inclusions. Proc. Natl. Acad. Sci. U. S. A. *102*, 11402–11407.

Smiljanic, K., Lavrnja, I., Mladenovic Djordjevic, A., Ruzdijic, S., Stojiljkovic, M., Pekovic, S., and Kanazir, S. (2010). Brain injury induces cholesterol 24-hydroxylase (Cyp46) expression in glial cells in a time-dependent manner. Histochem. Cell Biol. *134*, 159–169.

Smiljanic, K., Vanmierlo, T., Djordjevic, A.M., Perovic, M., Loncarevic-Vasiljkovic, N., Tesic, V., Rakic, L., Ruzdijic, S., Lutjohann, D., and Kanazir, S. (2013). Aging induces tissue-specific changes in cholesterol metabolism in rat brain and liver. Lipids *48*, 1069–1077.

Smith, G.A., Rocha, E.M., McLean, J.R., Hayes, M.A., Izen, S.C., Isacson, O., and Hallett, P.J. (2014). Progressive axonal transport and synaptic protein changes correlate with behavioral and neuropathological abnormalities in the heterozygous Q175 KI mouse model of Huntington's disease. Hum. Mol. Genet. *23*, 4510–4527.

Smith, L.L., Ray, D.R., Moody, J.A., Wells, J.D., and Van Lier, J.E. (1972). 24-hydroxycholesterol levels in human brain. J. Neurochem. *19*, 899–904.

Smith, Y., Bevan, M.D., Shink, E., and Bolam, J.P. (1998). Microcircuitry of the direct and indirect pathways of the basal ganglia. Neuroscience *86*, 353–387.

Sobo, K., Blanc, I.L., Luyet, P.-P., Fivaz, M., Ferguson, C., Parton, R.G., Gruenberg, J., and Goot, F.G. van der (2007). Late Endosomal Cholesterol Accumulation Leads to Impaired Intra-Endosomal Trafficking. PLOS ONE *2*, e851.

Söderberg, M., Edlund, C., Kristensson, K., and Dallner, G. (1990). Lipid compositions of different regions of the human brain during aging. J. Neurochem. *54*, 415–423.

Sodero, A.O., Trovò, L., Iannilli, F., Van Veldhoven, P., Dotti, C.G., and Martin, M.G. (2011a). Regulation of tyrosine kinase B activity by the Cyp46/cholesterol loss pathway in mature hippocampal neurons: relevance for neuronal survival under stress and in aging. J. Neurochem. *116*, 747–755.

Sodero, A.O., Weissmann, C., Ledesma, M.D., and Dotti, C.G. (2011b). Cellular stress from excitatory neurotransmission contributes to cholesterol loss in hippocampal neurons aging in vitro. Neurobiol. Aging *32*, 1043–1053.

Sodero, A.O., Vriens, J., Ghosh, D., Stegner, D., Brachet, A., Pallotto, M., Sassoè-Pognetto, M., Brouwers, J.F., Helms, J.B., Nieswandt, B., et al. (2012). Cholesterol loss during glutamate-mediated excitotoxicity. EMBO J. *31*, 1764–1773.

Song, W., Chen, J., Petrilli, A., Liot, G., Klinglmayr, E., Zhou, Y., Poquiz, P., Tjong, J., Pouladi, M.A., Hayden, M.R., et al. (2011). Mutant huntingtin binds the mitochondrial fission GTPase dynamin-related protein-1 and increases its enzymatic activity. Nat. Med. *17*, 377–382.

Sooksawate, T., and Simmonds, M.A. (2001). Effects of membrane cholesterol on the sensitivity of the GABAA receptor to GABA in acutely dissociated rat hippocampal neurones. Neuropharmacology *40*, 178–184.

Sorbi, S., Bird, E.D., and Blass, J.P. (1983). Decreased pyruvate dehydrogenase complex activity in Huntington and Alzheimer brain. Ann. Neurol. *13*, 72–78.

Sotrel, A., Paskevich, P.A., Kiely, D.K., Bird, E.D., Williams, R.S., and Myers, R.H. (1991). Morphometric analysis of the prefrontal cortex in Huntington's disease. Neurology *41*, 1117–1123.

Southwell, A.L., Smith-Dijak, A., Kay, C., Sepers, M., Villanueva, E.B., Parsons, M.P., Xie, Y., Anderson, L., Felczak, B., Waltl, S., et al. (2016). An enhanced Q175 knock-in mouse model of Huntington disease with higher mutant huntingtin levels and accelerated disease phenotypes. Hum. Mol. Genet.

Spann, N.J., and Glass, C.K. (2013). Sterols and oxysterols in immune cell function. Nat. Immunol. *14*, 893–900.

Spann, N.J., Garmire, L.X., McDonald, J.G., Myers, D.S., Milne, S.B., Shibata, N., Reichart, D., Fox, J.N., Shaked, I., Heudobler, D., et al. (2012). Regulated accumulation of desmosterol integrates macrophage lipid metabolism and inflammatory responses. Cell *151*, 138–152.

Srinivasan, K., Friedman, B.A., Larson, J.L., Lauffer, B.E., Goldstein, L.D., Appling, L.L., Borneo, J., Poon, C., Ho, T., Cai, F., et al. (2016). Untangling the brain's neuroinflammatory and neurodegenerative transcriptional responses. Nat. Commun. *7*, 11295.

Stary, C.M., Tsutsumi, Y.M., Patel, P.M., Head, B.P., Patel, H.H., and Roth, D.M. (2012). Caveolins: targeting pro-survival signaling in the heart and brain. Front. Physiol. *3*, 393.

Steffan, J.S., Kazantsev, A., Spasic-Boskovic, O., Greenwald, M., Zhu, Y.Z., Gohler, H., Wanker, E.E., Bates, G.P., Housman, D.E., and Thompson, L.M. (2000a). The Huntington's disease protein interacts with p53 and CREB-binding protein and represses transcription. Proc. Natl. Acad. Sci. U. S. A. *97*, 6763–6768.

Steffan, J.S., Kazantsev, A., Spasic-Boskovic, O., Greenwald, M., Zhu, Y.Z., Gohler, H., Wanker, E.E., Bates, G.P., Housman, D.E., and Thompson, L.M. (2000b). The Huntington's disease protein interacts with p53 and CREB-binding protein and represses transcription. Proc. Natl. Acad. Sci. U. S. A. *97*, 6763–6768.

Steffan, J.S., Bodai, L., Pallos, J., Poelman, M., McCampbell, A., Apostol, B.L., Kazantsev, A., Schmidt, E., Zhu, Y.Z., Greenwald, M., et al. (2001). Histone deacetylase inhibitors arrest polyglutamine-dependent neurodegeneration in Drosophila. Nature *413*, 739–743.

Strand, A.D., Baquet, Z.C., Aragaki, A.K., Holmans, P., Yang, L., Cleren, C., Beal, M.F., Jones, L., Kooperberg, C., Olson, J.M., et al. (2007). Expression profiling of Huntington's disease models suggests that brain-derived neurotrophic factor depletion plays a major role in striatal degeneration. J. Neurosci. Off. J. Soc. Neurosci. *27*, 11758–11768.

Stratton, B.S., Warner, J.M., Wu, Z., Nikolaus, J., Wei, G., Wagnon, E., Baddeley, D., Karatekin, E., and O'Shaughnessy, B. (2016). Cholesterol Increases the Openness of SNARE-Mediated Flickering Fusion Pores. Biophys. J. *110*, 1538–1550.

Subramaniam, S., Sixt, K.M., Barrow, R., and Snyder, S.H. (2009). Rhes, a striatal specific protein, mediates mutant-huntingtin cytotoxicity. Science *324*, 1327–1330.

Subtil, A., Gaidarov, I., Kobylarz, K., Lampson, M.A., Keen, J.H., and McGraw, T.E. (1999). Acute cholesterol depletion inhibits clathrin-coated pit budding. Proc. Natl. Acad. Sci. *96*, 6775–6780.

Suhr, S.T., Senut, M.C., Whitelegge, J.P., Faull, K.F., Cuizon, D.B., and Gage, F.H. (2001). Identities of sequestered proteins in aggregates from cells with induced polyglutamine expression. J. Cell Biol. *153*, 283–294.

Suzuki, S., Numakawa, T., Shimazu, K., Koshimizu, H., Hara, T., Hatanaka, H., Mei, L., Lu, B., and Kojima, M. (2004). BDNF-induced recruitment of TrkB receptor into neuronal lipid rafts. J. Cell Biol. *167*, 1205–1215.

Suzuki, T., Zhang, J., Miyazawa, S., Liu, Q., Farzan, M.R., and Yao, W.-D. (2011). Association of membrane rafts and postsynaptic density: proteomics, biochemical, and ultrastructural analyses. J. Neurochem. *119*, 64–77.

Svennerholm, L., Boström, K., Helander, C.G., and Jungbjer, B. (1991). Membrane lipids in the aging human brain. J. Neurochem. *56*, 2051–2059.

Svennerholm, L., Boström, K., and Jungbjer, B. (1997). Changes in weight and compositions of major membrane components of human brain during the span of adult human life of Swedes. Acta Neuropathol. (Berl.) *94*, 345–352.

Tai, Y.F., Pavese, N., Gerhard, A., Tabrizi, S.J., Barker, R.A., Brooks, D.J., and Piccini, P. (2007). Microglial activation in presymptomatic Huntington's disease gene carriers. Brain J. Neurol. *130*, 1759–1766.

Takabe, W., Urano, Y., Vo, D.-K.H., Shibuya, K., Tanno, M., Kitagishi, H., Fujimoto, T., and Noguchi, N. (2016). Esterification of 24S-OHC induces formation of atypical lipid droplet-like structures, leading to neuronal cell death. J. Lipid Res. *57*, 2005–2014.

Takamori, S., Holt, M., Stenius, K., Lemke, E.A., Grønborg, M., Riedel, D., Urlaub, H., Schenck, S., Brügger, B., Ringler, P., et al. (2006). Molecular Anatomy of a Trafficking Organelle. Cell *127*, 831–846.

Takano, H., and Gusella, J.F. (2002). The predominantly HEAT-like motif structure of huntingtin and its association and coincident nuclear entry with dorsal, an NF-kB/Rel/dorsal family transcription factor. BMC Neurosci. *3*, 15.

Tedde, A., Rotondi, M., Cellini, E., Bagnoli, S., Muratore, L., Nacmias, B., and Sorbi, S. (2006). Lack of association between the CYP46 gene polymorphism and Italian late-onset sporadic Alzheimer's disease. Neurobiol. Aging *27*, 773.e1-773.e3.

Telenius, H., Kremer, H.P., Theilmann, J., Andrew, S.E., Almqvist, E., Anvret, M., Greenberg, C., Greenberg, J., Lucotte, G., and Squitieri, F. (1993). Molecular analysis of juvenile Huntington disease: the major influence on (CAG)n repeat length is the sex of the affected parent. Hum. Mol. Genet. *2*, 1535–1540.

Teo, R.T.Y., Hong, X., Yu-Taeger, L., Huang, Y., Tan, L.J., Xie, Y., To, X.V., Guo, L., Rajendran, R., Novati, A., et al. (2016). Structural and molecular myelination deficits occur prior to neuronal loss in the YAC128 and BACHD models of Huntington disease. Hum. Mol. Genet. *25*, 2621–2632.

Testa, G., Staurenghi, E., Zerbinati, C., Gargiulo, S., Iuliano, L., Giaccone, G., Fantò, F., Poli, G., Leonarduzzi, G., and Gamba, P. (2016). Changes in brain oxysterols at different stages of Alzheimer's disease: Their involvement in neuroinflammation. Redox Biol. *10*, 24–33.

Teunissen, C.E., Dijkstra, C.D., Polman, C.H., Hoogervorst, E.L.J., von Bergmann, K., and Lütjohann, D. (2003). Decreased levels of the brain specific 24S-hydroxycholesterol and cholesterol precursors in serum of multiple sclerosis patients. Neurosci. Lett. *347*, 159–162.

Thal, D.R. (2012). The role of astrocytes in amyloid β-protein toxicity and clearance. Exp. Neurol. *236*, 1–5.

Thelen, K.M., Falkai, P., Bayer, T.A., and Lütjohann, D. (2006). Cholesterol synthesis rate in human hippocampus declines with aging. Neurosci. Lett. *403*, 15–19.

Thiele, C., Hannah, M.J., Fahrenholz, F., and Huttner, W.B. (2000). Cholesterol binds to synaptophysin and is required for biogenesis of synaptic vesicles. Nat. Cell Biol. *2*, 42–49.

Thompson, L.M., Aiken, C.T., Kaltenbach, L.S., Agrawal, N., Illes, K., Khoshnan, A., Martinez-Vincente, M., Arrasate, M., O'Rourke, J.G., Khashwji, H., et al. (2009). IKK phosphorylates Huntingtin and targets it for degradation by the proteasome and lysosome. J. Cell Biol. *187*, 1083–1099.

Tian, G., Kong, Q., Lai, L., Ray-Chaudhury, A., and Lin, C.G. (2010). Increased expression of cholesterol 24S-hydroxylase results in disruption of glial glutamate transporter EAAT2 association with lipid rafts: a potential role in Alzheimer's disease. J. Neurochem. *113*, 978–989.

de Tommaso, M., Nuzzi, A., Dellomonaco, A.R., Sciruicchio, V., Serpino, C., Cormio, C., Franco, G., and Megna, M. (2015). Dysphagia in Huntington's Disease: Correlation with Clinical Features. Eur. Neurol. *74*, 49–53.

Tong, X., Ao, Y., Faas, G.C., Nwaobi, S.E., Xu, J., Haustein, M.D., Anderson, M.A., Mody, I., Olsen, M.L., Sofroniew, M.V., et al. (2014). Astrocyte Kir4.1 ion channel deficits contribute to neuronal dysfunction in Huntington's disease model mice. Nat. Neurosci. *17*, 694–703.

Tong, Y., Ha, T.J., Liu, L., Nishimoto, A., Reiner, A., and Goldowitz, D. (2011). Spatial and Temporal Requirements for huntingtin (Htt) in Neuronal Migration and Survival during Brain Development. J. Neurosci. *31*, 14794–14799.

del Toro, D., Alberch, J., Lázaro-Diéguez, F., Martín-Ibáñez, R., Xifró, X., Egea, G., and Canals, J.M. (2009). Mutant huntingtin impairs post-Golgi trafficking to lysosomes by delocalizing optineurin/Rab8 complex from the Golgi apparatus. Mol. Biol. Cell *20*, 1478–1492.

del Toro, D., Xifró, X., Pol, A., Humbert, S., Saudou, F., Canals, J.M., and Alberch, J. (2010). Altered cholesterol homeostasis contributes to enhanced excitotoxicity in Huntington's disease. J. Neurochem. *115*, 153–167.

Travessa, A.M., Rodrigues, F.B., Mestre, T.A., and Ferreira, J.J. (2017). Fifteen Years of Clinical Trials in Huntington's Disease: A Very Low Clinical Drug Development Success Rate. J. Huntingt. Dis. *6*, 157–163.

Trettel, F., Rigamonti, D., Hilditch-Maguire, P., Wheeler, V.C., Sharp, A.H., Persichetti, F., Cattaneo, E., and MacDonald, M.E. (2000). Dominant phenotypes produced by the HD mutation in STHdh(Q111) striatal cells. Hum. Mol. Genet. *9*, 2799–2809.

Trushina, E., Dyer, R.B., Badger, J.D., Ure, D., Eide, L., Tran, D.D., Vrieze, B.T., Legendre-Guillemin, V., McPherson, P.S., Mandavilli, B.S., et al. (2004). Mutant huntingtin impairs axonal trafficking in mammalian neurons in vivo and in vitro. Mol. Cell. Biol. *24*, 8195–8209.

Trushina, E., Singh, R.D., Dyer, R.B., Cao, S., Shah, V.H., Parton, R.G., Pagano, R.E., and McMurray, C.T. (2006). Mutant huntingtin inhibits clathrin-independent endocytosis and causes accumulation of cholesterol in vitro and in vivo. Hum. Mol. Genet. *15*, 3578–3591.

Trushina, E., Canaria, C.A., Lee, D.-Y., and McMurray, C.T. (2014). Loss of caveolin-1 expression in knock-in mouse model of Huntington's disease suppresses pathophysiology in vivo. Hum. Mol. Genet. *23*, 129–144.

Tsai, Y.C., Leichner, G.S., Pearce, M.M.P., Wilson, G.L., Wojcikiewicz, R.J.H., Roitelman, J., and Weissman, A.M. (2012). Differential regulation of HMG-CoA reductase and Insig-1 by enzymes of the ubiquitin-proteasome system. Mol. Biol. Cell *23*, 4484–4494.

Twelvetrees, A.E., Yuen, E.Y., Arancibia-Carcamo, I.L., MacAskill, A.F., Rostaing, P., Lumb, M.J., Humbert, S., Triller, A., Saudou, F., Yan, Z., et al. (2010). Delivery of GABAARs to Synapses Is Mediated by HAP1-KIF5 and Disrupted by Mutant Huntingtin. Neuron *65*, 53–65.

Tydlacka, S., Wang, C.-E., Wang, X., Li, S., and Li, X.-J. (2008). Differential activities of the ubiquitin-proteasome system in neurons versus glia may account for the preferential accumulation of misfolded proteins in neurons. J. Neurosci. Off. J. Soc. Neurosci. *28*, 13285–13295.

Ulven, S.M., Dalen, K.T., Gustafsson, J.-Å., and Nebb, H.I. (2005). LXR is crucial in lipid metabolism. Prostaglandins Leukot. Essent. Fatty Acids *73*, 59–63.

Upadhyay, A., Amanullah, A., Mishra, R., Kumar, A., and Mishra, A. (2018). Lanosterol Suppresses the Aggregation and Cytotoxicity of Misfolded Proteins Linked with Neurodegenerative Diseases. Mol. Neurobiol. *55*, 1169–1182.

Urano, Y., Ochiai, S., and Noguchi, N. (2013). Suppression of amyloid-β production by 24S-hydroxycholesterol via inhibition of intracellular amyloid precursor protein trafficking. FASEB J. *27*, 4305–4315.

Uto, Y. (2015). Imidazo[1,2-a]pyridines as cholesterol 24-hydroxylase (CYP46A1) inhibitors: a patent evaluation (WO2014061676). Expert Opin. Ther. Pat. *25*, 373–377.

Valencia, A., Reeves, P.B., Sapp, E., Li, X., Alexander, J., Kegel, K.B., Chase, K., Aronin, N., and DiFiglia, M. (2010). Mutant huntingtin and glycogen synthase kinase 3-beta accumulate in neuronal lipid rafts of a presymptomatic knock-in mouse model of Huntington's disease. J. Neurosci. Res. *88*, 179–190.

Valenza, M., and Cattaneo, E. (2006). Cholesterol dysfunction in neurodegenerative diseases: is Huntington's disease in the list? Prog. Neurobiol. *80*, 165–176.

Valenza, M., and Cattaneo, E. (2011). Emerging roles for cholesterol in Huntington's disease. Trends Neurosci. *34*, 474–486.

Valenza, M., Rigamonti, D., Goffredo, D., Zuccato, C., Fenu, S., Jamot, L., Strand, A., Tarditi, A., Woodman, B., Racchi, M., et al. (2005). Dysfunction of the cholesterol biosynthetic pathway in Huntington's disease. J. Neurosci. Off. J. Soc. Neurosci. *25*, 9932–9939.

Valenza, M., Leoni, V., Tarditi, A., Mariotti, C., Björkhem, I., Di Donato, S., and Cattaneo, E. (2007a). Progressive dysfunction of the cholesterol biosynthesis pathway in the R6/2 mouse model of Huntington's disease. Neurobiol. Dis. *28*, 133–142.

Valenza, M., Carroll, J.B., Leoni, V., Bertram, L.N., Björkhem, I., Singaraja, R.R., Di Donato, S., Lutjohann, D., Hayden, M.R., and Cattaneo, E. (2007b). Cholesterol biosynthesis pathway is disturbed in YAC128 mice and is modulated by huntingtin mutation. Hum. Mol. Genet. *16*, 2187–2198.

Valenza, M., Leoni, V., Karasinska, J.M., Petricca, L., Fan, J., Carroll, J., Pouladi, M.A., Fossale, E., Nguyen, H.P., Riess, O., et al. (2010). Cholesterol defect is marked across multiple rodent models of Huntington's disease and is manifest in astrocytes. J. Neurosci. Off. J. Soc. Neurosci. *30*, 10844–10850.

Valenza, M., Marullo, M., Di Paolo, E., Cesana, E., Zuccato, C., Biella, G., and Cattaneo, E. (2015a). Disruption of astrocyte-neuron cholesterol cross talk affects neuronal function in Huntington's disease. Cell Death Differ. *22*, 690–702.

Valenza, M., Chen, J.Y., Di Paolo, E., Ruozi, B., Belletti, D., Ferrari Bardile, C., Leoni, V., Caccia, C., Brilli, E., Di Donato, S., et al. (2015b). Cholesterol-loaded nanoparticles ameliorate synaptic and cognitive function in Huntington's disease mice. EMBO Mol. Med. *7*, 1547–1564.

Vance, J.E., and Hayashi, H. (2010). Formation and function of apolipoprotein E-containing lipoproteins in the nervous system. Biochim. Biophys. Acta BBA - Mol. Cell Biol. Lipids *1801*, 806–818.

Ventura, I., Russo, M.T., De Nuccio, C., De Luca, G., Degan, P., Bernardo, A., Visentin, S., Minghetti, L., and Bignami, M. (2013). hMTH1 expression protects mitochondria from Huntington's disease-like impairment. Neurobiol. Dis. *49*, 148–158.

Videnovic, A., Leurgans, S., Fan, W., Jaglin, J., and Shannon, K.M. (2009). Daytime somnolence and nocturnal sleep disturbances in Huntington disease. Parkinsonism Relat. Disord. *15*, 471–474.

Vitali, C., Wellington, C.L., and Calabresi, L. (2014). HDL and cholesterol handling in the brain. Cardiovasc. Res. *103*, 405–413.

Vonsattel, J.P., and DiFiglia, M. (1998). Huntington disease. J. Neuropathol. Exp. Neurol. *57*, 369–384.

Vonsattel, J.P., Myers, R.H., Stevens, T.J., Ferrante, R.J., Bird, E.D., and Richardson, E.P. (1985). Neuropathological classification of Huntington's disease. J. Neuropathol. Exp. Neurol. *44*, 559–577.

Waelter, S., Scherzinger, E., Hasenbank, R., Nordhoff, E., Lurz, R., Goehler, H., Gauss, C., Sathasivam, K., Bates, G.P., Lehrach, H., et al. (2001). The huntingtin interacting protein HIP1 is a clathrin and α-adaptin-binding protein involved in receptor-mediated endocytosis. Hum. Mol. Genet. *10*, 1807–1817.

Wahrle, S.E., Jiang, H., Parsadanian, M., Legleiter, J., Han, X., Fryer, J.D., Kowalewski, T., and Holtzman, D.M. (2004). ABCA1 Is Required for Normal Central Nervous System ApoE Levels and for Lipidation of Astrocyte-secreted apoE. J. Biol. Chem. *279*, 40987–40993.

Waldvogel, H.J., Kim, E.H., Tippett, L.J., Vonsattel, J.-P.G., and Faull, R.L.M. (2015). The Neuropathology of Huntington's Disease. Curr. Top. Behav. Neurosci. *22*, 33–80.

Wang, B., and Tontonoz, P. (2018). Liver X receptors in lipid signalling and membrane homeostasis. Nat. Rev. Endocrinol.

Wang, J., Wang, C.-E., Orr, A., Tydlacka, S., Li, S.-H., and Li, X.-J. (2008a). Impaired ubiquitin-proteasome system activity in the synapses of Huntington's disease mice. J. Cell Biol. *180*, 1177–1189.

Wang, J.-Q., Chen, Q., Wang, X., Wang, Q.-C., Wang, Y., Cheng, H.-P., Guo, C., Sun, Q., Chen, Q., and Tang, T.-S. (2013). Dysregulation of Mitochondrial Calcium Signaling and Superoxide Flashes Cause Mitochondrial Genomic DNA Damage in Huntington Disease. J. Biol. Chem. *288*, 3070–3084.

Wang, W., Yang, L., and Huang, H.W. (2007). Evidence of Cholesterol Accumulated in High Curvature Regions: Implication to the Curvature Elastic Energy for Lipid Mixtures. Biophys. J. *92*, 2819–2830.

Wang, Y., Rogers, P.M., Su, C., Varga, G., Stayrook, K.R., and Burris, T.P. (2008b). Regulation of Cholesterologenesis by the Oxysterol Receptor, LXRα. J. Biol. Chem. *283*, 26332–26339.

Warby, S.C., Visscher, H., Collins, J.A., Doty, C.N., Carter, C., Butland, S.L., Hayden, A.R., Kanazawa, I., Ross, C.J., and Hayden, M.R. (2011). *HTT* haplotypes contribute to differences in Huntington disease prevalence between Europe and East Asia. Eur. J. Hum. Genet. *19*, 561–566.

Wasser, C.R., Ertunc, M., Liu, X., and Kavalali, E.T. (2007). Cholesterol-dependent balance between evoked and spontaneous synaptic vesicle recycling. J. Physiol. *579*, 413–429.

Weiss, A., Klein, C., Woodman, B., Sathasivam, K., Bibel, M., Régulier, E., Bates, G.P., and Paganetti, P. (2008). Sensitive biochemical aggregate detection reveals aggregation onset before symptom development in cellular and murine models of Huntington's disease. J. Neurochem. *104*, 846–858.

Weiss, A., Träger, U., Wild, E.J., Grueninger, S., Farmer, R., Landles, C., Scahill, R.I., Lahiri, N., Haider, S., Macdonald, D., et al. (2012). Mutant huntingtin fragmentation in immune cells tracks Huntington's disease progression. J. Clin. Invest. *122*, 3731–3736.

Werner, H.B., Krämer-Albers, E.-M., Strenzke, N., Saher, G., Tenzer, S., Ohno-Iwashita, Y., Monasterio-Schrader, P.D., Möbius, W., Moser, T., Griffiths, I.R., et al. (2013). A critical role for the cholesterol-associated proteolipids PLP and M6B in myelination of the central nervous system. Glia *61*, 567–586.

Wheeler, V.C., Gutekunst, C.-A., Vrbanac, V., Lebel, L.-A., Schilling, G., Hersch, S., Friedlander, R.M., Gusella, J.F., Vonsattel, J.-P., Borchelt, D.R., et al. (2002). Early phenotypes that presage late-onset neurodegenerative disease allow testing of modifiers in Hdh CAG knock-in mice. Hum. Mol. Genet. *11*, 633–640.

White, J.K., Auerbach, W., Duyao, M.P., Vonsattel, J.-P., Gusella, J.F., Joyner, A.L., and MacDonald, M.E. (1997). Huntingtin is required for neurogenesis and is not impaired by the Huntington's disease CAG expansion. Nat. Genet. *17*, 404–410.

White, M.A., Mast, N., Bjorkhem, I., Johnson, E.F., Stout, C.D., and Pikuleva, I.A. (2008). Use of complementary cation and anion heavy-atom salt derivatives to solve the structure of cytochrome P450 46A1. Acta Crystallogr. D Biol. Crystallogr. *64*, 487–495.

Wong, Y.C., and Holzbaur, E.L.F. (2014). The regulation of autophagosome dynamics by huntingtin and HAP1 is disrupted by expression of mutant huntingtin, leading to defective cargo degradation. J. Neurosci. Off. J. Soc. Neurosci. *34*, 1293–1305.

van der Wulp, M.Y.M., Verkade, H.J., and Groen, A.K. (2013). Regulation of cholesterol homeostasis. Mol. Cell. Endocrinol. *368*, 1–16.

Xiang, Z., Valenza, M., Cui, L., Leoni, V., Jeong, H.-K., Brilli, E., Zhang, J., Peng, Q., Duan, W., Reeves, S.A., et al. (2011). Peroxisome-proliferator-activated receptor gamma coactivator 1 α contributes to dysmyelination in experimental models of Huntington's disease. J. Neurosci. Off. J. Soc. Neurosci. *31*, 9544–9553.

Xie, C., Lund, E.G., Turley, S.D., Russell, D.W., and Dietschy, J.M. (2003). Quantitation of two pathways for cholesterol excretion from the brain in normal mice and mice with neurodegeneration. J. Lipid Res. *44*, 1780–1789.

Xu, P., Xu, H., Tang, X., Xu, L., Wang, Y., Guo, L., Yang, Z., Xing, Y., Wu, Y., Warner, M., et al. (2014). Liver X receptor β is essential for the differentiation of radial glial cells to oligodendrocytes in the dorsal cortex. Mol. Psychiatry *19*, 947–957.

Yamanaka, K., Saito, Y., Yamamori, T., Urano, Y., and Noguchi, N. (2011). 24(S)-hydroxycholesterol induces neuronal cell death through necroptosis, a form of programmed necrosis. J. Biol. Chem. *286*, 24666–24673.

Yamanaka, K., Urano, Y., Takabe, W., Saito, Y., and Noguchi, N. (2014). Induction of apoptosis and necroptosis by 24(S)-hydroxycholesterol is dependent on activity of acyl-CoA:cholesterol acyltransferase 1. Cell Death Dis. *5*, e990.

Yan, S., Tu, Z., Liu, Z., Fan, N., Yang, H., Yang, S., Yang, W., Zhao, Y., Ouyang, Z., Lai, C., et al. (2018). A Huntingtin Knockin Pig Model Recapitulates Features of Selective Neurodegeneration in Huntington's Disease. Cell *173*, 989-1002.e13.

Yang, C., McDonald, J.G., Patel, A., Zhang, Y., Umetani, M., Xu, F., Westover, E.J., Covey, D.F., Mangelsdorf, D.J., Cohen, J.C., et al. (2006). Sterol intermediates from cholesterol biosynthetic pathway as liver X receptor ligands. J. Biol. Chem. *281*, 27816–27826.

Yang, H.-M., Yang, S., Huang, S.-S., Tang, B.-S., and Guo, J.-F. (2017). Microglial Activation in the Pathogenesis of Huntington's Disease. Front. Aging Neurosci. *9*.

Yang, S.-H., Cheng, P.-H., Banta, H., Piotrowska-Nitsche, K., Yang, J.-J., Cheng, E.C.H., Snyder, B., Larkin, K., Liu, J., Orkin, J., et al. (2008). Towards a transgenic model of Huntington's disease in a non-human primate. Nature *453*, 921–924.

Yang, S.-T., Kreutzberger, A.J.B., Lee, J., Kiessling, V., and Tamm, L.K. (2016). The role of cholesterol in membrane fusion. Chem. Phys. Lipids *199*, 136–143.

Yu-Taeger, L., Petrasch-Parwez, E., Osmand, A.P., Redensek, A., Metzger, S., Clemens, L.E., Park, L., Howland, D., Calaminus, C., Gu, X., et al. (2012). A novel BACHD transgenic rat exhibits characteristic neuropathological features of Huntington disease. J. Neurosci. Off. J. Soc. Neurosci. *32*, 15426–15438.

Zala, D., Hinckelmann, M.-V., and Saudou, F. (2013a). Huntingtin's Function in Axonal Transport Is Conserved in Drosophila melanogaster. PLOS ONE *8*, e60162.

Zala, D., Hinckelmann, M.-V., Yu, H., Lyra da Cunha, M.M., Liot, G., Cordelières, F.P., Marco, S., and Saudou, F. (2013b). Vesicular Glycolysis Provides On-Board Energy for Fast Axonal Transport. Cell *152*, 479–491.

Zarrinpar, A., Bhattacharyya, R.P., and Lim, W.A. (2003). The structure and function of proline recognition domains. Sci. STKE Signal Transduct. Knowl. Environ. *2003*, RE8.

Zech, M., Nübling, G., Castrop, F., Jochim, A., Schulte, E.C., Mollenhauer, B., Lichtner, P., Peters, A., Gieger, C., Marquardt, T., et al. (2013). Niemann-Pick C Disease Gene Mutations and Age-Related Neurodegenerative Disorders. PLoS ONE *8*.

Zelcer, N., Khanlou, N., Clare, R., Jiang, Q., Reed-Geaghan, E.G., Landreth, G.E., Vinters, H.V., and Tontonoz, P. (2007). Attenuation of neuroinflammation and Alzheimer's disease pathology by liver x receptors. Proc. Natl. Acad. Sci. *104*, 10601–10606.

Zhang, J., Gregory, S., Scahill, R.I., Durr, A., Thomas, D.L., Lehericy, S., Rees, G., Tabrizi, S.J., Zhang, H., and TrackOn-HD investigators (2018). In Vivo Characterization of White Matter Pathology in Premanifest Huntington's Disease. Ann. Neurol.

Zhang, Y., Moheban, D.B., Conway, B.R., Bhattacharyya, A., and Segal, R.A. (2000). Cell surface Trk receptors mediate NGF-induced survival while internalized receptors regulate NGF-induced differentiation. J. Neurosci. Off. J. Soc. Neurosci. *20*, 5671–5678.

Zhang, Y., Leavitt, B.R., Raamsdonk, J.M. van, Dragatsis, I., Goldowitz, D., MacDonald, M.E., Hayden, M.R., and Friedlander, R.M. (2006). Huntingtin inhibits caspase-3 activation. EMBO J. *25*, 5896–5906.

Zhao, S., Hu, X., Park, J., Zhu, Y., Zhu, Q., Li, H., Luo, C., Han, R., Cooper, N., and Qiu, M. (2007). Selective expression of LDLR and VLDLR in myelinating oligodendrocytes. Dev. Dyn. *236*, 2708–2712.

Zheng, S., Clabough, E.B.D., Sarkar, S., Futter, M., Rubinsztein, D.C., and Zeitlin, S.O. (2010). Deletion of the Huntingtin Polyglutamine Stretch Enhances Neuronal Autophagy and Longevity in Mice. PLOS Genet. *6*, e1000838.

Zolotushko, J., Flusser, H., Markus, B., Shelef, I., Langer, Y., Heverin, M., Björkhem, I., Sivan, S., and Birk, O.S. (2011). The desmosterolosis phenotype: spasticity, microcephaly and micrognathia with agenesis of corpus callosum and loss of white matter. Eur. J. Hum. Genet. *19*, 942–946.

Zuccato, C., Ciammola, A., Rigamonti, D., Leavitt, B.R., Goffredo, D., Conti, L., MacDonald, M.E., Friedlander, R.M., Silani, V., Hayden, M.R., et al. (2001). Loss of huntingtin-mediated BDNF gene transcription in Huntington's disease. Science *293*, 493–498.

Zuccato, C., Tartari, M., Crotti, A., Goffredo, D., Valenza, M., Conti, L., Cataudella, T., Leavitt, B.R., Hayden, M.R., Timmusk, T., et al. (2003). Huntingtin interacts with REST/NRSF to modulate the transcription of NRSE-controlled neuronal genes. Nat. Genet. *35*, 76–83.

APPENDIX 1

CYP46A1 protects against NMDA-mediated excitotoxicity in Huntington's disease: Analysis of lipid raft content

Biochimie 153 (2018) 70–79

Contents lists available at ScienceDirect

Biochimie

journal homepage: www.elsevier.com/locate/biochi

Research paper

CYP46A1 protects against NMDA-mediated excitotoxicity in Huntington's disease: Analysis of lipid raft content

Lydie Boussicault [a, b], Radhia Kacher [b], Antonin Lamazière [c], Peter Vanhoutte [b], Jocelyne Caboche [b], Sandrine Betuing [b, *], Marie-Claude Potier [a, **]

[a] Institut du Cerveau et de la Moelle épinière (ICM), UMR-S975, Université Pierre et Marie Curie-Paris 6, Hôpital de la Salpêtrière, Paris, France
[b] Sorbonne Université, Faculté des Sciences et Ingénierie, INSERM/UMR-S 1130, CNRS/UMR 8246, Institute of Biology Paris-Seine, Neurosciences Paris Seine, Neuronal Signaling and Gene Regulation, IBPS-NPS, 75005, Paris, France
[c] LBM, Sorbonne Université, Faculté de Médecine, AP-HP, Hôpital Saint Antoine, 75012, Paris, France

ARTICLE INFO

Article history:
Received 26 February 2018
Accepted 27 July 2018
Available online 11 August 2018

Keywords:
Excitotoxicity
CYP46A1
Huntington's disease
Lipid rafts
GluN2B
Cholesterol

ABSTRACT

Huntington's Disease (HD) is an autosomal dominant neurodegenerative disease caused by abnormal polyglutamine expansion in huntingtin (mHtt) protein leading to degeneration of striatal neurons. Excitotoxicity, consecutive to overstimulation of N-methyl D-aspartate receptors (NMDARs) has a pivotal role in many neurological disorders including HD. Mutant Htt causes enhanced NMDA sensitivity, alteration of NMDAR expression and localization in neurons. Excitotoxic events initiate neuronal death in numerous ways, including activation of apoptotic cascades. Among the NMDAR subunits involved in glutamatergic-mediated excitotoxicity, GluN2B has been extensively reported. In addition to excitotoxicity, alteration of cholesterol metabolism has been observed in HD, with a decrease of cholesterol precursor synthesis along with an increase of cholesterol accumulation, which is deleterious for neurons. Expression of Cholesterol Hydroxylase enzyme, CYP46A1, which converts cholesterol into 24 S-hydroxycholesterol is down-regulated in HD. We found that CYP46A1 overexpression is beneficial in HD neurons and mouse model, but the mechanisms involved still remain unclear. In this study we addressed the effect of CYP46A1 on NMDAR-mediated excitotoxicity in HD primary neurons and its role in modulating cholesterol and localization of GLUN2B in lipid rafts. We showed that CYP46A1 is protective against NMDAR-mediated excitotoxicity in two different HD neuronal cell models. Cholesterol as well as GluN2B level in lipid raft, are significantly increased by mHtt. Despite a clear effect of CYP46A1 in reducing cholesterol content in lipid raft extracts from wild type neurons, CYP46A1 overexpression in HD neurons could not normalize the increased cholesterol levels in lipid rafts. This study highlights the beneficial role of CYP46A1 against NMDAR-mediated excitotoxicity and gives further insights into the cellular mechanisms underlying CYP46A1-mediated neuroprotection.

1. Introduction

Huntington's disease (HD) is an autosomal dominant neurodegenerative disease caused by an expansion of the CAG repeats in the first exon of the huntingtin gene, leading to a polyglutamine stretch in the N-terminus of the protein [1]. This mutation causes a progressive neurodegeneration affecting first striatal projection neurons (SPNs) and then cortical neurons, leading to characteristic motor, cognitive and psychiatric symptoms [2].

Among the cellular dysfunctions observed in HD, excitotoxicity has been extensively studied [3–6]. Excitotoxicity is mediated by elevated calcium influx through NMDA (N-Methyl-D-Aspartate) ionotropic glutamate receptors [7,8] leading to neuronal toxicity.

* Corresponding author. Sorbonne Université, Faculté des sciences et Ingénierie, Neuroscience Paris Seine, BAt A 3ème étage, 9 quai Saint Bernard, 75005 Paris, France.
** Corresponding author. ICM, Institut du Cerveau et de la Moelle, Hôpital de la Pitié Salpêtrière 47, Bd de l'Hôpital, 75013, Paris, France.
E-mail addresses: sandrine.betuing@upmc.fr (S. Betuing), marie-claude.potier@upmc.fr (M.-C. Potier).

https://doi.org/10.1016/j.biochi.2018.07.019
0300-9084/

NMDA receptors (NMDA-R) are hetero-tetramers containing two GluN1-NMDAR subunits associated to GluN2-NMDAR subunits (GluN2A and GluN2B) and/or GluN3 subunits with different properties [9–11]. Studies performed on cultured cortical or hippocampal neurons led to the conclusion that GluN2A-containing NMDARs are likely to promote cell survival, whereas GluN2B-containing NMDARs are preferentially associated to cell death signaling and contribute to NMDA-mediated excitotoxicity. Mutated Huntingtin (mHtt) has been reported to increase neuronal susceptibility to NMDA-induced excitotoxicity [3,12,13]. Indeed, in several HD animal models, increased NMDAR-mediated currents and enhanced excitotoxicity after NMDA stimulation were demonstrated at early stages of the disease [4,14–17]. Moreover, intrastriatal injections of NMDAR agonist in mice and primates reproduce the striatal degeneration observed in HD [18–21] underlying HD striatal neurons susceptibility to NMDAR-induced toxicity.

In addition to NMDAR-dependent signaling, cholesterol metabolism is also affected in HD, with a decrease of synthesis along with decreased levels of the rate-limiting enzyme for cholesterol degradation CYP46A1 [22–26]. Furthermore, cholesterol accumulation has been described in mHtt expressing neurons [27,28]. Cholesterol is an essential membrane component enriched in the central nervous system which, when dysregulated, strongly impacts normal cellular functions. In a wild type context, significant loss of membrane cholesterol as well as release of 24S-hydroxycholesterol has been observed after stimulation of post-synaptic NMDA [29]. Depletion of CYP46A1, prevented cholesterol loss, suggesting that cholesterol turnover at the membrane and NMDAR activation are tightly connected. Interestingly, CYP46A1 could interact indirectly with NMDA receptors as oxysterols were shown to interact with and modulate NMDA receptor activity whatever the subunit composition. Indeed, 24S-hydroxycholesterol was described as a potent positive allosteric modulator of NMDA-receptors able to enhance LTP in hippocampal slices [30] while 25S-hydroxycholesterol antagonized 24S-hydroxycholesterol effect [31,32]. CYP46A1 knock-out mice showed LTP and memory deficits that could be explained by an altered modulation of NMDAR activity by 24S-hydroxycholesterol. Accordingly, NMDAR activity was reduced in hippocampal slices derived from CYP46A1 KO mice while global synaptic transmission was not altered [32].

Lipid rafts are highly ordered membrane sub micrometric domains rich in cholesterol which play a role in neuronal communication [33]. These domains are essential for the clustering of neurotransmitter receptors and their downstream effectors. They can especially contribute to the regulation of ionotropic glutamate receptors function [34]. In cells expressing mHtt, cholesterol accumulates in membranes, which correlates with an increase of the lipid rafts [28]. Neurons expressing mHtt have an increased localization of GluN1-NMDAR and GluN2B-NMDAR subunits in lipid rafts [28]. Thus, NMDA-R enrichment in lipid raft could impact the excitotoxicity observed in HD. Studies focusing on lowering cholesterol, either inhibition of synthesis with simvastatin or by extracting cholesterol from cell membranes using cyclodextrins, showed a neuroprotective effect against NMDA-induced excitotoxicity associated to a redistribution of NMDA-R subunits in lipid rafts [28,35,36].

Finally, we demonstrated that regulating cholesterol homeostasis by overexpressing CYP46A1 has protective effect against mHtt induced toxicity *in vitro* and *in vivo* in HD models [25]. Giving the increasing evidence that cholesterol levels might influence NMDAR-mediated excitotoxicity, we focused on the role of CYP46A1 overexpression on the increased susceptibility to NMDA-induced excitotoxicity in HD neuronal models by analyzing cholesterol and GLUN2B content on lipid raft extracts.

2. Material and methods

2.1. Mice

YAC128 mice expressed a yeast artificial chromosome (YAC) sequence originally created to contain a modified version of the full-length human huntingtin gene (*HTT*) in exon 1 bearing 128 glutamines repetition (composed primarily of CAG codons but also containing 9 interspersed CAA codons). YAC128 mice were obtained from Jackson Laboratories. These mice were bred with FVB/NJ mice to generate male and female YAC128 and WT littermates. To determine mice genotype, extraction of genomic DNA was performed using the KAPA Mouse Genotyping Kit (Cliniscience, KK7302). A PCR was performed to confirm mice genotype using the following primers: Forward GGCTGAGGAAGCTGAGGAG and Reverse CGCCTCAGGTTCTGCTTTTA. The mice were housed in groups with a 12-h light/dark cycle and provided with food and water ad libitum. Animal care was conducted in accordance with standard ethical guidelines (U.S. National Institutes of Health publication no. 85–23, revised 1985, and European Committee Guidelines on the Care and Use of Laboratory Animals) and the local ethics committee approved the experiments (#01435.02 project).

2.2. Cell culture, infection and treatments

Primary striatal neurons were dissected from day 14.5 embryos from pregnant Swiss OF1 mice (Charles River Laboratory, France) as previously described [37]. Primary cortical neurons cultures were performed by dissecting P0 YAC128 new born mice. P0 cells were treated at DIV1 for 48H with AraC (10 μM, Sigma) to prevent glial cell proliferation. After 7 days *in vitro* (DIV) for striatal cell or 3 DIV for cortical YAC neurons, infections were performed with AAVrh10-CYP46A1-HA (1.10^12 vg/ml), AAVrh10-GFP (1.10^13 vg/ml), AAVrh2-Htt-18Q (1.10^13 vg/ml) and AAVrh2-Htt-82Q (1.10^13 vg/ml). For CYP46A1 and Htt co-infection, the total amount of viral particles was 1.10^13 vg/ml. All AAVrh10 vectors were produced and purified by Atlantic Gene therapies, Nantes, France. The viral constructs AAVrh10-GFP and AAVrh10-CYP46A1-HA contain the expression cassette consisting of either the GFP or the human CYP46A1, driven by a CMV/β-actin hybrid promoter (CAG) surrounded by inverted terminal repeats of AAV2. AAVrh2 expressing Htt-18Q or mhtt-82Q were kindly provided by Alexis Bemelmans (MIRCen, France). Theses AAV virus expressed the first 171 amino acid of the human Htt with 18 or 82 glutamine repetitions under the Chicken Beta Actin (CBA) promoter. These sequences were tagged by c-myc in C-terminal part.

2.3. NMDA treatment and cell immunostaining

After 21 DIV for striatal neurons or 10 DIV for cortical YAC128 neurons, cells were incubated with 100 μM NMDA (Sigma) for 10 min at 37 °C and 5% CO2 in Neurobasal medium (Invitrogen) without B27 supplement. Medium was replaced by fresh complete medium and cells were fixed 6 h after NMDA treatment with PFA-sucrose 4%. Briefly, cells were incubated 20 min at RT in PFA and then washed with PBS (Sigma). Neurons were detected with anti-rabbit MAP2 antibody (1:1000, Millipore), AAVrh10-CYP46A1-HA infected neurons were detected with anti-rat HA antibody (1:1000, Roche), while mHtt-82Q or Htt-18Q infected neurons were detected by anti-mouse 2b4 antibody (1:1000, Millipore) and with

appropriate anti-rabbit (CY5), anti-mouse (Alexa 488), or anti-rat (CY3) fluorophore-conjugated secondary antibodies (1:500, Invitrogen). Nuclei were stained by Dapi solution. Cell death was measured by quantification of pyknotic nuclei using ImageJ software. Infection rate was assessed by quantifying Htt positive cells in MAP2 positive cells population: (Number of Htt positive cell/number of MAP2 positive cell) ×100.

2.4. RNA extraction and LightCycler real time polymerase chain reaction

After 21 DIV (15 DIV post infection), cells were treated with NMDA 100 μM for 10 min. Six hours after treatment, cells were lysed in Trizol (Qiagen) following the manufacturer's instructions. Samples were stored at −80 °C until RNA extraction. RNA isolation was performed with miRNeasy Mini kit (Qiagen) according to the manufacturer's instructions. RNA concentrations were measured using a NanoDrop 2000 (ThermoScientific). Reverse transcription was performed with RevertAid First Strand cDNA synthesis kit (ThermoScientific). Quantitative real-time PCR reactions were performed using LightCycler480 SYBR-Green I Master according to manufacturer's protocol and run on LightCycler480 (Roche Diagnostics). The cycle threshold values were calculated automatically with the LightCycler480 SW 1.5 software with default parameters. The sequence of the primers used are the following: NeuN (Forward: ttgcttccaggtcgtgtat and Reverse: tggttccgatgctgtaggtt), DARPP32 (Forward: cacccaagtcgaagagacc and Reverse: tcctcctcatcatcctcctg), GluN2B (Forward: cctgtgtgagaggaatctcgg and Reverse: gctggatgccgggatagaa). Expression of hypoxanthine guanine phosphoribosyltransferase 1 (Hprt1) transcripts was used to normalize the amounts of cDNA, all groups were then normalized to the wild type group.

2.5. Rafts preparation

Rafts preparations were performed as described in Escartin et al. (2006) [38]. Briefly, lipid rafts purification is based on properties of resistance to nonionic detergent at low temperature and their floatability in low density fractions during gradient centrifugation. After 21 DIV (15 DIV post infection), striatal neurons were scraped on ice in MES (25 mM), NaCl (150 mM) buffer (Sigma) supplemented by protease inhibitors (Compete Mini, Roche). Six-well plates were pooled for each condition. Rafts were purified by 30 min incubation in 1% Brij-58 (Sigma) at 4 °C and fractionated through a discontinuous sucrose gradient following the protocol of Butchbach et al. [39]. From the top of the gradient, 10 fractions (400 μl) and the pellet were collected.

2.5.1. Cholesterol assay

Cholesterol content was measured in all fractions with Amplex Red Cholesterol assay kit (Invitrogen) following the manufacturer's instructions. By omitting cholesterol esterase, cholesterol levels, and not cholesteryl ester, were assessed.

2.5.2. Western blotting

An equal volume of each fraction (16 μl) was diluted in loading buffer (Biorad) and processed for immunoblotting. Samples from each fraction were loaded on polyacrylamide gel (4–12%, Biorad). Primary mouse monoclonal anti-GluN2B antibody (1:1000) (Millipore), and mouse monoclonal anti-flotilline 1 1:1000 antibody (BD Transduction Laboratories) were revealed with appropriate anti-mouse peroxidase-conjugated secondary antibodies (Invitrogen) and the ECL chemiluminescent reaction (Pierce).

2.5.3. Western blot quantification

Films were scanned, and optical density (OD) was measured using Image J software. Specific ODs in lipid rafts (fractions 3, 4 and 5) were normalized to flotillin 1 levels.

2.6. Gas chromatography - mass spectrometry

Cholesterol and 24(S)-hydroxycholesterol levels were determined from 3 million cultured cells by Gas Chromatography–Mass Spectrometry (GC–MS) using deuterium-labeled internal standards as described previously [25]. In Brief, the sterol fraction was silylated with Regisil® + 10% TMCS [bis(trimethylsilyl) trifluoroacetamide + 10% trimethylchlorosilane] (Regis technologies). The trimethylsilylether derivatives were then separated by gas chromatography (Hewlett-Packard 6890 series) in a medium polarity capillary column RTX-65 (65% diphenyl 35% dimethyl polysiloxane, length 30 m, diameter 0.32 mm, film thickness 0.25 μm; Restesk). The mass spectrometer (Agilent 5975 inert XL (Agilent Technologies, Palo Alto, CA)) was coupled to gas chromatography for detection of positive ions. Ions were produced in the electron impact mode at 70 eV. They were identified by the fragmentogram in the scanning mode and quantified by selective monitoring of the specific ions after normalization and calibration with the appropriate internal and external standards. Quantification of oxysterols was obtained with the isotope dilution method.

2.7. Statistics

Statistical analyses were performed with GraphPad Prism 5. All data are represented as mean ± SEM. Infection rate and aggregates percentage were analyzed by Two-way ANOVA followed by Bonferroni post hoc correction. For survival studies, results were analyzed by two-way ANOVA followed by Bonferroni post hoc correction. Cholesterol levels across fractions were analyzed by two-way ANOVA followed by Bonferroni post hoc correction. For GluN2B localization by immunoblotting, *t*-test was performed for each fraction. When only 2 groups were compared, student *t*-test were performed.

3. Results

3.1. Characterization of in vitro cellular model of Huntington's disease

Huntington's Disease (HD) is a complex pathology, which involves numerous cellular dysfunctions leading to striatal neurons death. Among these mechanisms, glutamate mediated-excitotoxicity and cholesterol dysregulation are of particular interest. In order to study the interplay between these two mechanisms, we developed a new cellular model consisting of primary striatal neuronal cultures infected with adeno-associated viral (AAV) constructs. To mimic HD pathology, we infected cells with either a mutated human version of Huntingtin bearing 82 glutamine repetitions (mHtt-82Q) or a non-toxic form of human Huntingtin bearing 18 glutamine repetitions (Htt-18Q) as a control (Fig. 1A–F). Infection rates were measured from one to 3 weeks post-infection, and showed a progressive increase followed by stabilization at around 65% of cells 3 weeks after either Htt-18Q or mHtt-82Q infection (Fig. 1B). As expected, neurons infected with Htt-18Q presented a diffuse Htt staining, while mHtt-82Q expressing neurons mainly showed aggregated Htt (Fig. 1A). The percentage of neurons bearing mHtt-82Q aggregates increased with time (Fig. 1D). At any time post-infection, striatal neurons expressing mHtt-82Q did not show any significant alteration of cell survival when compared to Htt-18Q-infected neurons, as indicated

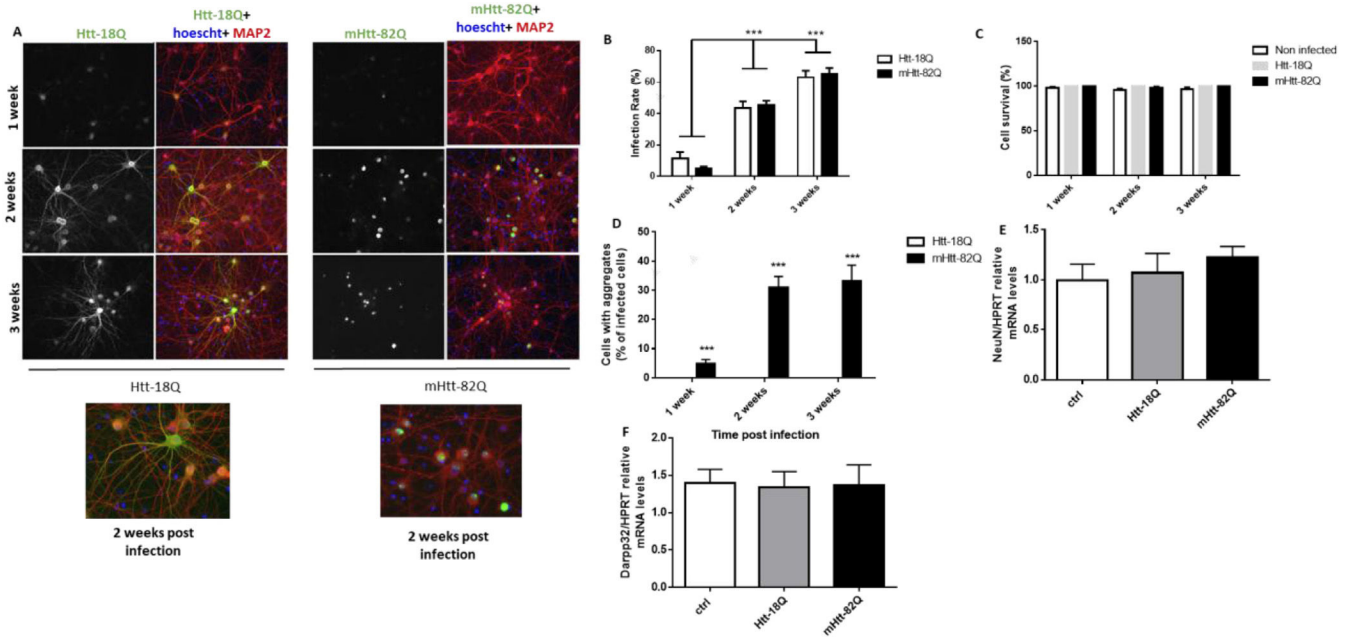

Fig. 1. Cellular model of Huntington's disease A. Huntingtin (Htt-18Q) and mutated Htt (mHtt-82Q) were expressed in primary striatal neurons by AAV infection. Cells were infected at 7 days *in vitro* (DIV) for 1, 2 or 3 weeks. Immunostaining of neuronal arborization (MAP2 in red) and Htt (in green) were performed 1, 2 or 3 weeks post infection. Infection rate (**B**), cell survival (**C**) and percentage of cells bearing aggregates (**D**) were quantified at each time point (Htt-18Q 1-week n = 146, 2 weeks n = 172, week 3 n = 191 neurons; mHtt-82Q 1-week n = 109, 2 weeks n = 247, week 3 n = 194 neurons, 4 culture). Neuronal (NeuN) and striatal (Darpp32) markers were measured by RT-qPCR (**E** and **F** respectively) 2 weeks post infection (n = 6 per condition, 2 independent cultures). Statistics: **B** and **D** 2-way ANOVA followed by Bonferroni post hoc test: ***p < 0.0001. Data are presented as mean ± SEM.

by analyzing the morphology of nuclei from infected neurons after Hoechst staining (Fig. 1C) or the levels of the neuronal marker NeuN transcripts (Fig. 1E). Finally, we found that Htt-18Q and mHtt-82Q had no effect on the level of striatal neuron marker DARPP32 transcripts (Fig. 1F).

3.2. CYP46A1 protects striatal neurons against NMDA-induced excitotoxicity

We showed in a previous study that the cholesterol 24-hydroxylase CYP46A1, an enzyme involved in brain cholesterol homeostasis, was neuroprotective from mHtt-induced neurotoxicity on HD cell lines and cultured striatal neurons [25]. Injection of AAV-CYP46A1 in the dorsal striatum of the R6/2 HD transgenic mouse model also protected from behavioral alterations and neuronal dysfunctions [25]. As an attempt to elucidate the cellular mechanisms underlying CYP46A1-mediated neuroprotective effect, we first studied NMDA-mediated excitotoxicity in mHtt-expressing neurons *in vitro*, as compared to normal Htt, in the presence or not of CYP46A1 (Fig. 2). High concentrations of NMDA (100 μM) were applied on striatal neurons infected with Htt-18Q or mHtt-82Q, and infected or not with AAV-rh10-CYP46A1 (Fig. 2A–D). Importantly, when Htt-18Q or mHtt-82Q were co-infected with CYP46A1, the co-infection rate reached 70% (Fig. 2B). Hoechst staining was used to detect condensed nuclei and hence neuronal death. In control condition (no treatment), few neurons contained condensed nuclei while NMDA treatment significantly increased the percentage of pyknotic nuclei (20%, Fig. 2C). In the meantime, MAP2 integrity was reduced by NMDA treatment reflecting both neuronal toxicity and cell death (Fig. 2D). Interestingly, CYP46A1 corrected both the number of pyknotic nuclei and MAP2 integrity following NMDA treatment, suggesting that CYP46A1 protected neurons against NMDA toxicity (Fig. 2D and E). We then applied the same protocol on striatal neurons infected with AAV constructs expressing Htt-18Q or mHtt-82Q with or without AAV-rh10-CYP46A1. Surprisingly, NMDA toxicity appeared to be similar in neurons expressing mHtt-82Q as compared to control or Htt-18Q conditions (Fig. 2D and E). However, in the presence of CYP46A1, striatal neurons expressing either Htt-18Q or mHtt-82Q became insensitive to NMDA-induced toxicity. To confirm this finding, CYP46A1 neuroprotection against NMDA-induced toxicity was tested in cultured cortical neurons from the HD YAC128 transgenic mice. As observed in striatal neurons infected with AAV expressing mHtt-82Q, CYP46A1 protected YAC128 neurons against NMDA-induced toxicity (Fig. 2E–G).

Altogether, these results suggest that CYP46A1 neuroprotective properties could be explained, at least partly, by an inhibition of toxicity mediated by NMDAR.

3.3. Regulation of cholesterol content and GluN2B localization by mHtt

Both cholesterol dysregulation and excitotoxicity mediated by NMDARs, in particular GluN2B containing NMDARs, were previously described in HD [28]. Using immunochemistry approach, it was shown that increase of cholesterol at the plasma membrane induces a relocalization of GluN2B in lipid rafts, leading to excitotoxicity [28].

Here we performed biochemical isolation of lipid rafts to characterize the effects of mHtt-82Q on both cholesterol content and GluN2B localization. We used a technique based on raft resistance to detergent. Cellular lysates were digested with Brij 58 and loaded on a discontinued 4 mL sucrose gradient. After overnight ultra-centrifugation, 10 fractions of 400 μl and the pellet were collected from top to bottom. Upper fractions (1–5) corresponded to detergent insoluble material while fractions 6 to 11 contained soluble material (Fig. 3A). To identify which fraction contained lipid rafts, we measured cholesterol and flotillin 1 levels

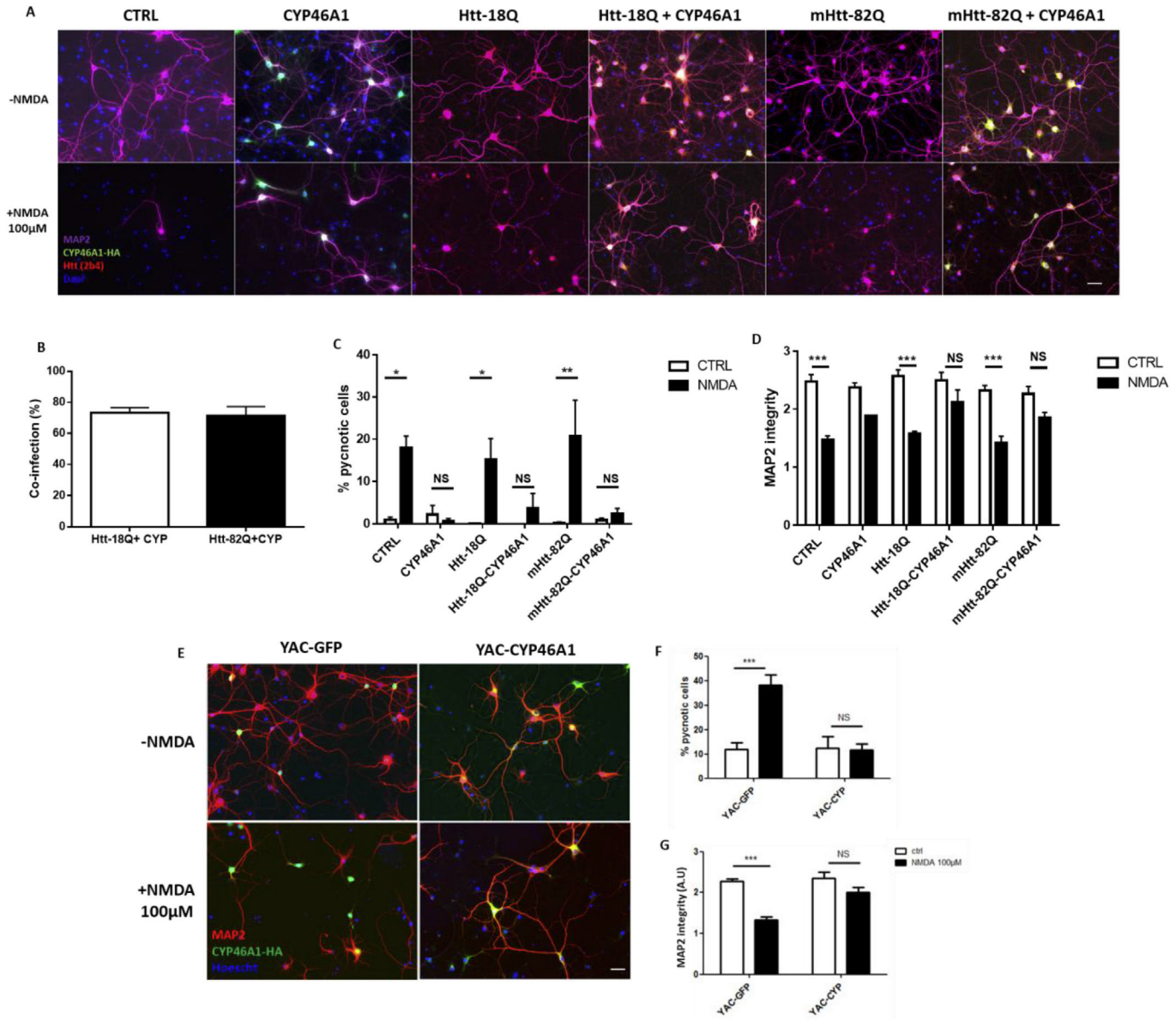

Fig. 2. CYP46A1 protects neurons against NMDA-induced excitotoxicity A. Striatal neurons were infected at DIV7 with Htt-18Q or mHtt-82Q ± CYP46A1-HA. High dose of NMDA (100 µM) was applied to neurons 2 weeks post-infection (DIV21) for 10 min and cells were fixed 4H after treatment. **B**. Htt-18Q or mHtt-82Q and CYP46A1 co-infection rates were estimated by calculating the percentage of cells positive for CYP46A1 and Htt. **C**. Cell death was measured by counting pyknotic nuclei based on Hoechst staining. **D**. MAP2 integrity was scored on the basis of MAP2 staining (3 = intact neurites, 2 = fragmented neurites, 1 = retracted neurites, 0 = absence of neurite). (CTRL, NMDA, Htt-18Q, Htt-18Q + NMDA n = 5; mHtt-82Q, mHtt-82Q + NMDA n = 4; CYP, CYP46A1+NMDA n = 2; Htt-18Q + CYP, Htt-18Q + CYP46A1+NMDA, mHtt-82Q + CYP46A1, mHtt-82Q + CYP46A1+NMDA n = 3, 3 independent cultures). Statistical analysis: Two-way ANOVA followed by Tukey's post-hoc test, *p < 0.05, **p < 0.01, ***p < 0.001. **E**. CYP46A1 protected YAC128 HD neurons against excitotoxicity. Cortical neurons from YAC128 HD new born mice (P0) were infected with CYP46A1-HA at DIV 2–3. NMDA treatment was applied at DIV 10 for 10 min and neurons were fixed 6 h later. Immunostaining for MAP2 (red), CYP46A1-HA (green) and nuclei (Blue) were performed. **F**. Percentages of pyknotic nuclei were measured and MAP2 integrity was assessed (**G**). n = 6 per condition, 2 independent cultures. Statistics: Two-way ANOVA followed by Bonferroni post hoc test. Scale bar = 40 µM. Data are expressed as mean ± SEM.

in each isolated fraction. In agreement with the literature [39], we found that fractions 3, 4 and 5 had the highest cholesterol concentrations and contained flotillin 1 (Fig. 3A). We then measured cholesterol content in fractions from striatal neurons infected with either Htt-18Q or mHtt-82Q. Striatal neurons expressing mHtt-82Q accumulated cholesterol in lipid rafts-containing fraction 3 as compared to 18Q expressing neurons (Fig. 3B). Cholesterol concentrations tended to be higher also in the detergent soluble fractions (7–9). However, total cholesterol content in cellular lysates measured by GC-MS remained unchanged after mHtt-82Q expression as compared to Htt-18Q expression (Table 1). Altogether these results suggest that mHtt-82Q specifically increased cholesterol levels in lipid rafts.

GluN2B localization was analyzed by western blot after biochemical lipid rafts isolation. We showed that mHtt-82Q expression induced a significant increase of GluN2B in lipid raft fractions 3 and 5 (Fig. 3C–D). Interestingly, this increase of GluN2B at the protein level was not explained by a regulation at the transcript level since GluN2B mRNA levels were not modified in mHtt-82Q-infected neurons (Fig. 3E). This observation agrees with

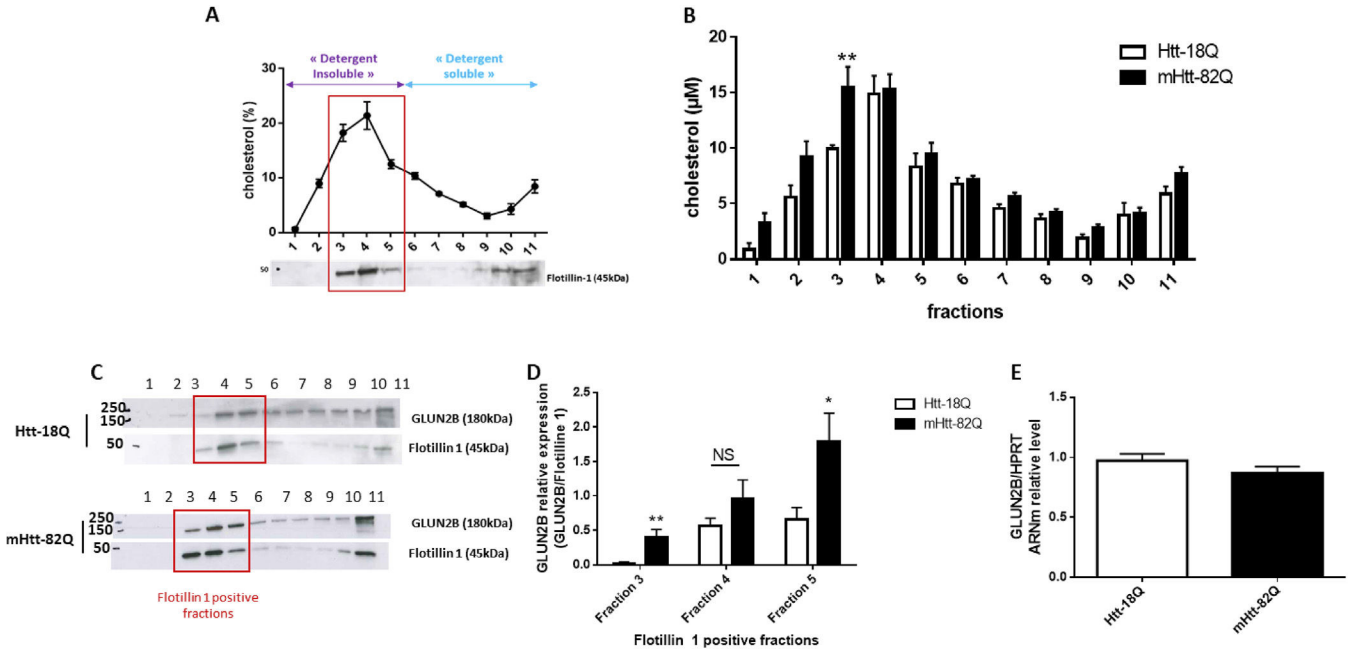

Fig. 3. MHtt-82Q induces an increase of cholesterol content and GluN2B localization in HD neurons lipid rafts Embryonic striatal neurons were infected with Htt-18Q or mHtt-82Q at DIV7. Two weeks post infection (DIV21) cells were collected, and lipid raft were isolated using sucrose gradient fractionation. **A**. Cholesterol concentrations were assessed in the 11 fractions obtained after ultracentrifugation. Flotillin 1, a protein marker of lipid rafts, levels were assessed by western blot in the 11 fractions. (n = 7, 3 independent cultures). **B**–**C**. GluN2B repartition in the 11 fractions was determined by western blot. GluN2B protein expression in lipid rafts was normalized with flotillin 1 expression. Htt-18Q n = 7, mHtt-82Q n = 13, 6 independent cultures, Statistics: *t*-test (inside each fraction), Welch's correction, $^{**}p < 0.01$. **E**. GluN2B transcript levels were measured by RT-qPCR on striatal neurons infected with Htt-18Q or mHtt-82Q at DIV7, 2 weeks post infection and normalized with HPRT transcript levels (n = 6 per conditions, 2 independent cultures). Data are represented as mean ± SEM.

Table 1
CYP46A1 decreases global cholesterol levels in striatal neurons. Embryonic striatal neurons were infected with Htt-18Q, mHtt-82Q, CYP46A1 or Htt-82Q + CYP46A1 at DIV7 (n = 3 per condition). Two weeks post infection (DIV21) cells were collected and GC-MS analysis was performed for cholesterol and 24S-OHC levels. Statistics: ANOVA One way, followed by Dunnett's post hoc test, $^{*}p < 0.05$. Data are represented as mean ± SEM.

	18Q	82Q	CYP46A1	82Q + CYP46A1
Cholesterol (ng/µg protein)	54,14 ± 8,96	48,92 ± 2,55	33,74 ± 1,61*	37,25 ± 1,80
24S-OHC/Chol (ng/µg protein)	0,00490 ± 0,00030	0,00409 ± 0,00048	0,00918 ± 0,00062*	0,00706 ± 0,00058

previous study showing that global GluN2B expression was unchanged in HD while its localization to the membrane was increased [6]. Furthermore, we confirm, using a biochemical assay on AAV-infected primary striatal neurons, that mHtt-82Q can induce a concomitant accumulation of cholesterol and GluN2B in lipid rafts.

3.4. Effect of CYP46A1 on cholesterol content and GluN2B localization in wild type striatal neurons

We then assessed whether CYP46A1 could influence cholesterol content in lipid rafts. Neurons were infected with AVVrh10-CYP46A1-HA and cholesterol levels were measured after fractionation. We found that CYP46A1 significantly decreased (−24%) cholesterol content in lipid rafts (Fig. 4A). This change was likely attributable to a global effect on cholesterol metabolism as suggested by results obtained by GC-MS (Table 1). CYP46A1 induced a 37% decrease of intracellular cholesterol in infected cells and a 87% increase of 24-OHC/cholesterol ratio without any change in flotillin 1 levels (Fig. 4B: compare lower panels in western blots from CTRL and CYP46A1). Altogether, these results strongly suggest that CYP46A1 decreased cholesterol concentration in lipid rafts rather than the amount of lipid rafts.

We thus showed that mHtt-82Q increased cholesterol levels in lipid raft fractions, CYP46A1 showed opposite effects (reduced cholesterol levels in lipid raft fractions), and CYP46A1 was protective against mHtt-82Q induced toxicity. As known, cholesterol induces a relocalization of NMDAR in lipid rafts and leads to excitotoxicity in HD [28]. We thus tested whether the neuroprotective effect of CYP46A1 in our HD model could be explained by a change of localization of GluN2B-containing NMDARs from inside to outside lipid rafts. With regard to GluN2B-containing NMDARs localization, we found that CYP46A1 expression left their localization unchanged (Fig. 4B and C).

3.5. Effect of CYP46A1 on cholesterol content and GluN2B-containing NMDAR localization in mHtt striatal neurons

We reasoned that despite its lack of effect on GluN2B-containing NMDARs localization in a wild type context, CYP46A1 could counteract the effects of mHtt on cholesterol content and GluN2B localization in lipid rafts. We measured cholesterol and GLUN2B contents in lipid rafts isolated from neurons co-infected with mHtt-82Q and CYP46A1 and compared to neurons infected with mHtt-82Q only (Fig. 5). There was no change either in cholesterol levels in lipid raft fractions (Fig. 5 A) or in global cholesterol content

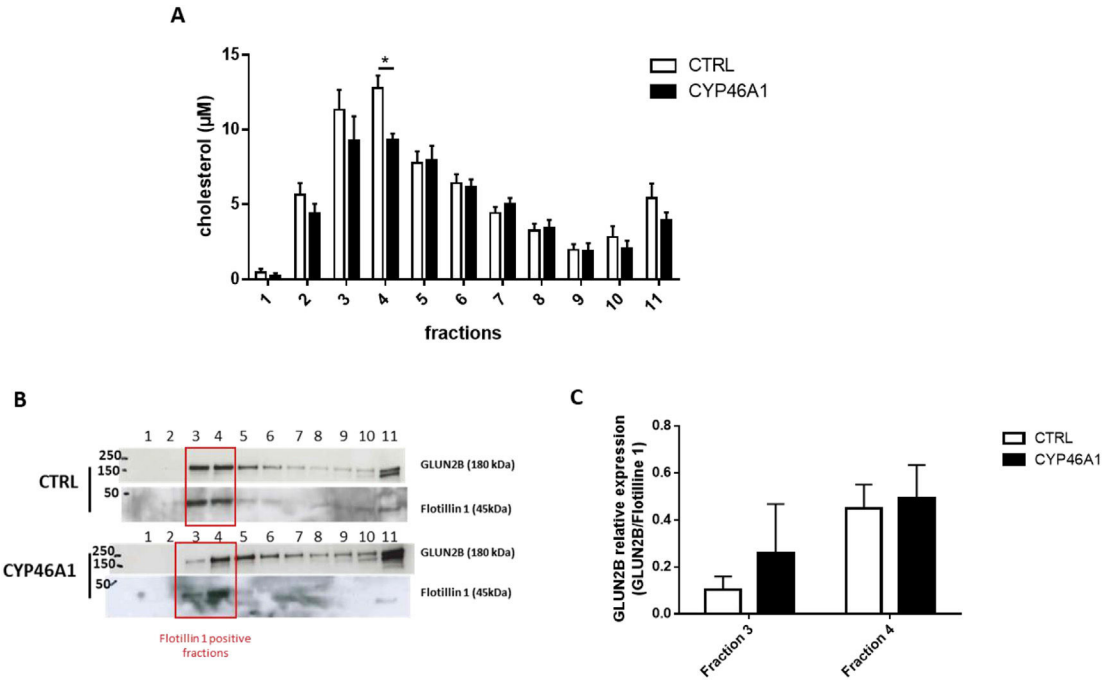

Fig. 4. CYP46A1 decreases cholesterol in lipid rafts, without affecting GluN2B-containing NMDARs localization in WT neurons **A**. Cholesterol content was assessed on striatal neurons infected or not with CYP46A1-HA. Neurons were infected at DIV7 and raft isolation were performed 2 weeks post infection. (CTRL n = 7, CYP46A1 n = 6, 3 independent cultures, Statistics: ANOVA Two way followed by Bonferroni's post hoc test, Interaction: NS, Fraction: ****, CYP46A1-HA: *). **B**. GluN2B distribution was determined using western blot. **D**. Quantification of GluN2B was normalized with flotillin 1 expression. CTRL n = 5, CYP46A1-HA n = 4, 3 independent cultures, Statistics: *t*-test, Welch's correction. Data are expressed as mean ± SEM.

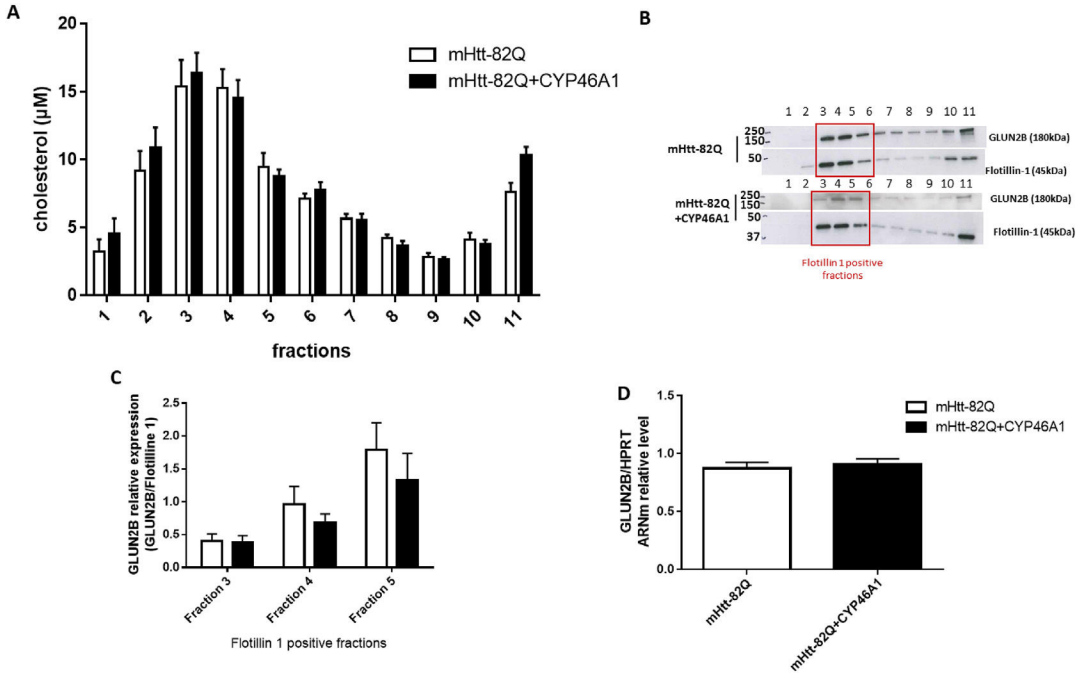

Fig. 5. CYP46A1 does not normalize cholesterol content in mHtt-82Q infected neurons A. Striatal neurons were infected at DIV7 with mHtt-82Q ± CYP46A1-HA. Two weeks post infection lipid rafts were isolated and cholesterol content was measured. (mHtt-82Q n = 14, mHtt-82Q + CYP46A1-HA n = 8, 6 independent cultures, Statistics: Two-way ANOVA). **B**. GluN2B distribution in all fractions was determined by western blot. **C**. Quantification of GluN2B signal obtained by western blot. GluN2B expression was normalized with flotillin 1 expression (mHtt-82Q n = 14, mHtt-82Q + CYP46A1-HA n = 8, 6 independent cultures). **D**. GluN2B transcript levels were measured by RT-qPCR on striatal neurons infected with mHtt-82Q ± CYP46A1-HA at DIV7, 2 weeks post infection, normalized with HPRT transcript levels. (n = 6 per conditions, 2 independent cultures). Data are represented as mean ± SEM.

following CYP46A1 expression despite a strong tendency to reduce cholesterol content in mHtt-82Q + CYP46A1 (Table 1). We concluded that CYP46A1-mediated decrease of cholesterol in lipid rafts was not sufficient to counterbalance mHtt-82Q induced cholesterol increase in lipid rafts. Similarly to the WT context (Fig. 4B and C), CYP46A1 did not restore GluN2B distribution in lipid rafts (Fig. 5B and C).

4. Discussion

It has been shown that in mHtt expressing cells, cholesterol content is increased especially in highly ordered domains such as lipid rafts, along with an enrichment of GluN2B in these domains [28]. Treatment with inhibitors of cholesterol synthesis is protective against NMDA induced neuronal death and is associated with a decrease of NMDAR in lipid raft [31]. We previously showed that the expression of CYP46A1, the rate limiting enzyme for cholesterol degradation, is neuroprotective in HD *in vivo* and *in vitro* [25]. Considering previous evidence for cholesterol involvement in excitotoxicity, especially in lipid raft organization, we focused this study on the potential role of CYP46A1 on cholesterol content and GluN2B localization in lipid rafts. We showed that, in striatal cultures, CYP46A1 expression protects against NMDA induced excitotoxicity. Moreover, mHtt containing neurons showed an increase in cholesterol content in lipid raft fractions, along with an accumulation of GluN2B. These results are consistent with the literature [28], and bring, using a different approach, evidence to confirm cholesterol dysregulation and GluN2B-NMDAR mislocalization in an HD context. In wild type striatal neurons, CYP46A1 induced cholesterol depletion from the cell and from lipid raft fractions as previously demonstrated [40], without changing GluN2B localization.

In neurons expressing mHtt, CYP46A1 overexpression does not rescue neither cholesterol content nor GluN2B localization suggesting that the observed neuroprotective effects of CYP46A1 in neuronal cultures treated with high doses of NMDA and in animal models of HD [25] are not mediated by a restoration of cholesterol and GluN2B content in lipid rafts. Whether CYP46A1 treatment could act on NMDA signaling or on other NMDA receptors subunits (GluN3 for instance) or coupling needs to be investigated. In the present study, we show that mHtt-82Q and CYP46A1 expression modified cholesterol content in lipid rafts in opposite directions but when co-expressed together CYP46A1 could not counteract mHtt-82Q effect. Whether mHtt-82Q increases cholesterol concentration without affecting the number of lipid rafts or rather increases the total number of lipid raft with unchanged cholesterol concentration remains to be determined. Interestingly, mHtt-82Q interacts with numerous proteins and lipids and could disturb raft content by modifying proteins interaction inside lipid raft thereby trapping cholesterol and making rafts less dynamic [41,42]. In cultured neurons CYP46A1 decreased lipid raft cholesterol concentration by a global effect on cholesterol clearance from the cell, without affecting the expression of cholesterol synthesis enzymes (Supplementary Fig. 1). Altogether, these results suggest that CYP46A1 does not act on lipid raft protein composition and interaction, therefore failing to restore mHtt-82Q specific alteration of lipid rafts.

The percentage of infected neurons, which is 65% 3 weeks post-infection, could be seen as a limiting factor in this study. However, it should be pointed out that the levels of mHtt and CYP46A1 co-infection is 78%, which should be enough to counteract the increase of cholesterol observed in the mHtt expressing neurons. Moreover, despite this infection rate, mHtt effect on cholesterol and GluN2B localization in lipid raft was largely detectable by biochemical technic.

We did not observe the increased sensibility of neurons expressing mHtt to excitotoxicity described in the literature [6]. However, we used striatal culture without cortical afference. Using co-cultures of cortical and striatal neurons could be an interesting option to recreate cortico-striatal synapses and thus favor striatal neurons sensibility to excitotoxicity [6]. Indeed, studies showed that the excitotoxicity observed in HD, is likely due to an extra-synaptic localization of GluN2B containing NMDARs [5,43].

Alternative methods such as fluorescence correlation spectroscopy could be used to confirm that NMDA receptor subunits localization in lipid rafts is not corrected by CYP46A1 expression, either in the control situation or while expressing mHtt-82Q [44]. The use of newly developed probes for assessing specifically calcium signaling in lipid rafts would also be very useful to evaluate the effect of CYP46A1 on NMDAR activity after excitotoxic stimulation.

Other pathways could be involved in CYP46A1-mediated neuroprotection. NMDAR induced excitotoxicity can induce CYP46A1 expression and triggers cholesterol loss at the membrane, allowing TrkB (tropomyosine receptor kinase B) activation, which induces signaling pathway known to promote neuronal survival [29,45–48]. A recent study also showed that overexpression of CYP46A1 activates TrkB, which can then interact and activate the enzyme geranylgeranyltransferase-I (GGTase-I), promoting dendritic outgrowth [49]. Another pathway responsible for the increase of cell survival following CYP46A1 expression may involve GSk3β, which is highly associated to lipid rafts and is increased in HD, triggering apoptosis [50]. Interestingly, the metabolite of cholesterol produced by CYP46A1, 24S hydroxycholesterol (24S-OHC), is an endogenous ligand for the Liver X receptors (LXR) [51,52], which can exert neuroprotective effects after brain injury [53]. Post-translational regulation can also participate to the protection against excitotoxicity. Indeed, the study of knock-out mice for CYP46A1 showed a significant difference, compared to wild type, in the brain phospho-proteome and in the ubiquitination of protein involved in energy production and cytoskeleton functions [54].

In this study, we focused on CYP46A1 effects on neuronal cultures. However, it is well known that astrocytes are key elements for cholesterol metabolism. Indeed, in the adult brain, astrocytes are the main cells that produce cholesterol, which is then transported to neurons complexed with ApoE containing lipoproteins [55]. In HD models, cholesterol synthesis is decreased, along with a decreased expression of ApoE in astrocytes [56,57]. It would be interesting to study CYP46A1 effect on co-cultures of neurons and astrocytes to include the synthesis of cholesterol in astrocytes and its transport to neurons. Cholesterol degradation by CYP46A1 leads to the production of 24S-OHC, which could be excreted by neurons and transported to astrocytes. Since 24S-OHC is a ligand of LXR that can induce the transcription of ApoE [52,58], it could thus increase the production of ApoE by astrocyte and the transport of cholesterol to neurons. Thus, using co-cultures of astrocytes and neurons could bring broader insights into the role of newly synthesized cholesterol in the turnover of cholesterol in lipid rafts.

5. Conclusion

Altogether, we showed that CYP46A1 is protective against NMDAR mediated excitotoxicity, and its expression can regulate cholesterol content in lipid rafts. However, CYP46A1 cholesterol regulation could not counteract mHtt alterations in lipid raft content. The mechanisms underlying CYP46A1 neuroprotection in mHtt expressing neurons needs to be further studied, by exploring other pathways involving for example cortico-striatal connections in an exitotoxic context.

Funding

This work was supported in part by Agence Nationale de la Recherche “13-BSV1-022-01” grant, DIM Biotherapy Region Ile de France grant, Groupama Fondation Maladies Rares, Centre National de la Recherche Scientifique; Institut National de la Santé et de la Recherche Médicale and Sorbonne Université, Faculté des Sciences et Ingénierie. The research leading to these results has received funding from the program “Investissements d'avenir” (ANR-10-IAIHU-06).

Conflicts of interest

The authors declare no conflict of interest.

Acknowledgements

The authors gratefully acknowledge Dr. Alexis Bemelmans (CEA, Molecular Imaging Research Center (MIRCen)) for his kind gift of AAVrh2-Htt18Q and AAVrh2-82Q viral vectors. The authors wish to thank the CELIS-IPS stem cells core facility (Institut de la Moelle Epinière et du Cerveau).

Appendix A. Supplementary data

Supplementary data related to this article can be found at https://doi.org/10.1016/j.biochi.2018.07.019.

References

[1] M.E. MacDonald, C.M. Ambrose, M.P. Duyao, R.H. Myers, C. Lin, L. Srinidhi, G. Barnes, S.A. Taylor, M. James, N. Groot, H. MacFarlane, B. Jenkins, M.A. Anderson, N.S. Wexler, J.F. Gusella, G.P. Bates, S. Baxendale, H. Hummerich, S. Kirby, M. North, S. Youngman, R. Mott, G. Zehetner, Z. Sedlacek, A. Poustka, A.-M. Frischauf, H. Lehrach, A.J. Buckler, D. Church, L. Doucette-Stamm, M.C. O'Donovan, L. Riba-Ramirez, M. Shah, V.P. Stanton, S.A. Strobel, K.M. Draths, J.L. Wales, P. Dervan, D.E. Housman, M. Altherr, R. Shiang, L. Thompson, T. Fielder, J.J. Wasmuth, D. Tagle, J. Valdes, L. Elmer, M. Allard, L. Castilla, M. Swaroop, K. Blanchard, F.S. Collins, R. Snell, T. Holloway, K. Gillespie, N. Datson, D. Shaw, P.S. Harper, A novel gene containing a trinucleotide repeat that is expanded and unstable on Huntington's disease chromosomes, Cell 72 (1993) 971–983, https://doi.org/10.1016/0092-8674(93)90585-E.

[2] E.H. Aylward, A.M. Codori, A. Rosenblatt, M. Sherr, J. Brandt, O.C. Stine, P.E. Barta, G.D. Pearlson, C.A. Ross, Rate of caudate atrophy in presymptomatic and symptomatic stages of Huntington's disease, Mov. Disord. 15 (2000) 552–560, https://doi.org/10.1002/1531-8257(200005)15. :3<552::AID-MDS1020>3.0.CO;2-P.

[3] H. Zhang, Q. Li, R.K. Graham, E. Slow, M.R. Hayden, I. Bezprozvanny, Full length mutant huntingtin is required for altered Ca2+ signaling and apoptosis of striatal neurons in the YAC mouse model of Huntington's disease, Neurobiol. Dis. 31 (2008) 80–88, https://doi.org/10.1016/j.nbd.2008.03.010.

[4] R.K. Graham, M.A. Pouladi, P. Joshi, G. Lu, Y. Deng, N.-P. Wu, B.E. Figueroa, M. Metzler, V.M. André, E.J. Slow, L. Raymond, R. Friedlander, M.S. Levine, B.R. Leavitt, M.R. Hayden, Differential susceptibility to excitotoxic stress in YAC128 mouse models of Huntington disease between initiation and progression of disease, J. Neurosci. Off. J. Soc. Neurosci. 29 (2009) 2193–2204, https://doi.org/10.1523/JNEUROSCI.5473-08.2009.

[5] A.J. Milnerwood, C.M. Gladding, M.A. Pouladi, A.M. Kaufman, R.M. Hines, J.D. Boyd, R.W.Y. Ko, O.C. Vasuta, R.K. Graham, M.R. Hayden, T.H. Murphy, L.A. Raymond, Early increase in extrasynaptic NMDA receptor signaling and expression contributes to phenotype onset in Huntington's disease mice, Neuron 65 (2010) 178–190, https://doi.org/10.1016/j.neuron.2010.01.008.

[6] A.J. Milnerwood, A.M. Kaufman, M.D. Sepers, C.M. Gladding, L. Zhang, L. Wang, J. Fan, A. Coquinco, J.Y. Qiao, H. Lee, Y.T. Wang, M. Cynader, L.A. Raymond, Mitigation of augmented extrasynaptic NMDAR signaling and apoptosis in cortico-striatal co-cultures from Huntington's disease mice, Neurobiol. Dis. 48 (2012) 40–51, https://doi.org/10.1016/j.nbd.2012.05.013.

[7] D.W. Choi, Ionic dependence of glutamate neurotoxicity, J. Neurosci. 7 (1987) 369–379.

[8] D.W. Choi, J.Y. Koh, S. Peters, Pharmacology of glutamate neurotoxicity in cortical cell culture: attenuation by NMDA antagonists, J. Neurosci. 8 (1988) 185–196.

[9] Cull-Candy, S.G., Brickley, S. & Farrant, M. NMDA receptor subunits: diversity, development and disease. Curr. Opin. Neurobiol. 11, 327-335, ResearchGate. (n.d.). https://www.researchgate.net/publication/11941061_Cull-Candy_SG_Brickley_S_Farrant_M_NMDA_receptor_subunits_diversity_development_and_disease_Curr_Opin_Neurobiol_11_327-335 (accessed February 12, 2018).

[10] P. Paoletti, J. Neyton, NMDA receptor subunits: function and pharmacology, Curr. Opin. Pharmacol. 7 (2007) 39–47, https://doi.org/10.1016/j.coph.2006.08.011.

[11] P. Paoletti, C. Bellone, Q. Zhou, NMDA receptor subunit diversity: impact on receptor properties, synaptic plasticity and disease, Nat. Rev. Neurosci. 14 (2013) 383–400, https://doi.org/10.1038/nrn3504.

[12] M.M. Zeron, O. Hansson, N. Chen, C.L. Wellington, B.R. Leavitt, P. Brundin, M.R. Hayden, L.A. Raymond, Increased sensitivity to N-Methyl-D-Aspartate receptor-mediated excitotoxicity in a mouse model of Huntington's disease, Neuron 33 (2002) 849–860, https://doi.org/10.1016/S0896-6273(02)00615-3.

[13] J. Fan, C.M. Cowan, L.Y.J. Zhang, M.R. Hayden, L.A. Raymond, Interaction of postsynaptic density protein-95 with NMDA receptors influences excitotoxicity in the yeast artificial chromosome mouse model of Huntington's disease, J. Neurosci. Off. J. Soc. Neurosci. 29 (2009) 10928–10938, https://doi.org/10.1523/JNEUROSCI.2491-09.2009.

[14] M.S. Levine, G.J. Klapstein, A. Koppel, E. Gruen, C. Cepeda, M.E. Vargas, E.S. Jokel, E.M. Carpenter, H. Zanjani, R.S. Hurst, A. Efstratiadis, S. Zeitlin, M.-F. Chesselet, Enhanced sensitivity to N-methyl-D-aspartate receptor activation in transgenic and knockin mouse models of Huntington's disease, J. Neurosci. Res. 58 (1999) 515–532, https://doi.org/10.1002/(SICI)1097-4547(19991115)58. :4<515::AID-JNR5>3.0.CO;2-F.

[15] C. Cepeda, J.N. Itri, J. Flores-Hernández, R.S. Hurst, C.R. Calvert, M.S. Levine, Differential sensitivity of medium- and large-sized striatal neurons to NMDA but not kainate receptor activation in the rat, Eur. J. Neurosci. 14 (2001) 1577–1589, https://doi.org/10.1046/j.0953-816x.2001.01783.x.

[16] R.K. Graham, Y. Deng, E.J. Slow, B. Haigh, N. Bissada, G. Lu, J. Pearson, J. Shehadeh, L. Bertram, Z. Murphy, S.C. Warby, C.N. Doty, S. Roy, C.L. Wellington, B.R. Leavitt, L.A. Raymond, D.W. Nicholson, M.R. Hayden, Cleavage at the caspase-6 site is required for neuronal dysfunction and degeneration due to mutant huntingtin, Cell 125 (2006) 1179–1191, https://doi.org/10.1016/j.cell.2006.04.026.

[17] L.A. Raymond, V.M. André, C. Cepeda, C.M. Gladding, A.J. Milnerwood, M.S. Levine, Pathophysiology of Huntington's disease: time-dependent alterations in synaptic and receptor function, Neuroscience 198 (2011) 252–273, https://doi.org/10.1016/j.neuroscience.2011.08.052.

[18] E.G. Mcgeer, P.L. Mcgeer, Duplication of biochemical changes of Huntington's chorea by intrastriatal injections of glutamic and kainic acids, Nature 263 (1976) 517–519, https://doi.org/10.1038/263517a0.

[19] O. Isacson, P. Brundin, F.H. Gage, A. Björklund, Neural grafting in a rat model of huntington's disease: progressive neurochemical changes after neostriatal ibotenate lesions and striatal tissue grafting, Neuroscience 16 (1985) 799–817, https://doi.org/10.1016/0306-4522(85)90095-8.

[20] M.F. Beal, N.W. Kowall, D.W. Ellison, M.F. Mazurek, K.J. Swartz, J.B. Martin, Replication of the neurochemical characteristics of Huntington's disease by quinolinic acid, Nature 321 (1986) 168–171, https://doi.org/10.1038/321168a0.

[21] M.F. Beal, R.J. Ferrante, K.J. Swartz, N.W. Kowall, Chronic quinolinic acid lesions in rats closely resemble Huntington's disease, J. Neurosci. 11 (1991) 1649–1659.

[22] J.M. Karasinska, M.R. Hayden, Cholesterol metabolism in Huntington disease, Nat. Rev. Neurol. 7 (2011) 561–572, https://doi.org/10.1038/nrneurol.2011.132.

[23] M. Valenza, E. Cattaneo, Emerging roles for cholesterol in Huntington's disease, Trends Neurosci. 34 (2011) 474–486, https://doi.org/10.1016/j.tins.2011.06.005.

[24] V. Leoni, C. Caccia, The impairment of cholesterol metabolism in Huntington disease, Biochim. Biophys. Acta 1851 (2015) 1095–1105, https://doi.org/10.1016/j.bbalip.2014.12.018.

[25] L. Boussicault, S. Alves, A. Lamazière, A. Planques, N. Heck, L. Moumné, G. Despres, S. Bolte, A. Hu, C. Pagès, L. Galvan, F. Piguet, P. Aubourg, N. Cartier, J. Caboche, S. Betuing, CYP46A1, the rate-limiting enzyme for cholesterol degradation, is neuroprotective in Huntington's disease, Brain J. Neurol. 139 (2016) 953–970, https://doi.org/10.1093/brain/awv384.

[26] F. Kreilaus, A.S. Spiro, C.A. McLean, B. Garner, A.M. Jenner, Evidence for altered cholesterol metabolism in Huntington's disease post mortem brain tissue, Neuropathol. Appl. Neurobiol. 42 (2016) 535–546, https://doi.org/10.1111/nan.12286.

[27] E. Trushina, R.D. Singh, R.B. Dyer, S. Cao, V.H. Shah, R.G. Parton, R.E. Pagano, C.T. McMurray, Mutant huntingtin inhibits clathrin-independent endocytosis and causes accumulation of cholesterol in vitro and in vivo, Hum. Mol. Genet. 15 (2006) 3578–3591, https://doi.org/10.1093/hmg/ddl434.

[28] D. del Toro, X. Xifró, A. Pol, S. Humbert, F. Saudou, J.M. Canals, J. Alberch, Altered cholesterol homeostasis contributes to enhanced excitotoxicity in Huntington's disease, J. Neurochem. 115 (2010) 153–167, https://doi.org/10.1111/j.1471-4159.2010.06912.x.

[29] A.O. Sodero, J. Vriens, D. Ghosh, D. Stegner, A. Brachet, M. Pallotto, M. Sassoè-Pognetto, J.F. Brouwers, J.B. Helms, B. Nieswandt, T. Voets, C.G. Dotti, Cholesterol loss during glutamate-mediated excitotoxicity, EMBO J 31 (2012) 1764–1773, https://doi.org/10.1038/emboj.2012.31.

[30] S.M. Paul, J.J. Doherty, A.J. Robichaud, G.M. Belfort, B.Y. Chow, R.S. Hammond, D.C. Crawford, A.J. Linsenbardt, H.-J. Shu, Y. Izumi, S.J. Mennerick, C.F. Zorumski, The major brain cholesterol metabolite 24(S)-

hydroxycholesterol is a potent allosteric modulator of N-methyl-D-aspartate receptors, J. Neurosci. Off. J. Soc. Neurosci. 33 (2013) 17290–17300, https://doi.org/10.1523/JNEUROSCI.2619-13.2013.
[31] A.J. Linsenbardt, A. Taylor, C.M. Emnett, J.J. Doherty, K. Krishnan, D.F. Covey, S.M. Paul, C.F. Zorumski, S. Mennerick, Different oxysterols have opposing actions at N-methyl-D-aspartate receptors, Neuropharmacology 85 (2014) 232–242, https://doi.org/10.1016/j.neuropharm.2014.05.027.
[32] M.-Y. Sun, A. Taylor, C.F. Zorumski, S. Mennerick, 24S-hydroxycholesterol and 25-hydroxycholesterol differentially impact hippocampal neuronal survival following oxygen-glucose deprivation, PLoS One 12 (2017), e0174416, https://doi.org/10.1371/journal.pone.0174416.
[33] J.A. Allen, R.A. Halverson-Tamboli, M.M. Rasenick, Lipid raft microdomains and neurotransmitter signalling, Nat. Rev. Neurosci. 8 (2007) 128–140, https://doi.org/10.1038/nrn2059.
[34] C. Frank, S. Rufini, V. Tancredi, R. Forcina, D. Grossi, G. D'Arcangelo, Cholesterol depletion inhibits synaptic transmission and synaptic plasticity in rat hippocampus, Exp. Neurol. 212 (2008) 407–414, https://doi.org/10.1016/j.expneurol.2008.04.019.
[35] A. Abulrob, J.S. Tauskela, G. Mealing, E. Brunette, K. Faid, D. Stanimirovic, Protection by cholesterol-extracting cyclodextrins: a role for N-methyl-D-aspartate receptor redistribution, J. Neurochem. 92 (2005) 1477–1486, https://doi.org/10.1111/j.1471-4159.2005.03001.x.
[36] J. Ponce, N.P. de la Ossa, O. Hurtado, M. Millan, J.F. Arenillas, A. Dávalos, T. Gasull, Simvastatin reduces the association of NMDA receptors to lipid rafts: a cholesterol-mediated effect in neuroprotection, Stroke 39 (2008) 1269–1275, https://doi.org/10.1161/STROKEAHA.107.498923.
[37] D. Charvin, P. Vanhoutte, C. Pagès, E. Borrelli, E. Borelli, J. Caboche, Unraveling a role for dopamine in Huntington's disease: the dual role of reactive oxygen species and D2 receptor stimulation, Proc. Natl. Acad. Sci. U.S.A. 102 (2005) 12218–12223, https://doi.org/10.1073/pnas.0502698102.
[38] C. Escartin, E. Brouillet, P. Gubellini, Y. Trioulier, C. Jacquard, C. Smadja, G.W. Knott, L. Kerkerian-Le Goff, N. Déglon, P. Hantraye, G. Bonvento, Ciliary neurotrophic factor activates astrocytes, redistributes their glutamate transporters GLAST and GLT-1 to raft microdomains, and improves glutamate handling in vivo, J. Neurosci. Off. J. Soc. Neurosci. 26 (2006) 5978–5989, https://doi.org/10.1523/JNEUROSCI.0302-06.2006.
[39] M.E.R. Butchbach, G. Tian, H. Guo, C.-L.G. Lin, Association of excitatory amino acid transporters, especially EAAT2, with cholesterol-rich lipid raft microdomains: importance for excitatory amino acid transporter localization and function, J. Biol. Chem. 279 (2004) 34388–34396, https://doi.org/10.1074/jbc.M403938200.
[40] E. Hudry, D. Van Dam, W. Kulik, P.P. De Deyn, F.S. Stet, O. Ahouansou, A. Benraiss, A. Delacourte, P. Bougnères, P. Aubourg, N. Cartier, Adeno-associated virus gene therapy with cholesterol 24-hydroxylase reduces the amyloid pathology before or after the onset of amyloid plaques in mouse models of Alzheimer's disease, Mol. Ther. J. Am. Soc. Gene Ther. 18 (2010) 44–53, https://doi.org/10.1038/mt.2009.175.
[41] J. Suopanki, C. Götz, G. Lutsch, J. Schiller, P. Harjes, A. Herrmann, E.E. Wanker, Interaction of huntingtin fragments with brain membranes–clues to early dysfunction in Huntington's disease, J. Neurochem. 96 (2006) 870–884, https://doi.org/10.1111/j.1471-4159.2005.03620.x.
[42] K.A. Burke, K.M. Hensal, C.S. Umbaugh, M. Chaibva, J. Legleiter, Huntingtin disrupts lipid bilayers in a polyQ-length dependent manner, Biochim. Biophys. Acta BBA - Biomembr. 1828 (2013) 1953–1961, https://doi.org/10.1016/j.bbamem.2013.04.025.
[43] S. Okamoto, M.A. Pouladi, M. Talantova, D. Yao, P. Xia, D.E. Ehrnhoefer, R. Zaidi, A. Clemente, M. Kaul, R.K. Graham, D. Zhang, H.-S. Vincent Chen, G. Tong, M.R. Hayden, S.A. Lipton, Balance between synaptic versus extrasynaptic NMDA receptor activity influences inclusions and neurotoxicity of mutant huntingtin, Nat. Med. 15 (2009) 1407–1413, https://doi.org/10.1038/nm.2056.
[44] C. Marquer, V. Devauges, J.-C. Cossec, G. Liot, S. Lécart, F. Saudou, C. Duyckaerts, S. Lévêque-Fort, M.-C. Potier, Local cholesterol increase triggers amyloid precursor protein-Bace1 clustering in lipid rafts and rapid endocytosis, Faseb. J. 25 (2011) 1295–1305, https://doi.org/10.1096/fj.10-168633.
[45] A.O. Sodero, L. Trovò, F. Iannilli, P. Van Veldhoven, C.G. Dotti, M.G. Martin, Regulation of tyrosine kinase B activity by the Cyp46/cholesterol loss pathway in mature hippocampal neurons: relevance for neuronal survival under stress and in aging, J. Neurochem. 116 (2011) 747–755, https://doi.org/10.1111/j.1471-4159.2010.07079.x.
[46] A.O. Sodero, C. Weissmann, M.D. Ledesma, C.G. Dotti, Cellular stress from excitatory neurotransmission contributes to cholesterol loss in hippocampal neurons aging in vitro, Neurobiol. Aging 32 (2011) 1043–1053, https://doi.org/10.1016/j.neurobiolaging.2010.06.001.
[47] M. Martin, C.G. Dotti, M.D. Ledesma, Brain cholesterol in normal and pathological aging, Biochim. Biophys. Acta 1801 (2010) 934–944, https://doi.org/10.1016/j.bbalip.2010.03.011.
[48] M.G. Martin, L. Trovò, S. Perga, A. Sadowska, A. Rasola, F. Chiara, C.G. Dotti, Cyp46-mediated cholesterol loss promotes survival in stressed hippocampal neurons, Neurobiol. Aging 32 (2011) 933–943, https://doi.org/10.1016/j.neurobiolaging.2009.04.022.
[49] M. Moutinho, M.J. Nunes, J.C. Correia, M.J. Gama, M. Castro-Caldas, A. Cedazo-Minguez, C.M.P. Rodrigues, I. Björkhem, J.L. Ruas, E. Rodrigues, Neuronal cholesterol metabolism increases dendritic outgrowth and synaptic markers via a concerted action of GGTase-I and Trk, Sci. Rep. 6 (2016) 30928, https://doi.org/10.1038/srep30928.
[50] A. Valencia, P.B. Reeves, E. Sapp, X. Li, J. Alexander, K.B. Kegel, K. Chase, N. Aronin, M. DiFiglia, Mutant huntingtin and glycogen synthase kinase 3-β accumulate in neuronal lipid rafts of a presymptomatic knock-in mouse model of Huntington's disease, J. Neurosci. Res. 88 (n.d.) 179–190. doi:https://doi.org/10.1002/jnr.22184.
[51] J.M. Lehmann, S.A. Kliewer, L.B. Moore, T.A. Smith-Oliver, B.B. Oliver, J.-L. Su, S.S. Sundseth, D.A. Winegar, D.E. Blanchard, T.A. Spencer, T.M. Willson, Activation of the nuclear receptor LXR by oxysterols defines a new hormone response pathway, J. Biol. Chem. 272 (1997) 3137–3140, https://doi.org/10.1074/jbc.272.6.3137.
[52] K. Abildayeva, P.J. Jansen, V. Hirsch-Reinshagen, V.W. Bloks, A.H.F. Bakker, F.C.S. Ramaekers, J. de Vente, A.K. Groen, Cheryl L. Wellington, F. Kuipers, M. Mulder, 24(S)-Hydroxycholesterol participates in a liver X receptor-controlled pathway in astrocytes that regulates apolipoprotein E-mediated cholesterol efflux, J. Biol. Chem. 281 (2006) 12799–12808, https://doi.org/10.1074/jbc.M601019200.
[53] O. Cheng, R.P. Ostrowski, W. Liu, J.H. Zhang, Activation of liver X receptor reduces global ischemic brain injury by reduction of nuclear factor-kappaB, Neuroscience 166 (2010) 1101–1109, https://doi.org/10.1016/j.neuroscience.2010.01.024.
[54] N. Mast, J.B. Lin, K.W. Anderson, I. Bjorkhem, I.A. Pikuleva, Transcriptional and post-translational changes in the brain of mice deficient in cholesterol removal mediated by cytochrome P450 46A1 (CYP46A1), PLoS One 12 (2017), e0187168, https://doi.org/10.1371/journal.pone.0187168.
[55] J. Zhang, Q. Liu, Cholesterol metabolism and homeostasis in the brain, Protein Cell 6 (2015) 254–264, https://doi.org/10.1007/s13238-014-0131-3.
[56] M. Valenza, M. Marullo, E. Di Paolo, E. Cesana, C. Zuccato, G. Biella, E. Cattaneo, Disruption of astrocyte-neuron cholesterol cross talk affects neuronal function in Huntington's disease, Cell Death Differ. 22 (2015) 690–702, https://doi.org/10.1038/cdd.2014.162.
[57] M. Valenza, V. Leoni, J.M. Karasinska, L. Petricca, J. Fan, J. Carroll, M.A. Pouladi, E. Fossale, H.P. Nguyen, O. Riess, M. MacDonald, C. Wellington, S. DiDonato, M. Hayden, E. Cattaneo, Cholesterol defect is marked across multiple rodent models of Huntington's disease and is manifest in astrocytes, J. Neurosci. Off. J. Soc. Neurosci. 30 (2010) 10844–10850, https://doi.org/10.1523/JNEUROSCI.0917-10.2010.
[58] J. Fan, R.Q. Zhao, C. Parro, W. Zhao, H.-Y. Chou, J. Robert, T.Z. Deeb, C. Raynoschek, S. Barichievy, O. Engkvist, M. Maresca, R. Hicks, J. Meuller, S.J. Moss, N.J. Brandon, M.W. Wood, I. Kulic, C.L. Wellington, Small molecule inducers of ABCA1 and apoE that act through indirect activation of the LXR pathway, J. Lipid Res. 59 (2018) 830–842, https://doi.org/10.1194/jlr.M081851.

Abstract

Huntington's disease (HD) is an autosomal dominant neurodegenerative disease caused by abnormal CAG expansion on huntingtin's gene. Recently, altered brain cholesterol homeostasis has been implicated in HD. Particularly, the expression of CYP46A1, the rate-limiting enzyme for cholesterol degradation in the brain, is decreased in patients' post-mortem putamen and in the striatum of the zQ175 Knock-In HD mouse model. We restored CYP46A1 expression into the striatum of zQ175 mice at a pre-symptomatic stage. Behavioral, neuropathological and molecular tests were performed and showed an improvement of locomotor activity and histological landmarks. Cholesterol homeostasis was restored with an increase of cholesterol degradation and cholesterol synthesis. CYP46A1 induced a new transcriptional signature, with restoration of pathways involved in autophagy, proteasome, synaptic communication and axonal transport, which are known to be dysfunctional in HD. Thus, we explored these mechanisms to decipher CYP46A1 role in this restoration. CYP46A1 improved the synaptic transmission in the striatum of zQ175 mice, with increased spines density and synaptic connectivity. Aggregate clearance mediated by autophagy and proteasome was increased after CYP46A1 expression. Finally, BDNF and TrkB transport were enhanced by CY46A1 in HD *in vitro* models. Overall, CYP46A1 restoration alleviates the pathological phenotype of zQ175 mice through a global compensation. To gain further insights into CYP46A1-mediated neuroprotection, a cell sorting strategy was set up to study the transcriptomic and lipidomic signature in purified neurons and astrocytes from mouse striatum. This method will lead to a greater understanding of cell-type-specific regulations and cell-to-cell communication. Altogether, this project gave new insights into the potential application of CYP46A1 restoration as a therapeutic strategy in HD.

Résumé

La maladie de Huntington (MH) est une maladie génétique autosomique dominante, causée par une augmentation du nombre de CAG sur le gène de la huntingtin. L'homéostasie du cholestérol cérébral est altérée dans la MH. L'expression de CYP46A1, enzyme neuronale catabolisant le cholestérol dans le cerveau, est diminuée dans le putamen des patients ainsi que dans le striatum de souris modèles de la MH. Après restauration de l'expression de CYP46A1 dans le striatum des souris Knock-In zQ175, les capacités locomotrices sont améliorées, l'agrégation de la huntingtine mutée est diminuée, l'atrophie neuronale est limitée et le métabolisme du cholestérol est stimulé. Une nouvelle signature transcriptionnelle est induite par CYP46A1, avec une restauration des voies impliquées dans l'autophagie, le protéasome, la communication synaptique et le transport axonal, connues pour leur dysfonctionnement dans la MH. Ainsi, nous avons exploré ces mécanismes pour préciser le rôle de CYP46A1 dans ces restaurations. CYP46A1 améliore la transmission synaptique dans le striatum des souris, avec une augmentation de la densité en épines synaptiques et de la connectivité synaptique. L'élimination des agrégats par autophagie et par le protéasome est augmentée avec CYP46A1. Enfin, le transport de BDNF et de TrkB est amélioré par CYP46A1 dans un modèle *in vitro* de la MH. Ces résultats révèlent l'effet pléiotrope et bénéfique de la régulation du métabolisme du cholestérol dans le contexte de la MH. Pour approfondir cette étude, une technique de tri cellulaire a été mise au point, afin de séparer et purifier les neurones et les astrocytes à partir de striatum de souris, pour étudier les régulations transcriptomique et lipidomique de ces deux populations cellulaires. Cette étude permettra d'identifier de nouvelles cibles moléculaires pertinentes impliquées dans la neuroprotection par CYP46A1 et pouvant présenter un intérêt thérapeutique dans la MH.